NUREG/CR-7185
ANL-14/10

Effects of Thermal Aging and Neutron Irradiation on Crack Growth Rate and Fracture Toughness of Cast Stainless Steels and Austenitic Stainless Steel Welds

Manuscript Completed: September 2014
Manuscript Published: October 2014

Prepared by Omesh K. Chopra
Argonne National Laboratory, Argonne, IL 60439

Appajosula S. Rao, NRC Technical Monitor & Project Manager

Prepared for
Division of Engineering
Office of Nuclear Regulatory Research
U.S. Nuclear Regulatory Commission
Washington, DC 20555
NRC Job Code V6455

Abstract

Cast austenitic stainless steel (CASS) materials and austenitic stainless steel (SS) welds, both of which have a duplex structure, are susceptible to thermal aging embrittlement during reactor service. In addition, prolonged exposure of these materials used in core support structure and reactor internals to neutron irradiation changes their microstructure and microchemistry, which further degrades their fracture properties. The purpose of this paper is to review and evaluate the existing thermal aging and neutron irradiation embrittlement data on these materials to update the methodology developed earlier at Argonne National Laboratory (Argonne) for estimating the degradation of mechanical properties of these materials during reactor service. The methodology developed earlier to determine the kinetics and extent of thermal embrittlement from known material information as a function of time and temperature of service has been reviewed and, where necessary, updated to incorporate recent data published after the Argonne reports. The updated results are used to estimate the fracture toughness J-R curve of thermally aged CASS materials as a function of time and temperature of service. The existing data on irradiated materials have also been evaluated to define a threshold fluence level above which irradiation effects on materials properties are significant. The paper also examines the combined effects of thermal and neutron embrittlement, which can degrade the fracture toughness of these materials more than predicted from either of the processes independently. Potential information gaps in the data needed to adequately address these issues are also identified.

Paperwork Reduction Act Statement

This U.S. Nuclear Regulatory Commission Report (NUREG) does not contain information collection requirements and, therefore, is not subject to the requirements of the Paperwork Reduction Act of 1995 (44 United States Code [U.S.C.] 3501 et seq.).

Public Protection Notification

The U.S. Nuclear Regulatory Commission (NRC) may not conduct or sponsor, and a person is not required to respond to, a request for information or an information collection requirement unless the requesting document displays a current valid Office of Management and Budget (OMB) control number.

This page is intentionally left blank.

Foreword

The internal components of light water reactor (LWR) pressure vessels are fabricated primarily with austenitic stainless steels (SSs) because of their relatively high strength, ductility, and fracture toughness. In addition, cast austenitic stainless steel (CASS) materials are used for reactor pressure-boundary components, such as valve bodies, pump casings, primary coolant piping, and some reactor core internal components. Although austenitic SSs are completely austenitic in the wrought condition, welded SSs and CASS materials have a duplex structure consisting of austenite and ferrite phases. The ferrite phase increases the tensile strength and improves resistance to stress corrosion cracking (SCC). However, the duplex structure of ferrite and austenite phases is susceptible to thermal embrittlement after service at reactor operating temperatures. In addition, during normal reactor operational conditions the reactor core internal components are exposed to high-energy neutron irradiation and high-temperature reactor coolant. Exposure to neutron irradiation for extended periods changes the microstructure and microchemistry (radiation-induced segregation) of wrought and CASS materials and their welds, thus degrading the component fracture properties and increasing their susceptibility to irradiation-assisted stress corrosion cracking (IASCC).

These mechanical property changes are caused by a complex interaction among irradiation, temperature, stress, and environment (viz. boiling water reactor [BWR] and pressurized water reactor [PWR] environments). As nuclear power plants age and neutron irradiation dose increases, the degradation of the reactor components becomes more likely. This represents an important safety issue associated with long-term operation of nuclear power plants. The U.S. Nuclear Regulatory Commission (NRC) has been sponsoring research on reactor core internals, in particular the duplex steels and welds, to (a) define the screening criteria for the minimum acceptable level of percent delta ferrite in these duplex steels, above which significant decreases in the fracture toughness of these components begin due to both thermal and neutron fluence levels; (b) develop disposition curves for IASCC growth rates; and (c) assess the significance of both thermal and neutron embrittlement on the structural and functional integrity of these CASS components and welds.

The objective of this report is to summarize the current knowledge associated with the effect of the reactor environment and with the thermal and neutron irradiation effects on the mechanical properties of the reactor components that are fabricated using CASS and welds; and to identify gaps in this knowledge that could affect the long-term performance of these components. The purpose of this report is to (a) compile and review thermal and neutron embrittlement and IASCC crack growth rate (CGR) data on austenitic SS welds and CASS materials; (b) summarize the compiled data and reevaluate its impact on the threshold fluence levels for susceptibility to IASCC and neutron embrittlement; and (c) identify information gaps in the data needed to address the effects of thermal and neutron embrittlement on the structural and functional integrity of austenitic SS welds and CASS materials in LWR systems. Furthermore, limited data suggest that the concurrent exposure to neutron irradiation during reactor service can result in a combined effect wherein the service-degraded fracture toughness can be less than that predicted for either thermal or neutron irradiation embrittlement independently. The combined effects of these two embrittlement processes are also discussed.

The results of this final report may be used to (a) To determine when aging management of reactor vessel internal (RVI) components manufactured from CASS materials is needed for license renewal (LR) of LWRs under 10 CFR Part 54; (b) to support revision of the Generic Aging Lessons Learned (GALL) report; (c) determine appropriate inspection and flaw disposition procedures for reactor internals for use in American Society of Mechanical Engineers (ASME)

code development, and for developing needed conditions within Title 10, Section 50.55a, “Codes and Standards,” of the Code of Federal Regulations (10 CFR 50.55a); and (d) identify issues related to screening criteria for the lower bound value of the delta ferrite limit at which significant loss of the fracture toughness of the CASS components and the welds occur during the normal operation of the nuclear power plants. This report will also be used by the NRC to evaluate the acceptability of planned industry and NRC-sponsored research to address gaps identified in this report.

Brian Thomas,
Director Division of Engineering
Office of Nuclear Regulatory Research
U.S. Nuclear Regulatory Commission

Table of Contents

Figures

Tables

Executive Summary

Background

Austenitic stainless steels (SSs) are used extensively as structural alloys in light water reactor (LWR) systems, including reactor core internal components, because of their excellent ductility, high notch toughness, corrosion resistance, and good formability. In addition, cast austenitic stainless steel (CASS) materials are used for reactor pressure-boundary components, such as valve bodies, pump casings, primary coolant piping, and some reactor core internal components. Although austenitic SSs are completely austenitic in the wrought condition, welded SSs and CASS materials have a duplex structure consisting of austenite and ferrite phases. The ferrite phase increases the tensile strength and improves resistance to stress corrosion cracking (SCC). However, exposure to neutron irradiation for extended periods changes the microstructure (radiation hardening) and microchemistry (radiation-induced segregation) of wrought and CASS materials and their welds, degrades their fracture properties, and increases their susceptibility to irradiation-assisted stress corrosion cracking (IASCC). Furthermore, CASS materials and austenitic SS welds are susceptible to thermal embrittlement of the ferrite phase after extended operation at reactor operating temperatures.

The scope of this report is to compile and evaluate the thermal and neutron embrittlement data on CASS materials and austenitic SS welds since the Argonne topical reports on these subjects have been published, and (a) update the methodology for estimating the loss of fracture toughness of these materials during extended service at reactor operating temperatures, (b) define the threshold neutron fluence above which irradiation effects on mechanical properties are significant and develop disposition curves for IASCC growth rates for these materials used in the reactor core internals, and (c) identify information gaps in the data needed to address the effects of thermal and neutron embrittlement on the structural and functional integrity of CASS components and austenitic SS welds in LWR systems.

The purpose of this report is to (a) compile and review thermal and neutron embrittlement and IASCC crack growth rate (CGR) data on austenitic SS welds and CASS materials, (b) summarize the compiled data and reevaluate its impact on the threshold fluence levels for susceptibility to IASCC and neutron embrittlement, and (c) identify information gaps in the data needed to address the effects of thermal and neutron embrittlement on the structural and functional integrity of austenitic SS welds and CASS materials in LWR systems. Furthermore, limited data suggest that the concurrent exposure to neutron irradiation during reactor service can result in a combined effect wherein the service-degraded fracture toughness can be less than that predicted for either thermal or neutron irradiation embrittlement independently. The combined effects of these two embrittlement processes are also evaluated.

Thermal Embrittlement

CASS Materials

Thermal aging of these materials increases their hardness and tensile strength and decreases ductility, impact strength, and fracture toughness. The low-C CF-3 steels are the most resistant to thermal embrittlement, and the Mo-bearing, high-C CF-8M steels are the least resistant. The formation of Cr-rich α' regions in the ferrite is the primary mechanism for thermal embrittlement. The α' phase strengthens the ferrite matrix, which promotes brittle fracture even at higher temperatures. Furthermore, precipitation and/or growth of phase boundary carbides or nitrides results in a brittle failure due to phase boundary separation, and may facilitate cleavage of the ferrite by particle cracking. The degree of embrittlement and, hence, the toughness of the

material, is controlled by the amount of brittle fracture. Consequently, the amount, size, and distribution of the ferrite phase in the duplex structure have a strong effect on the extent of embrittlement.

Significant variations in ferrite content have been observed within CASS components. For example, the ferrite content ranged from 3.0 to 22.5% with an average of 13.3% ferrite for a hot-leg elbow, and from 1.5 to 15.0% with an average of 9.8% ferrite for the crossover-leg elbow removed from the Ringhals reactor in Sweden. Similarly, the ferrite contents in centrifugally cast pipes were higher near the outer than the inner surface. In general, ferrite contents estimated from the material chemical composition using the Hull's equivalent factors compared well with the measured values. These observations indicate that when measured ferrite content is used for design analyses, it is important to ensure that it is representative of the entire component. The distribution and morphology of ferrite in CASS materials is discussed. Parametric studies of the manufacturing process parameters indicate that spinodal decomposition of the ferrite at reactor temperatures is very sensitive to the initial state of the ferrite. Process parameters that improve the homogeneity of the ferrite solid solution delay the beginning of the decomposition, which results in a more aging-resistant CASS material.

The degree of thermal embrittlement is characterized in terms of the room temperature (RT) Charpy-impact energy. All CASS materials reach "saturation" RT impact energy, the minimum impact energy that can be achieved for a material after long-term aging. The actual saturation impact energy for a specific CASS material is independent of aging temperature but depends strongly on the chemical composition of the steel. It is lower for CF-8M steels than for CF-3 or CF-8 steels, and decreases with an increase in ferrite content and the concentration of C or N in the steel. The kinetics of thermal embrittlement are also discussed. The activation energy for the process of thermal embrittlement is estimated from the chemical composition of the material; the values range between 65 and 105 kJ/mole (15 and 25 kcal/mole).

A methodology developed earlier in NUREG/CR-4513, Rev. 1 for estimating the Charpy-impact energy and fracture toughness J-R curve of CASS components under LWR operating conditions from material information readily available in certified material test records has been reviewed and, if necessary, updated to incorporate recent data published after the Argonne report was published. The extent of thermal embrittlement as a function of time and temperature of reactor service is estimated from the extent of embrittlement at saturation and from the correlations describing the kinetics of embrittlement, which are expressed in terms of the chemical composition of the material. The fracture toughness J-R curve is then obtained from the correlation between the fracture toughness parameters and the RT Charpy-impact energy. Common lower-bound J-R curves at RT and 290–320°C for static and centrifugally cast CF-3, CF-8, and CF-8M steels with <10%, 10–15%, 15–25%, and 25–40% ferrite are also defined. A significant modification of the earlier methodology is that separate expressions are proposed for CF-8M steels containing less than 10% Ni and those containing equal to or greater than 10% Ni. The latter are most susceptible to thermal embrittlement compared with the other grades.

The screening criteria established by the NRC to determine the susceptibility of CASS materials to thermal aging embrittlement have also been reviewed to evaluate their validity. The results indicate that for low-Mo CF-3 and CF-8 materials, the existing criterion for potentially susceptible material of greater than 20% ferrite for static-cast material and all centrifugally-cast material are valid and somewhat conservative in some cases. For CF-8M materials, the existing criterion for potentially susceptible material of greater than 14% ferrite for static-cast material and greater than 20% ferrite for centrifugally-cast material, has been updated. The criterion for static-cast and centrifugally-cast CF-8M materials has been decreased to 13%

ferrite and 17% ferrite, respectively, for materials with less than 10% Ni, and to 10% ferrite and 13% ferrite, respectively, for materials with equal to or greater than 10% Ni.

A flow diagram of the methodology for estimating mechanical properties of thermally aged CASS materials in LWR systems has also been updated. Three schemes are presented for estimation of mechanical properties of CASS material of (a) unknown composition, (b) known composition and unknown service history, and (e) known composition and service history. Lower bound fracture toughness J-R curves at room temperature and 290–320°C are presented for static-cast and centrifugally-cast CASS materials containing 25–40%, 15–25%, 10–15%, and <10% ferrite. However, the updated methodology does not consider the effect of reactor coolant environment on fracture toughness. Recent data indicate about 40% reduction in fracture toughness J-R curve data of long-term aged CF-8 steel at 54°C in PWR shutdown water chemistry (SWC) relative to that in air. Additional fracture toughness tests on thermally aged CASS materials are needed to better understand the possible effects of LWR environments on fracture toughness.

Austenitic Stainless Steel Welds

Austenitic SS welds typically contain 5–15% ferrite. However, they do not have a single representative microstructure. Four distinct ferrite morphologies have been identified in austenitic SS welds: vermicular, acicular, lacy, and globular. The vermicular morphology is most commonly observed in welds with 5–15% ferrite, and a lacy or acicular morphology is observed in welds containing 13–15% ferrite. However, the mechanical properties of austenitic SS welds differ from those of CASS materials. For a given ferrite content, the tensile strength of welds is higher and fracture toughness is lower than that of CASS materials. The gas tungsten arc (GTA) welds exhibit the highest toughness and submerged arc (SA) welds the lowest. The toughness of shielded metal arc (SMA) welds is either comparable or slightly superior to that of SA welds. The J_{Ic} values for the SA welds are about one-third those for the GTA welds. In SS welds, failure is controlled by void formation near inclusions or other flaws in the material.

The mechanism of thermal embrittlement of austenitic SS welds is the same as that of CASS materials. However, since the ferrite content in welds is limited to about 15%, the degradation of mechanical properties occurs primarily as a result of the presence of grain/phase boundary carbides and second phase inclusions. The results of an earlier Argonne study indicated that the fracture toughness J-R curve for thermally aged austenitic SS welds might be decreased by up to 40%. The Argonne study defined a lower-bound J-R curve for thermally aged SS welds. Furthermore, recent data indicate significant environmental effects on the fracture toughness of SS welds; fracture toughness in LWR environments can be up to 40% lower than in air. Additional data are needed to establish fracture toughness degradation of SS welds in LWR environments.

IASCC Crack Growth Rates

The effects of material parameters (such as composition, thermo-mechanical treatment, microstructure, microchemistry, yield strength, and stacking fault energy) and environmental parameters (such as water chemistry, irradiation temperature, dose, and dose rate) on IASCC susceptibility of austenitic SSs were discussed in an early study at Argonne, in NUREG/CR-7027 (2010), and are summarized in this report. The existing data indicate that, in the normal water chemistry (NWC) of boiling water reactors (BWRs), neutron irradiation up to 0.42 dpa has no effect on CGRs. The CGRs for materials irradiated above 0.42 dpa are above the NUREG-0313 disposition curve for nonirradiated materials in high-purity water containing 8 ppm

dissolved oxygen (DO). The CGRs can be up to a factor of 40 higher for materials irradiated to higher neutron dose levels. The growth rates for some irradiated SSs are a factor of 2–3 higher than the Electric Power Research Institute (EPRI) disposition curve for BWR core internal components. The data for highly irradiated materials show anomalous behavior. The CGRs in an NWC BWR environment, for SSs irradiated to 19 or 38 dpa, are below the NUREG-0313 disposition curve for nonirradiated SSs.

The SCC growth rates in the hydrogen water chemistry (HWC) BWR environment show a significant decrease relative to those in the NWC BWR environment for SSs irradiated to less than 2.2 dpa. The CGRs increase rapidly at neutron dose levels above 2.2 dpa, and above about 4.0 dpa, the CGRs in HWC BWR environment are comparable to those in NWC BWR environment. This behavior is observed at least at stress intensity factor (K) values above 18 MPa $m^{1/2}$. Additional CGR data on SSs irradiated to 3–8 dpa are needed to better define the threshold neutron dose for IASCC susceptibility in low-potential environments.

The SCC growth rates in PWR environment show significant variability. The CGRs for the same material and irradiation condition increase with increasing temperature. The CGRs obtained at different temperatures have been normalized to 320°C using an activation energy of 100 kJ/mol. In PWR water at 320°C, the CGRs for SSs irradiated above 3 dpa may be up to an order of magnitude above the NUREG-0313 curve for nonirradiated materials in high-purity water with 0.2 ppm DO. The CGRs for SSs irradiated to 11–25 dpa may be up to two orders of magnitude above the same curve. As observed earlier for HWC BWR water, the CGRs in the PWR environment of SSs irradiated to 37.5 dpa exhibit anomalous behavior as the rates are only marginally above the NUREG-0313 curve. The reasons for the high CGRs for some SSs irradiated to 7–18 dpa and relatively low CGRs in SSs irradiated to 37.5 dpa are not known.

The limited IASCC CGR data indicate that the CGRs for austenitic SS welds and weld heat affected zone (HAZ) materials, as well as CASS materials in NWC BWR environments, are comparable to those for wrought austenitic SSs. The CGRs increase rapidly for materials irradiated above 0.42 dpa. The growth rates for materials irradiated to 2.0–2.5 dpa may be up to an order of magnitude higher than the CGRs predicted by the NUREG-0313 curve for nonirradiated sensitized austenitic SSs in high-purity water with 8 ppm DO. The very limited CGR data for these materials in HWC BWR environments are mostly below the 0.2-ppm-DO NUREG-0313 curve; however, there are no data for dose levels above about 2.3 dpa. Additional IASCC CGR data in LWR environments are needed for irradiated Type 316 or 316L welds. IASCC CGR data are also needed for CASS materials and austenitic SS welds and HAZ materials irradiated above 2.2 dpa, in HWC BWR environment at 288°C or PWR primary water chemistry at 320°C. Furthermore, the effect of irradiation temperature should be established to better understand the IASCC susceptibility of austenitic SSs in PWR environments.

Neutron Embrittlement

The fracture toughness of austenitic SSs has been divided into three broad categories. The fracture toughness (J_{IC}) is above 150 kJ/m^2 for Category III materials, and 30–150 kJ/m^2 for Category II materials. These materials fracture after stable crack extension at stresses well above or close to the yield stress. Category I materials fracture at stress levels well below the yield stress by unstable crack extension, and their fracture toughness, as characterized with the critical stress intensity factor (K_{IC}), is less than 75 MPa $m^{1/2}$. Nonirradiated wrought and cast austenitic SSs and their welds typically fall in Category III. However, neutron irradiation degrades the fracture toughness of austenitic SSs to the level of Category II or even I at high dose levels.

The fracture toughness data on irradiated wrought and cast austenitic SSs and their welds were compiled and evaluated in NUREG/CR-7027 (2010) to define the threshold neutron dose above which fracture toughness of these materials is reduced significantly. The existing fracture toughness data on austenitic SSs irradiated in LWRs indicate little or no loss of fracture toughness below an exposure of about 0.5 dpa and a substantial and rapid decrease at exposures of 1–5 dpa. In addition, fracture toughness appears to saturate at approximately 10 dpa. A similar trend was observed earlier for austenitic SSs irradiated in high-flux fast reactors at 350–427°C and tested at 300–427°C. However, for the LWR-irradiated materials, the saturation fracture toughness (K_{Ic} or K_{Jc}) values are in the range of 36.8–40.3 MPa $m^{1/2}$ (33.5–36.6 ksi $in.^{1/2}$), and samples at this toughness typically fail without stable ductile crack extension. These values are lower than the K_{Jc} of 75 MPa $m^{1/2}$ (68.2 ksi $in.^{1/2}$) observed for fast-reactor-irradiated materials.

In NUREG/CR-7027, existing fracture toughness data were evaluated to develop a fracture toughness trend curve that includes (a) a threshold neutron exposure for radiation embrittlement of austenitic SSs and a minimum fracture toughness for these materials irradiated to less than the threshold value, (b) a saturation neutron exposure and a saturation fracture toughness for materials irradiated to greater than this value, and (c) a description of the change in fracture toughness between the threshold and saturation neutron exposures. A review of the existing data indicated very limited data on (a) materials irradiated in LWRs to neutron dose levels of 0.1–1.0 dpa or above 10 dpa, and (b) LWR-irradiated CASS materials and austenitic SS welds. The contribution of additional precipitate phases, voids, and cavities on the fracture toughness of these materials is not accurately known.

The limited data indicate that for the same irradiation conditions, the fracture toughness of thermally aged CASS materials and austenitic SS welds is lower than that of austenitic SS HAZ material, which, in turn, is lower than that of solution-annealed wrought SSs. However, the lower-bound fracture toughness trend curves developed in the Argonne studies may not be adequate for Type 316 welds. Furthermore, the available data also indicate that LWR environments can also decrease fracture toughness J-R curve of some of these materials. Typically, the effect of environment is larger for materials with higher fracture toughness. Furthermore, for some materials, the fracture toughness considering the effect of the reactor coolant environment is below the lower-bound curve. Additional data are needed to accurately establish the bounding fracture toughness of CASS materials and austenitic SS welds for LWR applications.

Combined Effects of Thermal and Neutron Embrittlement

For reactor core internal components, concurrent exposure to neutron irradiation can result in a combined effect wherein the service-degraded fracture toughness can be less than that predicted for either thermal embrittlement or neutron irradiation embrittlement independently. The existing fracture toughness data on austenitic SS welds and associated HAZ materials, as well as CASS materials, indicate that some of the data for austenitic SS welds, particularly Type 316 welds, may not be bounded by the lower-bound fracture toughness versus neutron dose curve proposed in NUREG/CR-7027. The limited data on J-R curve tests in LWR coolant environments indicate that the reactor coolant environment can further decrease fracture toughness of these materials relative to that obtained in air. For some heats, fracture toughness in coolant environment is likely to be below the lower bound trend curve proposed in NUREG/CR-7027.

The available fracture toughness data are inadequate to evaluate the combined effects of thermal and neutron embrittlement on the threshold dose for embrittlement. Additional data are needed to better establish the potential loss of fracture toughness due to combined effects of thermal and neutron embrittlement in these materials in the transition dose range of 0.05 to 2.0 dpa.

Acronyms and Abbreviations

AMP	aging management program
APFIM	atom probe field ion microscopy
Argonne	Argonne National Laboratory
ASME	American Society of Mechanical Engineers
ASTM	American Society for Testing and Materials
AWS	American Welding Society
BWR	boiling water reactor
CGR	crack growth rate
CASS	cast austenitic stainless steels
CGR	crack growth rate
CMTR	certified material test record
CNSR	Chevron notch short rod
CR	composition ratio
CT	compact tension
CTOD	crack tip opening displacement
CW	cold worked
DBTT	ductile-brittle transition temperature
DO	dissolved oxygen
dpa	displacements per atom
EdF	Electricité de France
EPFM	elastic-plastic fracture mechanics
EPRI	Electric Power Research Institute
FN	ferrite number
FRA	Framatome
GE	General Electric
GF	George Fischer
GTA	gas tungsten arc
HAZ	heat-affected zone
HWC	hydrogen water chemistry
IASCC	irradiation-assisted stress corrosion cracking
IG	intergranular
IASCC	irradiation-assisted stress corrosion cracking
IGSCC	intergranular stress corrosion cracking
ISI	in-service inspection
JAPEIC	Japan Power Electric Engineering and Inspection Corp.
J-R	J-integral resistance
LEFM	linear-elastic fracture mechanics
LWR	light water reactor
MEA	Materials Engineering Associates, Inc.

MMA	manual metal arc
MRP	Materials Reliability Program
MSIP	mechanical stress improvement process
NDT	nil-ductility transition
NP	National Power
NRC	Nuclear Regulatory Commission
NWC	normal water chemistry
PIFRAC	pipe fracture (database)
PWR	pressurized water reactor
RIS	radiation-induced segregation
RT	room temperature
SA	submerged arc
SANS	small angle neutron scattering
SCC	stress corrosion cracking
SE(B)	single edge bend
SFE	stacking fault energy
SMA	shielded metal arc
SS	stainless steel
SSRT	slow strain rate tensile
TEM	transmission electron microscopy
TG	transgranular
TWI	The Welding Institute
USE	upper-shelf energy
WH	Westinghouse

Nomenclature

a	Crack length
B	Specimen thickness
B_{eff}	Effective specimen thickness
C	Coefficient of the power-law J-R curve
Cr_{eq}	Chromium equivalent for the material
C_V	Room-temperature "normalized" Charpy-impact energy, i.e., Charpy-impact energy per unit fracture area, at any given service and aging time (J/cm^2). The fracture area for a standard Charpy V-notch specimen (ASTM Specification E 23) is 0.8 cm^2. The value of impact energy in J has been divided by 0.8 to obtain "normalized" impact energy in J/cm^2.
C_{Vint}	Initial room–temperature "normalized" Charpy-impact energy of a material, i.e., unaged material (J/cm^2).
C_{Vsat}	Room-temperature "normalized" Charpy-impact energy of a material at saturation, i.e., the minimum impact energy that would be achieved for the material after long–term service (J/cm^2).
D	Neutron dose
da	Increment in crack length
E	Elastic modulus
F	Neutron fluence
J	J integral, a mathematical expression used to characterize the local stress-strain field at the crack tip region (parameter J represents the driving force for crack propagation)
J_d	Deformation J per ASTM Specification E 813-85 or E 1152–87 (kJ/m^2)
J_{Ic}	Value of J near the onset of crack extension
K	Stress intensity factor
K_{Ic}	Critical stress intensity factor
K_{Jc}	Equivalent critical stress intensity factor
K_{max}	Maximum stress intensity factor
K_{min}	Minimum stress intensity factor
M	Constraint factor
n	Exponent of the power-law J-R curve
Ni_{eq}	Nickel equivalent for the material
P	Aging parameter, i.e., the log of the time of aging at 400°C
Q	Activation energy for the process of thermal embrittlement (kJ/mole)
R	load ratio
S	Stress
t	Service or rest or aging time
t_{eff}	Effective time of loading
t_r	Rise time
T	Tearing modulus or temperature
W	Specimen width
α	Shape factor of the curve for the change in room-temperature Charpy-impact energy with time and temperature of aging

β	Half the maximum change in room-temperature Charpy-impact energy
δ_C	Ferrite content calculated from the chemical composition of a material (%)
υ	Poisson ratio
θ	Aging behavior at 400°C, i.e., the log of the time to achieve β reduction in impact energy at 400°C.
$\bar{\sigma}$	Von Mises effective stress
σ_f	Flow stress, defined as the average of yield and ultimate stress
σ_u	Ultimate stress
σ_y	Yield stress
ϕ	Material parameter

In this report, all values of impact energy have been normalized with respect to the actual cross-sectional area of the Charpy-impact specimen. Thus, for a standard Charpy-V-notch specimen per American Society for Testing and Materials (ASTM) Specification E 23 (i.e., 10 x 10-mm cross section and 2-mm V notch), impact energy value in J has been divided by 0.8 cm^2 to obtain impact energy in J/cm^2. Impact energies obtained on subsize specimens were normalized with respect to the actual cross-sectional area and appropriate correction factors were applied to account for size effects. Similarly, impact energies from other standards such as U-notch specimen were converted to a Charpy-V-notch value by appropriate correlations.

SI units of measurements have been used in this report. Conversion factors for measurements in British units are as follows:

To convert from	to	multiply by
in.	mm	25.4
J*	ft·lb	0.7376
kJ/ m^2	$in.-lb/in.^2$	5.71015
kJ/mole	kcal/mole	0.239

* When impact energy is expressed in J/cm^2, first multiply by 0.8 to obtain impact energy of a standard Charpy V-notch specimen in J.

Acknowledgments

This work is sponsored by the Office of Nuclear Regulatory Research, U.S. Nuclear Regulatory Commission, under Job Code V6455; Program Manager: Appajosula S. Rao.

This page is intentionally left blank.

1. Introduction

Austenitic stainless steels (SSs) are used extensively as structural alloys in light water reactor (LWR) systems, including reactor core internal components, because of their excellent ductility, high notch toughness, corrosion resistance, and good formability. In addition, cast austenitic stainless steel (CASS) materials are used in LWR systems for reactor pressure-boundary components, such as valve bodies, pump casings, primary coolant piping, and some reactor core internal components. Although these steels are completely austenitic in the wrought condition, welded SSs and CASS materials have a duplex structure consisting of austenite and ferrite phases. The ferrite phase provides additional benefits; it increases tensile strength and improves resistance to stress corrosion cracking (SCC).

However, exposure to neutron irradiation for extended periods changes the microstructure (radiation hardening) and microchemistry (radiation-induced segregation, or RIS)[1–5] of wrought and cast austenitic SSs and their welds, degrades their fracture properties[6–21] and increases their susceptibility to irradiation-assisted stress corrosion cracking (IASCC).[20–29] Furthermore, CASS materials and austenitic SS welds, which have a duplex structure, are susceptible to thermal embrittlement after extended operation at reactor operating temperatures,[30–53] typically 282°C (540°F) for boiling water reactors (BWRs), 288–327°C (550–621°F) for pressurized water reactor (PWR) primary coolant piping, and 343°C (650°F) for PWR pressurizers. In such instances, a fracture mechanics methodology, such as elastic-plastic fracture mechanics (EPFM) or linear-elastic fracture mechanics (LEFM) is needed for analysis of structural integrity and development of inspection guidelines. The former involves the J integral-resistance (J-R) curve approach, used where failure is caused by plastic deformation. The J integral is a mathematical expression used to characterize the local stress-strain field at the crack tip region (parameter J represents the driving force for crack propagation), and the J-R curve characterizes the resistance of the material to stable crack extension. The fracture toughness of such materials is represented by fracture mechanics parameters such as J_{Ic}, the value of J near the onset of crack extension, and the tearing modulus, T, which characterizes the slope of the J-R curve:

$$T = (dJ/da)(E/\sigma_f^2), \tag{1}$$

where E is the elastic modulus, a is the crack length, and σ_f is the flow stress defined as the average of the yield stress (σ_y) and ultimate stress (σ_u). The LEFM methodology is used where failure involves negligible plastic deformation. The fracture toughness of such materials is represented by the parameter K_{Ic} (i.e., plane strain fracture toughness), which characterizes the resistance of the material to unstable crack extension. For small-scale yielding (such as deep cracks in bending in sufficiently large specimens), the fracture toughness can be characterized by J_{Ic}. Since J_{Ic} and K_{Ic} have different units, it is often convenient to represent J_{Ic} in terms of a parameter K_{Jc}, which has the units of the stress intensity factor and is determined from the J_{Ic} value using the relationship

$$K_{Jc} = (E' J_{Ic})^{1/2}, \tag{2}$$

where the normalized elastic modulus is given by $E' = E/(1 - \upsilon^2)$, E is the elastic modulus, and υ is the Poisson ratio. Only in cases where LEFM is applicable, is K_{Jc} equal to the critical stress intensity.

The fracture toughness of austenitic SSs has been divided into three broad categories.[8] Category III corresponds to high toughness materials with J_{Ic} above 150 kJ/m^2 (857 in.-lb/in.^{2}).

In these materials, fracture occurs after stable crack extension at stresses well above the yield stress. Category II corresponds to materials with intermediate toughness and with J_{Ic} in the range of 30–150 kJ/m^2 (171–857 in.-lb/in.^{2}). In Category II materials, fracture occurs by stable or unstable crack extension at stress levels close to the yield stress. Category I corresponds to low-toughness materials with J_{Ic} < 30 kJ/m^2 (< 171 in.-lb/in.^{2}), and fracture occurs below the yield stress with little or no controlled crack extension.

Nonirradiated wrought and CASS materials fall in Category III. The J_{Ic} values for Type 304 and 316 SS at temperatures up to 125°C (257°F) vary between 169 and 1660 kJ/m^2 (965 and 9479 in.-lb/in.^{2}), with a median value of 672 kJ/m^2 (3837 in.-lb/in.^{2}).[8] The J_{Ic} values at 400–550°C (752–1022°F) are approximately 35% lower, with a median value of 421 kJ/m^2 (2404 in.-lb/in.^{2}). Fracture in such high-toughness materials is by the nucleation and coalescence of microvoids and is characterized by a dimpled fracture-morphology.

Although CASS materials and SS welds exhibit ductile fracture at temperatures up to 550°C (1022°F), their fracture toughness is lower than that of the wrought SSs. In addition, a dimpled fracture-morphology is observed in SS welds.[53] Because of a high density of inclusions in the weld, the dimples are relatively small and shallow, and often associated with inclusions. The overall fracture toughness of CASS materials and SS welds, is controlled by the density and morphology of second-phase inclusions in these materials and varies with the cast or weld process. For example, static cast products have lower fracture toughness than centrifugally-cast pipes. Gas tungsten arc (GTA) welds exhibit the highest toughness; shielded metal arc (SMA) welds have intermediate toughness; and submerged arc (SA) welds have the lowest toughness.[8] The median value of J_{Ic} is 492 kJ/m^2 (2809 in.-lb/in.^{2}) for GTA welds and 147 kJ/m^2 (839 in.-lb/in.^{2}) for SA welds at temperatures up to 125°C (257°F).

Welding of austenitic SSs results in a heat affected zone (HAZ) adjacent to the fusion zone, where the material microstructure and microchemistry are greatly altered because of the precipitation of Cr-rich carbides at the grain boundaries. The formation of the carbides depletes Cr from the grain-boundary region thereby creating a region that is susceptible to SCC. However, the fracture toughness of HAZ material is generally superior to that of the weld metal and may be comparable to that of the base metal.

A critical assessment of the susceptibility of austenitic SSs to IASCC was presented in U.S. Nuclear Regulatory Commission (NRC) topical report NUREG/CR-7027.[21] The existing data were evaluated to establish the effects of material parameters (such as composition, thermo-mechanical treatment, microstructure, microchemistry, yield strength, and stacking fault energy) and environmental parameters (such as water chemistry, irradiation temperature, dose, and dose rate) on IASCC susceptibility. The results were used to (1) define a threshold-fluence above which irradiation effects on susceptibility to IASCC and fracture toughness of wrought and CASS materials and their welds are significant and (2) evaluate the potential of neutron embrittlement under LWR operating conditions. A superposition model is used to represent the fatigue crack growth rates (CGRs). The results indicate that for the same irradiation conditions, the fracture toughness of thermally aged CASS material and austenitic SS weld metal is lower than that of the HAZ of SS base materials, which, in turn, is lower than that of solution-annealed SS base materials. The potential deficiencies or knowledge gaps in the existing experimental data on degradation of LWR core internal materials due to neutron irradiation are also discussed.

The thermal embrittlement of CASS materials and austenitic SS welds has also been investigated at Argonne National Laboratory (Argonne) and the results were published in

several NRC topical reports.[48–53] A procedure and correlations have been developed at Argonne for estimating fracture toughness, tensile, and Charpy-impact properties of CASS components during service from known material information.[50] The Argonne estimation scheme is applicable to compositions within the American Society for Testing and Materials (ASTM) Specifications A 351 for Grades CF-3, CF-3A, CF-8, CF-8A, and CF-8M. A correlation for Charpy-impact energy at saturation (i.e., the minimum impact energy that would be achieved for the material after long-term aging) is given in terms of chemical composition. Change in impact energy as a function of time and temperature of service is estimated from saturation impact energy and from the correlations that describe the kinetics of embrittlement, which are also given in terms of chemical composition. The fracture toughness J-R curve for the material is then obtained from the correlation between the fracture toughness parameters and the Charpy-impact energy. Tensile yield and flow stresses, and Ramberg/Osgood parameters are estimated from the flow stress of the unaged material and the kinetics of embrittlement.[52]

Although austenitic SS welds have a duplex structure, and their chemical compositions are similar to those of CASS materials, the Argonne correlations for CASS materials are not applicable to austenitic SS welds. The correlations account for mechanical-property degradation of typical heats of CASS, and do not consider the effects of compositional or structural differences that may arise from various welding processes, and that typically change the failure mechanism of the material. Degradation of fracture toughness and Charpy-impact energy of several SS pipe welds was evaluated in another NRC report, NUREG/CR-6428.[53] The welds were aged for 7,000 to 10,000 h at 400°C (752°F) to simulate saturation conditions; the lowest impact energy that would be achieved by the material after long-term aging. The results were compared with data from other studies.

Furthermore, limited data suggest that the concurrent exposure to neutron irradiation during reactor service can result in a combined effect wherein the service-degraded fracture toughness can be less than that predicted for either thermal or neutron irradiation embrittlement independently. The combined effects of these two embrittlement processes are also evaluated.

The scope of this report is to compile and evaluate the thermal and neutron embrittlement data on CASS materials and austenitic SS welds since the Argonne topical reports were published, as well as the following:

(a) Update the methodology for estimating the loss of fracture toughness of these materials during extended service at reactor operating temperatures,

(b) Define the threshold neutron fluence above which irradiation effects on mechanical properties are significant and develop disposition curves for IASCC growth rates for these materials used in the reactor core internals, and

(c) Identify information gaps in the data needed to address the effects of thermal and neutron embrittlement on the structural and functional integrity of CASS components and austenitic SS welds in LWR systems.

Data have been obtained on thermally aged and unaged CASS materials (with ferrite content up to 40%) and austenitic SS welds with and without neutron irradiation. The methodology presented in NUREG/CR-4513, Rev. 1 for predicting the loss of fracture toughness of CASS components due to thermal aging during service at reactor operating temperatures has been updated to include CASS materials with up to 40% ferrite. The combined effects of thermal and neutron embrittlement on loss of fracture toughness of these materials have also been included. In addition, an assessment presented in NUREG/CR-6428 (1996) of aging degradation effects on mechanical properties of austenitic SS welds has been updated to establish the lower-bound

fracture toughness J-R curve for SS welds during extended reactor operation. The effect of thermal and neutron irradiation on the bounding values of IASCC CGRs for these materials is evaluated as a function of neutron dose. The combined effects of thermal and neutron embrittlement as a function of ferrite content are also summarized.

2. Thermal Embrittlement of Duplex Stainless Steels

It has been known that binary iron-chromium alloys and ferritic SSs are susceptible to severe embrittlement when exposed to temperatures in the range of 270 to 475°C (518 to 887°F).[54–57] The potential for significant embrittlement of cast duplex SSs, consisting of both austenite and ferrite phases, has been confirmed by studies at Argonne[48–53] and elsewhere[30–34,42–44] on materials that were aged at temperatures between 290–450°C (554–842°F) for times up to 70,000 h (~8 yr). The results indicate that thermal aging of CASS materials (ASTM Specification A-351 for Grades* CF-3, CF-3A, CF-8, CF-8A, and CF-8M) at reactor operating temperatures of 270–350°C (518–662°F) increases their hardness and tensile strength; decreases ductility, impact strength, and fracture toughness; and shifts the Charpy transition curve to higher temperatures. The effect of thermal aging is observed to decrease at temperatures above 400°C (752°F). For example, the extent of thermal embrittlement in CASS materials aged at 450°C (842°F) is less than that in materials aged for similar times at 400°C (752°F).[20]

Various grades and heats of CASS exhibit varying degrees of thermal embrittlement. The low-C CF-3 steels are the most resistant to thermal embrittlement, and the Mo-bearing, high-C CF-8M steels are the least resistant. Ferrite morphology had a strong effect on the degree or extent of embrittlement, whereas small changes in material composition significantly altered the kinetics of embrittlement. In addition, the results of studies on the kinetics of thermal aging demonstrate that thermal embrittlement of cast duplex SSs can occur during the reactor design life of 40 yr.[48]

In austenitic SS welds, the ferrite phase is desired for controlling the weld solidification behavior and inhibiting the formation of low-melting-point compounds such as sulfides and phosphides, which promote microfissuring.[8] Since the ferrite phase is brittle at low temperatures, austenitic SS welds also exhibit a ductile-brittle transition temperature (DBTT) phenomenon. However, at ambient and elevated temperatures, the ferrite phase shows a ductile deformation behavior. The fracture toughness of Type 304/308 and 316/16-8-2 welds is dependent on the weld process but not composition.[8] For a given weld process, both these weld metals exhibit similar fracture toughness.[40] In general, the GTA welds exhibit the highest toughness and SA welds the lowest. The J_{Ic} values for the SA welds are about one-third those for the GTA welds.

Type 308 SS welds generally contain 5–15% ferrite, but their mechanical properties typically differ from those of CASS materials. Earlier studies conducted at Argonne[53] indicated that for a given ferrite content, the tensile strength of austenitic SS welds is higher and fracture toughness is lower than that of CASS materials. Experimental data[53] indicate that CASS materials with very poor fracture toughness are relatively insensitive to thermal aging. In these steels, failure is controlled by void formation near inclusions or other flaws in the material (i.e., by processes that are not sensitive to thermal aging). These results suggest that austenitic SS welds with poor fracture toughness (e.g., SA and SMA welds) should be relatively less sensitive to thermal aging than GTA welds.

2.1 Mechanism of Thermal Embrittlement

Fracture of the 300 series austenitic SSs is essentially by nucleation, growth, and coalescence of microvoids resulting in a dimpled fracture morphology, irrespective of test temperature.[8] The heat-to-heat variability is due to the differences in the density and morphology of inclusions such as carbides, calcium aluminates, and manganese sulfides, which serve as nucleation sites for

*The CF-3A and CF-8A grades represent high tensile strength material. The chemical composition of these grades is further restricted within the composition limits of CF-3 and CF-8, to obtain a ferrite/austenite ratio that results in higher ultimate and yield strengths. In this report, they are considered equivalent to CF-3 and CF-8 grades.

void formation. Large inclusions or inclusion clusters aligned in the working direction fail early in the deformation process, thereby resulting in poor fracture toughness. In relatively tough materials, microvoids are nucleated away from the primary fracture plane, and significant plastic deformation is required for void coalescence.

A similar fracture behavior is also observed in CASS materials and austenitic SS welds. Fracture occurs by microvoid coalescence. In CASS materials, voids nucleate preferentially within the ferrite phase, or at inclusions and phase boundaries, whereas in austenitic SS welds, microvoids forms at manganese silicates and silicides, oxides, and delta ferrite.[8,41,43] In both materials, the overall fracture toughness is controlled by the density and morphology of the second phase particles, and for CASS materials, to some extent by the volume fraction of ferrite. The fracture toughness of austenitic SS welds is generally lower than that of cast or wrought austenitic SSs because of the higher density of inclusions. Among austenitic SS welds, the SA and SMA welds have poor fracture toughness relative to the GTA welds; they have a high density of manganese- and silicon-rich silicates and silicides. High silicon contents are generic to the SA and SMA welds because of silicon pickup from the flux. Typically SA welds have 0.6–1.0% Si, SMA welds have 0.5–0.8% Si, and GTA welds have less than 0.5% Si.[8]

Furthermore, in materials with a duplex structure, such as CASS and austenitic SS welds, the ferrite phase exhibits a ductile-to-brittle-transition temperature. Its plastic straining capacity is substantially decreased at low temperatures. However, the ferrite phase is ductile at room temperature and higher temperatures. Therefore, in the unaged condition, both CASS materials and austenitic SS welds exhibit a ductile dimpled fracture. The transition temperatures of unaged materials are relatively low. The differences in the transition temperature for the various unaged heats and grades of CASS materials are due to the amount of ferrite and the differences in the mechanism of brittle fracture. The high-carbon CF-8 or CF-8M steels have a higher transition temperature than CF-3 steels because of the presence of phase boundary carbides. The carbides weaken the boundaries and lead to premature phase boundary separation with little or no strain hardening. For austenitic SS welds, since the ferrite volume fraction is typically less than 15%, the ferrite content has little effect on the overall fracture toughness of welds.

The available data indicate that the fracture toughness of wrought austenitic SSs and their welds is strongly influenced by specimen orientation. For austenitic SS pipe welds, specimens with a crack propagating in the axial direction (C-L orientation)* exhibit fracture toughness J_{Ic} and tearing modulus values that are 60–70% lower than those propagating in the circumferential direction (L-C orientation).[41] This behavior has been attributed to the alignment of stringers in the primary working direction (axial or longitudinal). When stringers are aligned parallel to the crack propagation direction C-L orientation), tear ridges are nucleated ahead of the crack front, the coalescence of which results in premature crack advance without extensive plastic deformation. When stringers are normal to the crack propagation direction (L-C orientation), microvoids are very deep and equiaxed, which blunts the advancing crack tip, and significant plastic deformation is needed for failure. Similarly, fracture toughness J-R tests on Type 304 control-rod and Type 304L top guide materials irradiated to 4.7–12.0 dpa in a BWR, showed lower fracture toughness in the T-L orientation than in the L-T orientation.[10] The lower fracture toughness along the T-L orientation is also due to the presence of stringers consisting of long, narrow particles oriented in the rolling direction, which result in a long and narrow quasi-cleavage structure parallel to the crack advance, thereby accelerating the crack advance.

*The first letter represents the direction perpendicular to the plane of the crack and the second letter represents the direction of crack advance. L = longitudinal or rolling direction; C = circumferential direction for pipes; T = transverse direction for plates.

The available data also indicate that thermal aging of CASS materials and austenitic SS welds at 290–450°C (554–842°F) results in thermal embrittlement of the ferrite, and the ductile-to-brittle-transition temperature for these materials is increased to higher temperatures.[8,48–52] Thermal aging of CASS materials at 290–450°C leads to (a) spinodal decomposition of the ferrite into high-Cr α' and low-Cr α regions; (b) nucleation and growth of the high-Cr α' phase; (c) precipitation of a Ni- and Si-rich G phase, $M_{23}C_6$, and γ_2 (austenite); and (d) additional precipitation and/or growth of existing carbides at ferrite/austenite phase boundaries.[42,58–66] Thermal aging has little or no effect on the austenite phase. The formation of Cr-rich α' regions in the ferrite is the primary mechanism for thermal embrittlement. The α' phase strengthens the ferrite matrix and increases strain hardening, which raises the local tensile stresses above the critical value for brittle fracture at higher temperatures. The formation of G phase and precipitation and growth of carbides or nitrides at phase boundaries also contribute to some extent, particularly in high-C and Mo-bearing materials. Furthermore, the presence of these phases leads to a brittle failure by phase boundary separation, and may facilitate cleavage of the ferrite by particle cracking.

Thermal aging of austenitic SS welds leads to spinodal decomposition of the ferrite to form the α' phase, formation of Ni- and Ti-rich silicides (the G phase, $Ti_6Ni_{16}Si_7$) in the ferrite, precipitation of $M_{23}C_6$ carbides on the phase boundaries, and limited M_6C carbides in the matrix.[8] However, the degradation of fracture toughness occurs primarily due to the presence of grain boundary or phase boundary carbides, which initiate localized intergranular cracking. Fracture occurs along the delta ferrite regions where the second phase particles initiate voids/cracks either by decohesion of the ferrite/austenite interphase or particle cracking.[40] The dominant failure process is transgranular dimple fracture, and intergranular cracking is limited to a few isolated regions.[8]

A study conducted at Electricité de France (EdF) on the evolution of thermally aged CASS materials, using Charpy U-notch impact test specimens, indicated that at room temperature, the brittle transgranular fracture of ferrite takes place primarily by cleavage; some twinning is also observed in highly embrittled material.[43] Multiple-cleavage of ferrite islands is observed throughout the material. The cleavage facets are all parallel to each other, irrespective of the geometry of the individual islands. The percent of cleavage increases with increase in the degree of thermal embrittlement, or with decrease in test temperature. At higher temperature, although cleavage of the ferrite is reduced, twinning appears to plays an important role in brittle failure of ferrite. The ferrite/austenite phase boundary exhibits a jagged appearance with very fine lines and straight deformation bands within the ferrite islands (most likely slip bands and twins).[43] The fracture behavior of the austenite also changes from a dimple fracture to shear fracture. The presence of completely embrittled ferrite skeleton promotes the low-energy failure mode of ductile shearing or tearing of the austenite ligaments between the islands of ferrite.[37] Typically, in duplex materials, cavities initiate from the cleavage cracks in the ferrite and not from matrix-inclusion decohesions.

Another study on microstructural characterization and fracture behavior of unaged and aged CF-8M steel at room temperature using Charpy V-notch and fracture toughness compact tension (CT) specimens also showed similar failure mechanisms.[67] At room temperature, fully ductile dimple fracture was observed for unaged material and material aged up to 40,000 h at 300°C (572°F). Ductile dimple fracture and brittle cleavage facets were observed for material aged up to 10,000 h at 350 and 400°C (662 and 752°F). In addition to these two fracture modes, ferrite/austenite phase boundary separation was also observed in materials aged at 450°C (842°F). Phase boundary separation is generally observed in high-C CASS materials aged at high temperatures (i.e., 400 or 450°C). Fractographic evaluation of both Charpy V-notch and fracture toughness CT specimens

showed similar fracture modes for aged CF-8M material. The only difference was that longer aging times were needed before brittle cleavage fracture was observed in the CT specimens. Although only room-temperature tests were conducted in this study, tests at higher temperatures are expected to show a larger fraction of ductile dimple fracture and less brittle fracture.

Thus, severely embrittled CASS materials generally exhibit large areas of brittle transgranular fracture of ferrite, linked by ductile shearing or tearing of the austenite ligaments. At room temperature, brittle fracture of the ferrite is in the form of cleavage facets. The degree of embrittlement and, hence, the toughness of the material, is controlled by the amount of brittle fracture. CASS materials with poor toughness and impact strength exhibit greater fraction of brittle fracture. For some CASS materials, although a fraction of the material may fail in a brittle fashion, the surrounding austenite provides ductility and toughness. Such materials have adequate toughness even after long-term aging. A predominantly brittle failure occurs when either the ferrite phase is continuous (e.g., in cast material with a large ferrite content) or the ferrite/austenite phase boundary provides an easy path for crack propagation (e.g., in high-C grades of cast steel with large phase-boundary carbides). For CASS materials with lacy ferrite morphology, a ferrite content of about 10% or greater can provide a continuous ferrite phase. Consequently, the amount, size, and distribution of the ferrite phase in the duplex structure, and the presence of phase-boundary carbides are important parameters in controlling the degree or extent of thermal embrittlement.

Cleavage of ferrite occurs when the local tensile stress reaches the critical cleavage fracture stress. At low temperatures (i.e., high values of yield stress), cleavage cracks nucleate in the ferrite in the plastic zone near the notch tip at loads that are below general yielding. At high temperatures (i.e., low values of yield stress), strain hardening is needed to raise the local tensile stress to the cleavage fracture stress. Ductile fracture results when strain hardening is insufficient to raise the tensile stress to the critical value. The relationship between the degree of cleavage fracture and toughness, however, is complex since cleavage cracks can be initiated by several mechanisms (i.e., dislocation pile up, cracking of carbide or nitride particles, and cracking of twin intersections). Each of the mechanisms requires a unique stress level. Thus, for the same amount of cleavage fracture, the toughness may vary in different cast materials.

The time-temperature curves for the formation of various phases and the change in impact strength of thermally aged cast duplex stainless steel[32] indicate that at temperatures above 550°C (1022°F), the embrittlement is largely due to formation of sigma phase, and below 500°C (932°F), precipitation of α' phase leads to embrittlement. Furthermore, the time-temperature transformation curves for Fe-Cr alloys indicate that the α' phase is not stable at 550°C (1022°F). At 550°C, the iron-chromium alloys are embrittled after aging for >10 h, owing to the formation of a sigma phase.[33] Consequently, the fracture toughness of embrittled CASS materials can be recovered virtually completely by annealing for 1 h at 550°C (1022°F) and water quenching. This short heat treatment dissolves the α' phase but prevents formation of sigma phase;[48] the dissolution of α' has been confirmed by microstructural studies.[42]

2.2 Distribution and Morphology of Ferrite

2.2.1 Ferrite Morphology

2.2.1.1 CASS Materials

The degree and kinetics of thermal embrittlement of duplex structures such as CASS materials are controlled primarily by the amount, size, and distribution of the ferrite phase, and to some

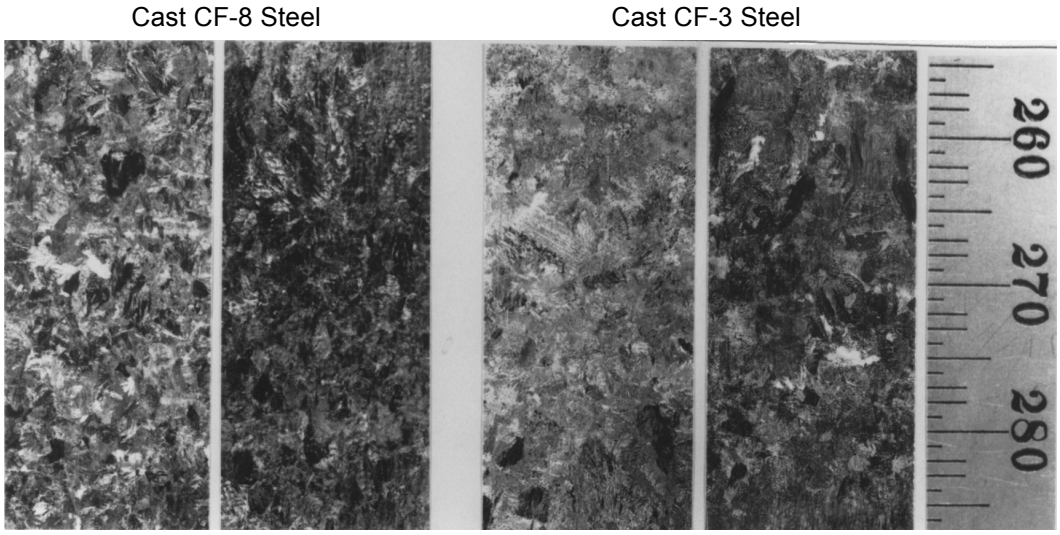

Figure 1. Microstructure along the axial and circumferential sections of centrifugally-cast CF-8 and CF-3 stainless steel pipes showing equiaxed grain structure.

extent the presence of carbides or nitrides at the phase boundaries. These material parameters in turn depend on the chemical composition and the manufacturing process. Differences in the thermal aging behavior have been observed is austenitic SS castings produced by different foundries, suggesting that manufacturing parameters may also be important for thermal aging.

The effect of manufacturing process on the thermal embrittlement of CASS materials has been investigated by Massoud et al.[68] The manufacturing process for castings consists of solidification of the material from a liquid state at around 1500°C (2732°F), followed by a homogenizing heat treatment of the solid at 1050–1150°C (1922–2102°F) and water quenching. Duplex SSs with high Cr contents solidify into a primary δ ferrite phase. The high-Cr SSs are also more sensitive to thermal aging. Typically, the core of the large sand-cast components consists of equiaxed grains, and the surface regions contain columnar grains, elongated in the direction of the temperature gradient; steeper temperature gradients result in smaller and more elongated columnar grains.[68] Examples of equiaxed and columnar grain structures are shown in Figs. 1 and 2, respectively.

During cooling of the solidified material, if the concentrations of the γ-forming elements such as C, N, Mn, and Ni, are sufficient, a fraction of the δ-ferrite transforms to γ-austenite by solid-state δ to γ transformation. Furthermore, if the cooling rate between 900 and 600°C (1652 and 1112°F) is slow, δ ferrite can transform to the brittle sigma (σ) phase, and $M_{23}C_6$ carbides can also precipitate at the δ/γ phase boundaries, both of which lead to degradation of the mechanical properties of the material.[68] Therefore, the manufacturing processes require that the casting must be annealed at around 1100°C (2012°F) followed by a rapid quench to avoid the formation of these deleterious precipitates.

The significant results of the parametric study of the manufacturing process parameters conducted by Massoud et al.[68] are as follows:

- The solidification speed affects the morphology of the ferrite-austenite microstucture and the characteristics of the toughness transition curve, but does not seem to affect the aging behavior of the steel.

Figure 2. Microstructure along axial section of a check valve from the decommissioned Shippingport reactor showing columnar grains.

- The homogenizing temperature especially affects the ferrite content of the material and the chemical composition of each phase. Thus, it affects the aging behavior of the steel.
- The homogenizing treatment holding time and the quenching rate affect the beginning of the decomposition of the ferrite and consequently the overall kinetics of aging.

The results indicate that the microstructural changes in the ferrite by spinodal decomposition during thermal aging at temperatures between 290 and 400°C (554 and 752°F), are very sensitive to the initial state of the ferrite in the as-quenched condition. Any manufacturing process parameter that improves the homogeneity of the ferrite solid solution, such as long homogenizing heat treatments and rapid quench, delay the beginning of the ferrite decomposition, which results in a more aging-resistant CASS material.

The ferrite morphology of the various CASS materials varies with the ferrite content, chemical composition, and size of the casting. Studies conducted at Argonne on 30 heats of CF-3, CF-8, and CF-8M CASS materials showed that globular ferrite morphology was observed for materials containing <5% ferrite.[48] Some differences in morphology were observed between the different grades of CASS materials containing >5% ferrite. The CF-8 and CF-8M steels had a lacy morphology, while the CF-3 cast steels showed a mixture of lacy and acicular ferrite. Significant variations in ferrite content within a CASS component have been observed in hot-leg and crossover-leg elbows removed from the Ringhals reactor.[69] The material of the elbows was ASTM 351 CF-8M steel, with ferrite content determined from the modified Schaefler diagram, of 20.1% for the hot-leg and 19.8% for the crossover-leg elbow. Test rings were cut from the two elbows and the ferrite content measured with a ferritemeter at the inside surface at three different heights of the ring, as well as through the thickness of the ring. The results from around 700 measurements showed that the ferrite content varies significantly in the actual components. The ferrite content for the hot-leg elbow ranged from 3.0 to 22.5% with an average of 13.3% ±4.2% ferrite, and for the crossover-leg elbow ranged from 1.5 to 15.0% with an average of 9.8% ±3.4% ferrite. The results also indicate that for both elbows, the measured average ferrite contents are comparable with the values estimated from the material chemical composition using the Hull's equivalent factors or the ASTM A800/A800M methodology (see Section 2.2.2).

Significant variations in the ferrite content were also observed in the Argonne studies on CASS materials, which were obtained from actual components. The morphology and measured ferrite content along circumferential sections of centrifugally-cast CF-8 (Heat P1) and CF-3 (Heat P2) pipes from regions near the inside and outside diameter, and two vanes of a static cast CF-3 pump impeller (Heat I) are shown in Fig. 3. The results indicate that for both centrifugally-cast

Centrifugally-cast CF-8 Stainless Steel (Heat P1) Pipe

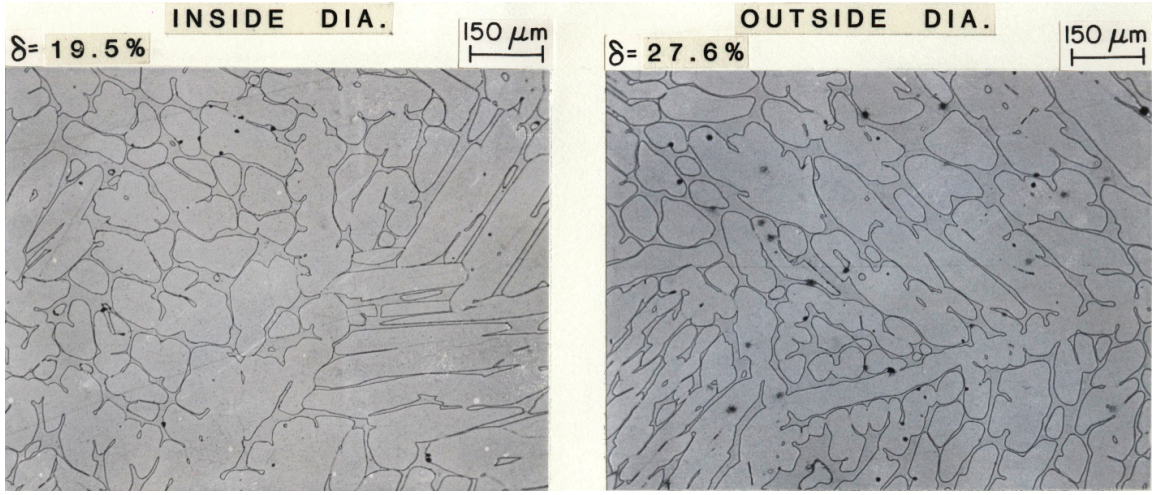

Centrifugally-cast CF-3 Stainless Steel (Heat P2) Pipe

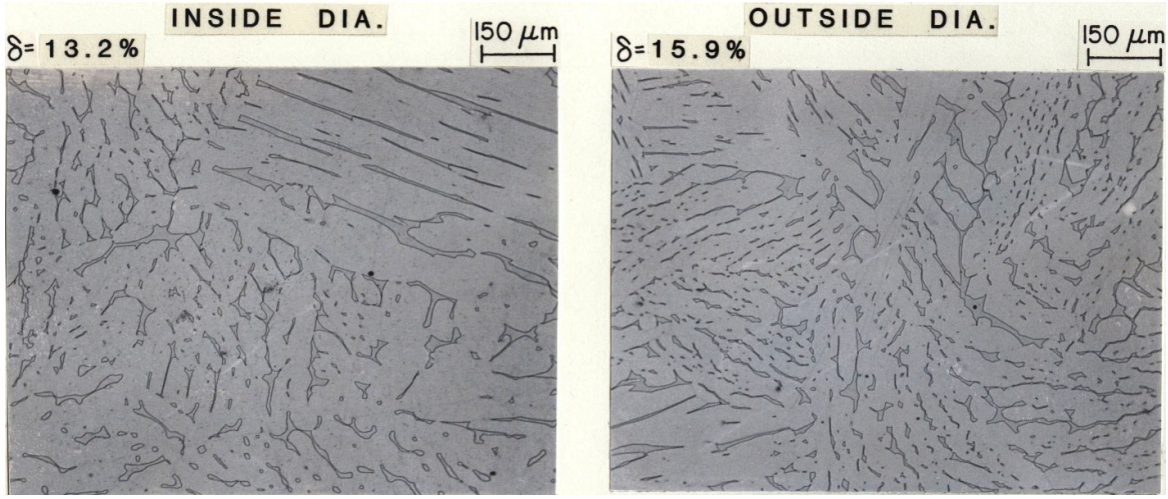

Static cast CF-3 Stainless Steel (Heat I) Pump Impeller

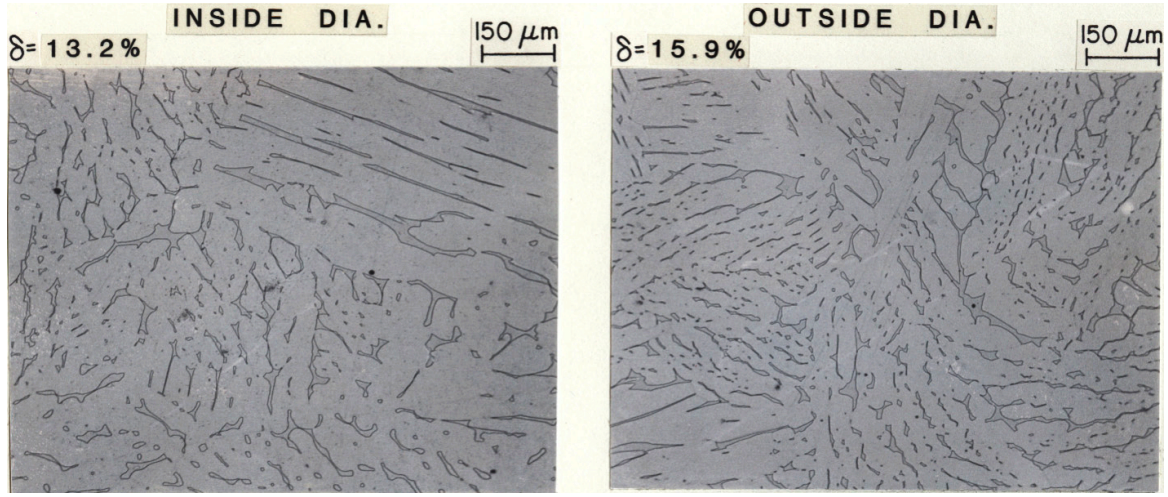

Figure 3. Ferrite content and morphology along circumferential section of centrifugally-cast CF-8 (Heat P1) and CF-3 (Heat P2) pipes from regions near the inside and outside diameter, and two vanes of a static cast CF-3 pump impeller (Heat I).

pipes, the ferrite contents are higher near the outer surface than the inner surface. The values are about 20% higher for the CF-3 pipe (Heat P2) and 40% higher for the CF-8 pipe (Heat P1). In addition, the ferrite content of pump impeller vane 3 was about 40% higher than that of Vane 1. The ferrite contents estimated from the chemical composition using Hull's equivalent factors, were 17.7%, 15.6%, and 17.1 % for CF-8 pipe, CF-3 pipe, and CF-3 pump impeller, respectively. The estimated values are comparable to the measured ferrite contents for the CF-3 pipe and pump impeller, but are lower than the measured values for the CF-8 pipe.

These observations indicate that if measured value of ferrite content is used for design calculations or analyses, several locations should be selected across the length and width of the component to ensure that it is representative of the entire component. The results also indicate that for centrifugally-cast SS pipes, the extent of embrittlement is likely to increase from the inner surface towards the surface because of the increasing ferrite content.

2.2.1.2 Austenitic Stainless Steel Welds

A duplex structure is also observed in austenitic SS welds, with ferrite being the minor phase distributed in various forms in the austenite matrix. Similar to the CASS materials, the solidification behavior and subsequent solid state transformation within the weld metal during cooling control the microstructural characteristics of the weld. The solidification sequences in Type 308 SS welds include primary crystallization of δ-ferrite with subsequent envelopment by austenite, followed by further transformations from liquid to γ and δ to γ.[70] As the sample cools to a temperature below that of the solidus, the transformation at the liquid-g interface is completed, leaving behind a skeletal network of untransformed d ferrite along the cores of the primary and secondary dendrite arms. This residual ferrite is rich in Cr, which makes it very stable.[70] However, primary ferrite with a lower average Cr concentration of about 24–25 wt.%, may transforms into Widmanstatten austenite and ferrite during rapid cooling. These two types of transformations involve extensive solute redistribution by diffusion, and may be used to explain the various ferrite morphologies observed in austenitic SS welds.[70]

Austenitic SS welds do not have a single representative microstructure. Examples of typical ferrite morphology of four different welds is shown in Fig. 4. PWWO is a 0.305-m (12-in.) schedule 100 pipe mockup weld with overlays, PWCE is a 0.71-m (28-in.) Type 304 pipe weld, PWDR is a 0.254-m (10-in.) Type 304 SS pipe weld after service in the Dresden reactor, and PWMS is a 0.71-m (28-in.) SS pipe weld treated by the Mechanical Stress Improvement Process (MSIP). In another study on the ferrite morphology and variations in ferrite content in two austenitic SS welds, four distinct ferrite morphologies were identified in Type 308 SS multipass welds: vermicular, lacy, acicular, and globular.[70] These morphologies were observed on the same multipass weld. The welds were deposited by the GTA process on a 25-mm thick Type 304L SS plate (0.019 C, 1.75 Mn, 0.63 Si, 0.029 P, 0.006 S, 10.0 Ni, 18.55 Cr, and balance Fe [wt.%]) containing a single-V butt joint, using Type 308 SS filler metal (0.016 C, 1.95 Mn, 0.35 Si, 0.029 P, 0.004 S, 9.76 Ni, 20.14 Cr, and balance Fe [wt.%], and Cr_{eq}/Ni_{eq} = 1.66). One of the welds was made with the joint surfaces buttered with the weld metal and the other without buttering. Ferrite number (FN) was measured using a Magne-gage in accordance with American Welding Society (AWS) A4.2-74 (see Section 2.2.2).[71]

The average FNs of the root pass deposited in the buttered and not buttered weld were 13 and 8, respectively. The lower ferrite content of the weld prepared without buttering was attributed to weld-metal dilution with the base metal; it is indicative of a change in weld metal composition. Furthermore, the FN value of the root pass decreased further after the second and third passes because of the dilution of ferrite from the thermal effects to which the root pass is subjected

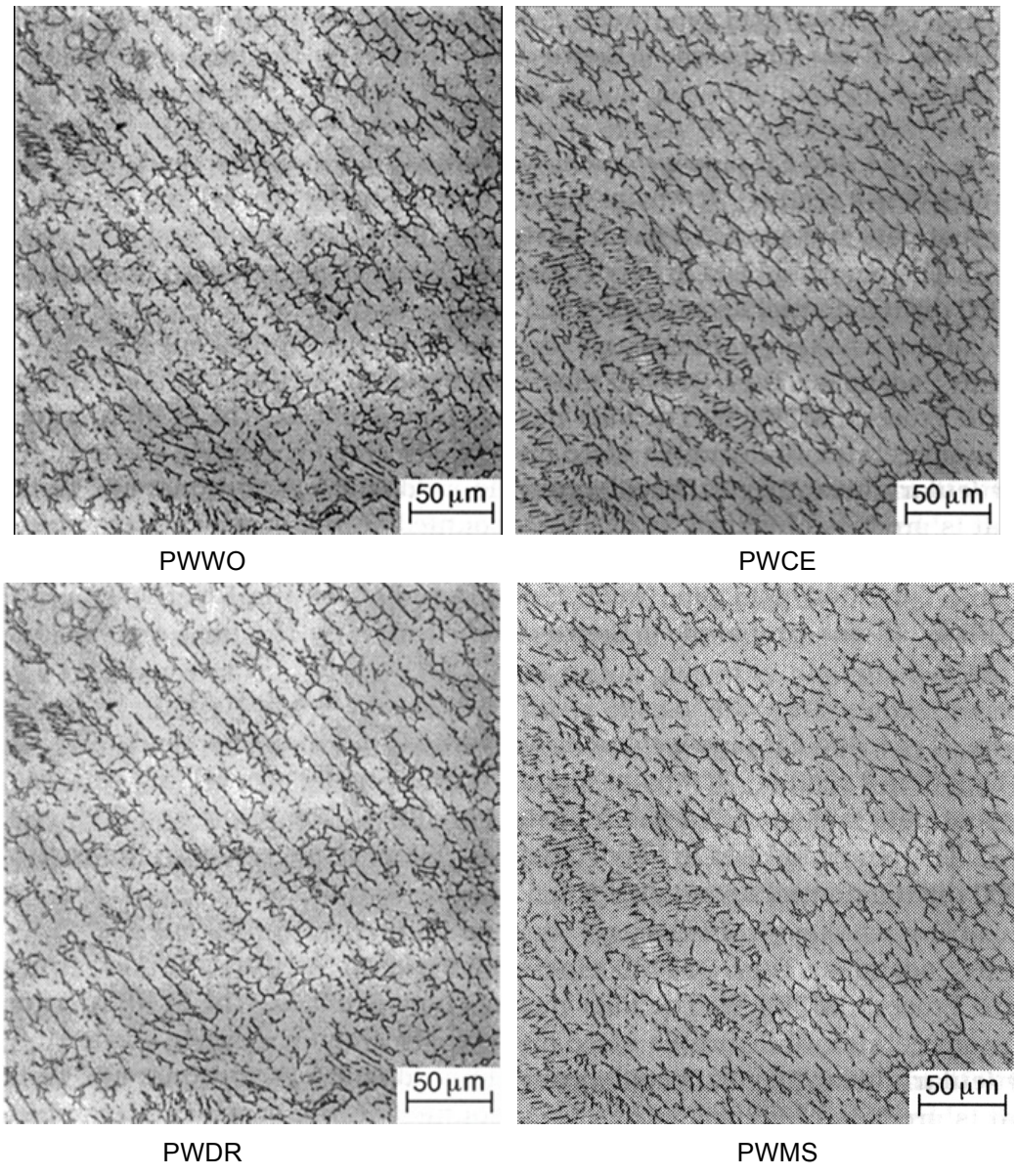

Figure 4. Typical ferrite morphology of four different welds.

during a multipass weld. Variations in ferrite content were also observed in both welds within a cross section of the bead, along the length and width of the weld. The FN values* at various weld locations varied from 9 to 13 and 5 to 14 for the buttered and not-buttered welds, respectively. Based on the composition of the weld metal, the calculated ferrite content for the weld, without dilution, is 8.1% from Hull's equivalent factor,[72] 5.9 from the ASTM A800/A800M methodology (based on the Schoefer diagram),[73,74] and about 13.8% from the modified Schaeffler (or Delong) diagram.[75,76]

The value based on the ASTM A800 methodology is significantly lower than the average measured value of FN 11 for the buttered weld. However, since the ferrite measurements were made using a Magne-gage, such instruments are very sensitive to surface roughness or surface curvature. Furthermore, phases other than ferrite and austenite may form at higher

* FN values determined from the modified Schaeffler diagram.

temperatures during welding, which may alter the magnetic response of the material such that the indicated ferrite content is quite different than of the same material not subjected to the welding process. It should also be mentioned that the variations in ferrite content in part might be due to differences in the N pickup during welding.[70]

The vermicular morphology is most commonly observed in austenitic SS welds with FN 5–15, and was predominantly observed in the weld root pass and the two subsequent passes. The ferrite content varied between FN 9 and 12. The vermicular (meaning the form, markings, motion, or tracks of worms) morphology, depending on the sectional cut viewed, appears as an aligned skeletal network of ferrite or as a curved skeletal form. The alignment is along the heat flow direction, which is also the primary dendrite growth direction.

A lacy morphology was observed predominantly in the third pass of the weld; the ferrite content varied between FN 13 and 15. The lacy structure looked very regular and aligned. The lacy form of ferrite is characterized by long columns of interlaced ferrite oriented along the growth direction in an austenite matrix. Most likely, it forms by the transformation of primary δ-ferrite to Widmanstatten austenite and ferrite.

An acicular morphology was present in the sixth and crown passes of the weld; the ferrite content was about FN 14. However, unlike the previous two morphologies, the acicular structure had no directionality and did not conform to the solidification substructure in any way. This morphology is typical of weld metals with Cr_{eq}/Ni_{eq} = 2. It also forms by the low-temperature transformation of primary ferrite to austenite and ferrite.

The globular form is characterized by ferrite in the form of globules randomly distributed in a matrix of austenite. The structure has no directionality and is not related to the overall solidification substructure. It was commonly observed in weld passes 4, 5, and 6 of the multi-pass weld. The ferrite content was around FN 10. A globular morphology is formed because of thermal instability of any of the other forms of ferrite, particularly the acicular form.

It should be noted that these ferrite morphologies may appear continuous or discontinuous depending on the section of the weld viewed. Therefore, caution must be exercised in such characterization of the ferrite since only vermicular and lacy morphologies are continuous.

2.2.2 Estimation of Ferrite Content

As discussed above, the ferrite content in the CASS structure is essentially a function of the chemical composition and the manufacturing process history of the material. Typically, the ferrite content of the CASS duplex structures is determined by from the (a) chemical composition, (b) magnetic response, or (c) metallographic examination of the material. Among the magnetic methods, the Magne-Gage and Ferritescope are the most commonly used instruments for measuring the ferrite content in CASS materials or austenitic SS welds. The Magne-Gage is a continuous-reading instrument that utilizes a spring to measure the attraction between a magnet and the material of unknown ferrite content, and the response is compared with that of a calibrated sample. The Ferritescope operates on the magneto-induction principle where the relative magnetic permeability of the specimen is measured.

However, because the magnets or the probes of these instruments are small, the surface roughness or curvature of the sample is an important parameter that can vary the magnetic linkage with the material being measured. In addition, phases other than ferrite and austenite may form in the material during service, which may alter the magnetic response of the material

such that the indicated ferrite content is quite different from that of the same chemical composition that has undergone a different heat treatment.

Until 1973, ferrite contents in duplex structures such as CASS materials and austenitic SS welds were determined by metallographic examination of the structure. A sample of the material was polished and etched to reveal the ferrite and austenite phases, and a grid was superimposed over the image of an optical microscope to determine by point counting the percentage of ferrite in the sample. The main drawback with this method is that the point count estimates of ferrite may vary with the etching technique used to reveal the ferrite phase, and with the number of grid points used in the measurements. Furthermore, as discussed above, the ferrite content in most CASS components varies significantly in different regions of the component, and obtaining metallographic samples from various regions may not be practical.

Although a quantitative metallographic method provides the most accurate estimate of ferrite content, determination of ferrite percent from chemical composition of the material offers the most useful and most common method for ferrite control during solidification of the metal from a melt during casting or welding. However, the accuracy of these estimations depends on the accuracy of the chemical analysis procedure, and the degree of variability of composition within the casting or weld. The most commonly used methods are described below.

2.2.2.1 Hull's Equivalent Factor

When a certified material test record (CMTR) is available, the ferrite content is calculated from chemical composition in terms of Hull's equivalent factors for nickel and chromium given by

$$Cr_{eq} = Cr + 1.21(Mo) + 0.48(Si) – 4.99 \quad (3)$$

and

$$Ni_{eq} = (Ni) + 0.11(Mn) – 0.0086(Mn)^2 + 18.4(N) + 24.5(C) + 2.77, \quad (4)$$

where the concentrations of the various alloying and interstitial elements is in wt.%. The concentration of N is often not available in a CMTR; if not known, it is assumed to be 0.04 wt.%. The ferrite content δ_c is given by

$$\delta_c = 100.3(Cr_{eq}/ Ni_{eq})^2 – 170.72(Cr_{eq}/ Ni_{eq}) + 74.22. \quad (5)$$

The measured ferrite content and values calculated from Hull's equivalent factor for the various CASS heats used in studies at Argonne,[48] the Georg Fischer Co. (GF),[30] EdF,[43] National Power (NP),[44] Framatome (FRA),[34] and the Electric Power Research Institute (EPRI)[35] are shown in Fig. 5. For most heats, the difference between the estimated and measured values is ±6% ferrite. The results also indicate that the calculated ferrite content was generally lower than the measured values for CF-8M heats that contained ≥10% Ni.

2.2.2.2 ASTM A800/800M Methodology

The ferrite content of the casting shall be estimated from the central line of the of the diagram at the composition ratio of chromium equivalent, Cr_{eq}, to nickel equivalent, Ni_{eq}, determined from the following formula:

$$(Cr_{eq}/Ni_{eq}) = (Cr + 1.5Si + 1.4Mo + Nb – 4.99)/(Ni +30C + 0.5Mn + 26(N – 0.02) + 2.77) \quad (6)$$

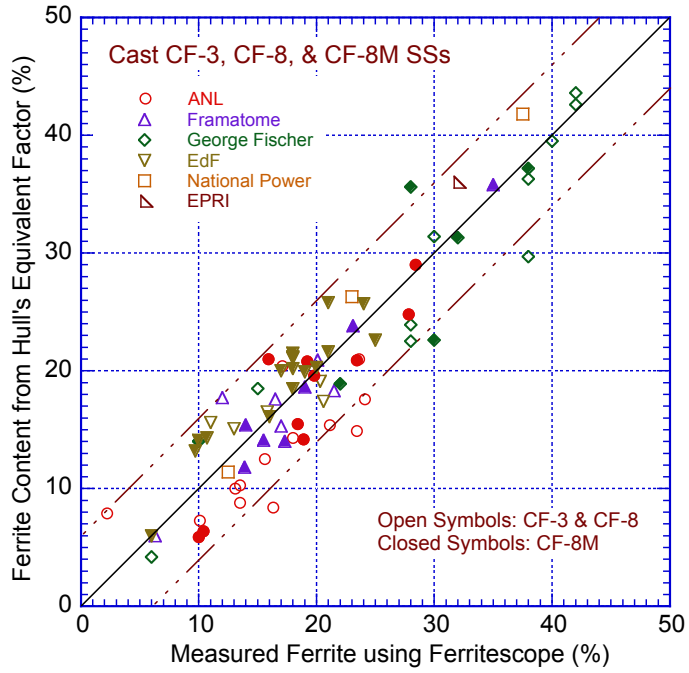

Figure 5.
Plots of measured ferrite content and values calculated from Hull's equivalent factor for various CASS materials.

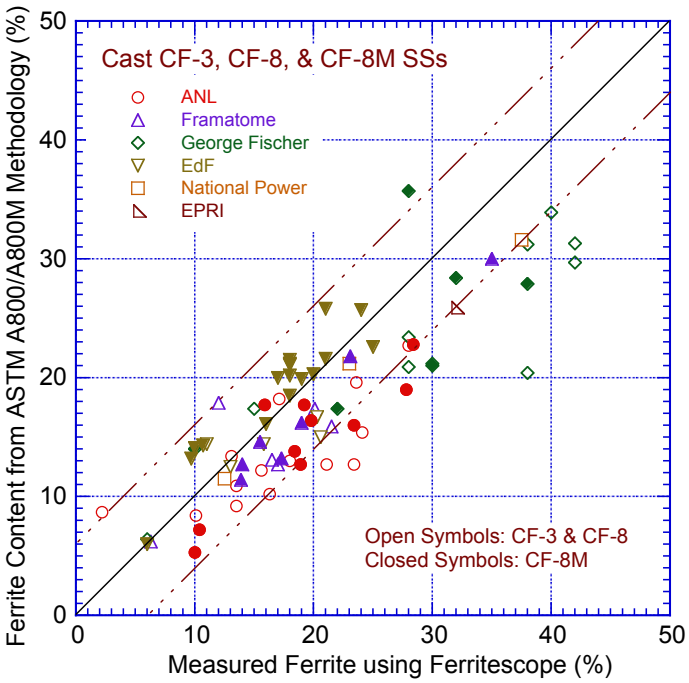

Figure 6.
Plots of measured ferrite content and values calculated from ASTM A800/A800M methodology for various CASS materials.

The values of the composition ratio (CR) for a given ferrite content (F), or vice versa, is then determined mathematically from the equation of the central line:

$$CR = 0.9 + 3.38883 \times 10^{-2}F - 5.58175 \times 10^{-4}F^2 + 4.22861 \times 10^{-6}F^3 \quad (7)$$

The measured ferrite content and values calculated from ASTM A800/A800M methodology for the same heats of CASS materials plotted in Fig. 5 are shown in Fig. 6. The results indicate that for ferrite contents greater than 20%, the calculated ferrite content for several heats is lower than the measured values. Most of these heats with significantly lower calculated values

contained 22.0–23.0 wt.% Cr and about 8.0–8.5 wt.% Ni. Compared to the ferrite content calculated from Hull's equivalent factor, the ASTM A800/A800M methodology under predicts the ferrite content for CASS materials with greater than 15% ferrite. The difference between the two methods can be seen clearly in Fig. 7.

The measured ferrite content and values calculated from Hull's equivalent factor or the ASTM A800/A800M methodology for several austenitic SS welds used in studies at Argonne and by Slama et al., Mills, and Lucas et al., are plotted in Figs. 8a and 8b, respectively. The results indicate that the measured ferrite contents in the welds are significantly higher than the calculated values. They are about 50% higher than the values calculated from Hull's equivalent factor, and are 80% higher than those determined from the ASTM A800 methodology. Furthermore, as seen before for CASS materials, the ferrite content calculated from the ASTM A800 methodology are about 20% lower than those calculated from the Hull's method.

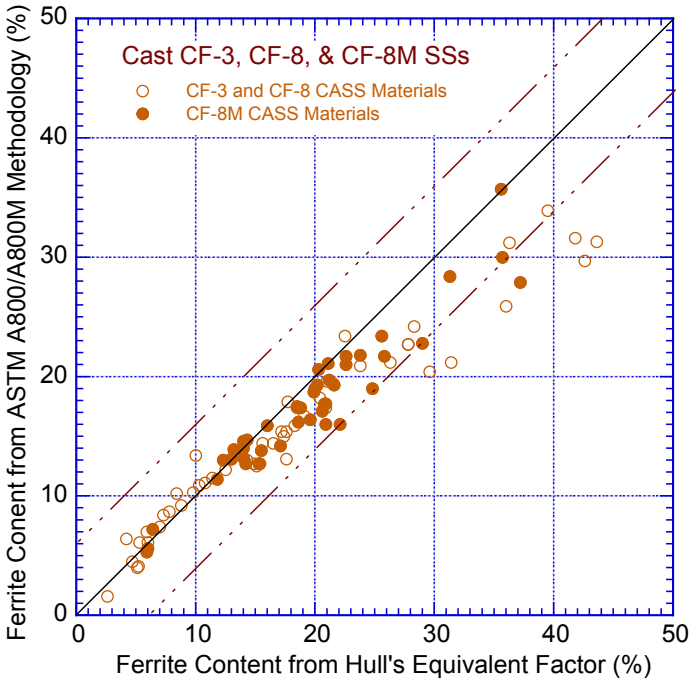

Figure 7.
Plots of ferrite content calculated from Hull's equivalent factor and those estimated from the ASTM A800/A800M methodology for various CASS materials.

2.3 Kinetics of Thermal Embrittlement

The degree of embrittlement has generally been characterized in terms of Charpy-impact energy of notched toughness specimens. The current "best estimates" of the degree of embrittlement at reactor operating temperatures are obtained from Arrhenius extrapolations of laboratory data obtained at higher temperatures.[30] The aging time to reach a given degree of embrittlement at different temperatures is determined from the equation:

$$t = 10^{P} \exp\left[\frac{Q}{R}\left\{\frac{1}{T} - \frac{1}{673}\right\}\right] \qquad (8)$$

where Q is the activation energy, R the gas constant, T the absolute temperature, and P an aging parameter that describes the combined effect of time and temperature on aging represents the degree of aging reached after 10^{P} h at 400°C (752°F). Thus, P = 1 for aging

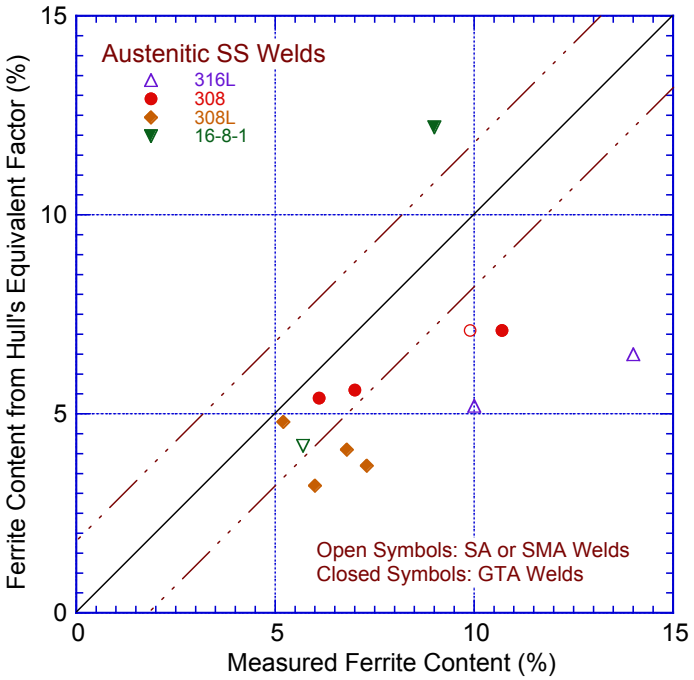

Figure 8a.
Plots of measured ferrite content and values calculated from Hull's equivalent factor for various austenitic SS welds.

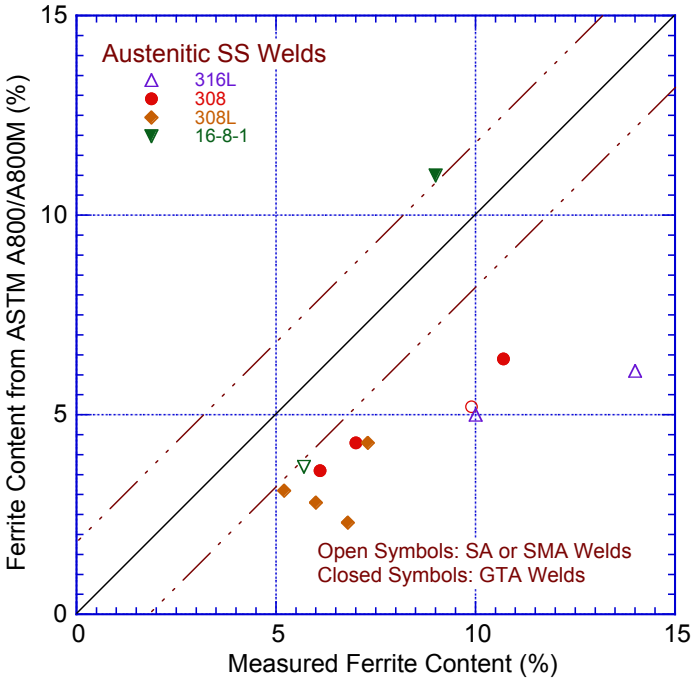

Figure 8b.
Plots of measured ferrite content and values calculated from ASTM A800/A800M methodology for various austenitic SS welds.

10 h at 400°C. The aging parameter for any given aging condition is obtained by rewriting Eq. 8 such that,

$$P = \log_{10}(t) - \frac{1000Q}{19.143}\left(\frac{1}{T_s + 273} - \frac{1}{673}\right). \quad (9)$$

The activation energy for the process of embrittlement has been described as a function of the chemical composition of the cast material.[34] Thus,

$$Q(\text{kJ/mole}) = -182.6 + 19.9(\%\ \text{Si}) + 11.08(\%\ \text{Cr}) + 14.4(\%\ \text{Mo}),$$

or

$$Q(\text{kcal/mole}) = -43.64 + 4.76(\%\ \text{Si}) + 2.65(\%\ \text{Cr}) + 3.44(\%\ \text{Mo}). \quad (10)$$

The activation energy calculated from Eq. 10 for the process of embrittlement, ranges between 65 and 105 kJ/mole (15 and 25 kcal/mole) for CF-3, CF-8, and CF-8M cast SSs. These values are significantly lower than the activation energy of spinodal decomposition in CASS materials. The spinodal decomposition and G-phase precipitation in low-temperature-aged cast duplex SS have been investigated by transmission electron microscopy (TEM), atom probe field ion microscopy (APFIM), small-angle neutron scattering (SANS), and extraction replica techniques.[58–66] The activation energy of the spinodal reaction in CF-3 SS was 250 ± 30 kJ/mole (~60 ± 7 kcal/mole).[63] This value is comparable to that for Cr diffusion in Fe-Cr alloys. The lower values of the activation energy of thermal embrittlement of CASS materials are most likely due to other factors, such as the effect of the formation of carbides and nitrides at the phase boundaries, or G-phase and/or γ_2 precipitation in ferrite, all of which may change the fracture mechanism of the aged material.

For example, precipitation of large carbides or nitrides at phase boundaries can initiate phase boundary separation by particle cracking. Consequently, a lower degree of spinodal decomposition (i.e., smaller amplitude of Cr fluctuation) is needed for a given change in mechanical properties. The material would show a faster reduction in impact strength relative to a material without phase boundary carbides. However, precipitation of carbides or nitrides occurs primarily at 400 or 450°C and is extremely slow at lower temperatures. Thus, the influence of phase boundary carbides would tend to increase the apparent activation energy of embrittlement measured from mechanical-property data.

The other factor that can influence the overall activation energy for embrittlement is the precipitation of other second-phase particles in ferrite, in particular the G phase, a multicomponent phase consisting of Ni, Si, Mo, Cr, Fe, and some Mn, and C.[61,65] The kinetics of G-phase precipitation depend on the chemical composition of the cast material.[42,58] For some heats, G phase is observed after times as short as 10,000 h at 400°C, while other heats require up to 70,000 h of aging at 400°C for G-phase formation. In general, precipitation of G phase is faster in the molybdenum-containing CF-8M steels.[42,58,59,61] The aging conditions for which G phase has been detected by TEM or SANS techniques in various cast SSs, are shown in Fig. 9. The kinetics for the decrease in the Charpy-impact energy of the aged CASS material are also plotted in the figure. The actual aging times for a given decrease in impact energy varied significantly for the various heats (shown by the horizontal scatter bars in Fig. 9). Generally, the aging times for the CF-8M steels were lower from those for the CF-3 or CF-8 steels.

At 400°C, the reduction in impact energy appears to be essentially complete before G phase is detected in any of the heats. For example, G phase was not detected in any of the heats aged for 3,000 h, whereas an 80% reduction in impact energy occurred by 4,600 h in all heats. However, at temperatures <350°C, G-phase precipitation and the decrease in impact energy occurred simultaneously. At 320°C, only a 50% reduction in strength occurred in most heats by 30,000 h, and G phase was observed in the specimens. These results indicate that the influence of G-phase

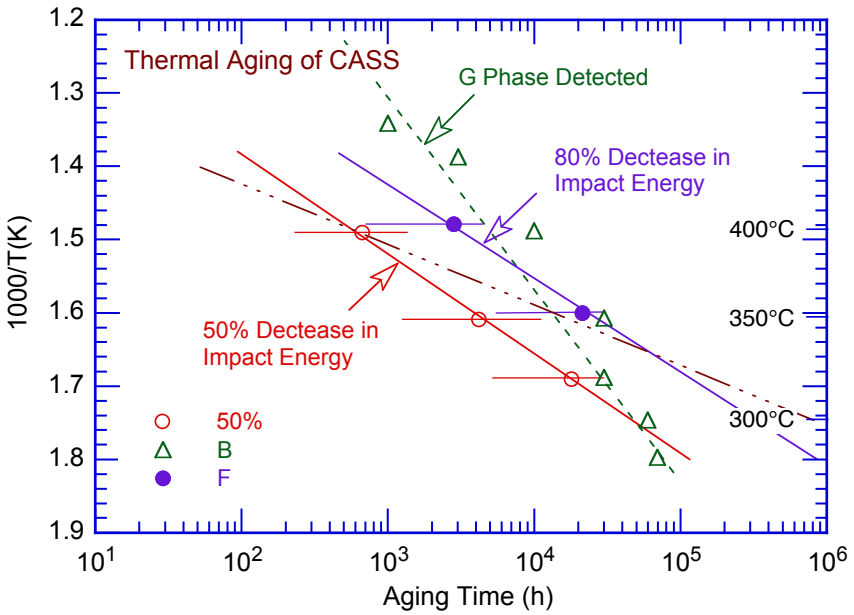

Figure 9. Arrhenius plots for the formation of G phase and reduction in impact energy.

precipitation on embrittlement would be greater at low temperatures, since at 400°C the kinetics of spinodal decomposition are much faster than G-phase precipitation, which follows nucleation and growth.

The mechanism by which the G phase influences thermal embrittlement of CASS materials is not well understood. The precipitation of G phase can influence the kinetics of embrittlement by either directly altering the kinetics of spinodal decomposition or changing the deformation and fracture behavior of the ferrite matrix and thereby influencing the effectiveness of spinodal decomposition. The only experimental data on the kinetics of spinodal decomposition in cast duplex SS were obtained by modeling the amplitude of Cr fluctuations, measured by APFIM, in thermally aged CF-3 steel.[63] The results yield an activation-energy of 250 kJ/mole. No G phase was observed in the steel after 5,000 h at 400 or 350°C. As shown in Fig. 9, most heats require ≥10,000 h at 400°C and ≥30,000 h at 350°C before G-phase precipitates are detected.

The low values of activation energy obtained from mechanical property data most likely are due to the effect of G-phase precipitation on the deformation behavior of the ferrite matrix. The concomitant precipitation of G phase may alter the frequency (spacing) of Cr fluctuations produced by spinodal decomposition, which would be more effective in strain hardening. Thus, a lower degree of spinodal decomposition (i.e., lower amplitude of the Cr fluctuations) would be needed for a given change in mechanical properties; embrittlement would be faster.

For a specific composition of the CASS material, Eqs. 9 and 10 can be used to determine the aging conditions that are representative of end-of-life reactor service. For a material with an activation energy of 100 kJ/mole (24 kcal/mole), the end-of-life condition for cold-leg piping (40 yr at 290°C [555°F]), is equivalent to 10,000 h at 400°C. The end-of-life condition for hot-leg piping (40 y at 320°C [610°F]), is equivalent to 30,000 h at 400°C. Consequently, the laboratory data obtained for materials aged at 400°C are currently used to predict the end-of-life impact strength at reactor temperatures.

The above methodology, however, assumes a unique aging behavior at 400°C (752°F), which is not observed for CASS materials produced at different foundries using different manufacturing processes. The decrease in room-temperature (RT) Charpy-impact energy during thermal aging at 400°C (752°F) of various heats of cast stainless steel[30,34,35,48,77,78] is shown in Fig. 10. The results indicate that all materials reach "saturation" RT impact energy (i.e., a minimum value that would be achieved by the material after long-term aging). The actual saturation value of RT impact energy for a specific CASS material is independent of aging temperature but depends strongly on the chemical composition of the steel. It is lower for the Mo-bearing CF-8M steels than for the Mo-free CF-3 or CF-8 steels, and decreases with an increase in ferrite content and the concentration of C or N in the steel.

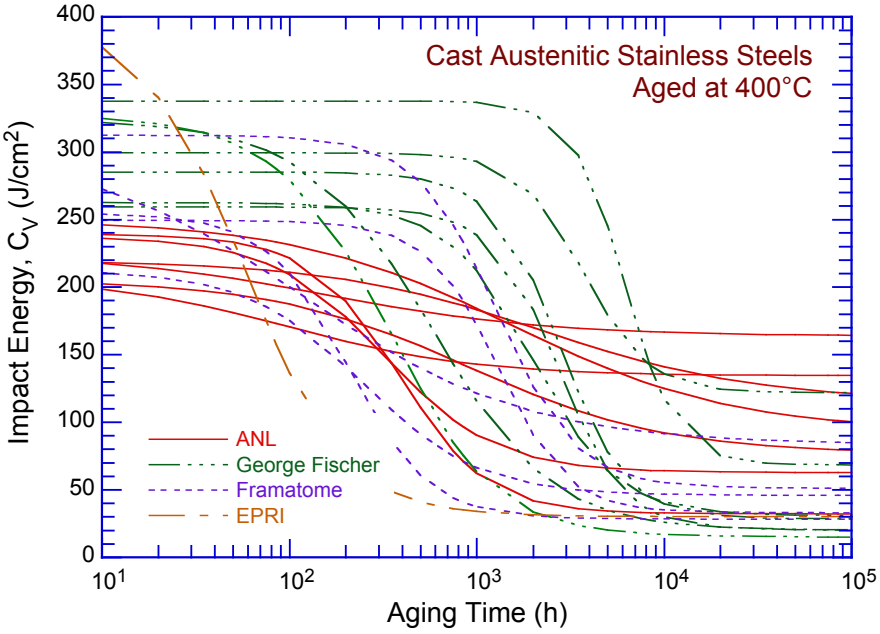

Figure 10. Decrease in Charpy-impact energy for various heats of cast austenitic SSs aged at 400°C.

However, Fig. 10 indicates that for a given decrease in the RT Charpy-impact energy, the time for aging at 400°C varies by more than two orders of magnitude for the various heats. For example, the time required for the impact energy to start decreasing varies from less than 100 h (e.g., the EPRI heat) to more than 1,000 h (GF heats). The time for the start of thermal aging effects varies from 50 to 500 h for the Argonne and FRA heats. Furthermore, for some materials, the decrease in impact energy is very fast (i.e., low activation energy) and for others it is slow (i.e., high activation energy). Typically, CASS materials that take longer for thermal embrittlement to start have low activation energy and materials that take short times for embrittlement to start have high activation energy. The results indicate that for most CASS materials, the time to reach saturation impact energy is the same for all grades and heats of CASS materials; the aging time for saturation is independent of material composition or manufacturing process. The logarithm of the aging time at 400°C (parameter θ) for a 50% reduction in RT Charpy-impact energy (parameter β) has been shown to be an important parameter for characterizing the kinetics of thermal embrittlement.[50] Table 1 lists the values of parameters β and θ for the various heats of CASS materials shown in Fig. 10; parameter α is a shape factor.

The activation energies of thermal aging embrittlement vary from 65 to 230 kJ/mole (15 to 55 kcal/mole).[30,34,43,48,50,58,59,77–79] Small changes in the composition of the material seem to cause the kinetics of thermal embrittlement to vary significantly. Microstructural examination of aged CASS materials suggests that steels that take longer for embrittlement to start at 400°C and have low activation energy are associated with clusters of Ni-Si, Mo-Si, and Ni-Si-Mo in the ferrite matrix.[42,58,59] These clusters are considered precursors of G-phase nucleation and precipitation. CASS materials with low activation energy (i.e., fast embrittlement) show G-phase precipitation after aging but embrittlement at 400°C takes longer to start. CASS materials with high activation energy (i.e., slow embrittlement) do not contain a G phase but embrittlement at 400°C takes relatively short time to start.[42,58–61] The presence of Ni-Si-Mo clusters in the ferrite matrix of an unaged material may be considered a signature of steels that are potentially sensitive to thermal embrittlement; steels with Ni-Si-Mo clusters in the ferrite matrix show low activation energy for thermal embrittlement but take longer to embrittle at 400°C.

Microstructural characterization and annealing studies on thermally aged cast stainless steel show that strengthening of ferrite is caused primarily by spinodal decomposition of ferrite to form Cr-rich α' phase.[42,48,49] Consequently, the kinetics of thermal embrittlement should be controlled by the amplitude and frequency of Cr fluctuations produced by spinodal decomposition (i.e., by the size and spacing of the α' phase). The low activation energies of thermal embrittlement are most likely caused by variations in the spacing of Cr fluctuations; atom probe field-ion microscopy studies indicate that the spacing between Cr fluctuations decreases with decreasing temperature.[60,64] During thermal aging, production heat treatment and possibly the casting process, both of which affect ferrite composition and microstructure of unaged material, can influence microstructural evolution and, therefore, the kinetics of embrittlement.

2.4 Extent of Thermal Embrittlement of CASS Materials

As discussed in the previous section, all CASS materials reach “saturation” RT impact energy (i.e., a minimum value that would be achieved by the material) after long-term aging. The actual value of saturation RT impact energy for a specific cast SS is independent of aging temperature but depends strongly on the chemical composition of the steel. It is lower for the Mo-bearing CF-8M steels than for the Mo-free CF-3 or CF-8 steels, and decreases with an increase in ferrite content or the concentration of C or N in the steel.[50] Typically, the extent of thermal embrittlement has been characterized by the RT “normalized” Charpy-impact energy (Charpy-impact energy per unit fracture area).

In the Argonne studies,[48–51] correlations were developed for the extent of thermal embrittlement at “saturation” (i.e., the minimum Charpy-impact energy that would be achieved for the material after long-term aging) in terms of the chemical composition of the material. The extent of thermal embrittlement as a function of time and temperature of reactor service was estimated from the extent of embrittlement at saturation and the correlations describing the kinetics of embrittlement, which are also given in terms of chemical composition. The fracture toughness J-R curve for the material was then obtained from the correlation between fracture toughness parameters and RT Charpy-impact energy used to characterize the extent of thermal embrittlement. A common lower-bound J-R curve for various grades of CASS materials of unknown chemical composition was defined for a given material specification, ferrite content, and temperature.

Table 1. Chemical composition, ferrite content, and kinetics of thermal embrittlement for various heats of CASS materials.

	Chemical Composition (wt.%)							Ferrite (%)		C_{Vsat}	Constants			Q
Heat	Cr	Mo	Si	Ni	Mn	C	N	Calc.	Mea	(J/cm^2)	β	θ	α	(kJ/mole)
Argonne National Laboratory														
52	19.49	0.35	0.92	9.40	0.57	0.009	0.052	10.3	13.5	161.8	–	–	–	–
51	20.13	0.32	0.86	9.06	0.63	0.010	0.058	14.3	18.0	115.9	0.139	3.53	1.15	204.7
47	19.81	0.59	1.06	10.63	0.60	0.018	0.028	8.4	16.3	163.7	0.069	2.29	1.20	195.7
P2	20.20	0.16	0.94	9.38	0.74	0.019	0.040	12.5	15.6	141.3	0.258	2.83	1.09	218.6
I	20.20	0.45	0.83	8.70	0.47	0.019	0.032	20.4	17.1	134.3	0.094	2.10	1.00	250.0
69	20.18	0.34	1.13	8.59	0.63	0.023	0.028	21.0	23.6	76.7	0.214	3.21	1.07	175.9
P1	20.49	0.04	1.12	8.10	0.59	0.036	0.057	17.6	24.1	53.7	0.305	2.57	0.75	252.7
61	20.65	0.32	1.01	8.86	0.65	0.054	0.080	10.0	13.1	93.3	0.214	3.48	1.20	197.8
59	20.33	0.32	1.08	9.34	0.60	0.062	0.045	8.8	13.5	89.1	0.197	3.14	1.20	249.4
68	20.64	0.31	1.07	8.08	0.64	0.063	0.062	14.9	23.4	47.1	0.301	2.88	0.68	161.1
60	21.05	0.31	0.95	8.34	0.67	0.064	0.058	15.4	21.1	44.8	0.291	2.89	0.88	210.9
56	19.65	0.34	1.05	9.28	0.57	0.066	0.030	7.3	10.1	117.6	–	–	–	–
74	19.11	2.51	0.73	9.03	0.54	0.064	0.048	15.5	18.4	63.1	0.269	3.44	0.70	95.0
75	20.86	2.58	0.67	9.12	0.53	0.065	0.052	24.8	27.8	32.1	0.436	2.82	0.51	139.0
66	19.45	2.39	0.49	9.28	0.60	0.047	0.029	19.6	19.8	87.9	0.208	3.16	1.57	163.9
64	20.76	2.46	0.63	9.40	0.60	0.038	0.038	29.0	28.4	41.1	0.338	2.81	0.60	147.3
65	20.78	2.57	0.48	9.63	0.50	0.049	0.064	20.9	23.4	59.7	0.260	2.99	0.59	153.8
P4	19.64	2.05	1.02	10.00	1.07	0.040	0.151	5.9	10.0	62.7	0.289	2.70	0.62	158.7
63	19.37	2.57	0.58	11.85	0.61	0.055	0.031	6.4	10.4	126.5	0.119	2.83	1.11	155.5
Georg Fischer Co.														
284	23.00	0.17	0.52	8.23	0.28	0.025	0.037	43.6	42.0	20.5	0.551	3.66	0.39	85.9
280	21.60	0.25	1.37	8.00	0.50	0.028	0.038	36.3	38.0	19.6	0.609	3.20	0.73	88.9
282	22.50	0.15	0.35	8.53	0.43	0.035	0.040	29.7	38.0	28.5	0.500	3.65	0.39	91.6
281	23.10	0.17	0.45	8.60	0.41	0.036	0.053	31.4	30.0	17.2	0.618	3.76	0.47	89.8
283	22.60	0.23	0.53	7.88	0.48	0.036	0.032	42.6	42.0	18.6	0.599	3.60	0.44	83.7
278	20.20	0.13	1.00	8.27	0.28	0.038	0.030	18.5	15.0	68.3	0.347	3.90	0.29	63.1
279	22.00	0.22	1.36	7.85	0.37	0.040	0.032	39.5	40.0	23.8	0.546	3.06	0.58	93.5
277	20.50	0.06	1.81	8.13	0.54	0.052	0.019	22.5	28.0	30.7	0.466	3.54	0.49	87.7
291	19.60	0.66	1.59	10.60	0.28	0.065	0.054	4.2	6.0	121.9	0.195	3.65	0.35	71.2
292	21.60	0.13	1.57	7.52	0.34	0.090	0.039	23.9	28.0	17.2	0.373	3.07	0.44	98.8
290	20.00	2.40	1.51	8.30	0.41	0.054	0.050	31.3	32.0	15.8	0.624	3.48	0.12	81.0
288	19.60	2.53	1.70	8.40	0.47	0.052	0.022	35.6	28.0	14.9	0.671	2.96	0.66	105.3
287	20.50	2.58	0.51	8.46	0.50	0.047	0.033	37.2	38.0	20.5	0.555	3.46	0.36	90.3
286	20.20	2.44	1.33	9.13	0.40	0.072	0.062	18.9	22.0	15.5	0.594	3.03	0.72	106.4
289	19.70	2.30	1.44	8.25	0.48	0.091	0.032	22.6	30.0	16.2	0.580	3.29	0.41	90.1
285	18.80	2.35	0.86	9.49	0.48	0.047	0.039	14.0	10.0	61.1	0.313	3.60	0.20	89.3
Framatome														
A	18.90	0.10	0.99	8.90	1.14	0.021	0.074	6.0	6.3	166.0	0.090	3.44	0.20	111.7
E	21.04	0.08	0.54	8.47	0.80	0.035	0.051	17.6	16.5	45.7	0.334	2.63	0.65	132.9
F	19.72	0.34	1.16	8.33	0.26	0.038	0.026	17.7	12.0	83.2	0.282	2.45	1.23	176.2
C	20.73	0.13	1.09	8.19	0.91	0.042	0.035	20.9	20.1	51.1	0.393	3.30	0.45	83.1
G	20.65	0.02	1.03	8.08	0.74	0.040	0.073	15.3	17.0	62.5	–	–	–	–
H	20.70	0.05	1.18	8.07	0.71	0.050	0.045	18.3	21.5	50.6	–	–	–	–
D	19.15	2.50	0.94	10.32	1.12	0.026	0.063	12.2	13.9	33.0	0.439	3.30	0.40	89.7
I	19.36	2.40	0.98	10.69	0.70	0.020	0.039	14.1	15.5	150.7	–	–	–	–
K	20.80	2.62	0.75	10.45	1.09	0.060	0.056	15.4	14.0	48.5	–	–	–	–
L	20.76	2.48	0.81	10.56	0.79	0.040	0.042	18.6	19.0	30.4	–	3.00	–	–
B	20.12	2.52	0.93	10.56	0.83	0.053	0.042	14.0	17.3	28.2	0.478	2.55	0.47	128.6
Westinghouse														
C148	20.95	2.63	0.53	9.48	1.02	0.061	0.056	22.1	14.0	53.1	–	2.80	–	–
Electric Power Research Institute														
EPRI	22.04	0.23	0.84	7.93	0.74	0.030	0.045	36.0	32.0	30.0	0.564	2.10	0.60	225.0

Correlations were also developed for estimating changes in tensile stress and Ramberg/Osgood parameters for tensile strain hardening.[52] However, only fracture toughness J-R curve data have been reevaluated and updated in this report.

2.4.1 Charpy-Impact Energy

In the Argonne studies,[48] different correlations were developed to estimate the saturation RT impact energy of the various grades of cast SS. To ensure that the estimates are either accurate or conservative for all heats, the saturation RT impact energy for a specific cast SS was determined by two different expressions between RT Charpy-impact energy and a material parameter that depends on material ferrite content and chemical composition. The lower value was used for estimating mechanical properties of thermally aged CASS materials. For CF-3 and CF-8 steels, the saturation value of RT impact energy, C_{Vsat}, is the lower value determined from

$$\log_{10}C_{Vsat} = 1.15 + 1.36\exp(-0.035\Phi), \tag{11}$$

where the material parameter Φ is expressed as

$$\Phi = \delta_c(Cr + Si)(C + 0.4N), \tag{12}$$

and from

$$\log_{10}C_{Vsat} = 5.64 - 0.006\delta_c - 0.185Cr + 0.273Mo - 0.204Si + 0.044Ni - 2.12(C + 0.4N). \tag{13}$$

For CF-8M steel with <10% Ni, the saturation value of RT impact energy C_{Vsat} is the lower value determined from

$$\log_{10}C_{Vsat} = 1.10 + 2.12\exp(-0.041\Phi), \tag{14}$$

where the material parameter Φ is expressed as

$$\Phi = \delta_c(Ni + Si + Mn)^2(C + 0.4N)/5; \tag{15}$$

and from

$$\log_{10}C_{Vsat} = 7.28 - 0.011\,\delta_c - 0.185Cr - 0.369Mo - 0.451Si - 0.007Ni - 4.71(C + 0.4N). \tag{16}$$

For CF-8M steel with ≥10% Ni, the saturation value of RT impact energy C_{Vsat} is the lower value determined from

$$\log_{10}C_{Vsat} = 1.10 + 2.64\exp(-0.064\Phi), \tag{17}$$

where the material parameter Φ is expressed as

$$\Phi = \delta_c(Ni + Si + Mn)^2(C + 0.4N)/5; \tag{18}$$

and from

$$\log_{10}C_{Vsat} = 7.28 - 0.011\,\delta_c - 0.185Cr - 0.369Mo - 0.451Si - 0.007Ni - 4.71(C + 0.4N). \quad (19)$$

If not known, the N content was assumed to be 0.04 wt.%. The correlations were optimized by using a larger database (≈80 compositions of CASS materials) and mechanical property results on materials that were aged up to ≈58,000 h at 290–350°C (554–662°F). The saturation values of RT impact energy for CF-3, CF-8, and CF-8M steels observed experimentally at Argonne,[48,77,78] GF,[30] Westinghouse (WH),[31] EdF,[43] NP,[44] FRA,[34] and EPRI[35] are plotted as a function of the material parameter ϕ in Fig. 11. The solid lines represent best-fit curves for the data (i.e., Eq. 11 for CF-3 or CF-8 steels and Eqs. 14 and 17 for CF-8M steel). The chemical composition, ferrite content, and saturation RT Charpy-impact energy of most of the materials are given in Table 1. The measured values of C_{Vsat} and those estimated from Eqs. 11–19 are plotted in Fig. 12. The difference between the predicted and observed values is less than ±15% for most of the CF-3 and CF-8 steels and less than ±25% for the CF-8M steels.

The expressions given in Eqs. 11–19 for estimating the saturation RT Charpy-impact energy for a specific CASS material, were correlated to the material ferrite and the chemical composition because a review of the thermal embrittlement data for aged CASS materials indicated that a correlation between Charpy-impact energy and ferrite content alone did not yield good results. The saturation RT impact energies for CF-3, CF-8, and CF-8M steels shown in Fig. 11 are plotted as a function of the material ferrite content in Fig. 13; the results show poor correlation.

2.4.2 Fracture Toughness J-R Curve

The saturation fracture toughness J-R curve for a specific CASS material can be estimated from its RT Charpy-impact energy at saturation. The J-R curve is expressed by the power-law relation $J_d = C\Delta a^n$, where J_d is deformation J per ASTM Specifications E 813-85 and E 1152-87, Δa is crack extension, and C and n are constants. The coefficient C at room temperature or are plotted in Fig. 14 using an updated fracture toughness database. Fracture toughness data from studies at Argonne,[48,77–79] FRA,[34,36] EdF,[38] EPRI,[35] The Welding Institute (TWI),[80] and Materials Engineering Associates, Inc. (MEA),[81] are included in the figure.

At both RT and reactor temperatures, the coefficient C decreases with a decrease in the RT Charpy-impact energy. Separate correlations are obtained for CF-3 and CF-8 steels and for CF-8M steels; the latter show larger decrease in fracture toughness for a given impact energy. Furthermore, for CF-8M steels, the decrease in the values of coefficient C is much greater for RT Charpy-impact energy values less than about 40 J/cm^2. As discussed later in this section, data on chemical compositions of CASS piping materials from a select sample of nuclear power plants indicate that at least 9% of the CF-8M materials that are currently in use in the U.S. nuclear power plants contain more than 25% ferrite. However, the methodology developed earlier in NUREG/CR-4513, Rev. 1 was not applicable for CASS materials with greater than 25% ferrite. The methodology for estimating thermal embrittlement has been extended to cover CASS materials containing greater than 25% ferrite. For CF-8M materials, a bilinear expression is developed between RT Charpy-impact energy and coefficient C of the power-law J-R curve.

To help ensure that the estimated J-R curve was conservative for all material and aging conditions, the correlations for estimating the J-R curves for static-cast materials are obtained by subtracting the value of standard deviation for the fit to the data from the best-fit curve in Fig. 14; these curves are shown as chain dot curves. For centrifugally-cast materials, the best-fit correlations are used. For CF-8M materials, the value of the RT Charpy-impact energy for

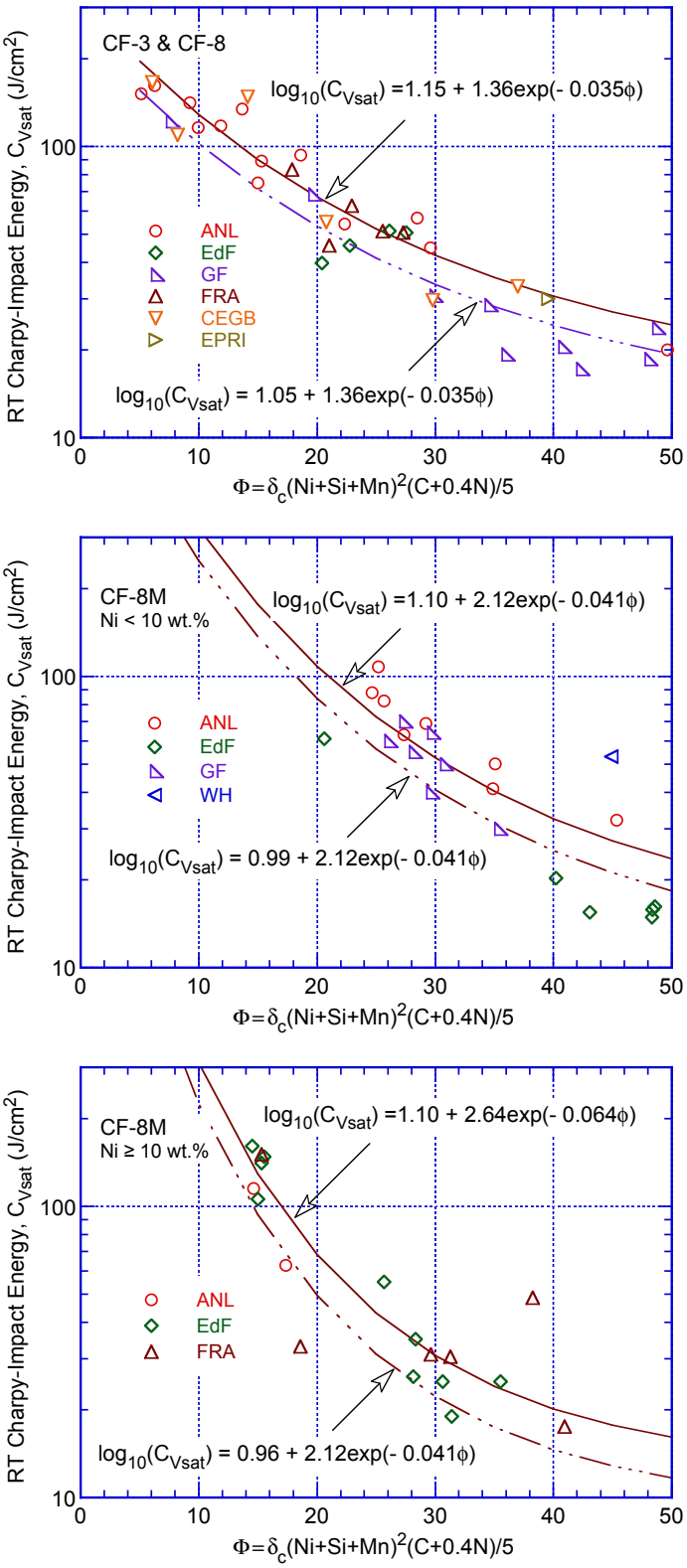

Figure 11. Correlation between RT Charpy-impact energy at saturation and the material parameter ϕ for CF-3, CF-8, and CF-8M steels.

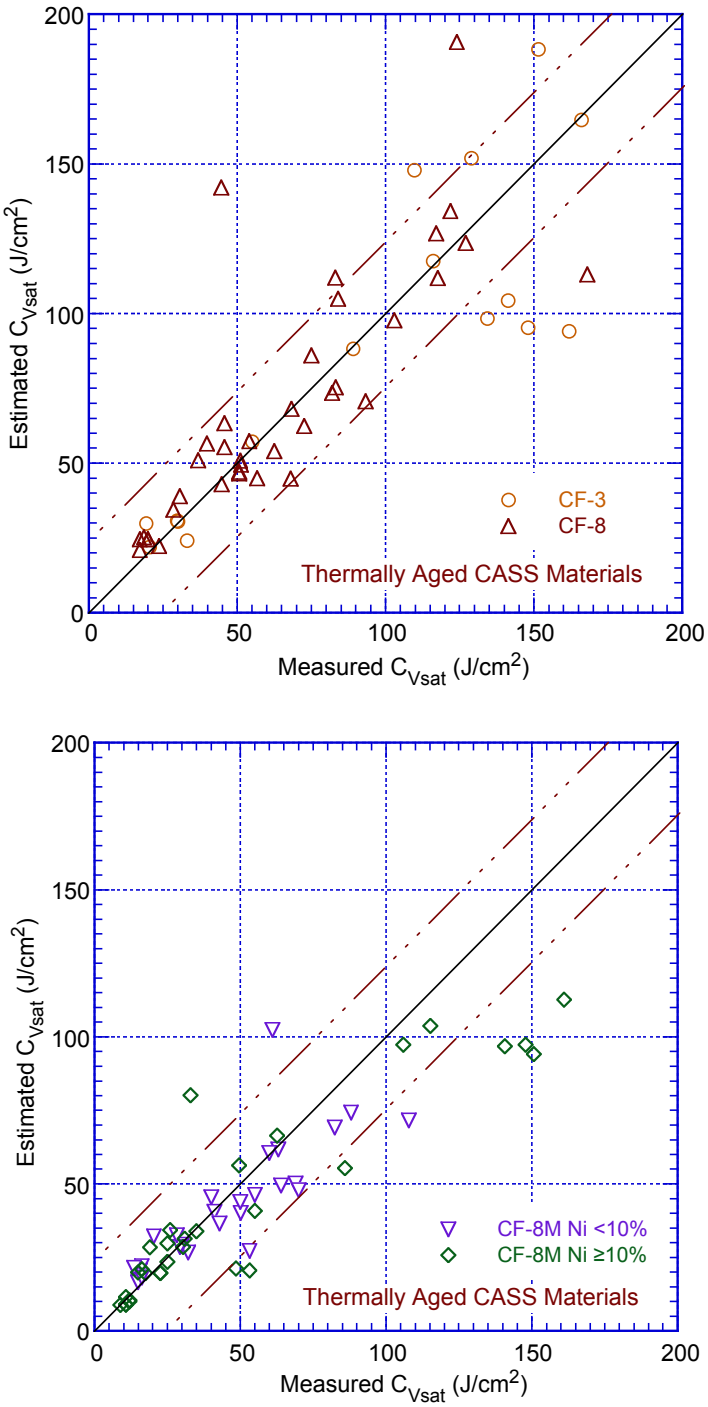

Figure 12. Measured and estimated values of saturation RT Charpy-impact energy for CF-3, CF-8, and CF-8M CASS materials.

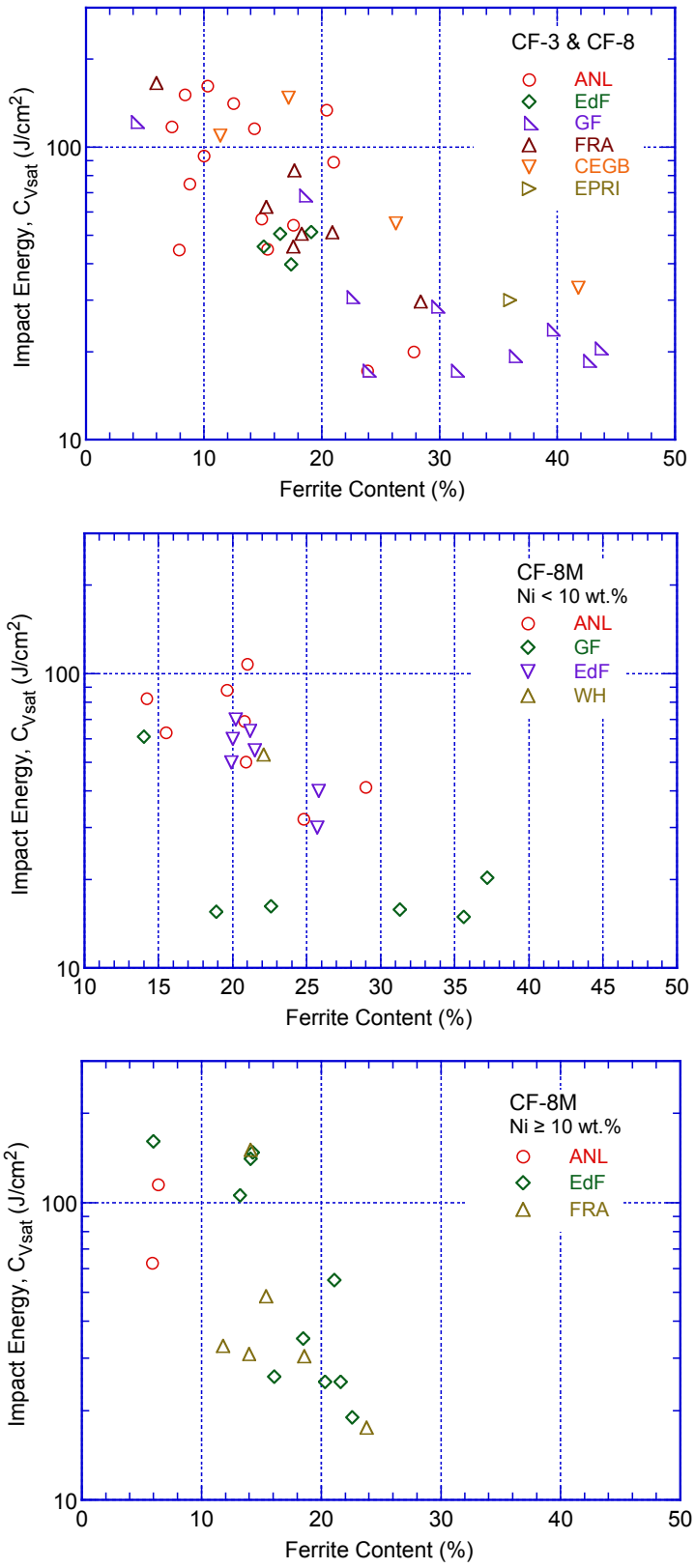

Figure 13. Correlation between RT Charpy-impact energy at saturation and the ferrite content for CF-3, CF-8, and CF-8M steels.

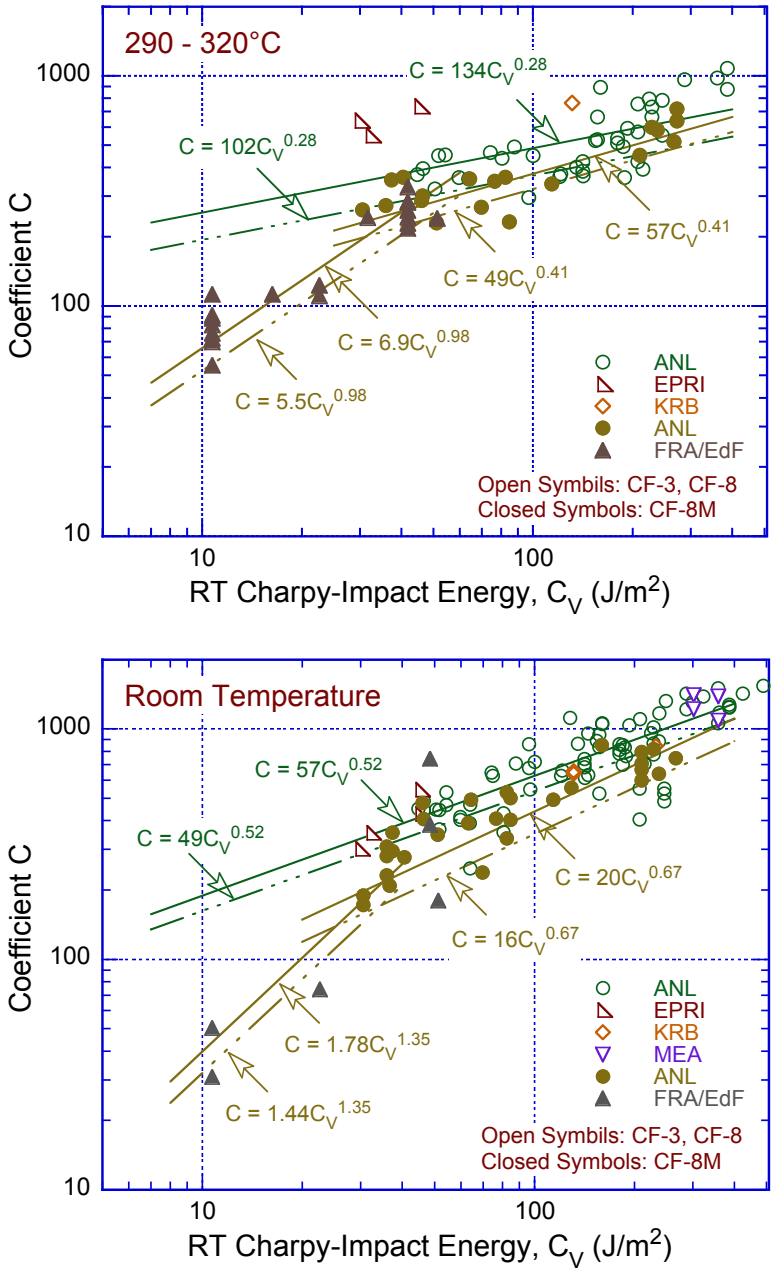

Figure 14. Correlation between RT Charpy-impact energy and coefficient C at 290–320°C and RT for CF-3, CF-8, and CF-8M CASS materials.

the transition from one expression to the other varies between 35 and 45 J/cm^2 because of the differences in the standard deviation for the fit to the individual set of data. For static-cast CASS materials, the coefficient C of the J-R curve at RT for CF-3 or CF-8 steels is expressed as

$$C = 49[C_V]^{0.52}, \tag{20}$$

and for CF-8M steels, for RT Charpy-impact energy values greater than 35 J/cm^2 as

$$C = 16[C_V]^{0.67}, \tag{21}$$

and for RT Charpy-impact energy values equal to or less than 35 J/cm^2 as

$$C = 1.44[C_V]^{1.35}. \quad (22)$$

For static-cast CASS materials, the coefficient C of the J-R curve at 290–320°C for CF-3 or CF-8 steels is expressed as

$$C = 102[C_V]^{0.28}, \quad (23)$$

and for CF-8M steels, for RT Charpy-impact energy values greater than 45 J/cm^2 as

$$C = 49[C_V]^{0.41}, \quad (24)$$

and for RT Charpy-impact energy values equal to or less than 45 J/cm^2 as

$$C = 5.5[C_V]^{0.98}. \quad (25)$$

For centrifugally-cast CASS materials, the coefficient C of the J-R curve at RT for CF-3 or CF-8 steels is expressed as

$$C = 57[C_V]^{0.52}, \quad (26)$$

and for CF-8M steels, for RT Charpy-impact energy values greater than 35 J/cm^2 as

$$C = 20[C_V]^{0.67}, \quad (27)$$

and for RT Charpy-impact energy values equal to or less than 35 J/cm^2 as

$$C = 1.78[C_V]^{1.35}. \quad (28)$$

For centrifugally-cast CASS materials, the coefficient C of the J-R curve at 290–320°C for CF-3 or CF-8 steels is expressed as

$$C = 134[C_V]^{0.28}, \quad (29)$$

and for CF-8M steels, for RT Charpy-impact energy values greater than 40 J/cm^2 as

$$C = 57[C_V]^{0.41}, \quad (30)$$

and for RT Charpy-impact energy values equal to or less than 40 J/cm^2 as

$$C = 6.9[C_V]^{0.98}. \quad (31)$$

The exponent n of Δa has also been correlated with the RT Charpy-impact energy C_V. To ensure that the estimated J-R curves were conservative, the correlations represented the lower bound values of the exponent n versus Charpy-impact energy experimental data. A review of the updated fracture toughness data for thermally aged CF-3, CF-8, CF-8M steels indicated that the existing correlation between RT Charpy-impact energy and the exponent n in the power-law J-R curve[50] were adequate and did not need to be updated. For example, the existing

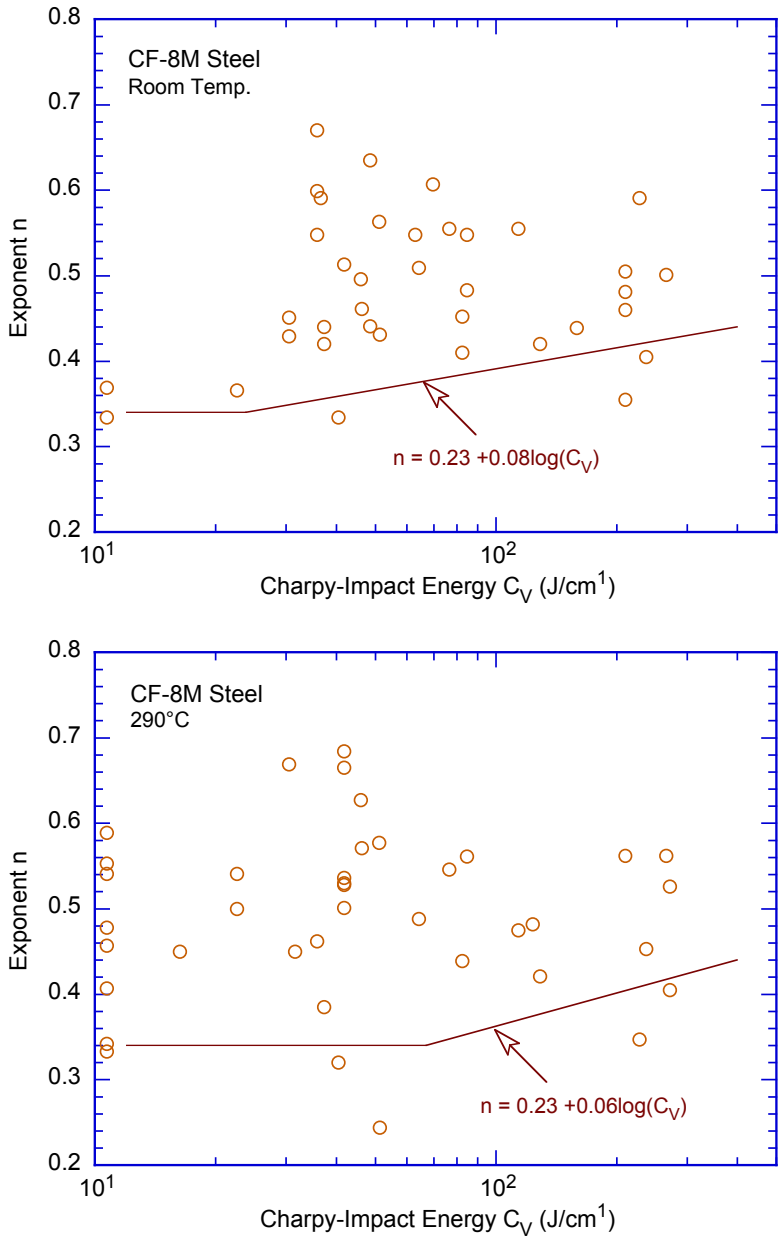

Figure 15. Correlation between RT Charpy-impact energy and exponent n of the power-law J-R curve at RT and 290°C for CF-8M materials. The solid line bounds the existing data for exponent n as a function of RT Charpy-impact energy.

correlation for CF-8M bound the updated data for RT Charpy-impact energy and exponent n shown in Fig. 15.

For static-cast or centrifugally-cast CASS materials, the exponent n at RT is given by the value larger of 0.34 and that determined for CF-3 steels from the expression

$$n = 0.15 + 0.16\log_{10}[C_V], \quad (32)$$

for CF-8 steels from

$$n = 0.20 + 0.12\log_{10}[C_V], \quad (33)$$

and for CF-8M steels from

$$n = 0.23 + 0.08\log_{10}[C_V]. \quad (34)$$

For static-cast or centrifugally-cast CASS materials, the exponent n at 290°C is given by the value larger of 0.34 and that determined for CF-3 steels from the expression

$$n = 0.17 + 0.12\log_{10}[C_V], \quad (35)$$

for CF-8 steels from

$$n = 0.21 + 0.09\log_{10}[C_V], \quad (36)$$

and for CF-8M steels from

$$n = 0.23 + 0.06\log_{10}[C_V]. \quad (37)$$

Equations 20–37 may be used to determine the fracture toughness J-R curve of static- or centrifugally-cast CF-3, CF-8, and CF-8M CASS materials from the RT Charpy-impact energy of the material. If the RT Charpy-impact energy is not known, then the saturation fracture toughness J-R curves for these CASS materials can be determined from their chemical composition available in the CMTRs using Eqs. 11–19 and Eqs. 20–37. In general, the following observations may be drawn from the study of thermal embrittlement of CASS materials:[82]

(a) Among the grades considered, CF-8M steels have the smallest J_d value for a given crack extension. The value of J_d at a given crack extension for CF-8M steels is generally about half of that of the other grades.
(b) CF-3, CF-3A, CF-8, and CF-8A steels show a similar extent of thermal aging. The value of J_d at a given crack extension for CF-8 and CF-8A steels is generally less than 10% lower than that for CF-3 and CF-3A steels.
(c) Static-cast CASS materials are more susceptible to thermal aging than the centrifugally-cast materials. The value of J_d at a given crack extension for static-cast SS is generally about 20% lower than that for the centrifugally-cast material with a similar ferrite content.
(d) Although CF-8M steels show a similar extent of thermal aging when the J-R curve is measured at both RT and at reactor operating temperature, the other grades considered show a decreased value of J_d at a given crack extension when the J-R curve is measured at reactor operating temperature. The value of J_d at a given crack extension for CF-3, CF-3A, CF-8, and CF-8A steels is generally about 20% lower when measured at reactor operating temperature than when measured at RT.

These correlations are valid for static- and centrifugally-cast CF-3, CF-3A, CF-8, CF-8A, and CF-8M steels defined by ASTM Specification A351. The criteria used in developing these correlations ensure that the estimated mechanical properties are adequately conservative for compositions of CASS materials within ASTM A351. The updated correlations are applicable to all compositions of CF-8M materials, including materials with ferrite contents above 25%. However, in the updated database, there were few or no fracture toughness J-R curve data for CF-3 and CF-8 materials with C_{Vsat} less than 30 J/cm^2 (17.7 ft·lb). Therefore, the correlations presented in this report may not be applicable for those compositions of CF-3 and CF-8

materials for which the estimated value of C_{Vsat} is less than 30 J/cm^2 (<17.7 ft·lb). Typically, such compositions would contain more than 30% ferrite. Furthermore, the correlations may not encompass all metallurgical factors that can arise from differences in production heat treatment or casting processes and may be overly conservative for some steels.

It should be noted that these correlations account for the degradation of mechanical properties of typical heats of CASS materials. They do not consider the initial fracture properties of the unaged material. Some CASS materials may have low initial fracture toughness and the estimated J-R curves may be higher than the initial value. Therefore, some knowledge regarding the initial fracture toughness of the material is needed to justify the use of the estimated fracture toughness. The initial fracture toughness J-R curves may be estimated from the RT Charpy-impact energy of the unaged material.

Flaw tolerance methods are often used to develop ASME Code Section XI flaw acceptance standards or to justify alternatives to the ASME Code Section XI in-service inspection (ISI) requirements. Recently, an EPRI Report 1019128 (December 2009),[83] presented a flaw tolerance approach based on elastic-plastic fracture mechanics considerations that could be used in combination with a demonstrated inspection method for managing the effects of aging of CASS piping, particularly with greater than 20% ferrite content. The report included a database of CASS CF-3, CF-8, CF-8A, and CF-8M piping materials. The sources of the CASS data included: (a) information obtained from a Westinghouse data search based on random sampling of heats of CASS material from 15 plants (see Table 2) and (b) data packages from the

Table 2. The primary circuit piping CASS material in Westinghouse designed plants.

Plant Name	Size (Mwe)	System Loops	Material Type
Beaver Valley 2	852	3	CF-8A
Callaway 1	1157	4	CF-8A
Catawba 1	1153	4	CF-8A
Catawba 2	1153	4	CF-8A
Comanche Peak 1	1150	4	CF-8A
Farley 1	829	3	CF-8A
Farley 2	829	3	CF-8A
McGuire 1	1180	4	CF-8A
McGuire 2	1180	4	CF-8A
Millstone 3	1150	4	CF-8A
North Anna 1	934	3	CF-8A
North Anna 2	788	3	CF-8A
South Texas 1	1250	4	CF-8A
South Texas 2	1250	4	CF-8A
Vogtle 1	1113	4	CF-8A
Vogtle 2	1113	4	CF-8A
Watts Bar 1	1177	4	CF-8A
Watts Bar 2	1177	4	CF-8A
Wolf Creek	1158	4	CF-8A
Beaver Valley 1	852	3	CF-8M
Cook 1	1090	4	CF-8M
Cook 2	1054	4	CF-8M
Kewaunee	560	2	CF-8M
Prairie Island 2	530	2	CF-8M
Sequoyah 1	1140	4	CF-8M
Sequoyah 2	1140	4	CF-8M

Sandusky Foundry and Machine Co., NUREG/CR-5024, and Structural Integrity Associates. The CASS data was used to estimate the ferrite contents of a representative sample of CASS CF-3, CF-8, CF-8A, and CF-8M materials, and perform statistical analyses to study the distribution of the ferrite contents of these materials. When information for the Mo and N contents was not available, values of 0.5 and 0.04 (wt.%), respectively, were assumed.

The results yielded mean ferrite content and standard deviation values of 15.9% and 4.9% for CF-8 material (total 333 data points), and 17.6% and 5.4% for CF-8M material (total 147 data points). The total data for CF-3 and CF-8 were too small (less than 15 data points) to provide meaningful estimates. The distribution of the ferrite content for CF-8M materials (Fig. 16) indicated that nearly 9% of the heats of CF-8M material contained greater than 25% ferrite. Therefore, the Argonne correlations presented earlier in NUREG/CR-4513, Rev. 1 would not be applicable to at least some of the heats of CF-8M material currently in use in the U.S. PWRs.

The updated expressions presented in Eqs. 20–31 should be used for these materials. However, since the updated database used in this report contained little or no fracture toughness J-R curve data for thermally aged CF-3 and CF-8 materials with more than 25% ferrite, the expressions presented in Eqs. 20–31 may not be applicable to such materials. The use of these expressions for CF-3 and CF-8 materials with more than 25% ferrite needs to be justified.

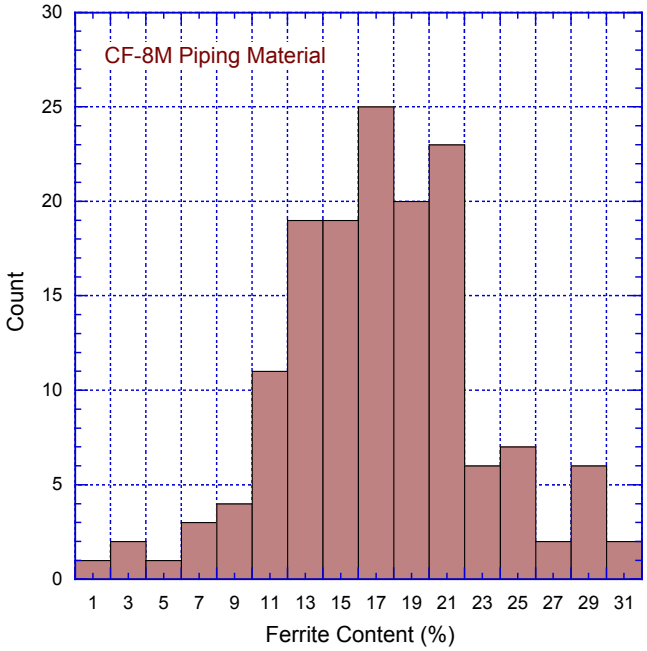

Figure 16.
Distribution of ferrite content in CASS CF-8M piping material in Westinghouse PWRs (Ref. EPRI 1019128).

2.5 Assessment of Thermal Embrittlement of CASS Materials

2.5.1 Estimation of Thermal Embrittlement of CASS Materials of Known Composition and Service Condition – Service Time Values

Room-temperature impact energy as a function of time and temperature of aging is estimated from the RT saturation impact energy C_{Vsat} and the kinetics of embrittlement. The decrease in RT Charpy-impact energy C_V with time is expressed as

$$\log_{10}C_V = \log_{10}C_{Vsat} + \beta\{1 - \tanh [(P - \theta)/\alpha]\}, \quad (38)$$

where the aging parameter P is determined from Eq. 9 The constants α and β can be determined from C_{Vint} and C_{Vsat} as follows:

$$\alpha = -0.585 + 0.795\log_{10}C_{Vsat} \quad (39)$$

and

$$\beta = (\log_{10} C_{Vint} - \log_{10}C_{Vsat})/2. \quad (40)$$

The CMTR for a specific CASS component provides information on chemical composition, tensile strength, and possibly Charpy-impact energy of the material. If C_{Vint} is not known, a typical value of 200 J/cm^2 [or 160 J (118 ft·lb) for a standard Charpy V-notch specimen] may be used. The value of θ is not available for CASS components in the field, and can only be obtained from aging archival material for 5,000–10,000 h at 400°C (752°F). However, parametric studies show that the aging response at reactor temperatures is relatively insensitive to the values of θ.[84] A value of 2.9 for θ (i.e., mean of the experimental data) is used to estimate thermal embrittlement at 280–330°C (536–626°F). A θ value of 3.3 is used for estimates at temperatures <280°C (<536°F) and 2.5 for estimates at 330–360°C (626–680°F). In the Argonne study, the activation energy for thermal embrittlement is expressed in terms of both chemical composition and the constant θ.[50] The activation energy Q in kJ/mole for CF-3 and CF-8 steels is given by

$$Q = 10 [74.52 - 7.20\ \theta - 3.46\ Si - 1.78\ Cr + 148\ N - 61\ C], \quad (41)$$

and for CF–8M steels by

$$Q = 10 [74.52 - 7.20\ \theta - 3.46\ Si - 1.78\ Cr - 4.35\ Mn + 23\ N]. \quad (42)$$

Equations 41 and 42 are slightly different from the expression proposed by Slama et al. 1983 (i.e. Eq. 10 presented earlier).[34] These equations are applicable to compositions within ASTM Specification A 351, with an upper limit of 1.2 wt.% for Mn content. Actual Mn content is used when CASS materials that contain up to 1.2 wt.% Mn; for steels containing greater than 1.2 wt.% Mn, 1.2 wt.% is assumed. Furthermore, the values of Q predicted from Eqs. 41 and 42 should be between 65 kJ/mole (15.5 kcal/mole) minimum and 250 kJ/mole (59.8 kcal/mole) maximum; Q is assumed to be 65 kJ/mole if the predicted values are lower, and 250 kJ/mole if the predicted values are higher. The above expressions for estimating activation energy Q for thermal aging embrittlement of CASS materials agree qualitatively with the microstructural and mechanical-property data. For example, an increase in the value of θ decreases the activation energy, as expected. The contribution of Si for all grades of CASS steels and of Mn for CF-8M steels are consistent with their effect on the formation of G-phase. These elements should promote precipitation of G phase: hence, the coefficients for these elements should have a negative sign, because activation energy for thermal embrittlement is low for steels that show G-phase precipitation. An increase in C or N in the steel will promote carbide or nitride precipitation at high temperatures and thus increase the activation energy. The positive sign of the constant for the N content agrees with this behavior. The constant for the C content in steel, however, has a negative sign. It is likely that C also promotes precipitation of G phase, a multicomponent phase consisting of Ni, Si, Mo, Cr, Fe, and some Mn and C.[61,66]

The RT Charpy-impact energy of a specific CASS material as a function of service time and temperature can be obtained from estimated C_{Vsat} (Eqs. 3–5 and 11–19) and the kinetics of

embrittlement (Eqs. 38–42). The initial Charpy-impact energy of the unaged steel is needed for estimating the decrease in impact energy as a function of time and temperature of service. The RT Charpy-impact energy observed experimentally and that estimated from the chemical composition and initial impact energy of the CASS materials used to develop these correlations are presented in Figs. 19 and 20 of NUREG/CR-4513, Rev. 1. A θ value of 2.9 was used for all temperatures of thermal aging. The estimated change in impact energy at temperatures less than or equal to 330°C (626°F) is either accurate or slightly conservative for most of the heats. A few heats show poor agreement because either the estimated C_{Vsat} is higher than the experimental value (Framatome Heat D and Argonne Heat 47) or the estimated activation energy is high (Framatome Heat C and Georg Fischer Heat 278). Even at 350°C, the estimated impact energies show good agreement with the experimental results because the θ values for most of the heats shown in the figures are either greater or only slightly lower than 2.9. The EPRI heat and an EdF heat (experimental θ is 2.1 for both heats) alone show nonconservative estimates at 350°C. A θ value of 2.5 rather than 2.9 should be used to ensure that the estimates at 330–360°C (626–680°F) are conservative.

Once the RT Charpy-impact energy C_V is known, the service-time coefficient C and exponent n of the fracture toughness J-R curve are determined from Eqs. 20–31 and 32–37, respectively. The methodology and expressions for estimating the change in tensile flow and yield stresses and the engineering stress-strain curve of CASS materials as a function of time and temperature of service, have been described earlier in NUREG/CR-6142.[52] The tensile properties of aged CASS materials are determined from known material information, (i.e., chemical composition and initial tensile strength of the steel). The fracture toughness J_{Ic} values for the service-aged CASS material can be determined from the estimated values of the fracture toughness J-R curve and flow stress. In Figs. 17–20, the change in the measured values of coefficient C as a function of aging time and temperature, are compared with those estimated from material composition and the initial RT Charpy-impact energy, for some of the CASS materials.

The results indicate that in general, the estimates at aging temperatures of 320 and 350°C, are either accurate or conservative for all of the materials. The proposed methodology can be used to estimate the change in fracture toughness of CASS materials for known material composition and service conditions, particularly for service temperature between 290 and 320°C.

2.5.2 Estimation of Thermal Embrittlement of CASS Materials of Unknown Composition – Lower-bound values

The Argonne methodology discussed above provides the expressions for estimating the fracture toughness J-R curves of unaged and aged CASS materials as a function of the RT Charpy-impact energy, which in turn is determined from the a material parameter that depends on the chemical composition and ferrite content of the material. However, for convenience, lower-bound J-R curves are defined as a function of ferrite content of the CASS material. The fracture toughness is defined by the J-R curve expressed by the power-law relation $J_d = C\Delta a^n$, where J_d is deformation J per ASTM Specifications E 813-85 and E 1152-87, Δa is crack extension, and C and n are constants. The coefficient C and exponent n for the lower-bound fracture toughness J-R curve are determined from the bounding value of C_{Vsat} for a range of ferrite content in the CASS material.

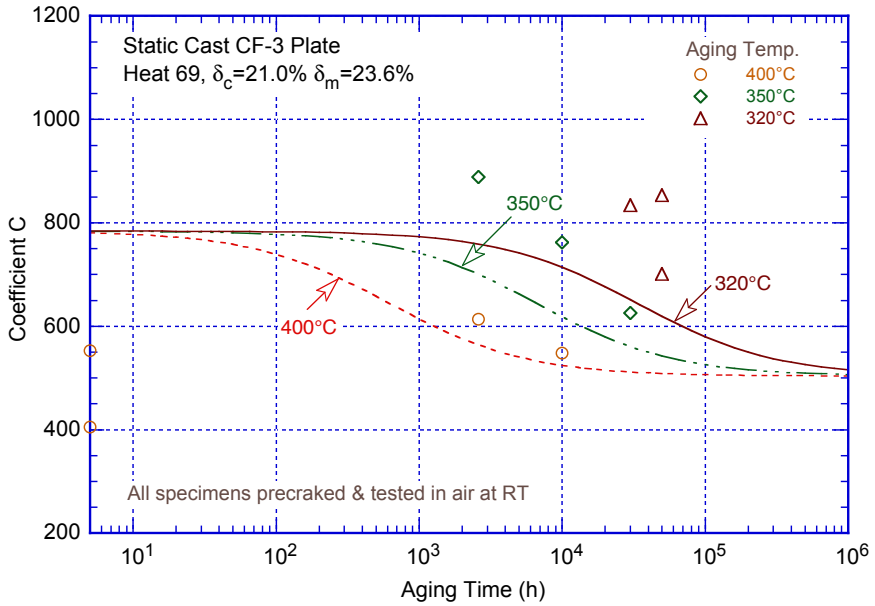

(a)

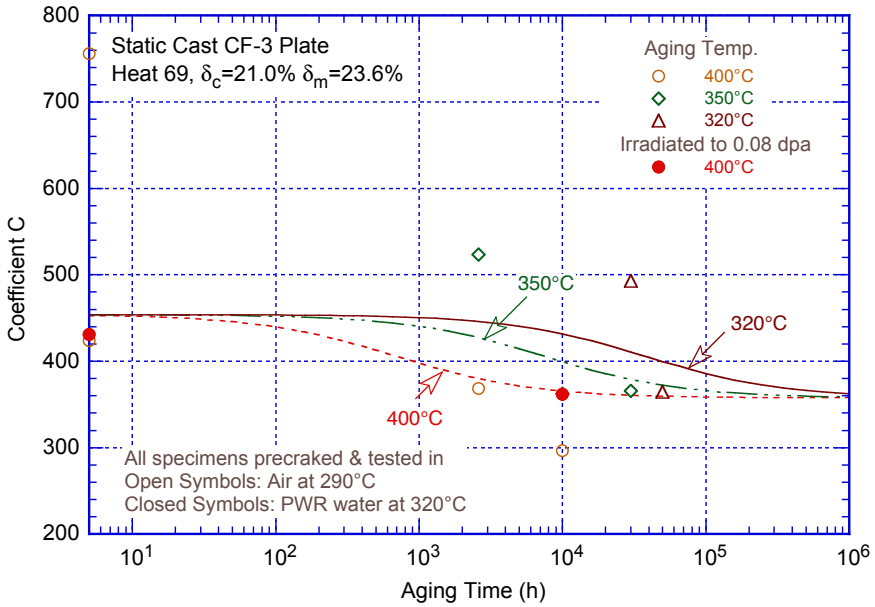

(b)

Figure 17. Comparison of the experimental values of coefficient C of the power-law J-R curve at (a) RT and (b) 290 or 320°C as a function of aging time and temperature for static-cast CF-3 plate with the values estimated from material composition and the initial RT Charpy-impact energy.

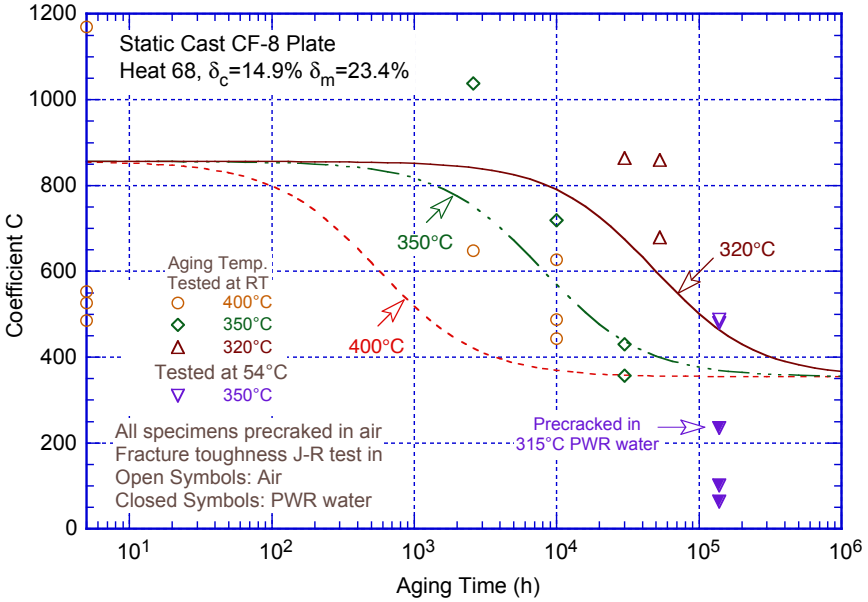

(a)

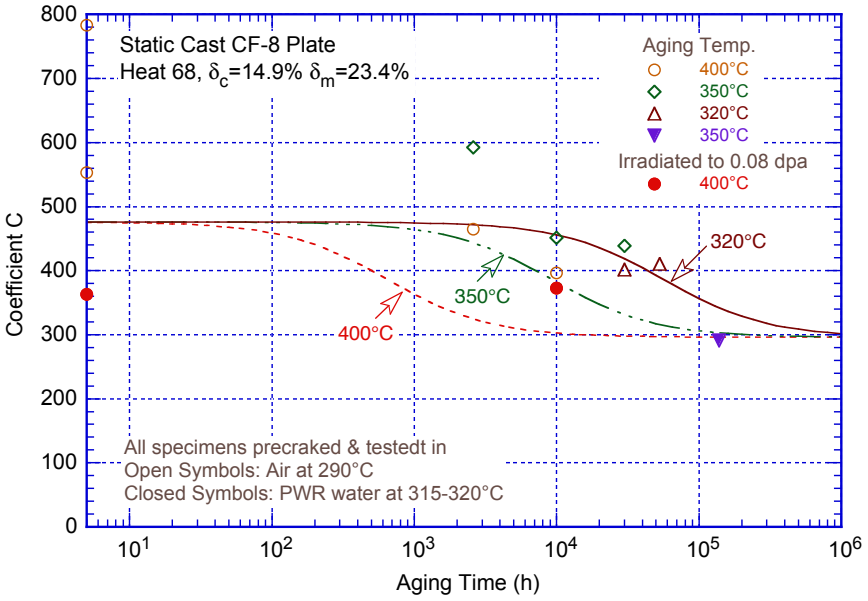

(b)

Figure 18. Comparison of the experimental values of coefficient C of the power-law J-R curve at (a) RT or 54°C and (b) 290 or 315–320°C as a function of aging time and temperature for static-cast CF-8 plate with the values estimated from material composition and the initial RT Charpy-impact energy.

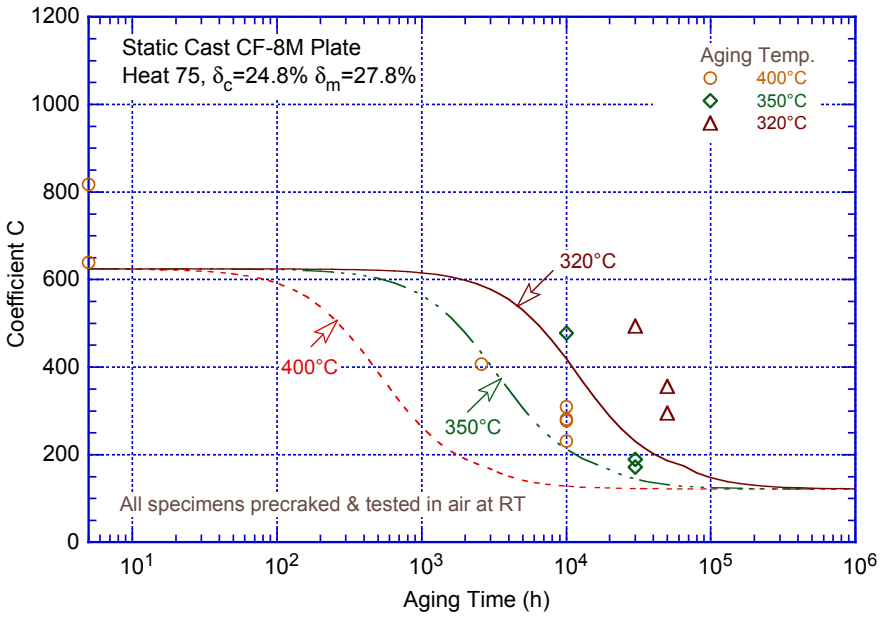

(a)

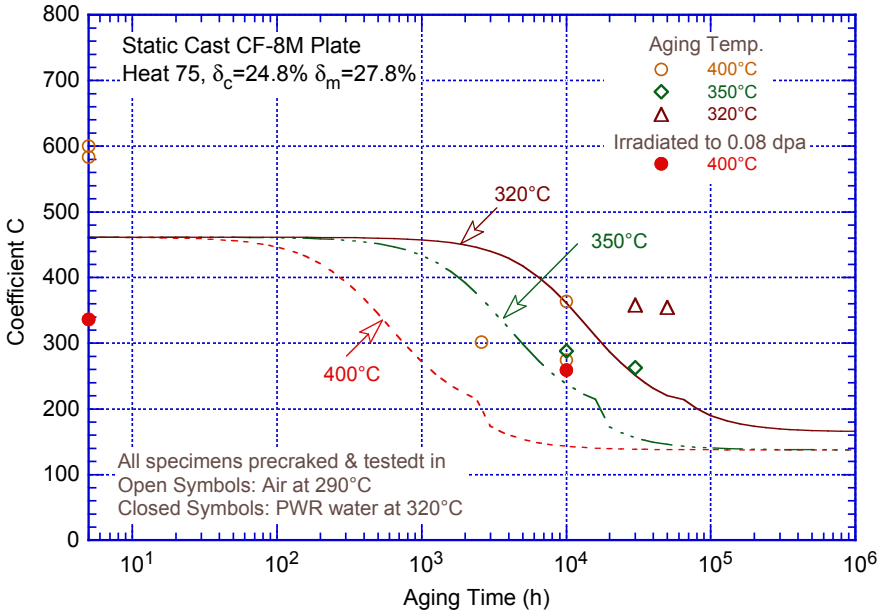

(b)

Figure 19. Comparison of the experimental values of coefficient C of the power-law J-R curve at (a) RT and (b) 290 or 320°C as a function of aging time and temperature for static-cast CF-8M plate with the values estimated from material composition and the initial RT Charpy-impact energy.

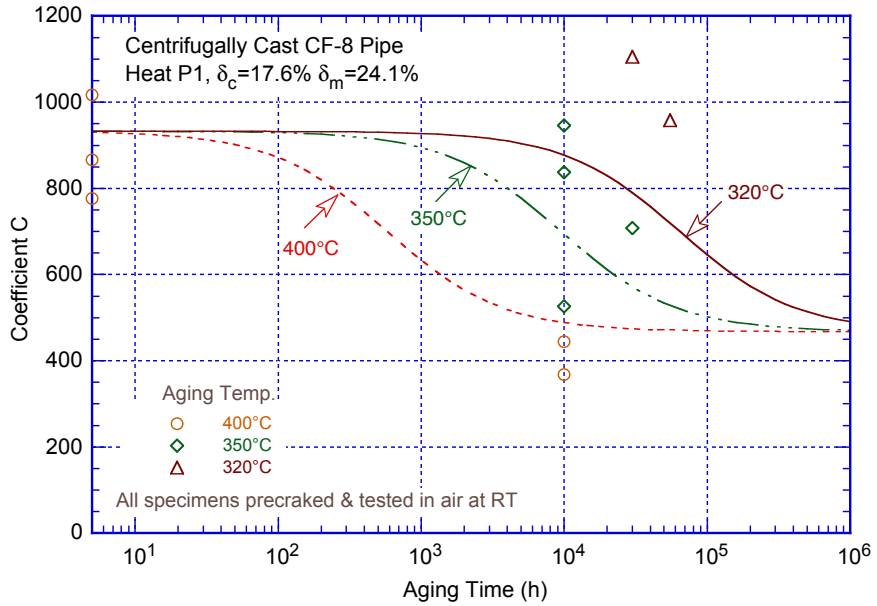

(a)

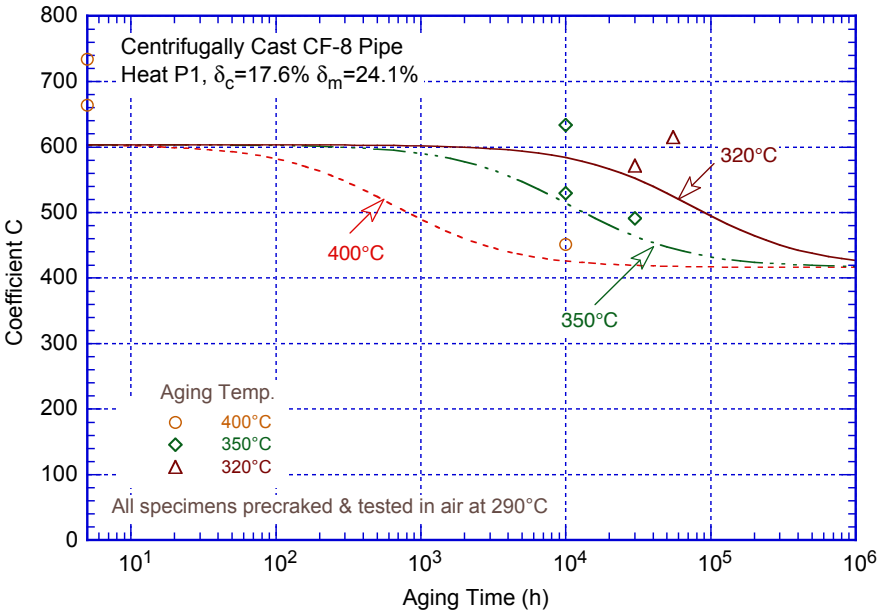

(b)

Figure 20. Comparison of the experimental values of coefficient C of the power-law J-R curve at (a) RT and (b) 290°C as a function of aging time and temperature for centrifugally-cast CF-8 pipe with the values estimated from material composition and the initial RT Charpy-impact energy.

Therefore, first, the bounding values of saturation RT Charpy-impact energy, C_{Vsat}, for ferrite contents of <10%, 10–15%, 15–25%, and 25–40% are established for each grade of CASS material, from the plots of estimated C_{Vsat} and ferrite content (Fig. 21). The saturation RT Charpy-impact energy, C_{Vsat}, for the different grades of CASS materials, is the lower value determined from the sets of expressions given in Eqs. 11–19. Separate expressions are

proposed for CF-8M steels containing less than 10% Ni and those containing equal to or greater than 10% Ni. The latter are most susceptible to thermal embrittlement than the other grades.

A value of 10% Ni is used in this study to differentiate whether primary γ (austenite) form during solidification of the castings from the liquid. For CASS CF-8M compositions containing less than 10% Ni, the solidification sequence is as follows: Liq. $\rightarrow$ Liq. + $\delta \rightarrow \delta$; with $\delta \rightarrow \gamma$ in the solid.[85] Austenite nucleates predominantly at the δ ferrite grain boundaries and to a lesser extent at interdendritic locations within the ferrite. For CF-8M compositions containing equal to or more than 10% Ni, the solidification sequence is likely to be as follows: Liq. $\rightarrow$ Liq. + $\delta \rightarrow$ Liq. + δ + $\gamma \rightarrow \delta$ + γ; with $\delta \rightarrow \gamma$ continuing in the solid.[85] The austenite forms first in the liquid as a secondary phase enveloping the primary δ ferrite. On further cooling, it grows in the remaining liquid as well as into ferrite. The latter reaction continues below the solidus line. The actual microstructures of the casting depend on the Cr/Ni ratio for the specific composition.

The lower-bound J-R curves at RT and 290–320°C determined from the estimated C_{Vsat} for static-cast and centrifugally-cast CASS materials with 25–40%, 15–25%, 10–15%, and <10% ferrite, are plotted in Figs. 22a, 22b, 23a and 23b. These plots are updated versions of Figs. 3 and 4 of NUREG/CR-4513, Rev. 1.[50] These lower-bound fracture toughness J-R curves can be used for completely embrittled CASS materials of unknown composition. The estimated C_{Vsat} and the corresponding values of coefficient C and exponent n of the J-R curve at RT and 290–320°C (550–608°F) for CF-3, CF-8, and CF-8M with <10 and ≥10% Ni are listed in Table 3.

Table 3. Coefficient C and exponent n for the lower-bound J-R curve at RT and at reactor operating temperatures for thermally aged CASS materials.

Material Grade	Estimated C_{Vsat} (J/cm^2)	Static Cast Material				Centrifugally-cast Material			
		Room Temp.		290–320°C		Room Temp.		290–320°C	
		C (kJ/cm^2)	n	C (kJ/cm^2)	n	C (kJ/cm^2)	n	C (kJ/cm^2)	n
Ferrite content 25–40%									
CF-3/CF-3A	29	285	0.39	263	0.35	331	0.39	346	0.35
CF-8/CF-8A	22	247	0.36	244	0.34	287	0.36	320	0.34
CF-8M (Ni <10%)	16	60	0.34	82	0.34	74	0.34	103	0.34
CF-8M (Ni ≥10%)	10	32	0.34	52	0.34	390	0.34	65	0.34
Ferrite content 15–25%									
CF-3/CF-3A	41	338	0.41	288	0.36	393	0.41	379	0.36
CF-8/CF-8A	29	285	0.38	263	0.34	331	0.38	346	0.34
CF-8M (Ni <10%)	24	102	0.34	121	0.34	127	0.34	152	0.34
CF-8M (Ni ≥10%)	15	57	0.34	79	0.34	70	0.34	100	0.34
Ferrite content 10–15%									
CF-3/CF-3A	68	438	0.44	332	0.39	510	0.44	436	0.39
CF-8/CF-8A	45	353	0.40	295	0.36	411	0.40	388	0.36
CF-8M (Ni <10%)	43	199	0.36	219	0.34	249	0.36	266	0.34
CF-8M (Ni ≥10%)	30	139	0.35	152	0.34	172	0.35	191	0.34
Ferrite content <10%									
CF-3/CF-3A	101	539	0.47	371	0.41	627	0.47	487	0.41
CF-8/CF-8A	62	419	0.42	324	0.37	487	0.42	425	0.37
CF-8M (Ni <10%)	69	274	0.38	279	0.34	342	0.38	324	0.34
CF-8M (Ni ≥10%)	50	220	0.37	244	0.34	275	0.37	284	0.34

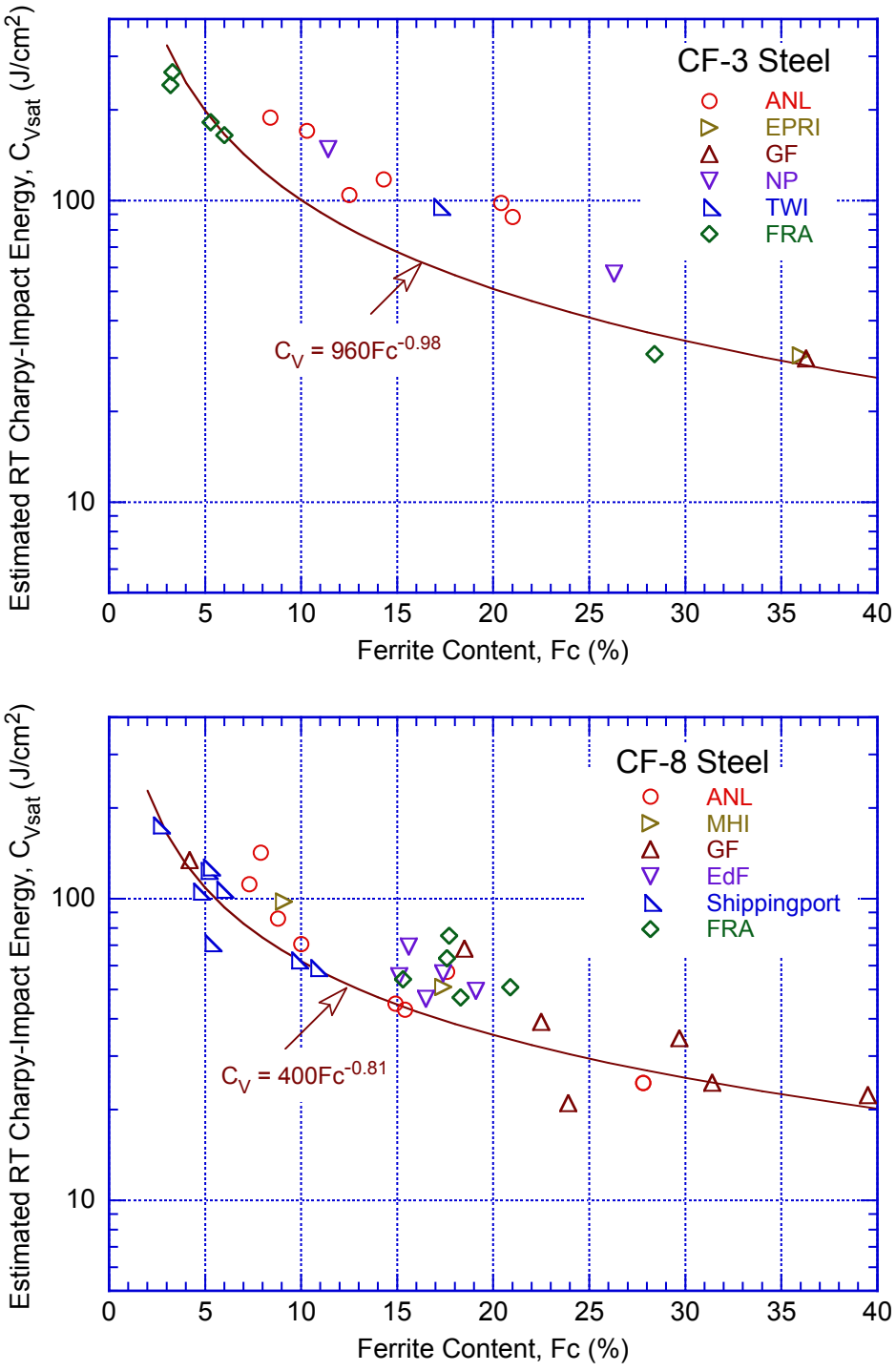

Figure 21. Correlation between saturation RT Charpy-impact energy and ferrite content for CF-3, CF-8, and CF-8M CASS materials.

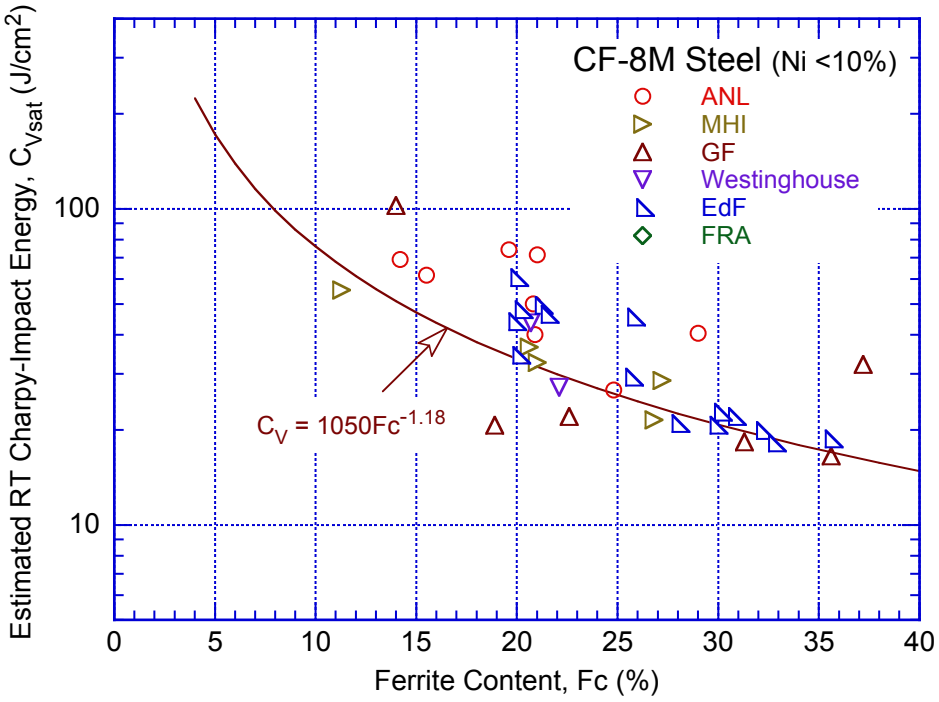

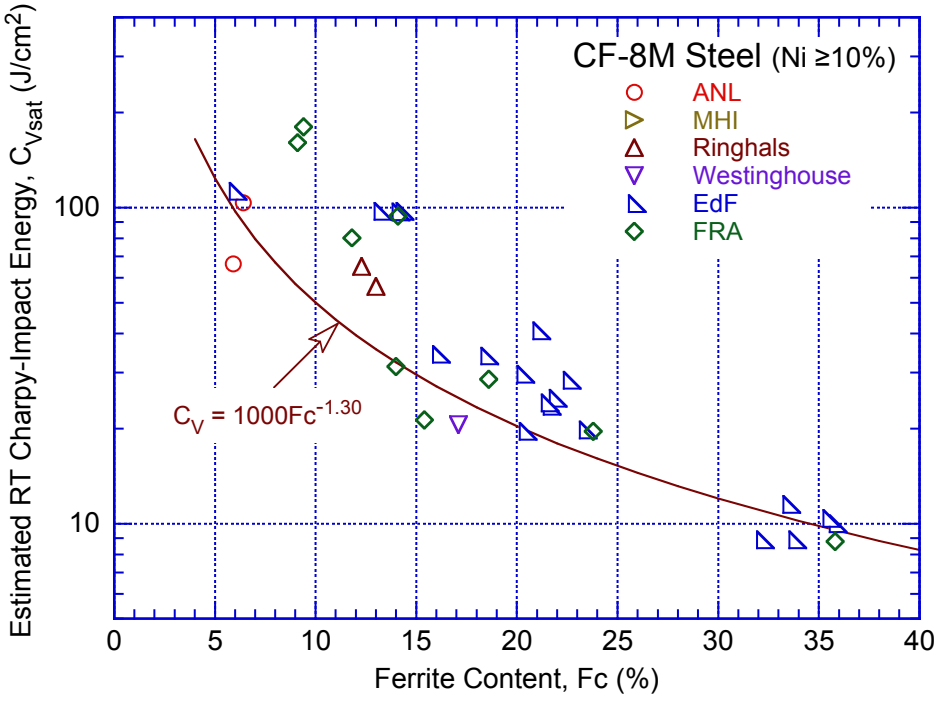

Figure 21 Continued.

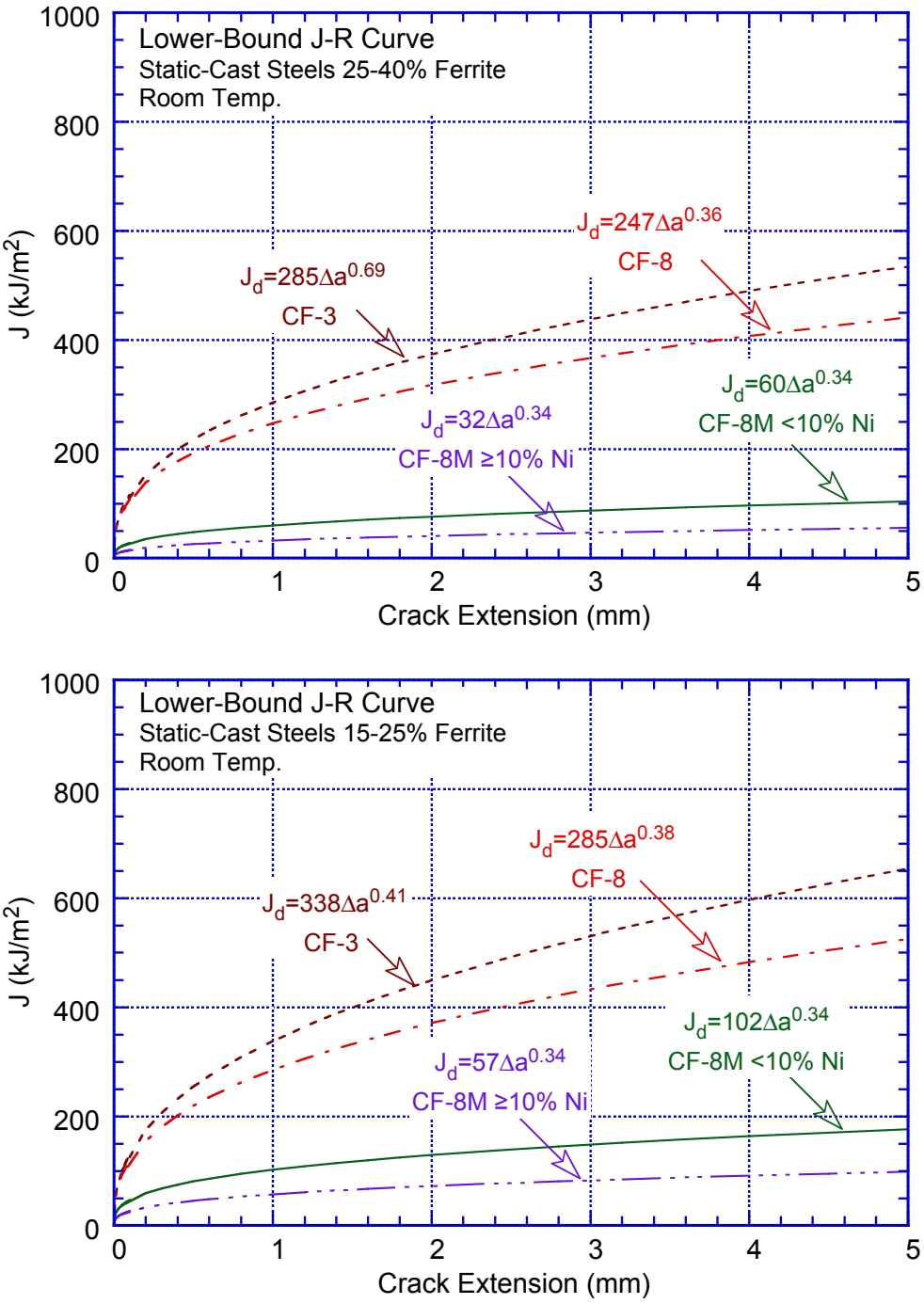

Figure 22a. Estimated lower-bound J-R curves at RT for static-cast CASS materials with ferrite contents of 25–40%, 15–25%, 10–15%, and <10%.

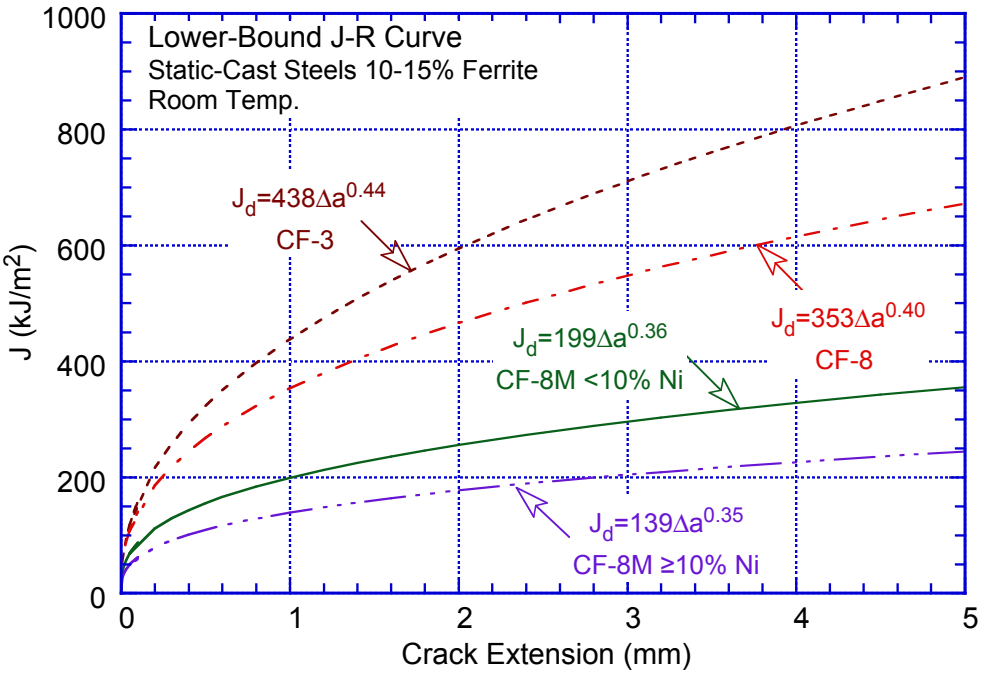

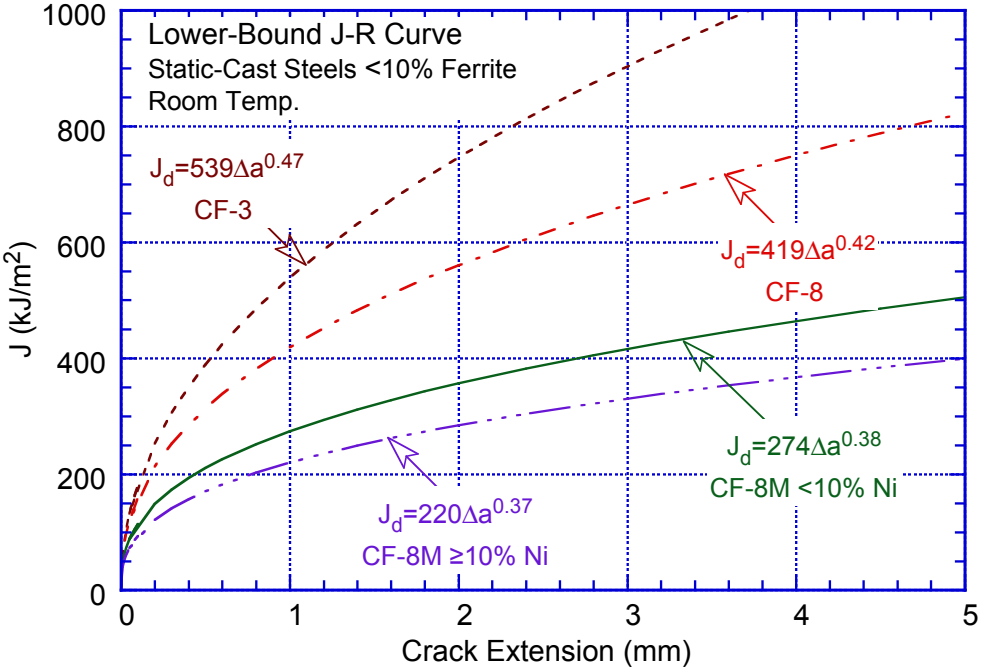

Figure 22a Continued.

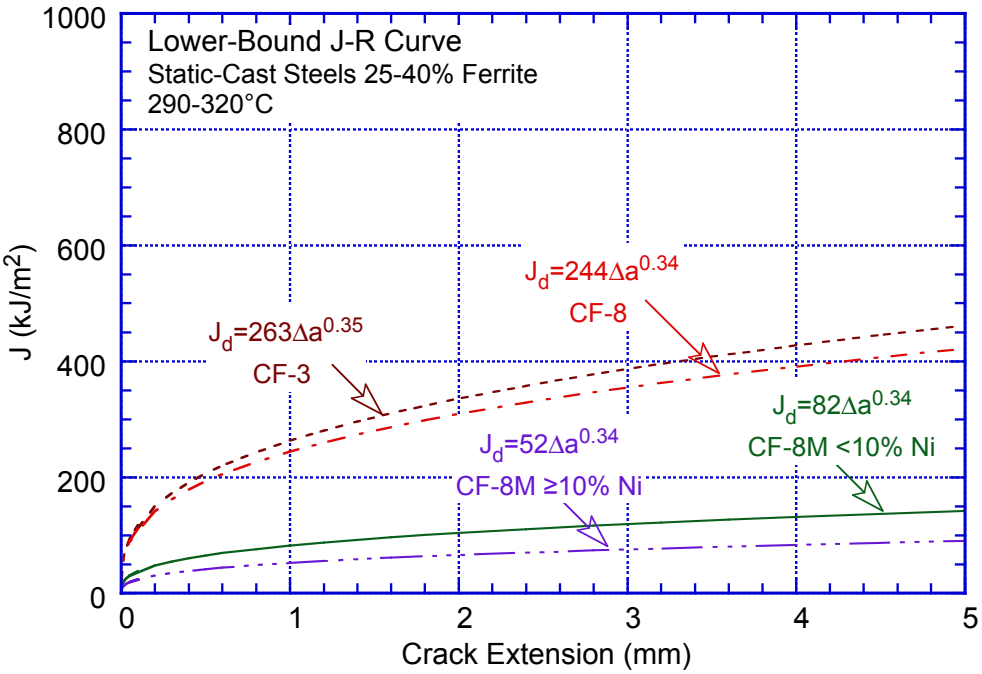

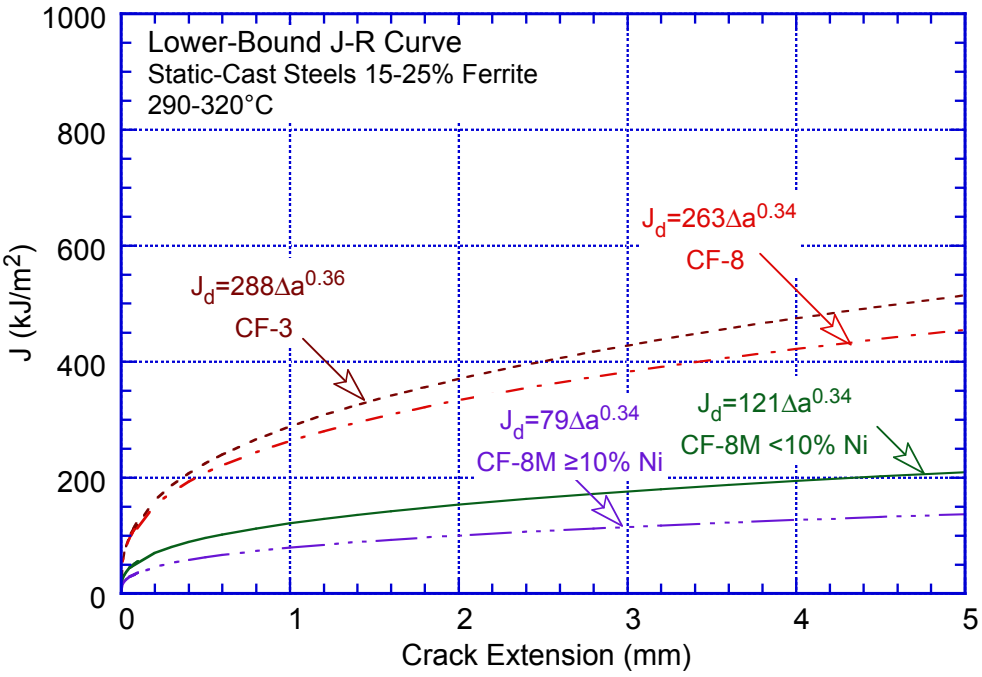

Figure 22b Estimated lower-bound J-R curves at 290–320°C for static-cast CASS materials with ferrite contents of 25–40%, 15–25%, 10–15%, <10%.

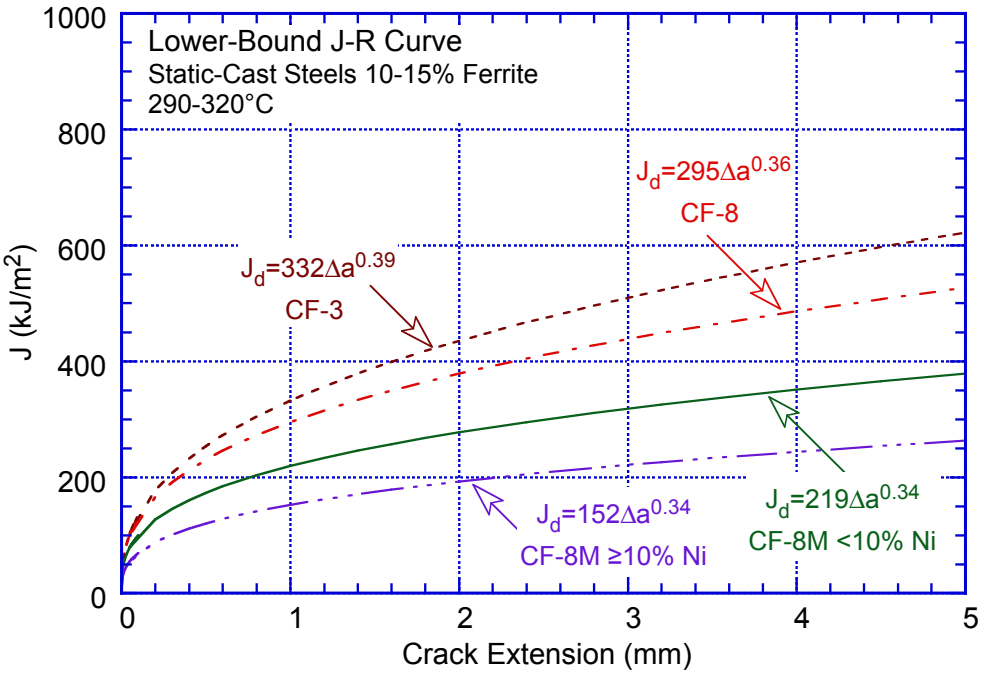

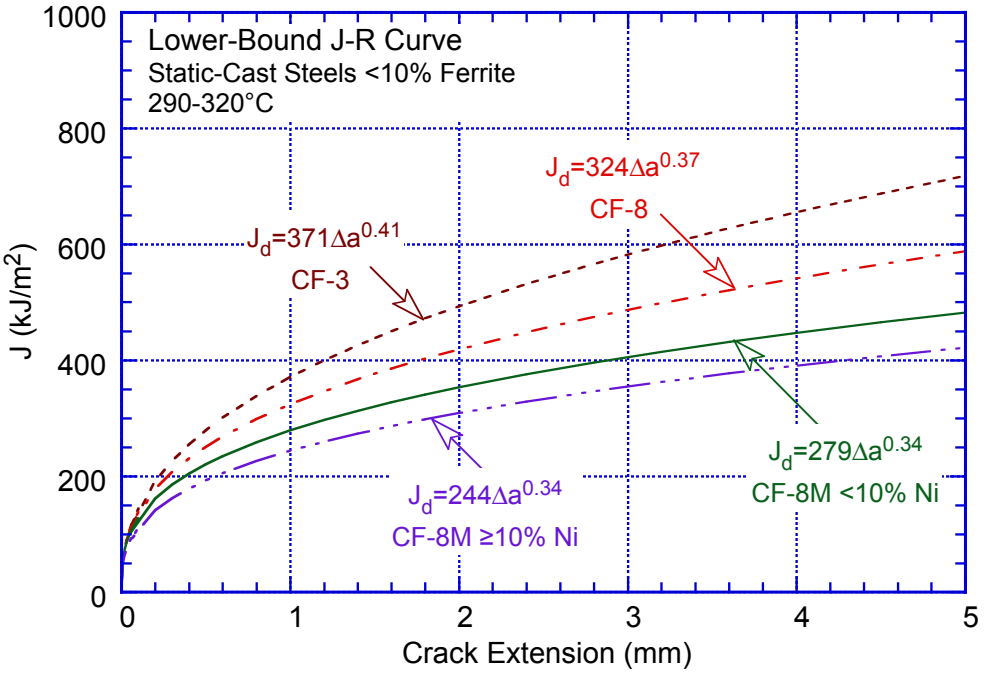

Figure 22b Continued.

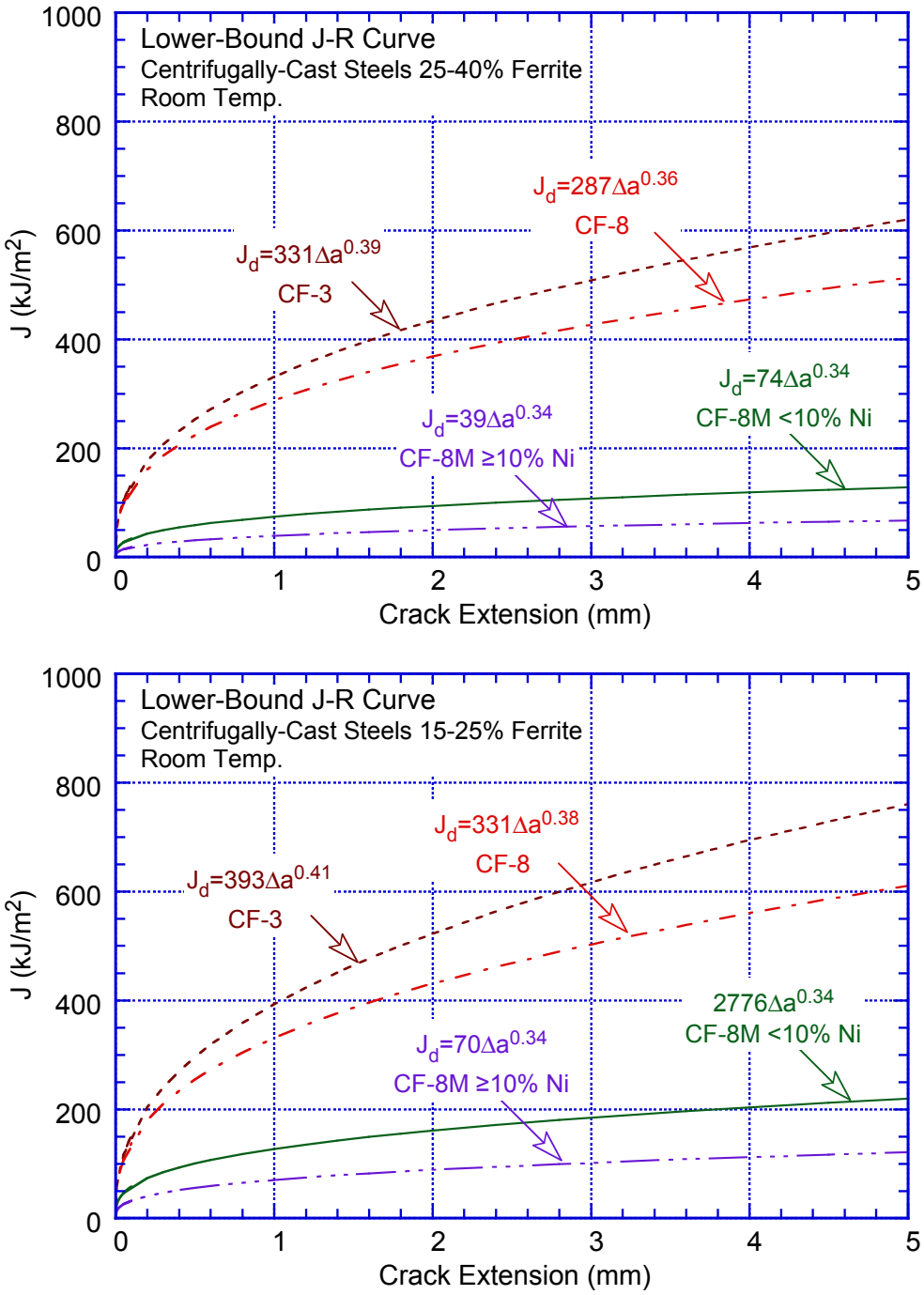

Figure 23a. Estimated lower-bound J-R curves at RT for centrifugally-cast CASS materials with ferrite contents of 25–40%, 15–25%, 10–15%, and <10%.

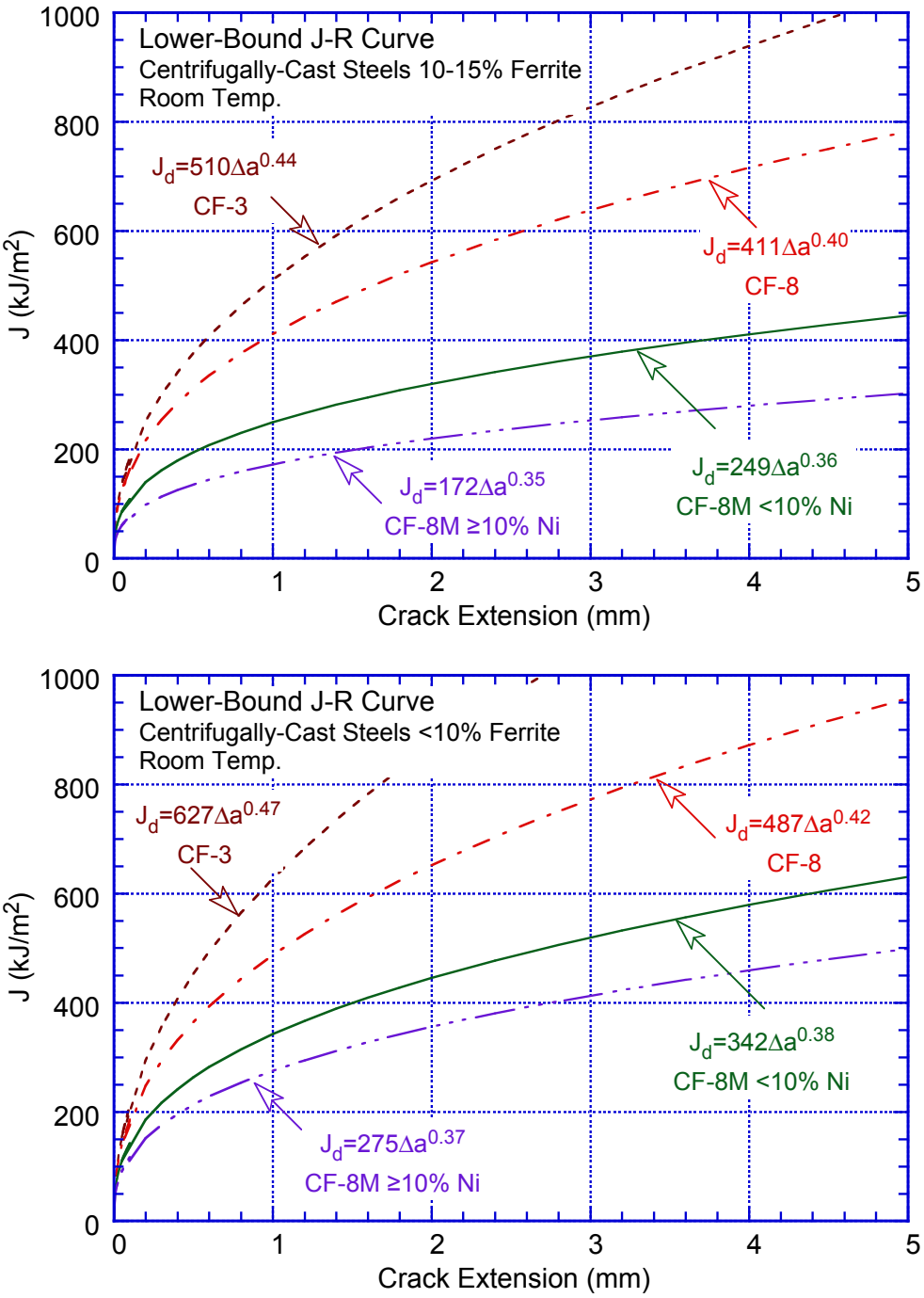

Figure 23a. Continued.

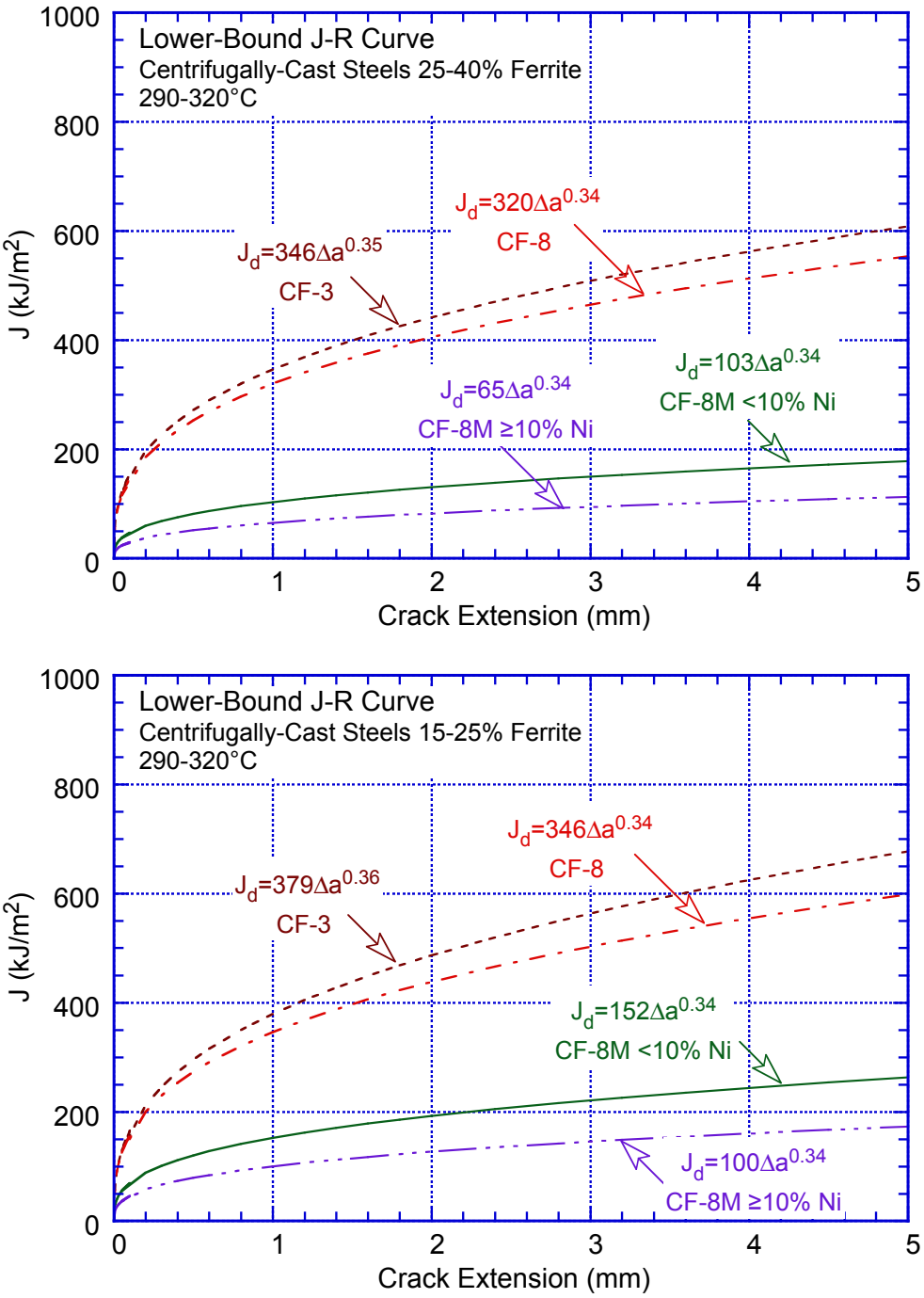

Figure 23b Estimated lower-bound J-R curves at 290–320°C for centrifugally-cast CASS materials with ferrite contents of 25–40%, 15–25%, 10–15%, and <10%.

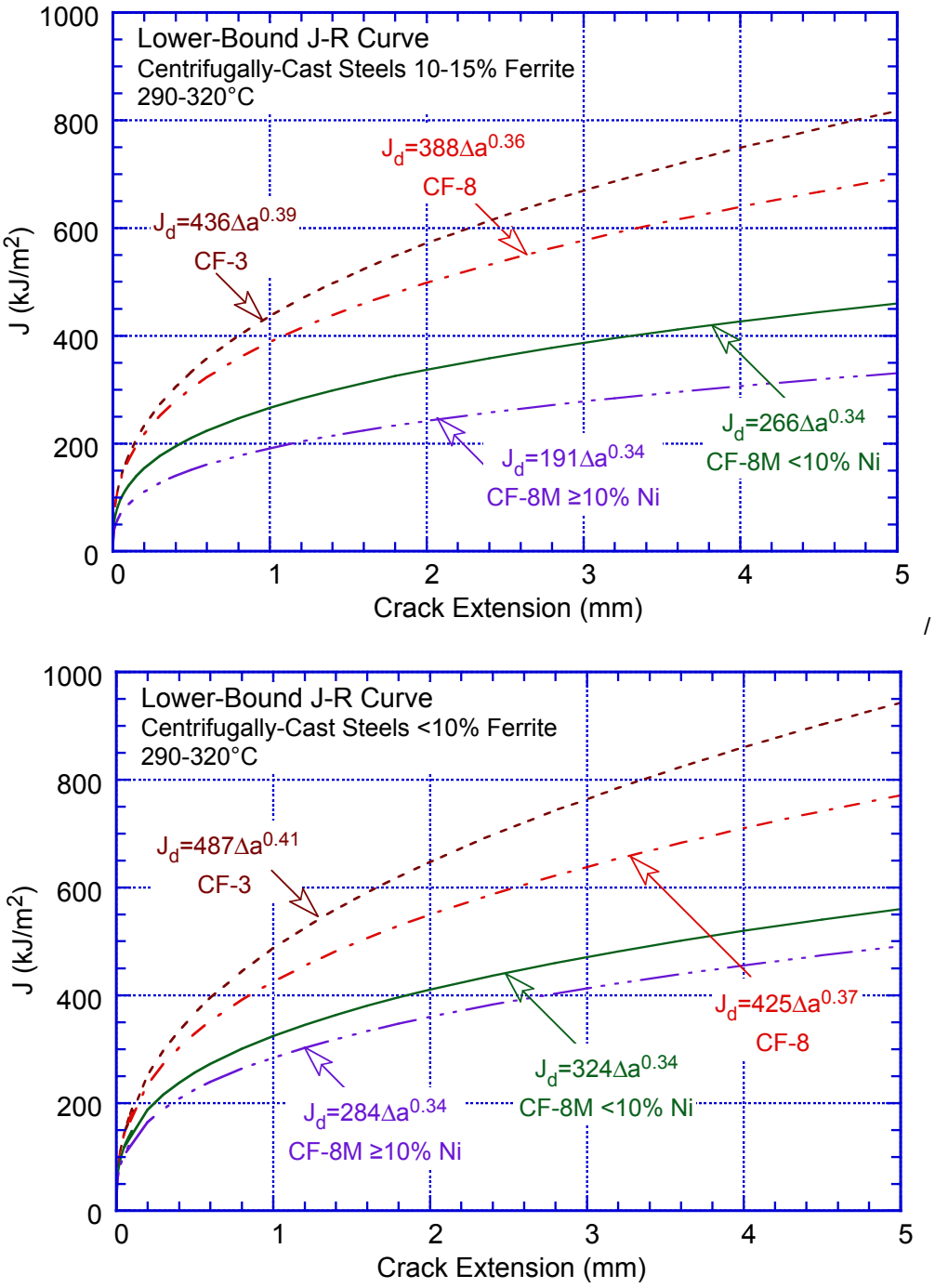

Figure 23b Continued.

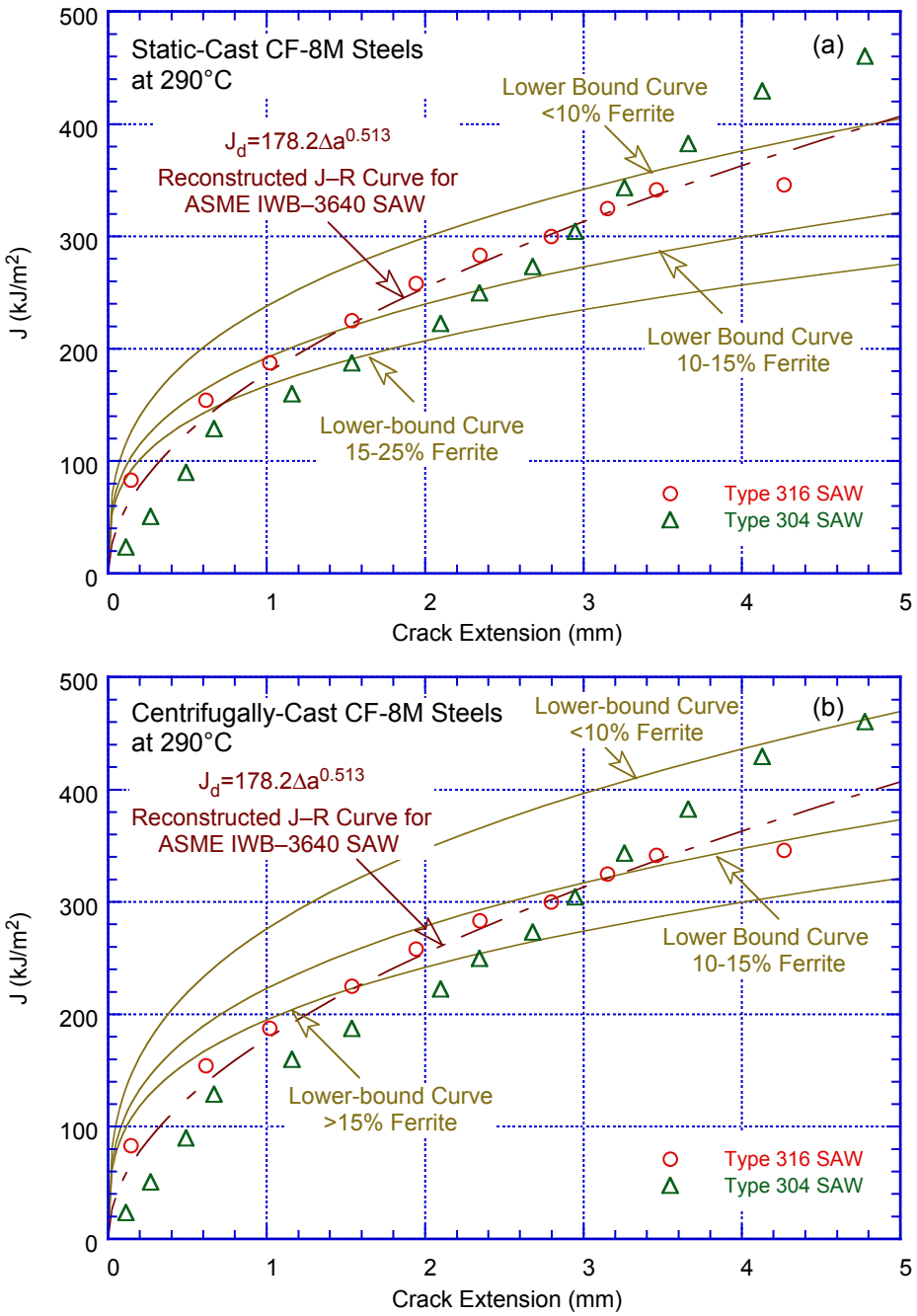

Figure 24. Comparison of the lower-bound fracture toughness J-R curve for thermally aged (a) static-cast and (b) centrifugally-cast CF-8M steels at 290°C estimated using the NUREG/CR-4513, Rev. 1 expressions, with the fracture toughness of SA welds used to develop ASME Section XI Subsection IWB-3640 evaluations.

The NRC staff compared the estimated lower-bound fracture toughness J-R curves developed by Argonne for thermally aged CASS materials with the fracture toughness used in American Society of Mechanical Engineers (ASME) Section XI Subsection IWB-3640 for evaluating flux welds.[82] The comparison is shown in Fig. 24 for static-cast and centrifugally-cast CASS materials. The results show that the lower-bound fracture toughness of thermally aged CASS material with up to 25% ferrite is similar to the fracture toughness J-R curve used in Section XI

IWB-3640 to evaluate SA welds. The procedures in ASME Section XI Subsection IWB-3640 reduce the load-bearing capacity of the SS component to account for the reduced fracture toughness of the SA welds, based on elastic-plastic fracture mechanics analyses.[86,87] Because the lower-bound fracture toughness of thermally aged CASS steel is similar to the fracture toughness of SA welds used in the elastic-plastic fracture mechanics analyses of IWB-3640, the procedures in IWB-3640 for SA welds are directly applicable to CASS materials.

Furthermore, since the flaw evaluation is based on the unaged material ultimate stress, this approach would be conservative. Experimental data indicate that the flow stress, that is, half of the sum of the ultimate and yield stresses, is increased by about 10%, 14%, and 24%, for CF-3 and CF-3A, CF-8 and CF-8A, and CF-8M materials, respectively.[50] A higher ultimate stress would increase the load bearing capability of a component. Therefore, the NRC staff has accepted the procedures developed in IWB-3640 of Section XI for SA welds for evaluating flaws in thermally aged CASS materials for addressing aging degradation concerns in license renewal applications.

The use of the IWB-3640 SA weld procedures for evaluating flaws in thermally aged CASS components are considered conservative because:

1. The lower-bound fracture toughness of thermally aged CASS is similar to the fracture toughness used in IWB-3640 to evaluate SA welds.

2. The actual fracture toughness of a thermally aged CASS component in a U.S. utility plant would likely be higher than the Argonne lower-bound fracture toughness.

3. The thermally aged components would be able to bear more load due to the increased ultimate stress resulting from thermal aging. This is not credited in this flaw evaluation procedure.

Thus, the use of the IWB-3640 SA weld procedures for evaluating flaws in thermally aged CASS components is considered as a "screening" step to determine whether further detailed flaw evaluation accounting for actual plant-specific material properties should be performed. The procedures in IWB-3640 for SA welds have been available since the winter 1985 Addenda of Section XI, and have been applied successfully by utilities without resulting in unnecessary component repairs or replacements. However, the Argonne methodology of NUREG/CR-4513, Rev. 1 was not applicable to CASS CF-8M materials with greater than 25% ferrite or for CF-8M materials containing more than trace amounts of Nb. Even then, the proposed flaw evaluation procedures based on the lower-bound fracture toughness of thermally aged CASS materials was expected to be sufficient for the vast majority of cases.

In this report, the plots in Fig. 24 have been updated to include a comparison of the new lower-bound fracture toughness J-R curve presented in Figs. 22 and 23 with the fracture toughness J-R curve of SA welds used to develop ASME Section XI Subsection IWB-3640 evaluations. The results are shown in Figs. 25 and 26 for static-cast and centrifugally-cast CASS materials, respectively. The results indicate that the fracture toughness J-R curve used in Section XI, Subsection IWB-3640 to evaluate SA welds bounds the lower-bound fracture toughness of thermally aged CASS material containing up to 25% ferrite except for CF-8M materials with ≥10% Ni. As seen in Figs. 25 and 26, the lower-bound fracture toughness J-R curve for CF-8M materials containing ≥10% Ni and 15–25% ferrite is lower than the J-R curve of SA weld. In addition, the estimated lower-bound J-R curve for thermally aged CASS materials with greater than 25% ferrite.

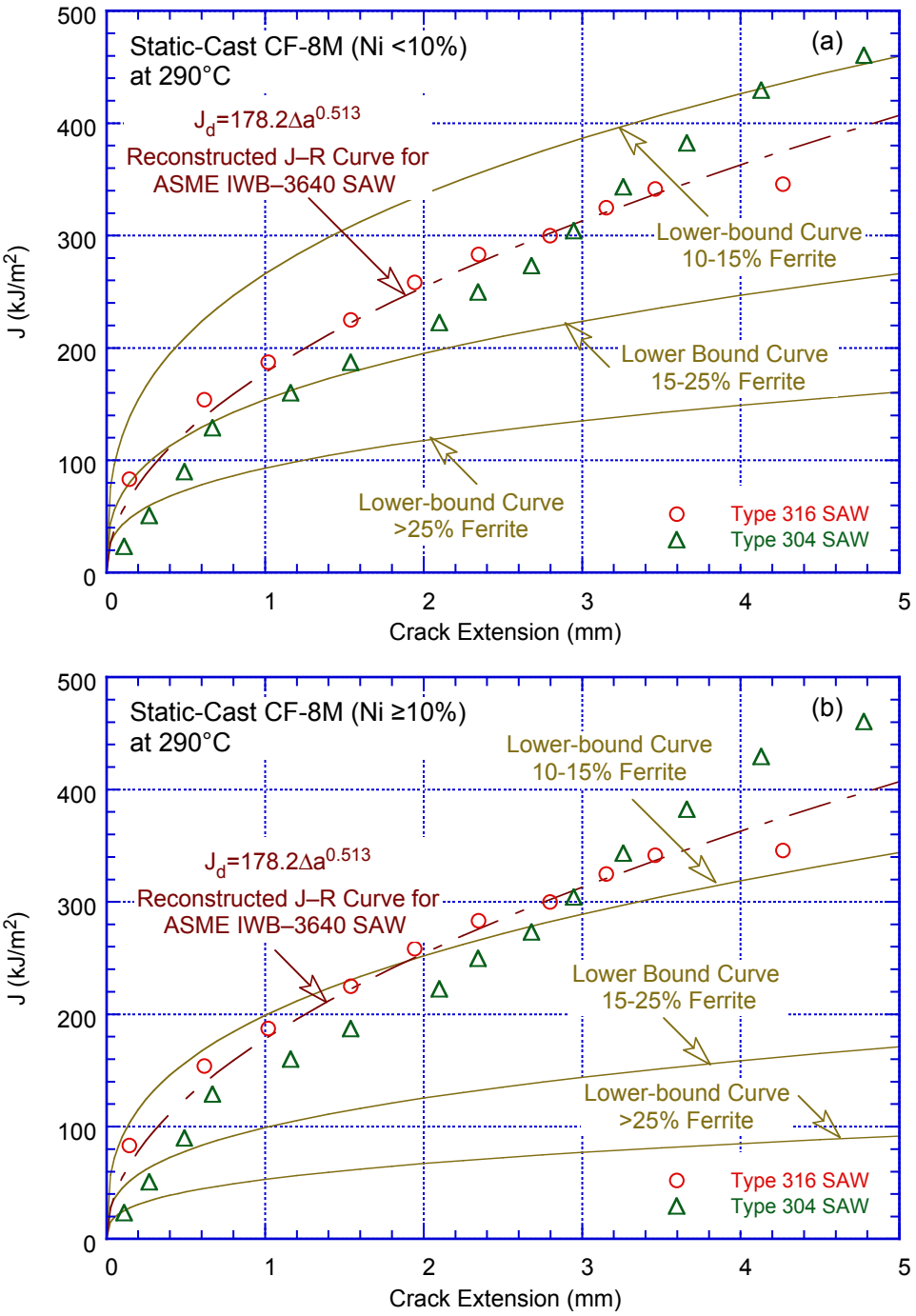

Figure 25. Comparison of the lower-bound fracture toughness J-R curve for thermally aged static-cast CF-8M steels containing (a) <10% Ni and (b) ≥10% Ni at 290°C estimated using the updated expressions presented in this report, with the fracture toughness of SA welds used to develop ASME Section XI Subsection IWB-3640 evaluations.

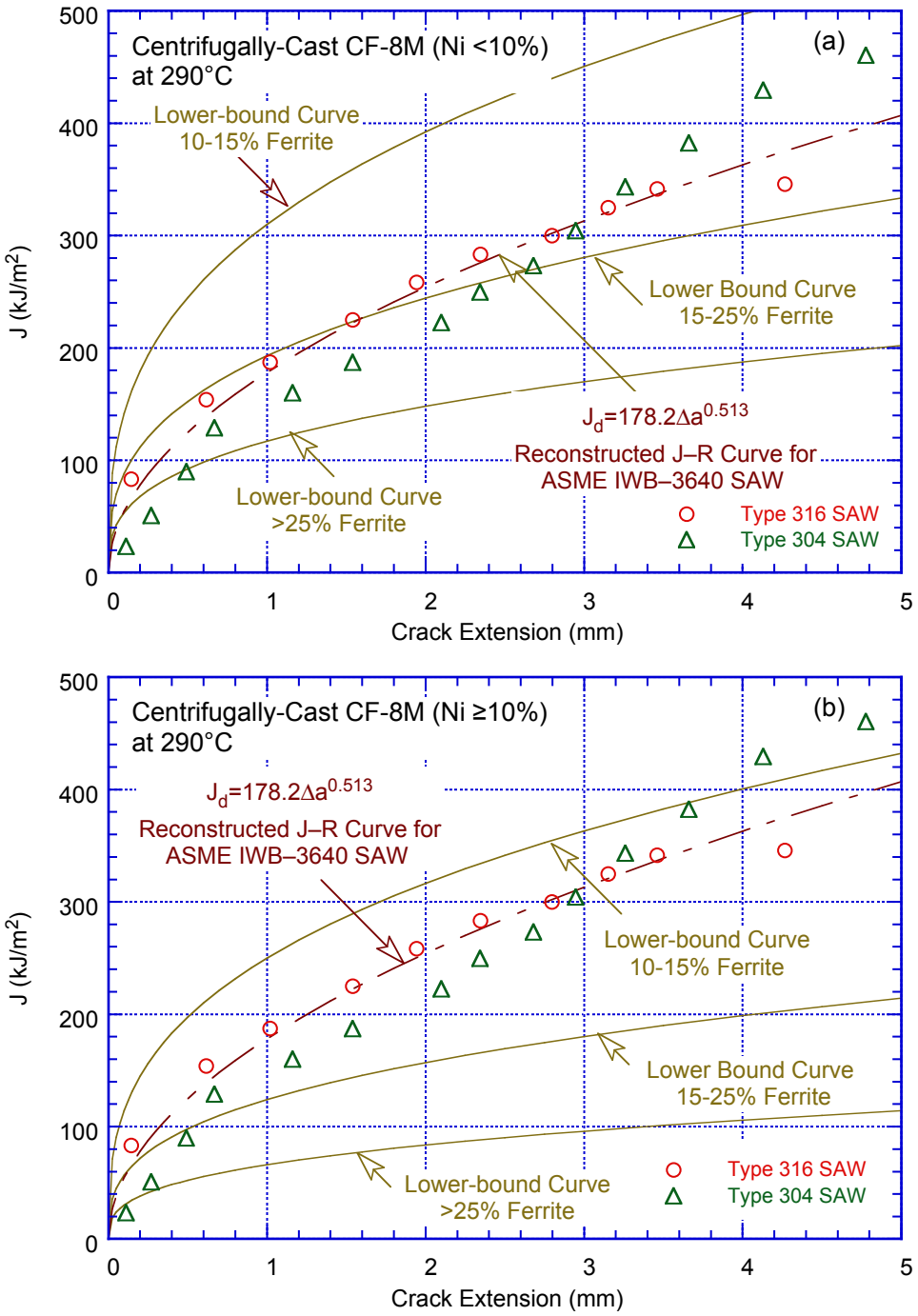

Figure 26. Comparison of the lower-bound fracture toughness J-R curve for thermally aged centrifugally-cast CF-8M steels containing (a) <10% Ni and (b) ≥10% Ni at 290°C estimated using the updated expressions presented in this report, with the fracture toughness of SA welds used to develop ASME Section XI Subsection IWB-3640 evaluations.

2.5.3 Updated Fracture Toughness Data for CASS Materials

Fracture toughness J-R curve data obtained on four heats of CF-8M material at EdF,[38] after the publication of NUREG/CR-4513, Rev. 1, are shown in Figs. 27 and 28. All heats except Heat EK contained ≥10% Ni, and all heats except DI contained >25% ferrite. The corresponding updated lower-bound J-R curve for the grade of material and range of ferrite content is also

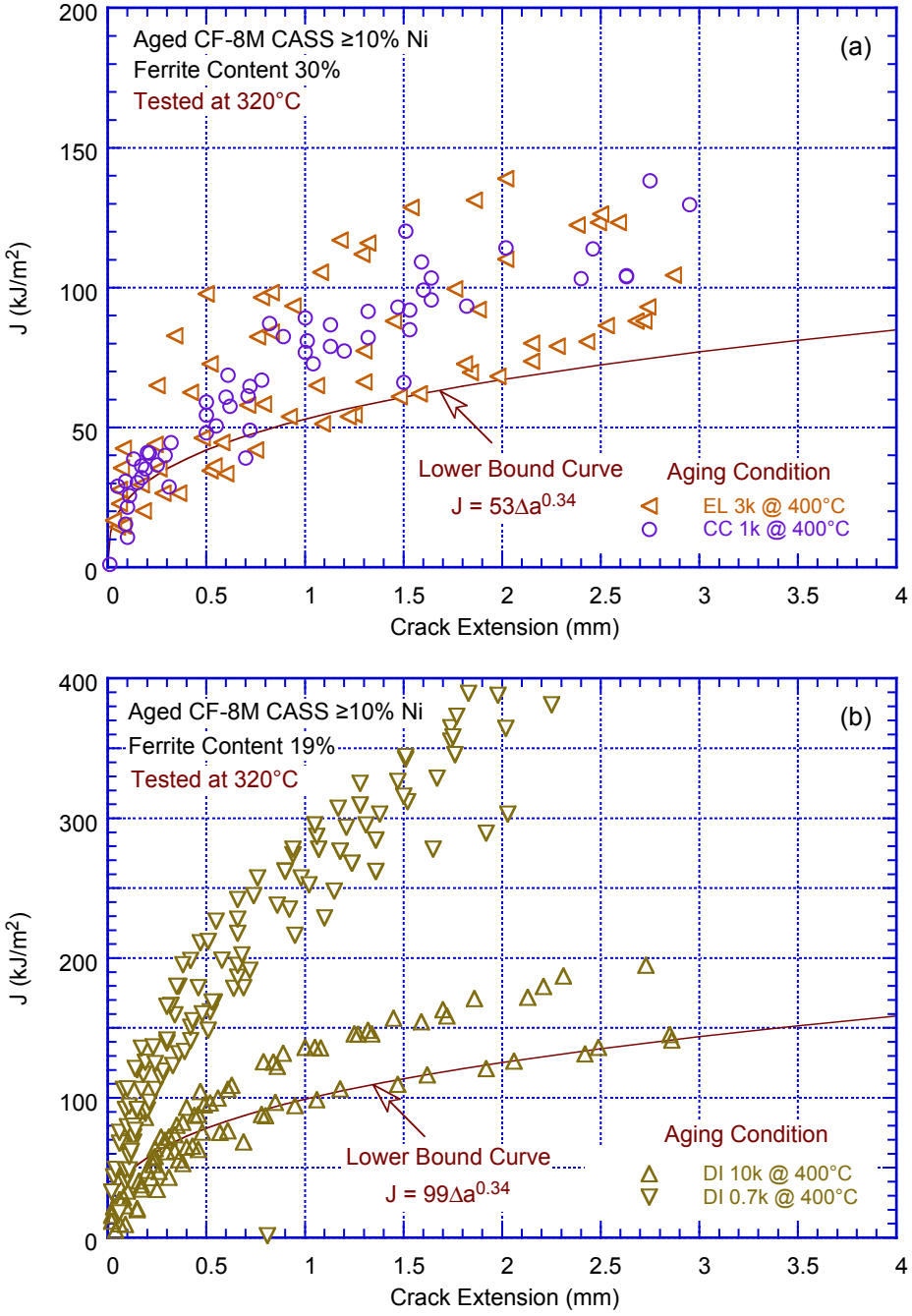

Figure 27. Fracture toughness J-R curve data at 320°C for static-cast and thermally aged plates (Heats CC and DI) and an elbow (Heat EL) of CF-8M material with ≥10% Ni and (a) >25% and (b) 15–25% ferrite (Ref. 38).

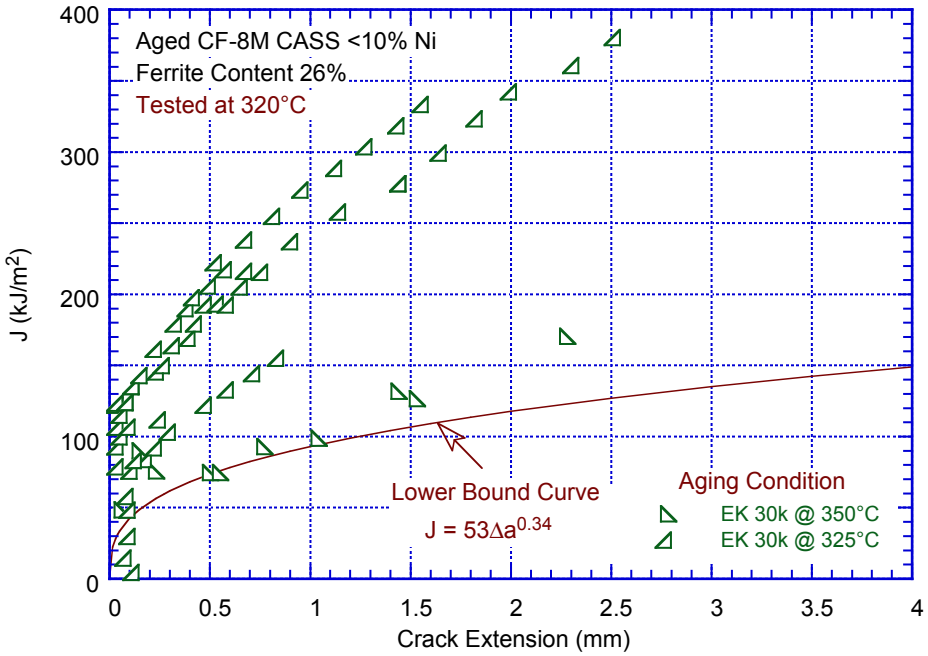

Figure 28. Fracture toughness J-R curve data at 320°C for static-cast and thermally aged elbow (Heat EK) of CF-8M material with <10% Ni and >25% ferrite (Ref. 38).

plotted in the figure (i.e., curves shown in Figs. 22 and 23 and associated power-law J-R curve parameters listed in Table 3). The results indicate that for all CF-8M materials, the applicable lower bound J-R curve bounds most of the J-R curve data. Some of the data obtained on materials that were aged to saturation condition (i.e. aged more than 3,000 h at 400°C) are below the lower-bound curve.

A recent scoping study on low-temperature crack propagation for CASS CF-8 material in PWR environments investigated the potential synergy between hydrogen embrittlement and thermal embrittlement associated with decomposition of the ferrite at reactor temperatures.[88] Fracture toughness J-R curve tests were conducted in air and PWR shutdown water chemistry (SWC) at 54°C on 1-T CT specimens of CF-8 material (Argonne Heat 68) that was thermally aged for about 138,000 h (about 15.8 yr) at 350°C. The ferrite content calculated from Hull's equivalent factors was 15%, and measured using a ferritescope was 23%. The specimens were either fatigue precracked in air at 54°C or fatigue plus SCC precracked in PWR water at 315°C. The fracture toughness J-R curve data for these tests are shown in Fig. 29. Note that one of the specimens that was precracked in PWR water at 315°C was inadvertently tested at elevated temperature of 315°C in PWR primary water chemistry. The updated lower-bound J-R curve at room temperature for CF-8 material with 15–25% ferrite is also shown in the figure for comparison.

The results indicate that at 54°C, the J-R curve data in air are bounded, with additional margin, by the updated lower-bound J-R curve. However, the J-R curve data for specimens precracked in air at 54°C and then tested in PWR (SWC) at 54°C are significantly below the lower-bound curve. These results show an apparent large effect of the coolant environment on fracture toughness; every material and test condition is identical for the two sets of duplicate tests except the one was tested in air and the other in water. The specimens that were precracked in PWR water at 315°C and then tested in PWR water at 54°C or 315°C also show reduced fracture toughness relative to that in air, but the difference is less. The J-R curve data for the

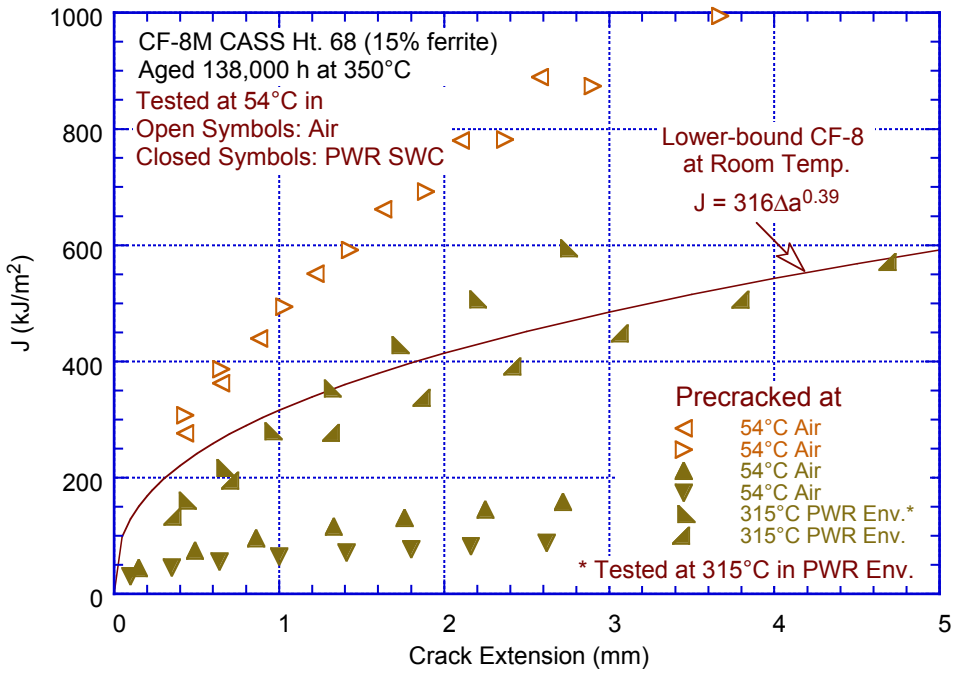

Figure 29. Fracture toughness J-R curve data for thermally aged Heat 68 of CF-8M plate at 54°C. The curve represent the lower bound curve at room temperature for static-cast CF-8 material (Ref. 88).

specimen that was cooled down to from 315°C and then tested at 54°C SWC are only marginally below the lower-bound J-R curve, and the data for the specimen that was precracked and tested at 315°C PWR primary water chemistry are slightly above the lower-bound curve.

The reason for the drastic reduction in fracture toughness in PWR SWC at 54°C relative to that in air at 54°C is not clear. Additional fracture toughness tests on thermally aged CASS CF-8 materials in air and LWR environments should be conducted to better understand the combined effects of hydrogen embrittlement and thermal embrittlement in LWR environments.

2.5.4 Screening Criteria for Susceptibility of CASS Materials to Thermal Embrittlement

An EPRI report on thermal aging embrittlement of CASS components proposed the use of the J value at a crack extension of 2.5 mm (0.1 in.), $J_{2.5}$, to differentiate between nonsignificant and potentially significant reductions in fracture toughness of thermally aged CASS materials.[46] Flaw tolerance evaluations were presented in Appendices A and B of the EPRI report to support the choice of a threshold value of $J_{2.5}$ = 255 kJ/m^2 (1456 in.-lb/in.^{2}). The NRC staff found that using $J_{2.5}$ = 255 kJ/m^2 is an acceptable screening approach for fracture toughness of CASS materials.[45] The screening criteria to determine the susceptibility of CASS components to thermal aging embrittlement are outlined in Table 4.[45]

The expressions presented in Fig. 21, and the methodology described in Section 2.4.2 for estimating the corresponding fracture toughness J-R curve for the RT Charpy-impact energy trend curves in Fig. 21, can be used to check the validity of the ferrite content criteria given in Table 4. The saturation values of J at 2.5 mm crack extension corresponding to the RT Charpy-impact energy trend curves in Fig. 21 are shown in Figs. 30 and 31 for static-cast and

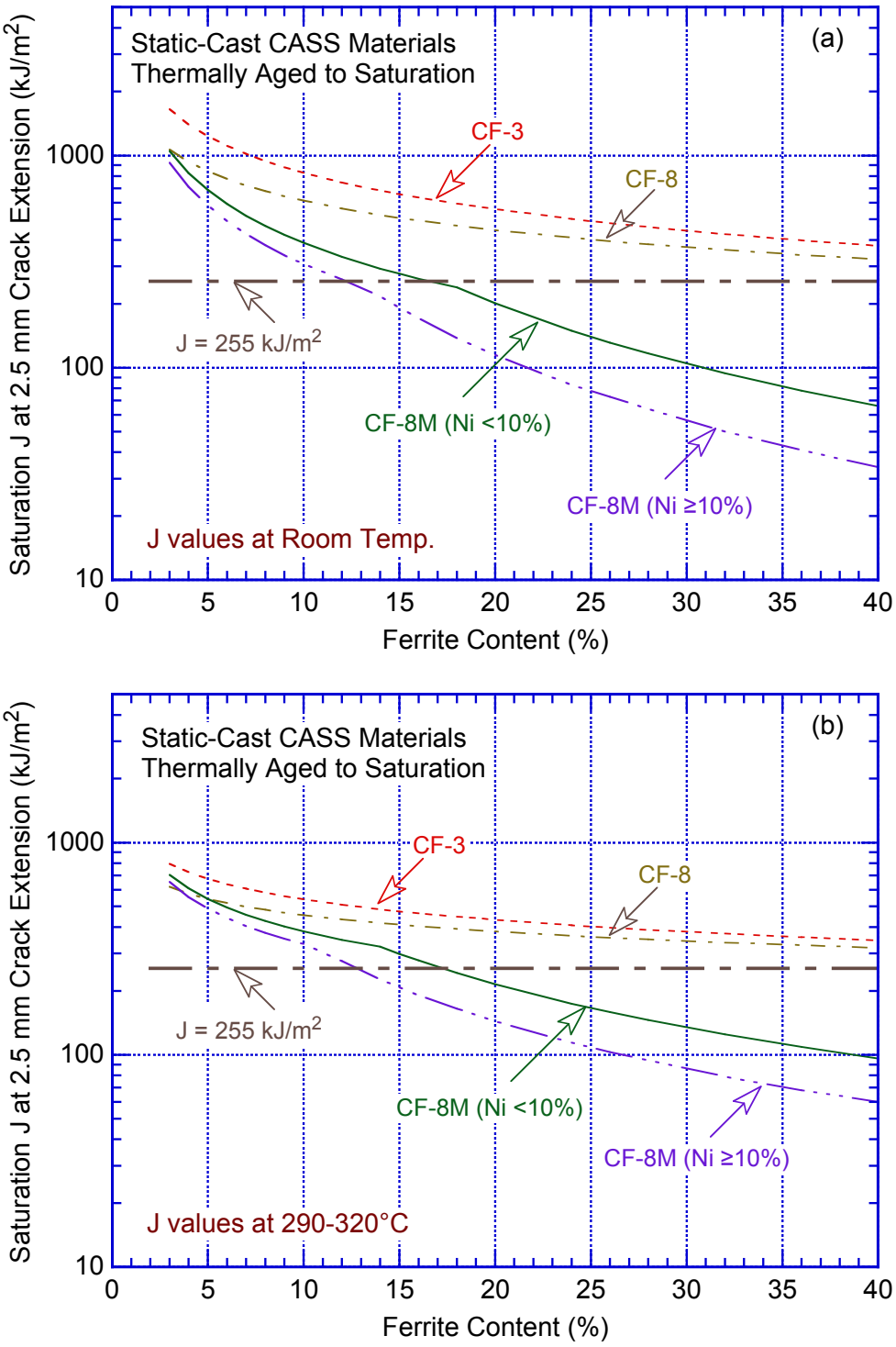

Figure 30. The change in saturation J at 2.5 mm crack extension determined at (a) RT and (b) 290-320°C as a function of ferrite content for static-cast CF-3, CF-8, and CF-8M CASS materials.

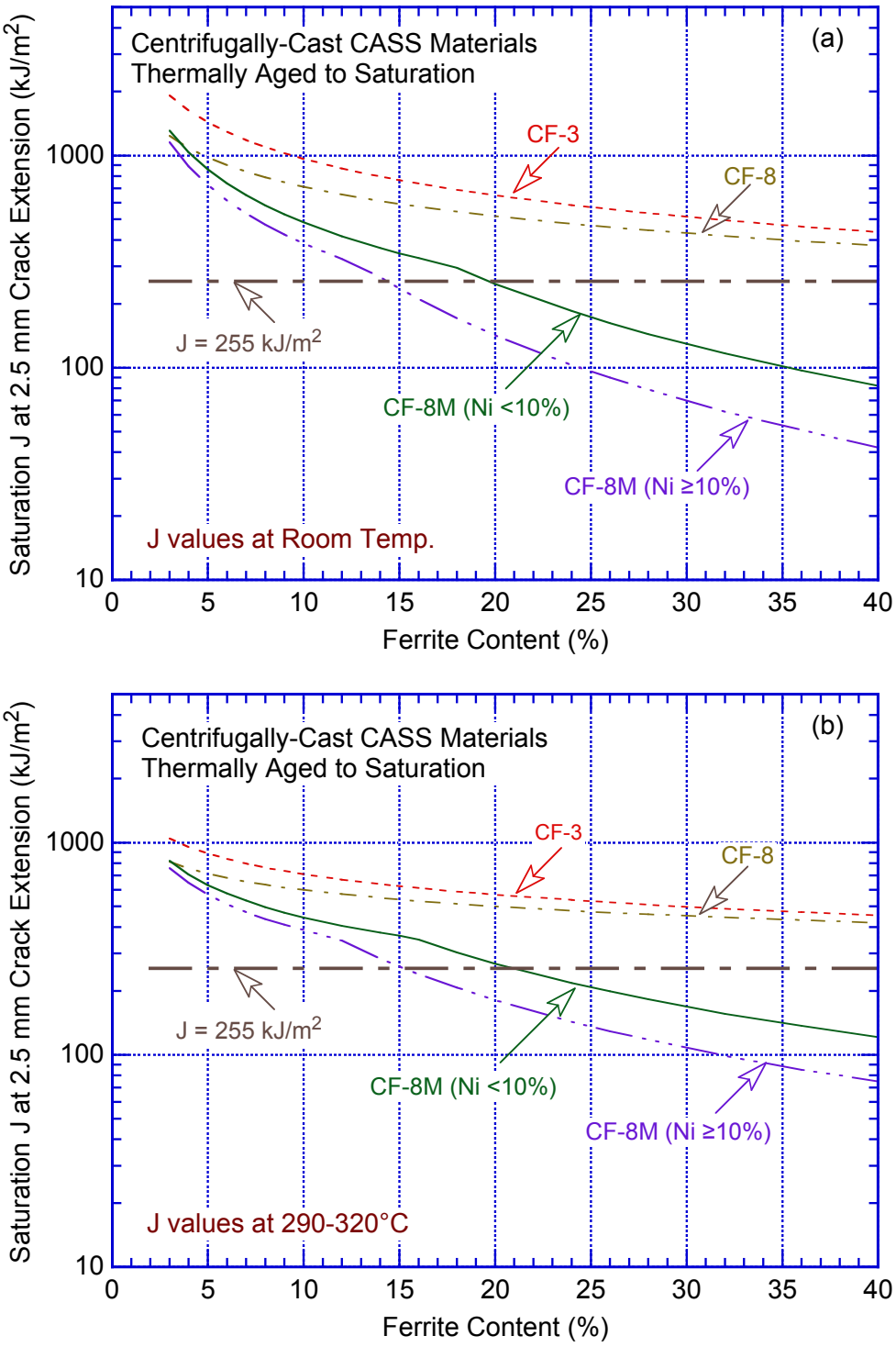

Figure 31. The change in saturation J at 2.5 mm crack extension determined at (a) RT and (b) 290-320°C as a function of ferrite content for centrifugally-cast CF-3, CF-8, and CF-8M CASS materials.

centrifugally-cast CASS materials, respectively. The results indicate that for CF-3 and CF-8 steels, values of $J_{2.5}$ for both static-cast and centrifugally-cast materials are significantly above the threshold value of 255 kJ/m^2, particularly for centrifugally-cast materials. Therefore, the screening criterion that the reduction in fracture toughness due to thermal embrittlement of centrifugally-cast CF-3 and CF-8 steels is "nonsignificant" is valid, and that the reduction in fracture toughness of static-cast CF-3 and CF-8 steels is "significant" only for steels with greater than 20% is a conservative criterion.

Table 4. Screening criteria for thermal-aging susceptibility of CASS CF-3, CF-8, and CF-8M materials.

Mo Content (wt.%)	Casting Method	Ferrite Content	Susceptibility Determination
High (2.0–3.0)	Static	≤14%	Not susceptible
		>14%	Potentially susceptible
	Centrifugal	≤20%	Not susceptible
		>20%	Potentially susceptible
Low (0.5 max.)	Static	≤20%	Not susceptible
		>20%	Potentially susceptible
	Centrifugal	All	Not susceptible

The results for CF-8M steels with <10% Ni indicate that the $J_{2.5}$ values are above the 255 kJ/m^2 threshold value for ferrite contents less than 17% for static-cast materials, and less than about 19% for centrifugally-cast materials. Similarly for CF-8M steels with ≥10% Ni, the $J_{2.5}$ values are above the 255 kJ/m^2 threshold value for ferrite contents less than 12% for static-cast materials, and less than about 14% for centrifugally-cast materials. Therefore, the existing screening criteria for the susceptibility of CF-8M materials to thermal embrittlement, needs to be revised. To provide the same level of safety margin as those for the CF-3 and CF-8 materials, the screening criteria is represented by the ferrite content where the $J_{2.5}$ values in Figs. 30 and 31 decrease below a threshold value of 300 kJ/m^2.

Thus, the threshold ferrite content above which CF-8M materials with <10% Ni are considered “potentially susceptible” to thermal embrittlement, should be decreased from 14% to 13% ferrite for static-cast materials, and from 20% to 17% for centrifugally-cast materials. For CF-8M materials with ≥10% Ni, the threshold ferrite content should be decreased from 14% to 10% for the static cast materials, and from 20% to 13% for the centrifugally-cast materials. The updated screening criteria for thermal-aging susceptibility of CASS CF-3, CF-8, and CF-8M materials are given in Table 5.

Table 5. Updated screening criteria for thermal-aging susceptibility of CASS CF-3, CF-8, and CF-8M materials.

Mo Content (wt.%)	Casting Method	Ferrite Content	Susceptibility Determination
High (2.0–3.0) With <10% Ni (≥10% Ni)	Static	≤13% (≤10%)	Not susceptible
		>13% (>10%)	Potentially susceptible
	Centrifugal	≤17% (≤13%)	Not susceptible
		>17% (>13%)	Potentially susceptible
Low (0.5 max.)	Static	≤20%	Not susceptible
		>20%	Potentially susceptible
	Centrifugal	All	Not susceptible

2.5.5 Methodology for Estimating Thermal Embrittlement of CASS Materials

A flow diagram for estimating mechanical properties of CASS materials during reactor service is shown in Fig. 32. The estimation scheme is divided into three sections based on available material information. In Section A of the flow diagram, "predicted lower-bound" fracture toughness is defined for CF-3, CF-8, and CF-8M steels of unknown composition (i.e., CMTR is not available). For materials with unknown composition, when the ferrite content of the steel is known, a different lower-bound fracture toughness and impact energy are defined for steels containing <10%, 10–15%, 15–25%, or 25–40% ferrite. However, as discussed in Section 2.2, the ferrite content used in this methodology should be representative of the material.

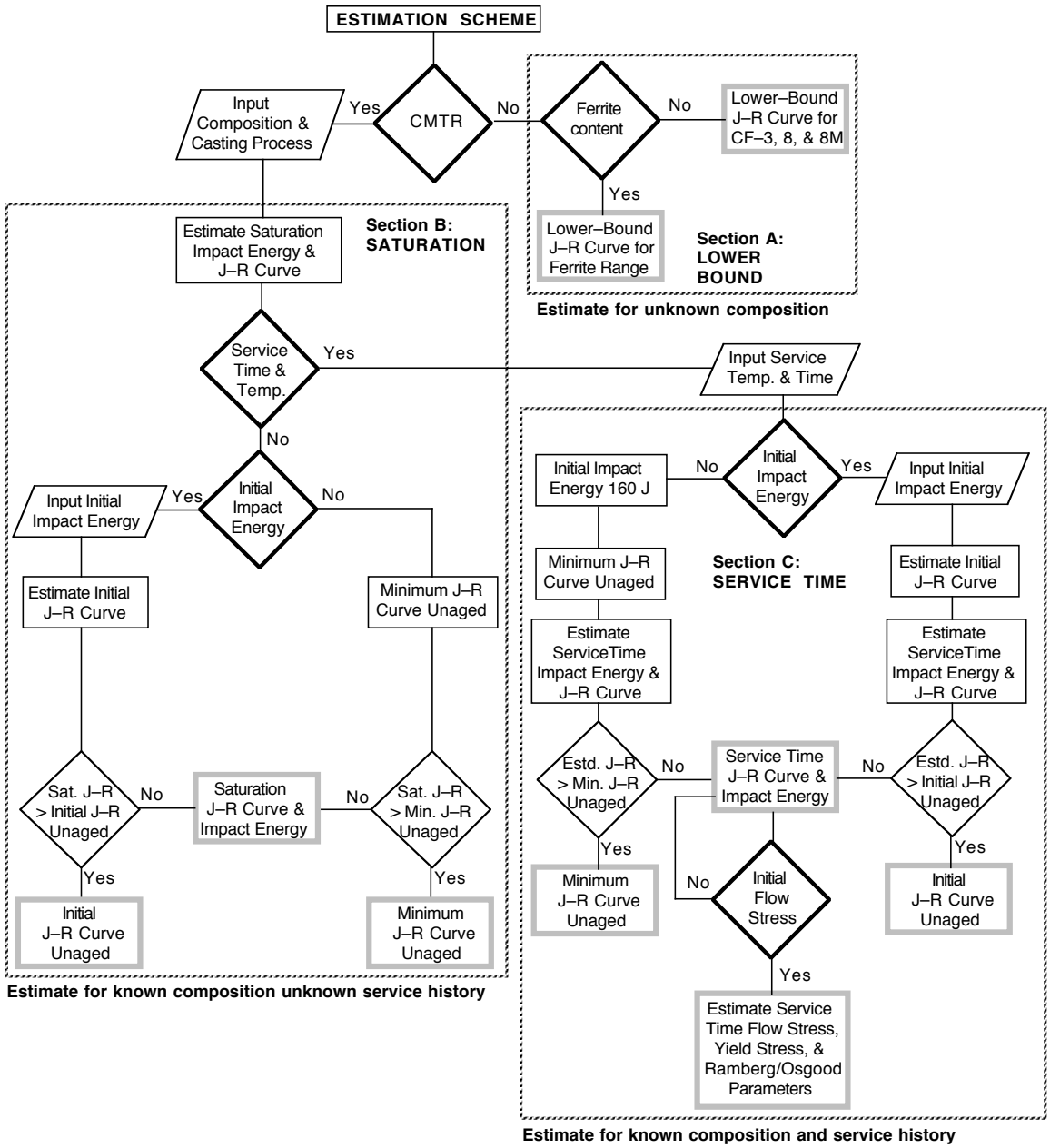

Figure 32. Flow diagram for estimating mechanical properties of thermally aged CASS materials in LWR systems.

The methodology for estimating mechanical properties when a CMTR is available (i.e., the chemical composition of the CASS material is known) is presented in Sections B and C of the flow diagram. Section B describes the estimation of "saturation" impact energy and fracture toughness J-R curve (i.e., the lowest values that would be achieved for a completely thermally-embrittled material). The only information needed for these estimations is the chemical composition of the material, which is used to estimate the saturation J-R curve for the thermally aged material. The correlations presented in this report account for the degradation of mechanical properties due to thermal aging. They do not explicitly consider the initial fracture properties of the unaged material. Some heats of inherently weak CASS materials may have poor fracture properties in the unaged condition, and estimations of saturation fracture toughness based on the methodology presented in this report may be higher than the fracture toughness of the unaged material. The available fracture toughness J-R curve data at 290–320°C (554–608°F) for unaged CASS materials indicate that the J-R curves for a few "weak" heats of static-cast steels may be lower than those for wrought SSs. Therefore, the saturation fracture toughness properties that should be used for design analyses for thermally aged CASS materials depend on whether or not the estimated saturation fracture toughness is lower than the initial fracture toughness of the unaged materials. The initial fracture toughness of the material can be estimated from its RT Charpy-impact energy.

The fracture toughness of the CASS material is not available in CMTRs. Two different options are used to establish the saturation fracture toughness of the thermally aged material. In the first option, the initial RT Charpy-impact energy of the unaged material is known, and this value is used to estimate the initial fracture toughness of the material. CASS materials with poor fracture properties are relatively insensitive to thermal aging and, typically, the fracture toughness of the material does not change significantly due to thermal aging during reactor service. Therefore, if the estimated saturation fracture toughness of aged material is higher than the fracture toughness of the unaged material, the latter is used as the worst-case toughness for that material.

In the second option, the initial RT Charpy-impact energy is not known and, therefore, the minimum fracture toughness of all unaged heats and heat treatment conditions of CASS materials is used as an upper bound for the estimated fracture toughness. This minimum upper-bound fracture toughness of unaged CASS materials is used as the worst-case fracture toughness for the material if the estimated saturation fracture toughness of thermally aged material is higher. The fracture toughness of unaged CASS materials is slightly higher at RT than at 290–320°C. However, for convenience, the minimum fracture toughness of unaged static-cast CASS materials at temperatures between RT and 320°C, can be expressed as

$$J_d = 400[\Delta a]^{0.40}, \tag{43}$$

and of centrifugally-cast CASS materials, as

$$J_d = 650[\Delta a]^{0.43}. \tag{44}$$

Estimation of mechanical properties at any given time and temperature of service (i.e., service time properties) is described in Section C. The initial impact energy of the unaged material is required for these estimations. If not known, the initial impact energy of 200 J/cm^2 (118 ft·lb) is assumed. However, similar to Section B, initial fracture toughness of the unaged material or the minimum fracture toughness of unaged cast stainless steels is used as an upper bound for the estimations. The initial tensile properties of the unaged material are needed for estimations of the tensile strength and Ramberg/Osgood strain hardening parameters. If the initial flow stress

of the CASS material is known, the J_{Ic} value and tearing modulus of the thermally aged material can then be determined from the estimated values of J-R curve and flow stress of the aged material.

However, as mentioned earlier, the above methodology for estimating fracture toughness of CASS materials in reactor service is not applicable for CF-8M materials with more than a trace amount of Nb (e.g., greater than 0.05%). The chemical requirements for ASTM A351 or A451 do not specify any upper limit for Nb. Typically, CF-8M steels contain only trace amounts of Nb. However, the Nb content could be high in castings produced using Type 347 scrap metal. For example, In the Argonne study, the measured RT Charpy-impact energy of a thermally aged heat of CF-8M steel with about 23% ferrite and containing 0.2% Nb, was significantly lower than that predicted from the above methodology. The fracture surface of the Charpy specimen showed that the phase boundaries were decorated with large Nb carbide particles that cracked easily. The available thermal embrittlement data on CF-8M materials is inadequate to accurately establish the threshold Nb content above which it contributes to increased embrittlement of the material. Therefore, for CF-8M materials with greater than 15% ferrite, it would be advisable to determine the Nb content of the material, and take appropriate action if the it is greater than 0.05%.

2.6 Extent of Thermal Embrittlement of Austenitic Stainless Steel Welds

In an earlier study at Argonne[48–51] on thermal embrittlement of CASS materials the methodology and correlations were developed for estimating fracture toughness, tensile, and Charpy-impact properties of CASS components during service from known material information. Although austenitic SS welds have a duplex structure and their chemical compositions are similar to those of CASS materials, the estimation scheme was not applicable to austenitic SS welds. The degradation of fracture toughness, tensile, and Charpy-impact properties of welds due to thermal aging was characterized in another report.[53] Five Type 304/308 or 308L welds were aged for 7,000–1,0000 h at 400°C to simulate saturation conditions (i.e., lowest impact energy that would be achieved by the material after long-term aging) and the results were compared with fracture toughness data from other studies. The ferrite morphologies of four of the five welds that were investigated are shown in Fig. 4. The J-R curves are expressed by the power-law relation $J_d = C(\Delta a)^n$ per ASTM Specifications E 813-85 and E 1152-87.

The results indicated that for austenitic SS welds, thermal aging resulted in moderate decreases in Charpy-impact strength and fracture toughness at both room temperature and 290°C. For the various welds, upper-shelf energy (USE) decreased by 50–80 J/cm^2 (30–47 ft·lb.). The decrease in the fracture toughness J-R curve or J_{Ic} was relatively small. Metallographic examination of the specimens indicated that failure occurred by the formation and growth of microvoids near hard inclusions. Such processes are relatively insensitive to thermal aging. Fracture resistance of the PWWO weld was inferior to that of the PWCE weld because of a higher density and a larger size of inclusions. Furthermore, the ferrite phase had little or no effect on the fracture properties of the welds because of its thin vermicular morphology and relatively low content (e.g., 6–8% ferrite).

The fracture toughness J-R curve data from the work conducted for the NRC and compiled in the Pipe Fracture (PIFRAC) Database* and from a few other sources,[40,89–93] are shown in Fig. 33. The PIFRAC database, consisting of the data from Refs. 94–98 was originally compiled at MEA,[99] and updated later by Battelle Memorial Institute.[100] The results indicate that fracture

* G. Wilkowski and N. Ghadiali, "Short Crack in Piping and Piping Welds," in Technical Data CD-ROM, Battelle Columbus Division, Columbus, OH (May 1995).

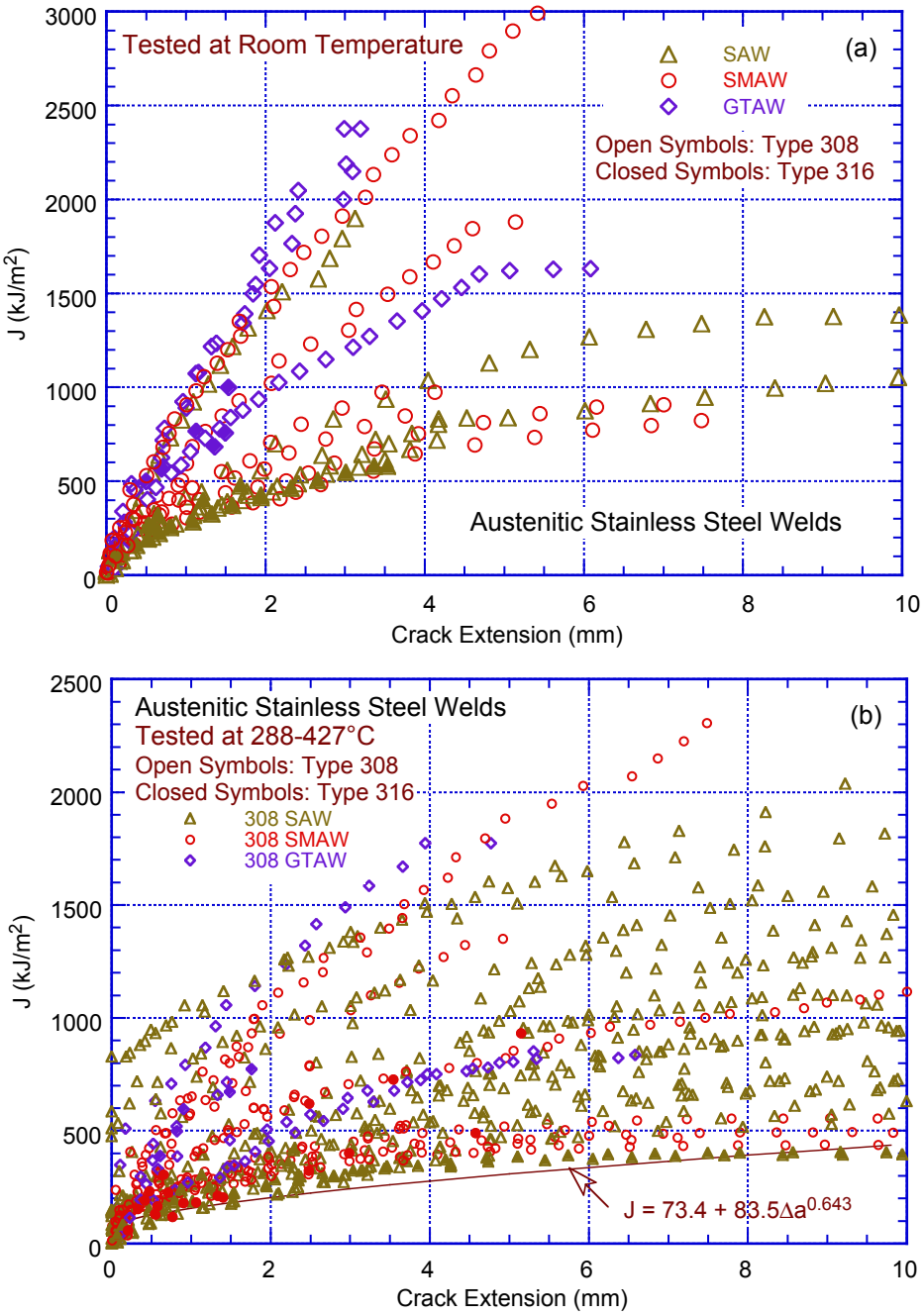

Figure 33. Fracture toughness J-R curves for stainless steel welds at (a) RT and (b) 288–427°C. Solid line represents lower-bound curve.

properties of SS welds are relatively insensitive to filler metal.[40] However, the welding process significantly affects fracture toughness. In general, GTA welds exhibit higher fracture resistance than SMAs or SA welds. The statistical differences in SA and SMA weld fracture toughness J-R curves have also been evaluated[101] and results indicate no difference between SA and SMA welds J-R curves. At 288°C, the lower-bound fracture toughness J-R curve for SA and SMA welds[101] is represented by

$$J(kJ/m^2) = 73.4 + 83.5\ \Delta a(mm)^{0.643} \quad (45)$$

where 73.4 kJ/m^2 is the fracture toughness J_{Ic}. The lower-bound curve for SA and SMA welds shows very good agreement with the data in Fig. 33. The fracture toughness data used in the analysis performed for the technical basis document for ASME Section XI Article IWB-3640 are somewhat higher than the curve given by Eq. 45. The data scatter in the fracture toughness J-R curve obtained at 200 and 288°C (392 and 550°F) for Linde 80 weld metal[102] is shown in Fig. 34. The J-R curve reconstructed form the data for the ASME IWB-3640 SA weld and the lower-bound J-R curve proposed in NUREG/CR-6004 for austenitic SS welds (i.e., Eq. 45), are also shown in the figure. The results indicate that most of the Linde 80 data are bounded by the lower-bound curve.

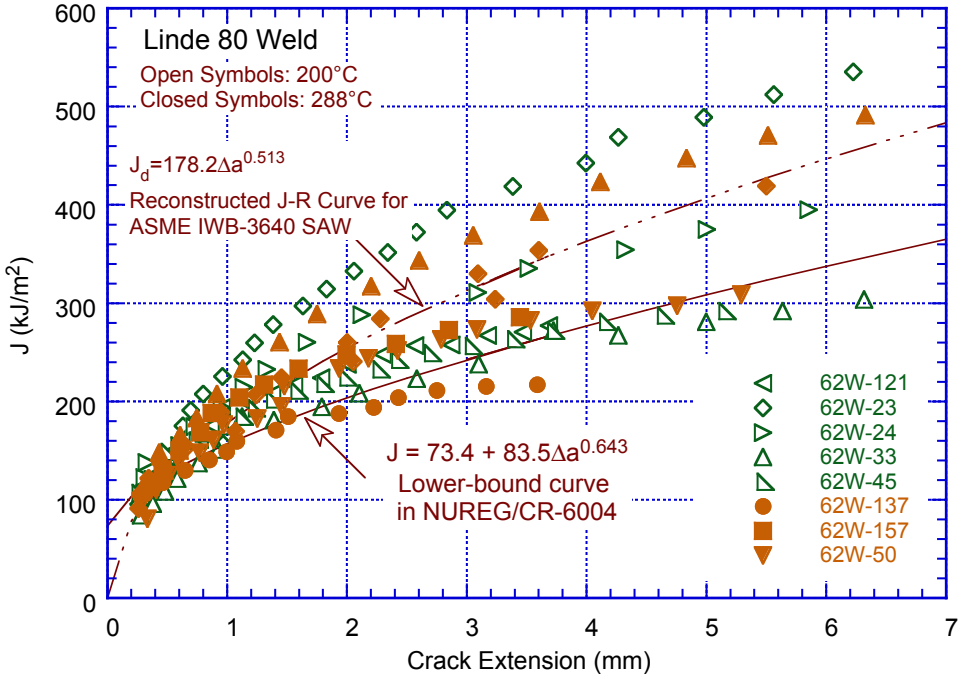

Figure 34. Fracture toughness J-R curves for Linde 80 welds at 200 and 288°C and the lower-bound J-R curve for unaged austenitic SS welds.

The available fracture toughness J-R curves for aged SMA, SA, and GTA welds are shown in Fig. 35.[41,90,103] In these studies, the time and temperature of aging was sufficient to achieve saturation toughness (i.e., the minimum value that could be achieved after long-term aging).

The J_{Ic} values for unaged and aged welds are plotted in Fig. 36. The results indicate that the J_{Ic} values for SA or SMA welds are generally lower than for the GTA welds. The one exception is the values for a Type 316L GTA weld, which are significantly lower than typically observed for GTA weld, both at RT and at 288°C. The reason for the low fracture toughness values is not known. The data also indicate that at reactor temperatures, the fracture toughness J_{Ic} of SS welds can be as low as 40 kJ/m^2. Hence, the fracture toughness J-R curves for fully embrittled SMA and SA welds can be lower than that predicted by Eq. 45; a conservative estimate for aged welds may be expressed as

$$J(kJ/m^2) = 40 + 83.5\ \Delta a(mm)^{0.643}. \qquad (46)$$

This curve is plotted in Fig. 35. The fracture toughness J-R curves for unaged and aged SS welds (i.e., Eqs. 45 and 46, respectively) are compared in Fig. 37 with the data for aged 316L

and CF-3 welds[90,104] and the data in the technical basis document for ASME Section XI Article IWB-3640.[95] Note that the data from Ref. 95 are modified J, and the deformation J values would be slightly lower.

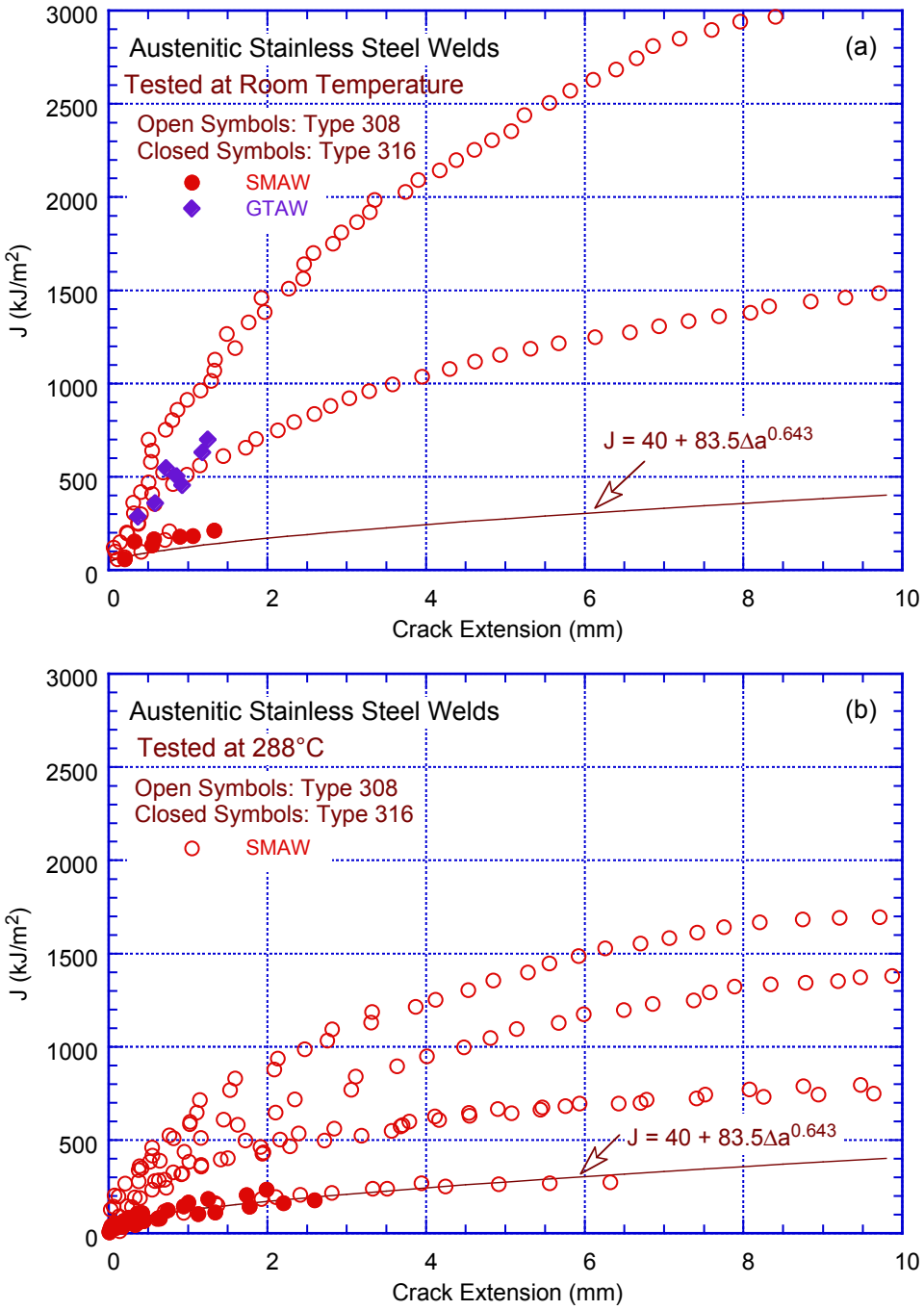

Figure 35. Fracture toughness J-R curves for aged stainless steel welds at (a) RT and (b) 288°C. Solid line represents lower-bound curve.

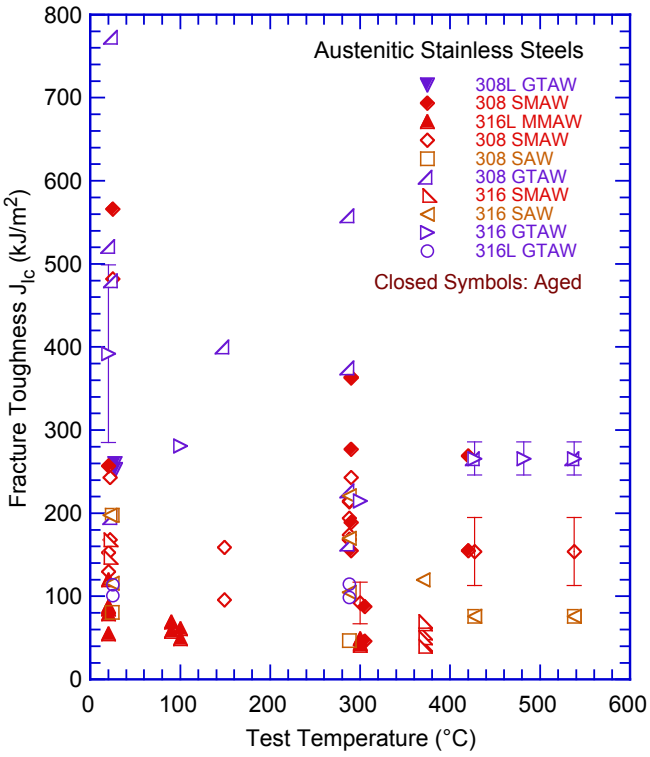

Figure 36.
Fracture toughness J_{Ic} for unaged and aged stainless steel welds.

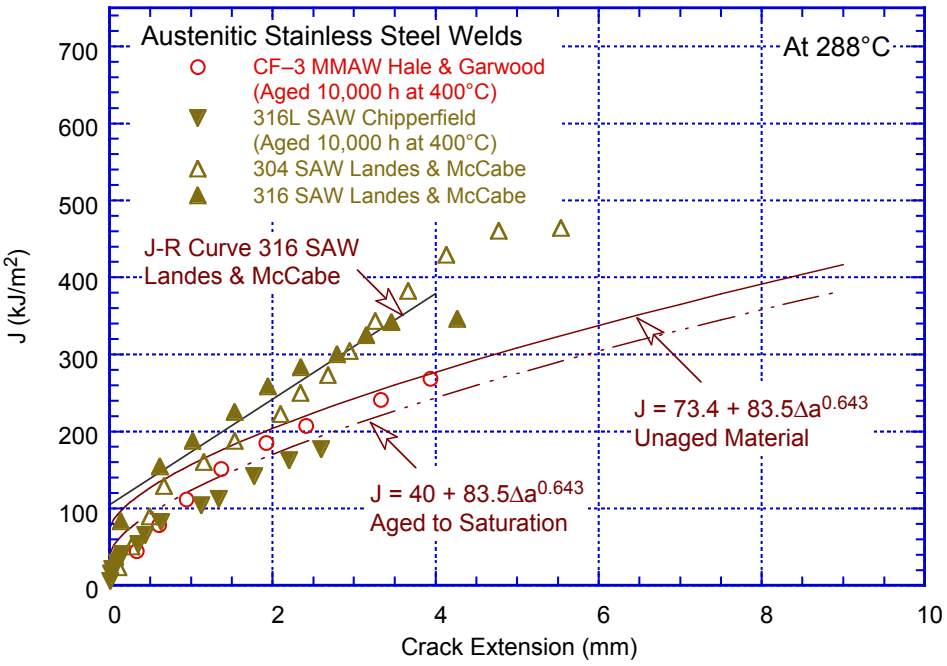

Figure 37. Fracture toughness lower-bound J-R curves and the data on unaged and aged 304, 316L, and CF-3 welds used to develop the ASME Code IWB-3640 analysis.

2.6.1 Update of Thermal Embrittlement Data for Austenitic Stainless Steel Welds

The J-R curve data for GTA, SMA, and SA welds of Type 308 and 16-8-1 SSs in air at 24 and 427°C is shown in Fig. 38.[40] The ferrite contents measured in the Type 16-8-1 GTA and SA welds were 5.7% and 9.0% respectively, and in the Type 308 GTA, SA, and SMA welds were 9.9%, 10.7%, and 7.0%, respectively. The results indicate that the fracture toughness of GTA weld is superior to that of SMA weld, which is superior to that of the SA weld. The fracture toughness at room temperature (i.e., closed symbols in the figure) is slightly higher than that at 427°C (i.e., open symbols). All of the data are bounded by the lower-bound J-R curve given by Eq. 45.

The fracture toughness J-R curve data for unaged and aged Type 308 SS GTA and SMA welds in air at 427°C is shown in Fig. 39.[41] The results indicate little or no effects of long-term aging (i.e., 10,000 h at 400°C) on the fracture toughness of GTA and SMA welds in air at 427°C. Little or no effect of thermal aging at 400°C on the fracture toughness of Type 304/308 SS pipe welds was also observed in an earlier study at Argonne.[53] The fracture toughness J-R curve data at 25 and 290°C for unaged and aged Type 304/308 pipe weld and a Type 304/308L pipe weld are shown in Figs. 40a and 40b, respectively.[53] The Type 308 weld was aged 10,000 h at 400°C and the Type 308L weld aged 7,700 h at 400°C. The measured ferrite content was 6.1% in the Type 304/308 and 6.8% in the Type 304/308L weld. The difference between the J-R curve data at both room temperature and 290°C, for unaged and aged welds is within the typical data scatter for fracture toughness tests. The results suggest that for Type 308 weld metal, thermal aging may not have a significant effect on its fracture toughness. However, the data for CF-3 MMA and 316L SA welds aged for 10,000 h at 400°C, the measured fracture toughness J-R curve data are both below the lower-bound J-R curve given by Eq. 45. A lower-bound J-R curve expressed by Eq. 46 was proposed in NUREG/CR-6428 for thermally aged austenitic SS welds.

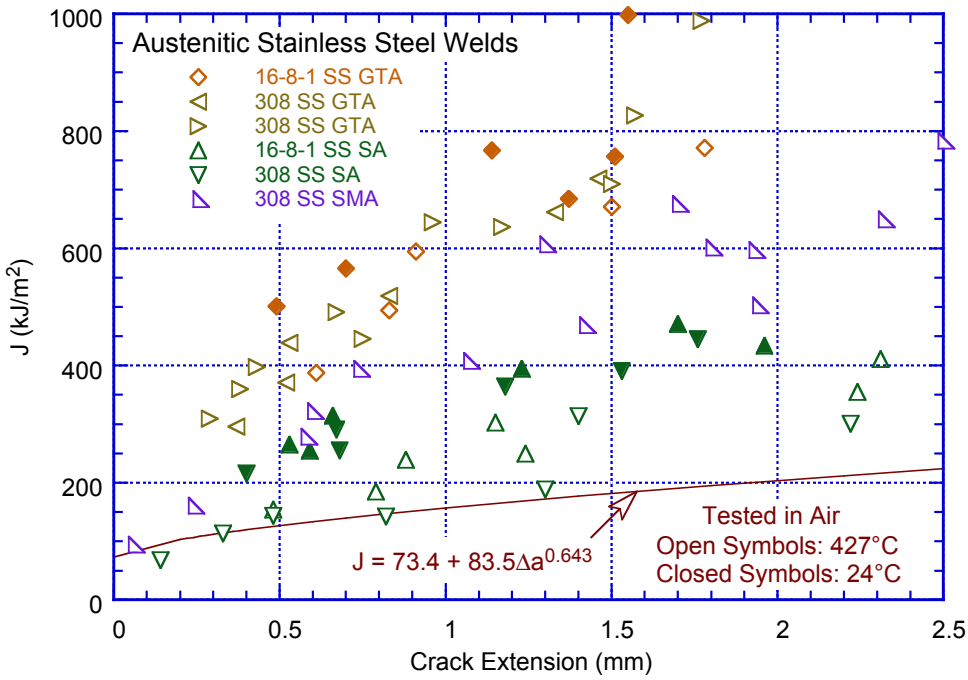

Figure 38. Fracture toughness J-R curve data for GTA, SMA, and SA welds in air at RT and 427°C (Ref. 40).

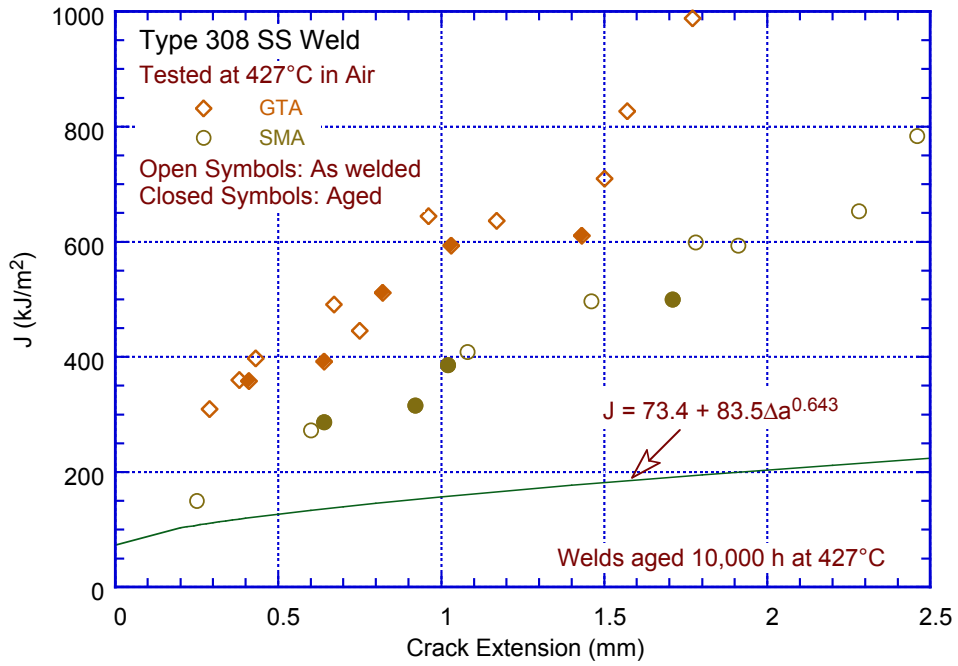

Figure 39. Fracture toughness J-R curve data for unaged and aged Type 308 SS GTA and SMA welds in air at 427°C (Ref. 40).

The fracture toughness J-R data obtained on two heats of Type 316L GTA weld obtained in air and in high-purity water with 300 ppb DO are plotted in Fig. 41.[105,106] The measured ferrite contents in the two welds were 10% and 14%. The results indicate that in-situ fracture toughness in the reactor coolant environment can result in a reduction of toughness by up to 40% relative to that in air. The in-situ properties degradation was attributed to absorption of hydrogen in the material during exposure to the high temperature aqueous environment.[105] The

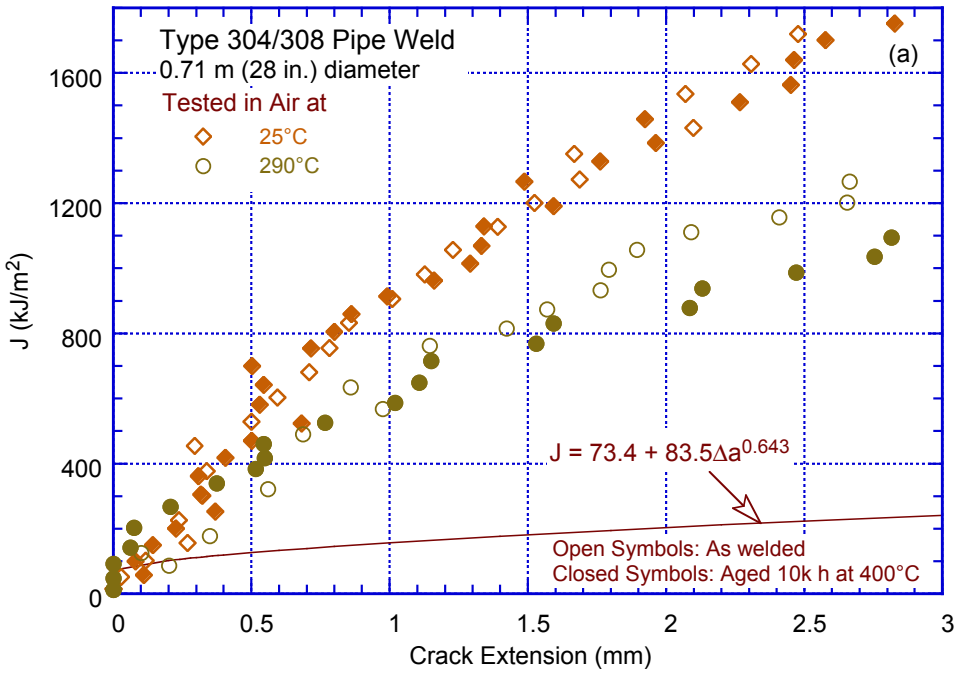

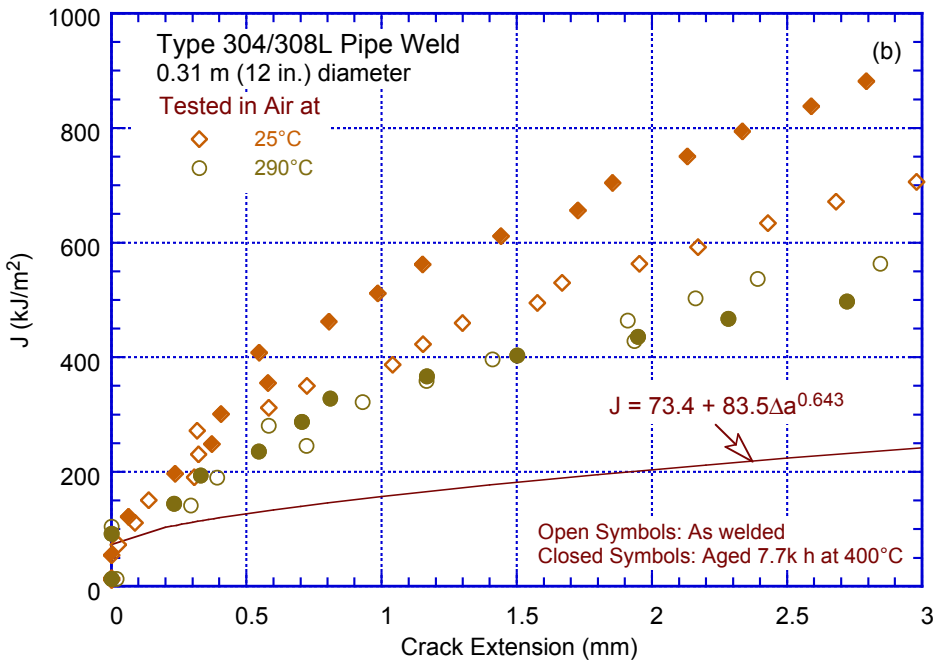

Figure 40. Fracture toughness J-R curve data for unaged and aged (a) Type 304/308 and (b) Type 304/308L pipe welds in air at 25 and 290°C (Ref. 53).

results also show that the fracture toughness of unaged austenitic SS welds in LWR environments may be below the lower-bound J-R curve for aged welds given by Eq. 46. Additional data are needed to establish the in-situ fracture toughness degradation of SS welds in LWR environments.

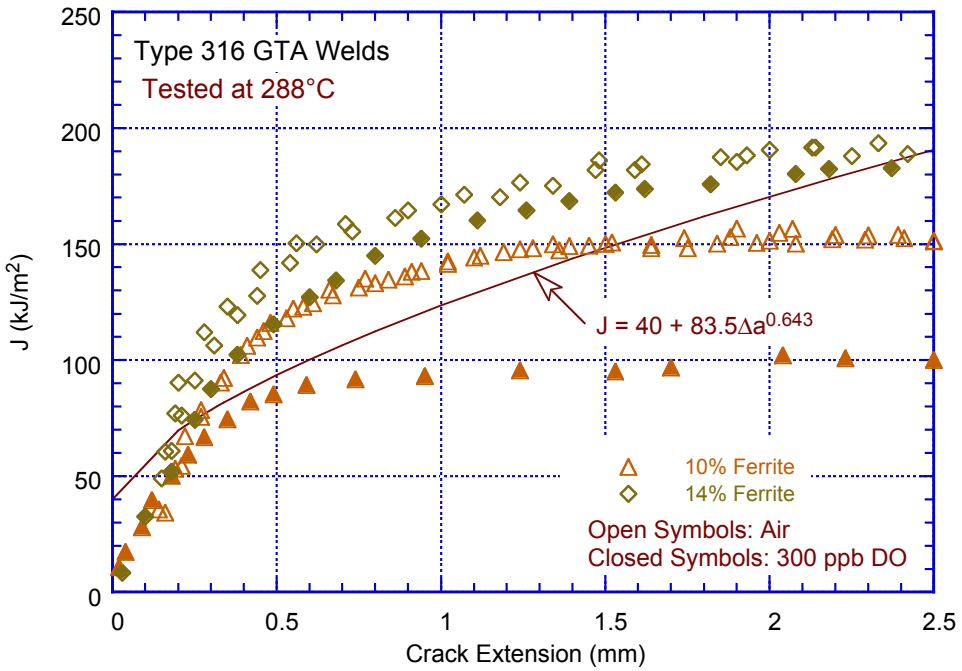

Figure 41. Fracture toughness J-R curve data for as-welded Type 316L GTA weld at 288°C in air and BWR environment with 300 ppb DO (Ref. 105).

This page is intentionally left blank.

3. IASCC Crack Growth Rates

A major concern regarding the structural and functional integrity of LWR core internal components is IASCC of structural materials (i.e., primarily austenitic SSs). Several incidents of IASCC have occurred since the mid-1970s in control blade handles and instrumentation tubes of BWRs, and since the 1990s, in BWR core shroud and PWR baffle bolts. As the name implies, IASCC is literally the irradiation-assisted enhancement of SCC susceptibility of materials. The susceptibility of austenitic SSs to IASCC has been investigated by conducting slow-strain-rate-tensile (SSRT), CGR, and crack initiation tests on irradiated material in simulated LWR environments[107–117]. The factors that influence IASCC of austenitic SSs include neutron irradiation conditions such as neutron fluence, flux, and energy spectrum, cold work, material composition, corrosion potential, water purity, temperature, and loading conditions. The susceptibility of austenitic SSs to IASCC increases with neutron fluence, corrosion potential, and water conductivity.

Furthermore, radiolysis of water leads to its dissociation into various molecular, ionic, and radical reaction products that interact to form H_2O_2, H_2, and O_2. In BWRs, these species increase the corrosion potential, which is known to increase the susceptibility of SSs to IASCC. Experimental data on Type 304 and 316 SSs irradiated up to 4.0×10^{21} n/cm^2 (6.0 dpa) show a beneficial effect of reducing the corrosion potential of the environment on IASCC susceptibility.[27,28] For example, the addition of H_2 to the reactor water greatly reduces the effect of radiolysis by scavenging the radiolysis products.[117] Since PWR coolants typically contain 2 ppm H_2 by weight or 30 cc/kg, radiolysis has no effect on the corrosion potential in PWRs. However, a low corrosion potential does not provide immunity to IASCC if the fluence is high enough; intergranular stress corrosion cracking (IGSCC) has been observed in baffle bolts in PWRs. Threshold fluence for IASCC is higher under low-potential BWR hydrogen water chemistry (HWC) or PWR primary water chemistry. It also varies with material composition and thermo-mechanical treatment.[27]

Laboratory SSRT data on irradiated austenitic SSs have been used to identify a threshold fluence above which IASCC is significant in austenitic SSs in normal water chemistry (NWC) BWR environments.[4,27,118,119] A threshold fluence level of 5×10^{20} n/cm^2 (E >1 MeV)* (0.75 dpa)† has been proposed for austenitic SSs in NWC BWR environments. However, the results in Fig. 42 indicate that the intergranular cracking susceptibility in some commercial-purity SSs increases rapidly at fluence levels above about 2×10^{20} n/cm^2 (0.3 dpa) and in high-purity heats of SSs at even lower fluence levels.

3.1 Effects of Material and Environmental Parameters on IASCC Susceptibility

In an earlier Argonne study,[21] the existing data have been reviewed to identify the key material parameters (such as composition, thermo-mechanical treatment, microstructure, microchemistry, yield strength, and stacking fault energy) and environmental parameters (such as water chemistry, irradiation temperature, dose, and dose rate) that influence IASCC, and to establish their effects on IASCC susceptibility of austenitic SSs. Discussions of some of those parameters follow.

* Unless otherwise mentioned otherwise all references to fluence levels are calculated for E ≥1 MeV.
† Conversion to dpa for LWRs, is E > 1 MeV and 10^{22} n/cm^2 ~ 15 dpa.

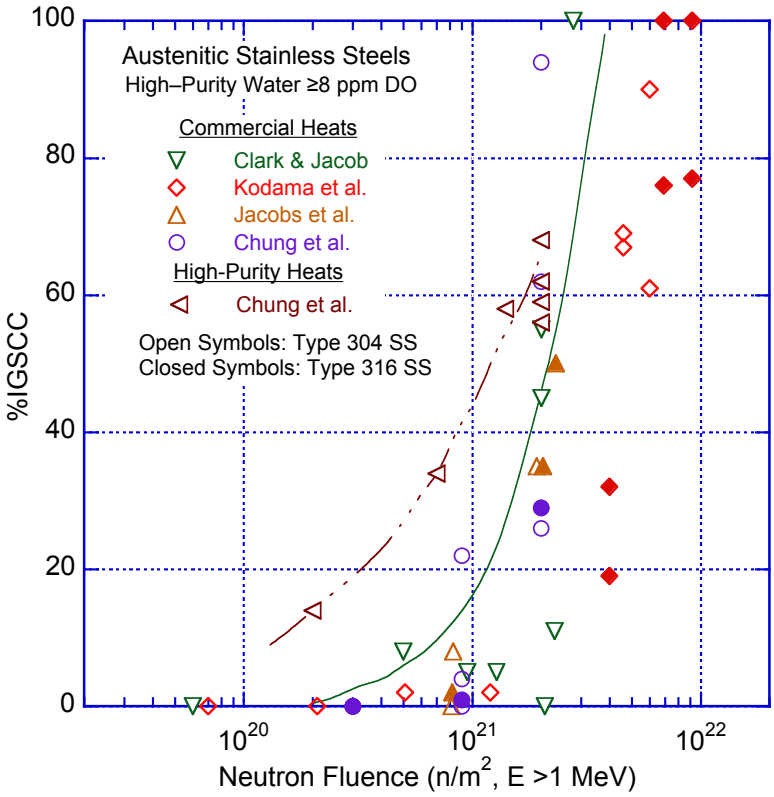

Figure 42. Susceptibility of irradiated austenitic SSs to IGSCC as a function of fluence in high-DO water.

3.1.1 Microstructure

The microstructural changes in austenitic SSs due to neutron irradiation vary with the material composition, irradiation temperature, and neutron fluence, flux, and energy spectrum. Irradiation damage is characterized by either the neutron fluence (n/cm^2) or the average number of displacements per atom (dpa). For BWR-irradiated SSs (i.e., irradiated at 275–300°C), the loop density saturates at about 1 dpa, and the average loop diameter saturates at 5 dpa. In general, the loop size increases and loop density decreases with irradiation temperature. Irradiation temperatures above 350°C lead to the formation of second phase particles.[5,23,120–123] Cavities and voids form at high doses and high temperatures. Under LWR conditions, metal carbides are the primary stable precipitates in 300-series SSs, although RIS of Ni and Si to sinks may lead to the formation of γ' phase (Ni_3Si) and G phase ($M_6Ni_{16}Si_7$). The microchemistry of the material is also changed due to RIS; Si, P, and Ni are enriched at regions such as grain boundaries, while Cr, Mo, and Fe are depleted. The extent of RIS depends on irradiation temperature and dose rate. At LWR temperatures, significant segregation is observed at an irradiation dose of 0.1 dpa, and the effect either saturates or changes very slowly beyond 5 dpa.

3.1.2 Microchemistry

Neutron irradiation also changes the microchemistry of the material due to RIS. The migration of vacancies and self-interstitial atoms to sinks, such as grain boundaries, dislocations, or precipitate surfaces, leads to local compositional changes. Elements such as Si, P, and Ni that are believed to migrate by interstitial mechanisms are enriched near regions that act as sinks for the point defects, while elements such as Cr, Mo, and Fe that exchange more rapidly with vacancies are depleted near sinks.[2,4,5] The extent of segregation or depletion depends on the

rate of generation and recombination of point defects (i.e., it depends on irradiation temperature and dose rate). Typically, RIS peaks at intermediate temperatures. It is reduced at low temperatures because of reduced mobility and at high temperatures due to back diffusion. For a specific neutron dose, RIS is greater at lower dose rate.

Most austenitic SSs show a rapid decrease in Cr to about 13 wt.% and an increase in Si to about 4 wt.% at 5 dpa.[23] The data at dose levels above 10 dpa are limited, but they indicate that Cr content can decrease to 8–10 wt.% and Si content increase to 6 wt.% in SSs irradiated in LWRs at 300–320°C up to 65 dpa.[23] Under similar irradiation conditions, grain boundary Ni concentrations increase to about 22 wt.% at 5 dpa and can be as high as 30 wt.% at 65 dpa. The RIS behavior of minor elements such as P, C, N, and B, all of which segregate at the boundary, is not well established.

3.1.3 Radiation Hardening

The point defect clusters and precipitates produced by irradiation act, to varying extent, as obstacles to dislocation motion, resulting in an increase in tensile strength and a reduction in ductility and fracture toughness of the material. In general, cavities (or voids) are strong barriers, large faulted Frank loops are intermediate barriers, and small loops and bubbles are weak barriers to dislocation motion.[1] The yield strength of irradiated SSs can increase up to five times that of the non-irradiated material after a neutron dose of about 5 dpa.[3] The yield and ultimate stresses increase and ductility decreases with irradiation. The extent of irradiation hardening and the increase in yield stress of austenitic SSs depend on the material composition and thermo-mechanical treatment, as well as the irradiation temperature. The greatest increase in yield strength for a given dose occurs at irradiation temperatures near 300°C (572°F). For a given neutron dose and irradiation temperature, the yield strength decreases with increasing test temperature.

At high neutron doses, as the irradiated yield strength approaches the ultimate strength of the material, there is a change in the deformation mode. Deformation by a planar slip mechanism is promoted, and the material exhibits strain softening.[114] This process can be explained by "dislocation channeling," whereby dislocation motion along a narrow band of slip planes clears the irradiation-induced defect structure, creating a defect-free channel that offers less resistance to subsequent dislocation motion or deformation. Nearly all SSs exhibit strain softening, and little or no uniform elongation, at irradiation dose above 3–5 dpa.[115,116] The enhanced planar slip also leads to a pronounced degradation in the fracture toughness of austenitic SSs.

3.1.4 Yield Strength

Three elements in combination influence IGSCC of austenitic SSs in BWR environments: a susceptible material, a significant tensile stress, and an aggressive environment. Low-C wrought austenitic SSs and weld metals are considered adequately resistant to sensitization by welding[126] and therefore are recommended to reduce the susceptibility to IGSCC. However, Andresen has shown that nonsensitized SSs are not immune to SCC; SSs with high yield strength are susceptible to IGSCC in ultra-high purity water.[117] The CGRs of austenitic SSs increase with increasing yield strength. The effect of yield strength on the SCC growth rates of LWR irradiated austenitic SSs in NWC and HWC BWR environments at 289°C is shown in Fig. 43.[20,124] Increases in yield strength can originate from surface or bulk cold work, weld shrinkage strain, precipitation hardening, oxide dispersion hardening, or even irradiation hardening; all of these increase SCC growth rates. At a given yield strength, a similar susceptibility to cracking is observed in high- and low-potential environments; however, the

CGRs in low potential water are an order of magnitude lower.[117] There is no significant difference among the different grades of SSs. The yield strength of irradiated austenitic SSs can increase up to five times that of the nonirradiated material after a neutron dose of about 5 dpa.[29] For austenitic SSs, the greatest increase in yield strength for a given irradiation level occurs at irradiation temperatures near 300°C (572°F).

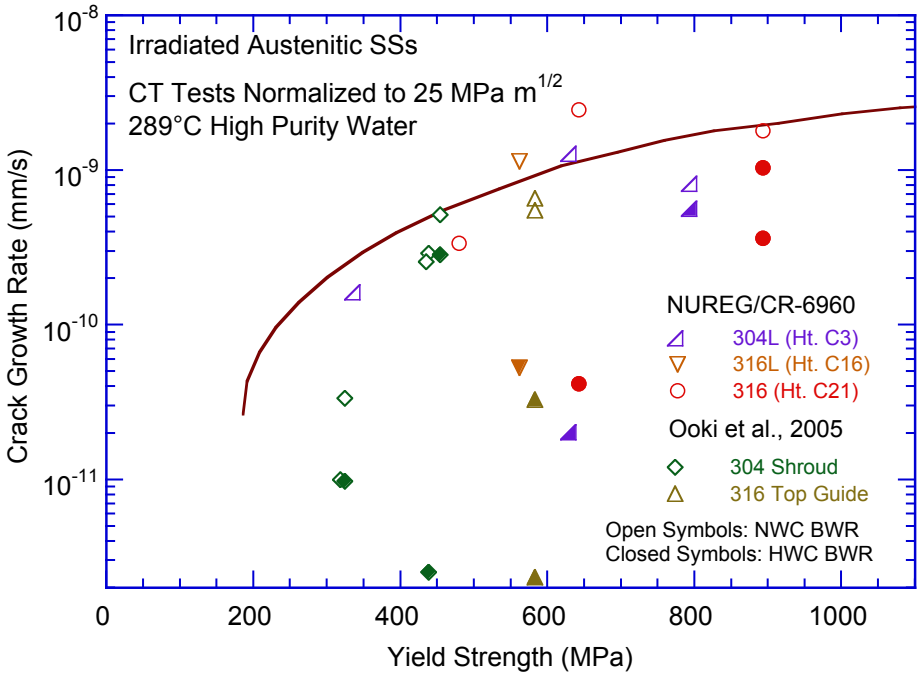

Figure 43. Change in SCC growth rates at 289°C of LWR irradiated austenitic SSs as a function of yield strength in NWC and HWC BWR environments (Refs. 20, 124).

3.1.5 Silicon Segregation

The increased susceptibility to IASCC and the loss of benefit of reducing potential in highly irradiated SSs have been attributed to the segregation of Si at the grain boundaries. The Si segregation is detrimental because at all relevant pH/potential conditions, Si oxidizes to SiO_2, which is highly soluble in hot water. Unusually high SCC growth rates have been observed in cold worked (CW) SSs, containing 1.5 to 5 wt.% Si, in high-purity water with 2 ppm (by weight) DO.[125] The CGR in 15% CW Type 304L SS with 5% Si (no Mo, Nb, or Ti additions) at 220°C (yield strength about 500 MPa) was 2.2×10^{-9} m/s at a stress intensity factor (K) of about 30 MPa $m^{1/2}$. The observed rate is a factor of 10 higher than the rates in most commercial SSs with similar levels of cold work/yield strength. More significant, the rate did not decrease when the environment was changed from high potential to low potential (95 ppb H_2). In addition, decreasing K resulted in an initial decrease in CGR, from 2.2 to 1×10^{-9} m/s, but thereafter the CGR remained constant as the K decreased from 30 to 15 MPa $m^{1/2}$ (Figs. 8 and 9 in Ref. 125).

In contrast to the increased susceptibility of high-Si materials indicated by crack growth tests, SSRT test data on irradiated Type 304 and 316 SSs with 0.5–1.8 wt.% Si show the opposite behavior. For the same fluence level, steels with 1.5 to 1.8 wt.% Si showed less irradiation hardening and greater elongation than steels containing 0.5 wt.% Si.[116] Because most commercial SSs contain about 0.5% Si, its effect on irradiation hardening is not likely to be significant. Available data suggest that high concentrations of Si at grain boundaries due to RIS

could increase susceptibility to IASCC. The absence of γ′ silicide (Ni_3Si) at the grain boundaries suggests that RIS of Ni and Si probably saturates at higher doses; however, there is no evidence that Si segregation saturates at high dose. The significance of Si segregation at grain boundaries on the SCC behavior of irradiated SSs is not clear, but Si segregation could be important.

3.1.6 Stacking Fault Energy

The stacking fault energy (SFE) is an important parameter that determines the deformation mode. Alloys with Ni concentration >18 wt.% are highly resistant to IASCC compared to Type 304 SS with 8 wt.% Ni.[3] Alloys with low SFE, such as SSs with 8 wt.% Ni, deform entirely by planar slip, whereas there is no evidence of planar slip in alloys with high SFE (with >20 wt.% Ni). The increased susceptibility to IASCC is attributed to absorption of dislocations at the grain boundaries, which may cause grain boundary sliding ahead of the crack tip, resulting in crack extension and IASCC. Alternatively, progressively higher stresses at the grain boundary can change the film rupture frequency, thereby exposing bare metal surface and leading to oxidation/dissolution and crack extension.

3.2 IASCC Crack Growth Rates

3.2.1 In BWR and PWR Environments

In an earlier study at Argonne,[21,29] the SCC CGR data for irradiated wrought and cast austenitic SSs as well as austenitic SS weld metal and weld HAZ materials in LWR environments were compiled and evaluated to define threshold fluence for IASCC and to develop disposition curves for cyclic and IASCC growth rates for reactor core internal materials. The importance of test procedures that closely reproduce the loading and environment conditions for reactor core internal components were discussed. The SCC CGRs for various grades and heats of austenitic SSs irradiated from 5×10^{20} to 2.5×10^{22} n/cm^2 (0.75 to 37.5 dpa) and tested in NWC and HWC BWR environments are shown in Figs. 44 and 45, respectively. The results are compared with the K versus CGR disposition curves proposed in the NRC report NUREG-0313 for nonirradiated sensitized austenitic SSs in high-purity water[126] and the curve proposed by EPRI for austenitic SS BWR core internal components.[127] The NUREG-0313 disposition curve is expressed as

$$da/dt\ (m/s) = A1\ (K)^{2.161}, \tag{47}$$

where the stress intensity factor, K, is in MPa m$^{1/2}$, and the magnitude of A1 depends on the water chemistry. The value of A1 is 2.1×10^{-13} in water with 8 ppm DO and 7.0×10^{-14} in water with 0.2 ppm DO. It is smaller in low-potential HWC BWR and PWR primary water environments. The EPRI disposition curve for use in BWR core environments is expressed as

$$da/dt\ (m/s) = A2\ (K)^{2.5}, \tag{48}$$

where the constant A2 is 4.564×10^{-13} in NWC BWR and 1.512×10^{-13} in HWC BWR environments. The EPRI correlations are based on two datasets; General Electric (GE) and Japan Power Engineering and Inspection Corp. (JAPEIC) data for SSs irradiated to 4.0–4.5 dpa,[127] and the Halden reactor data for Type 304, 347, and 316NG SSs that were irradiated to 13.5, 2.25, and 1.35 dpa.[128–132]

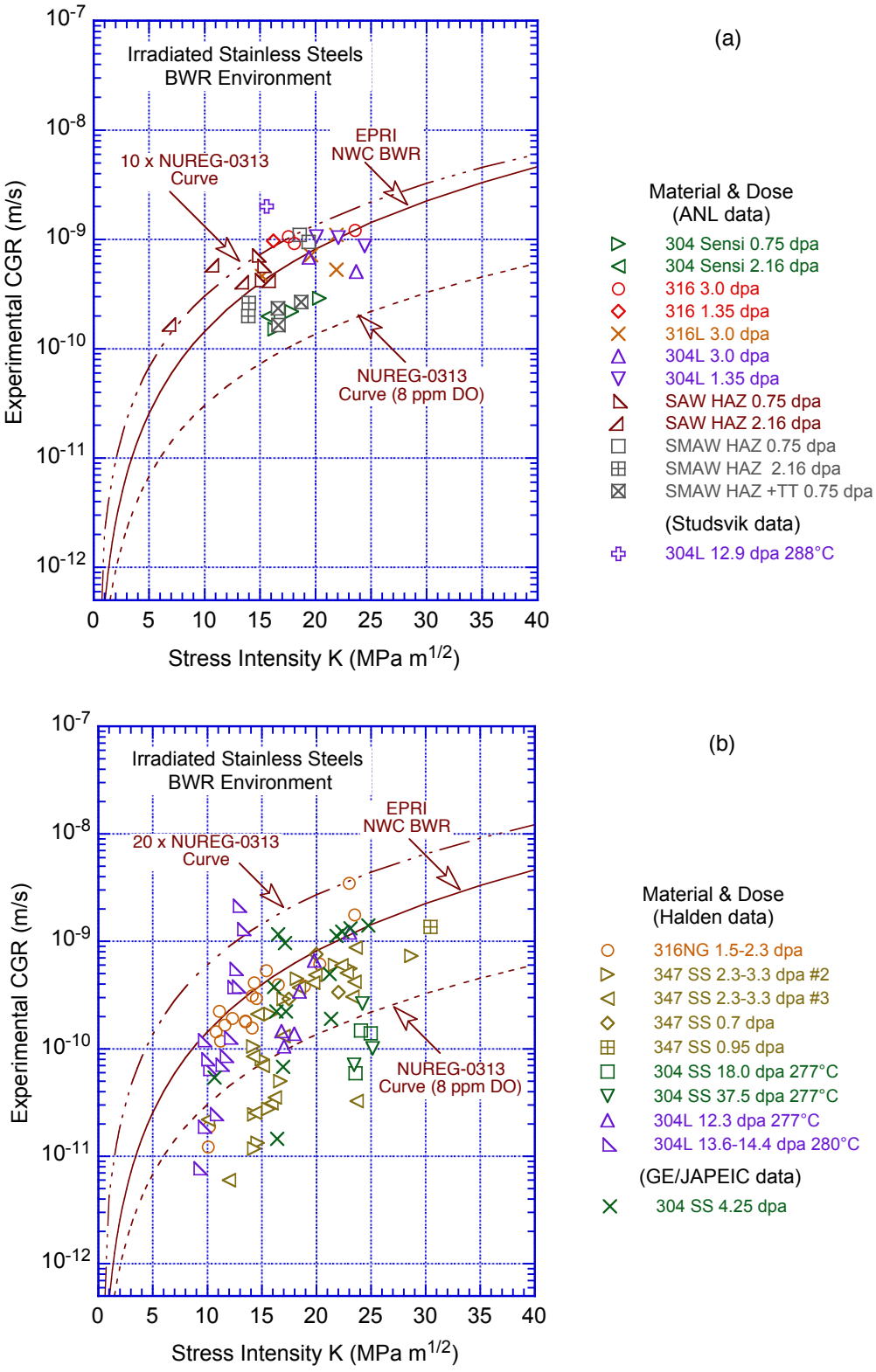

Figure 44. SCC growth rates in NWC BWR environment on austenitic SSs irradiated to 0.75–37.5 dpa (Refs. 20, 26, 128–133).

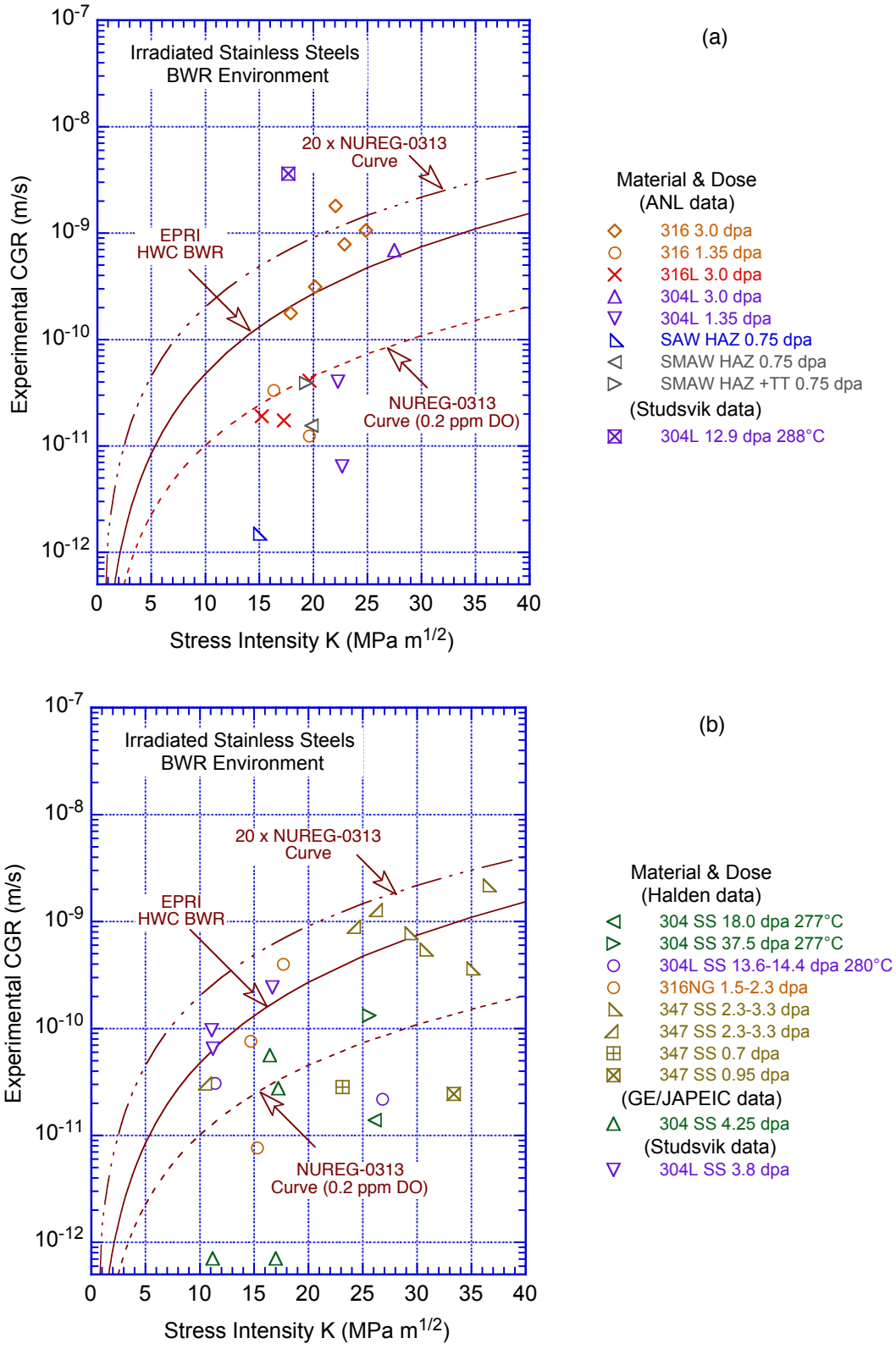

Figure 45. SCC growth rates in HWC BWR environment on austenitic SSs irradiated to 0.75–37.5 dpa (Refs. 20, 26, 128–133).

In the NWC BWR environment, the SCC CGRs of austenitic SSs irradiated to 5 dpa could be a factor of 10 higher and those irradiated to 10–12 dpa could be a factor of 25 higher than the NUREG-0313 disposition curve for nonirradiated SSs in 8 ppm water. The CGRs for SSs irradiated to 5–8 dpa (corresponding to a 60-year end-of-life neutron dose for a BWR) are a factor of 20 higher than the NUREG-0313 curve. However, the growth rates for highly irradiated materials show anomalous behavior. The CGRs for SSs irradiated in LWRs to 18 dpa or higher are below the NUREG-0313 disposition curve for nonirradiated SSs. The reasons for the low CGRs obtained for these highly irradiated materials in high-DO environment are not clear.

In the HWC BWR environment, the SCC CGRs show, a significant decrease relative to those in the NWC BWR environment for SSs irradiated to less than 3 dpa; little or no reduction for some SSs irradiated to dose levels as low as 3–4 dpa, at least at stress intensity factor (K) values above 18 MPa $m^{1/2}$; and no decrease for all SSs irradiated to 12–14.5 dpa. The CGRs for some of the materials irradiated to 3–4 dpa are above the CGR disposition curve proposed by EPRI for the HWC BWR environment. The tests that did not show the benefit of reduced corrosion potential on growth rates are often screened out because their loading conditions only marginally exceeded the proposed K/size criterion based on an effective yield stress. However, as discussed earlier in NUREG/CR-7027, none of these tests violated the K/size criteria and should be considered as valid tests.

Data on the SCC CGR for irradiated austenitic SSs in the PWR environment have been obtained at Halden[129–131] on BWR irradiated materials, at Studsvik[26] on BOR-60 irradiated materials, and from EPRI-sponsored studies on BWR and PWR irradiated materials. The materials were irradiated to 3.0–37.5 dpa at 288–340°C. The CGRs in the PWR environment show significant variability. For the same material and irradiation condition, the CGR increase with increasing temperature. The temperature dependence of SCC CGRs in irradiated and nonirradiated SSs yields activation energies between 60 and 150 kJ/mol. The data for CGRs of CW Type 316+Ti SS irradiated in a PWR yield an activation energy of 105 kJ/mol.[26] The experimental SCC CGRs for various grades and heats of austenitic SSs in a PWR environment are shown in Fig. 46; the data on materials irradiated in fast reactors are not included. The CGRs obtained at different temperatures have been normalized to a temperature of 320°C using an activation energy of 100 kJ/mol. Normalization did not significantly change the data scatter; it changed only the magnitude of the CGRs.

In PWR water at 320°C, the CGR data for SSs irradiated to 3 dpa are up to a factor of 12 above the NUREG-0313 curve for nonirradiated materials in high-purity water with 0.2 ppm DO. In addition, CGRs for SSs irradiated to 11–25 dpa are nearly two orders of magnitude above the same curve. As observed earlier for HWC BWR water, the CGRs in the PWR environment of SSs irradiated to 37.5 dpa are marginally above the NUREG-0313 curve for nonirradiated SSs in high-purity water with 0.2 ppm DO. The CGRs for SSs irradiated to 18 dpa show significant data scatter; CGRs obtained at K values between 7 and 9 MPa $m^{1/2}$ vary more than an order of magnitude; most values are above the NUREG-0313 curve. The reason is not known for the high CGRs for some SSs irradiated to 11.4 dpa and relatively low CGRs in SSs irradiated to 18 or 37.5 dpa. Additional data on PWR materials irradiated at temperatures of 300–350°C are needed to better understand the IASCC susceptibility of austenitic SSs in PWR environments.

All wrought and cast austenitic SSs and their welds, irradiated below the threshold neutron fluence are considered not susceptible to IASCC in a PWR environment. Based on laboratory SSRT data and PWR operating experience, a threshold fluence of 2×10^{21} n/cm^2 (3 dpa) has been proposed. For materials irradiated above this threshold, IASCC initiation data have been used to define for a given neutron dose, an apparent stress threshold below which IASCC

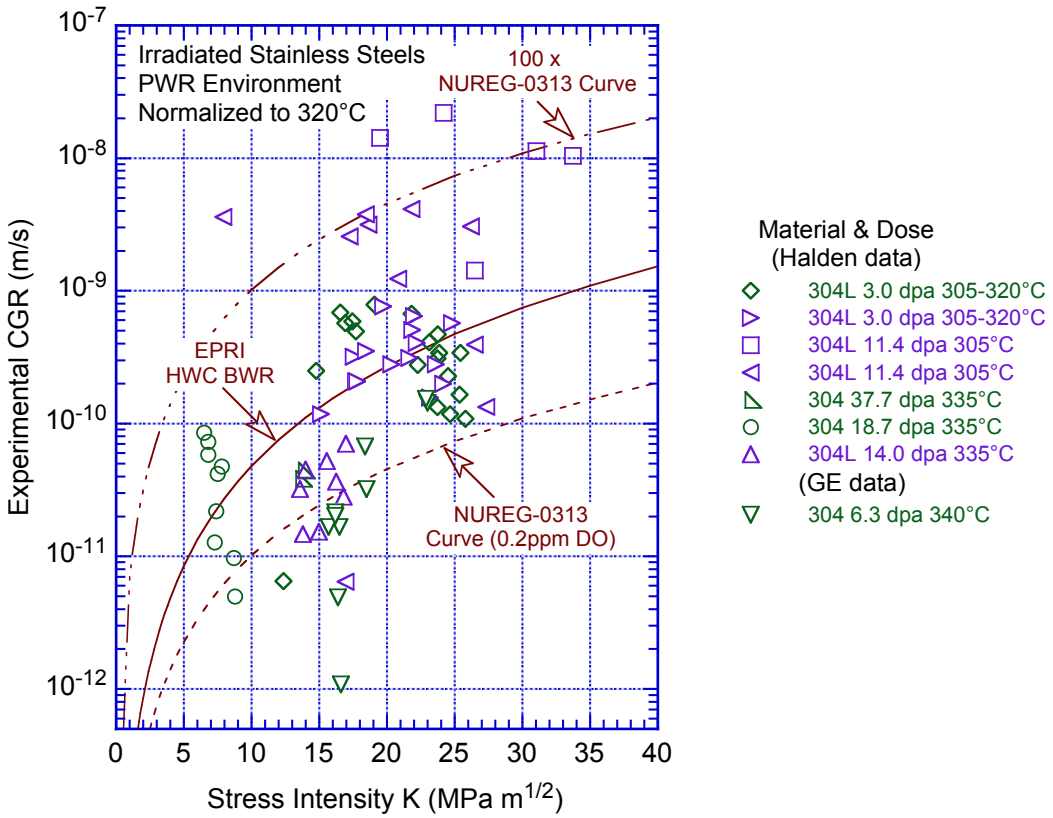

Figure 46. Normalized SCC growth rates in PWR environment for austenitic SSs irradiated to 0.75–37.5 dpa (Refs. 20, 26, 131).

initiation will not occur in a PWR environment. The existing IASCC initiation data have been reviewed to evaluate the adequacy of the database for developing screening criteria for the IASCC susceptibility of PWR core internal components. Most of the IASCC data have been obtained on CW Type 316 SS, while data on solution-annealed Type 304, 304L, or 316 SS are limited. There are no data on CASS materials and austenitic SS weld and weld HAZ materials. Several studies indicate that materials irradiated in fast reactors show lower susceptibility to IASCC than those irradiated in LWRs. The current IASCC initiation database, however, includes some tests on austenitic SS irradiated in the BOR-60 fast reactor.

In addition, although a threshold fluence of 3 dpa has been defined for IASCC in the PWR environment, no IASCC initiation data are available on austenitic SSs irradiated between 3 and 9.5 dpa. Furthermore, nearly all of the high fluence (>20 dpa) data and the majority of the low fluence data are for materials irradiated below 325°C and, therefore, do not include the potential effects of additional precipitate phases, voids/cavities, and He generation rate on IASCC. In reactor core internal components, IASCC is likely to occur under creviced conditions. Nearly all of the IASCC initiation tests have been conducted in the normal PWR environment.

3.2.2 Update of the CGR Data

The SCC CGRs for irradiated and nonirradiated Types 304 or 304L austenitic SS, SA or SMA weld HAZ materials, tested at 289°C in high-purity water with 600 ppb or <50 ppb DO are shown in Fig. 47.[20,124,134,135] The materials were irradiated between 5×10^{20} and

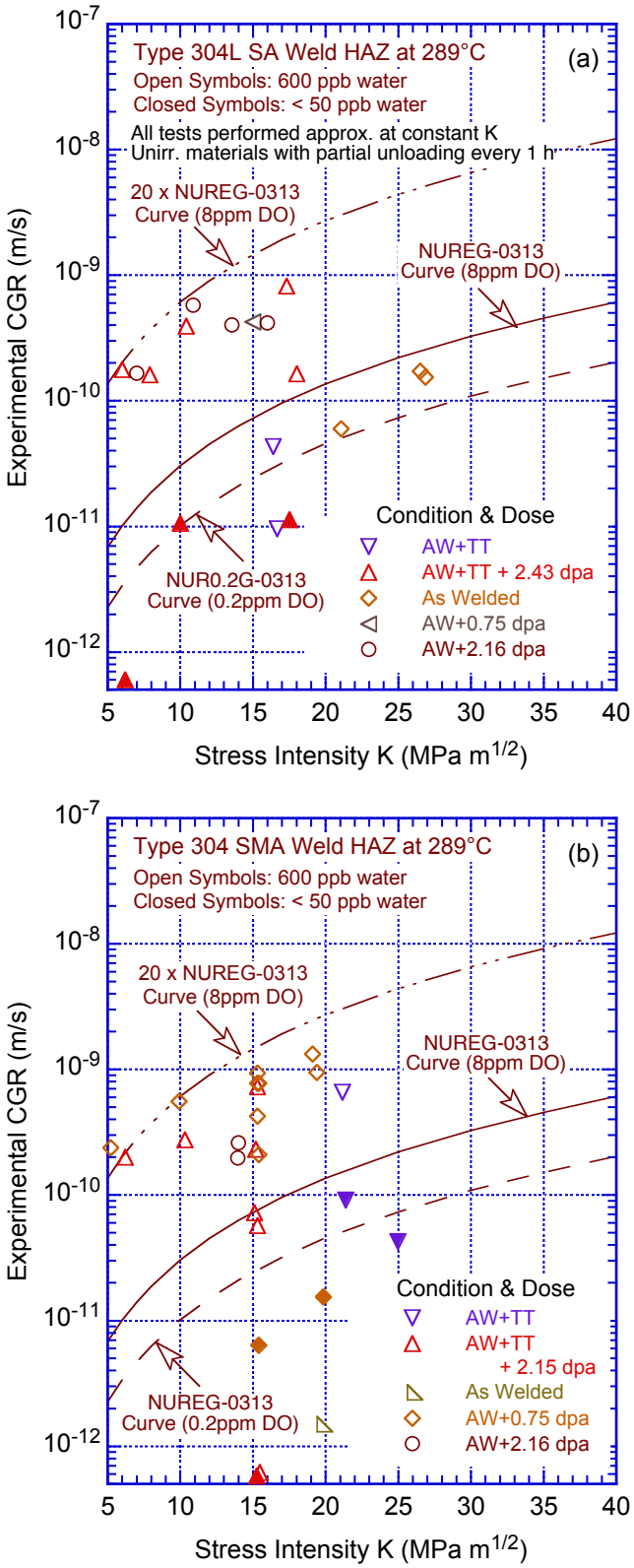

Figure 47. SCC growth rates for nonirradiated and irradiated austenitic SS (a) SA and (b) SMA weld HAZ materials at 289°C in high-purity water with 600 or <50 ppb DO (Refs. 20, 124, 134, 135).

2.5×10^{22} n/cm^2 (0.75 to 37.5 dpa). As before, the results are compared with the K versus CGR disposition curves proposed in the NRC report NUREG-0313 for nonirradiated sensitized austenitic SSs in high-purity water with 8 ppm or 0.2 ppm DO.[126]

The results indicate that in NWC BWR environment, the CGRs of Types 304 or 304L austenitic SS, SA, or SMA weld HAZ materials irradiated up to about 2.5 dpa are a factor of up to 20 higher than those predicted by the NUREG-0313 curve for nonirradiated sensitized austenitic SSs in high-purity water with 8 ppm DO. The CGRs in HWC BWR environment are generally below the NUREG-0313 curve for nonirradiated sensitized austenitic SSs in high-purity water with 0.2 ppm DO. These results suggest that the SCC CGRs for SA or SMA weld HAZ materials in NWC BWR environments are comparable to those for wrought austenitic SSs. For these materials, the CGRs in HWC BWR environments are mostly below the 0.2 ppm DO NUREG-0313 curve. However, the data are too limited to draw a conclusion.

The SCC CGRs for thermally aged and unaged Type 316L weld metal and irradiated and nonirradiated CASS materials, tested at 289 or 320°C in high-purity water with 300–2,000 or <50 ppb DO or PWR environments are shown in Fig. 48.[20,88,105,135,136] The materials were irradiated between 5×10^{20} and 2.5×10^{22} n/cm^2 (0.75 to 37.5 dpa). As before, the results are compared with the K versus CGR disposition curves proposed in the NRC report NUREG-0313 for nonirradiated sensitized austenitic SSs in high-purity water with 8 ppm or 0.2 ppm DO.[126]

The results indicate that the SCC CGRs for thermally aged and unaged Type 316L weld metal at 289°C in high-purity water with 300–2,000 ppb DO are bounded by the NUREG-0313 curve for nonirradiated sensitized austenitic SSs in high-purity water with 8 ppm DO. All of the data are below this curve. However, similar data for irradiated Type 316L weld metal are not available. The results also indicate that the CGRs for CF-8M CASS material irradiated to about 2.5 dpa and tested in high-DO water at 289°C are up to a factor of 6 higher than the NUREG-0313 curve for 8 ppm DO environment. The data in high-purity water with <50 ppb DO at 320°C indicate that the SCC CGRs for thermally aged and unaged CF-8M CASS materials irradiated to 0.08 dpa are all below the NUREG-0313 curve for nonirradiated sensitized austenitic SSs in high-purity water with 0.2 ppm DO. The limited data for CASS materials suggests that the 0.2 ppm DO curve for NUREG-0313 can be used for the CGRs of CASS materials irradiated up to 0.08 dpa in HWC BWR environments.

3.2.3 Effect of Neutron Fluence

The SCC growth rates for various grades and heats of austenitic SSs, irradiated from 5×10^{20} n/cm^2 to 2.5×10^{22} n/cm^2 (0.75 to 37.5 dpa) in NWC BWR and HWC BWR environments at 288°C and K = 20 MPa m$^{1/2}$ as a function of neutron dose, are shown in Figs. 49a and 49b, respectively.[21] All materials except those irradiated in a fast reactor were irradiated in BWRs at temperatures of 280–300°C; the fast reactor irradiations were at 320°C. In the NWC BWR environment, the CGR increases above the 8 ppm DO NUREG-0313 curve for neutron doses above 0.42 dpa. The CGR also increases with dose out to about 10 dpa, although there is variability in the data. In the HWC BWR environment, the CGRs do not exceed the 0.2 ppm DO NUREG-0313 curve for neutron doses above 2.2 dpa. The CGRs in HWC environment for materials irradiated 12–15 dpa are comparable to those observed in the NWC BWR environment. However, as noted previously, there are some anomalously data with very low growth rates; the CGRs of SSs irradiated to about 19 and 38 dpa are comparable to those for nonirradiated sensitized SSs in high-DO water. The curves in Fig. 49 bound approximately 75th percentile of the data in the NWC environment and even more for the HWC

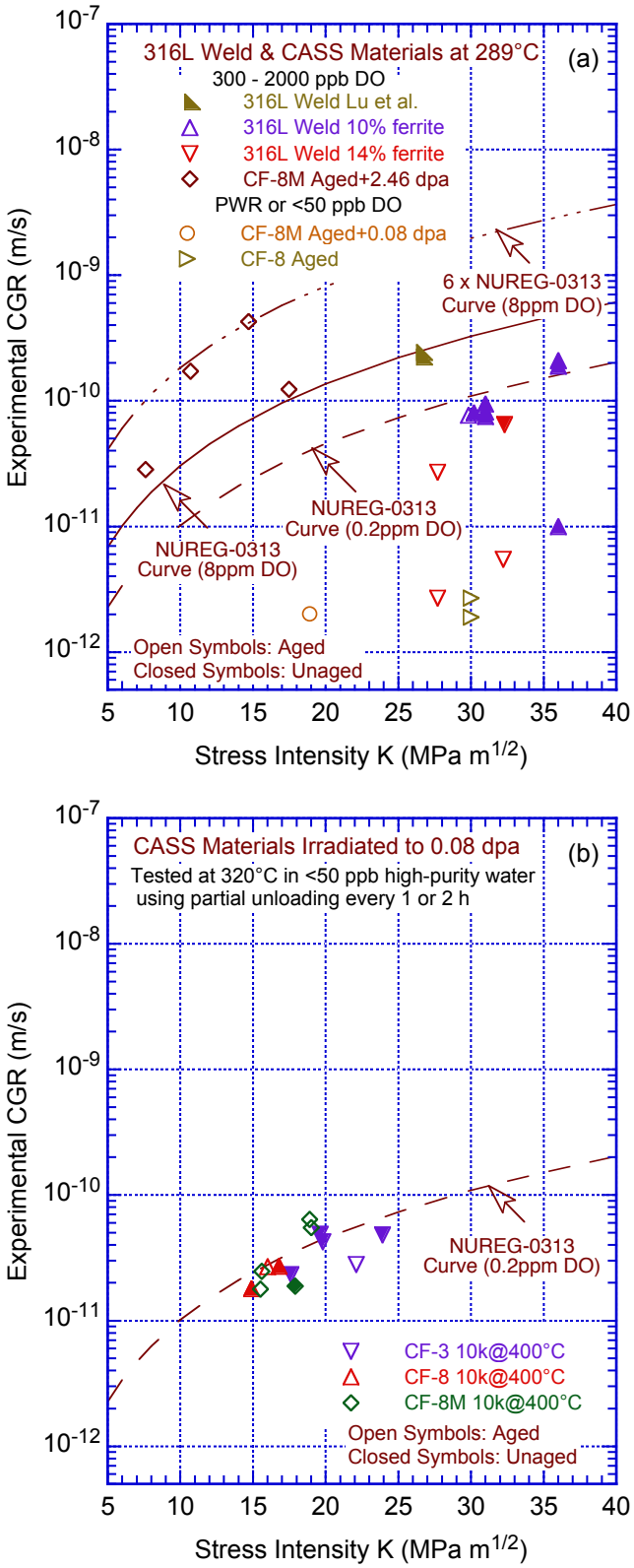

Figure 48. SCC growth rates for aged and unaged (a) Type 316L welds and (b) CASS materials in irradiated or nonirradiated conditions and tested at 289 or 320°C in high-purity water with 300–2,000 or <50 ppb DO (Refs. 20, 88, 105, 135, 136).

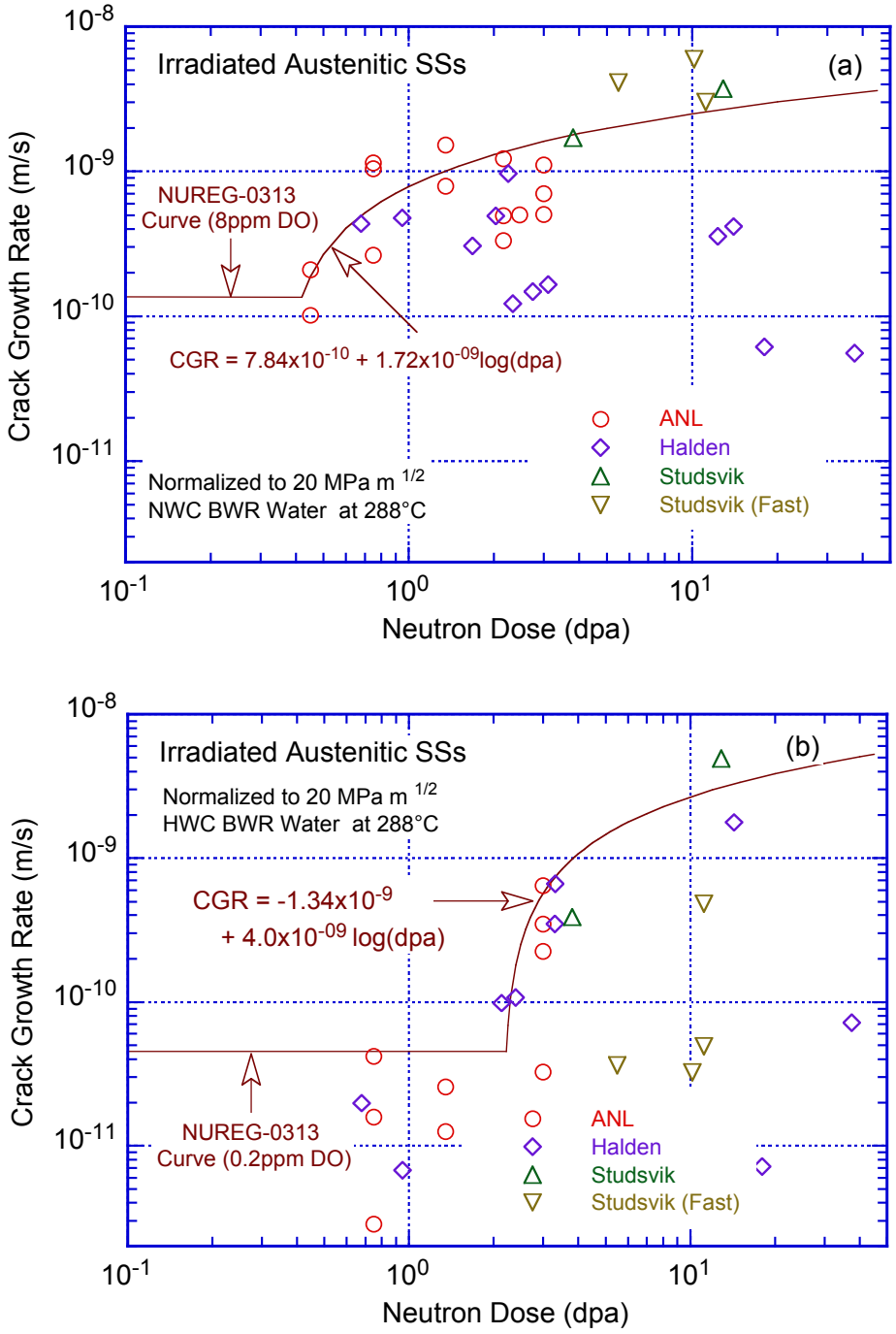

Figure 49. SCC growth rates of irradiated stainless steels in (a) NWC and (b) HWC BWR environments at 288°C and K of 20 MPa $m^{1/2}$ plotted as a function of neutron dose.

environment. The curves assume a threshold dose of 0.42 dpa and 2.2 dpa (or 2.8×10^{20} and approximately 1.47×10^{21} n/cm^2) in the NWC and HWC environment, respectively. The curves assume that constant A1 in the NUREG-0313 disposition curve (Eq. 47) varies with neutron dose. In the NWC environment A1 is taken as

$$A1 = 1.21 \times 10^{-12} + 2.65 \times 10^{-12} \log(\text{dpa}), \quad (49)$$

and in the HWC environment as

$$A1 = -2.07 \times 10^{-12} + 6.17 \times 10^{-12} \log(\text{dpa}). \quad (50)$$

Equation 50 is an updated version of the expression published earlier in NUREG/CR-2027 and Ref. 29. In addition, note that because Eqs. 49 and 50 define the constant A1 in Eq. 47, these values must be multiplied by $(20)^{2.161}$ to obtain the CGRs shown in Fig. 10.

The available SCC CGR data for austenitic SS welds and weld HAZ as well as CASS materials in NWC and HWC BWR environments are shown in Fig. 50.[20,105,124,134,135] The data plotted at 0.05 dpa are for nonirradiated material. These limited data indicate that in NWC BWR environment, the CGRs for nonirradiated materials or materials irradiated up to 0.42 dpa are below the NUREG-0313 curve for nonirradiated sensitized austenitic SSs in high-purity water with 8 ppm DO. For materials irradiated above 0.42 dpa, most of the data are bounded by the curve represented by Eqs. 47 and 49. In HWC BWR environment, the CGRs for nonirradiated materials or materials irradiated up to 2.2 dpa are below the NUREG-0313 curve for nonirradiated sensitized austenitic SSs in high-purity water with 0.2 ppm DO. However, there is little or no IASCC CGR data in HWC BWR environment on CASS materials or austenitic SS welds and HAZ materials irradiated above 2.2 dpa.

Figure 51a shows the SCC growth rates as a function of neutron dose for various grades and heats of austenitic SSs that had been irradiated to 0.7–37.5 dpa in HWC BWR water at 288°C or the PWR environment at 320°C, with K = 20 MPa $m^{1/2}$(from Ref. 21). All materials except those irradiated in a fast reactor were irradiated in BWRs at temperatures of 280–300°C; the fast reactor irradiations were at 320°C. The data for the HWC BWR or PWR environments may be represented by the bounding curves shown in the figure. The curve represents a variation of A1 in the NUREG-0313 disposition curve (Eq. 47) with neutron dose that is expressed by Eq. 50.

A few SCC CGR results for aged CF-8M CASS material in the nonirradiated condition and unaged and aged CF-3 CASS material irradiated to 0.08 dpa in PWR environment are shown in Fig. 51b. [88,136] The results are below the NUREG-0313 curve for nonirradiated sensitized austenitic SSs in high-purity water with 0.2 ppm DO.

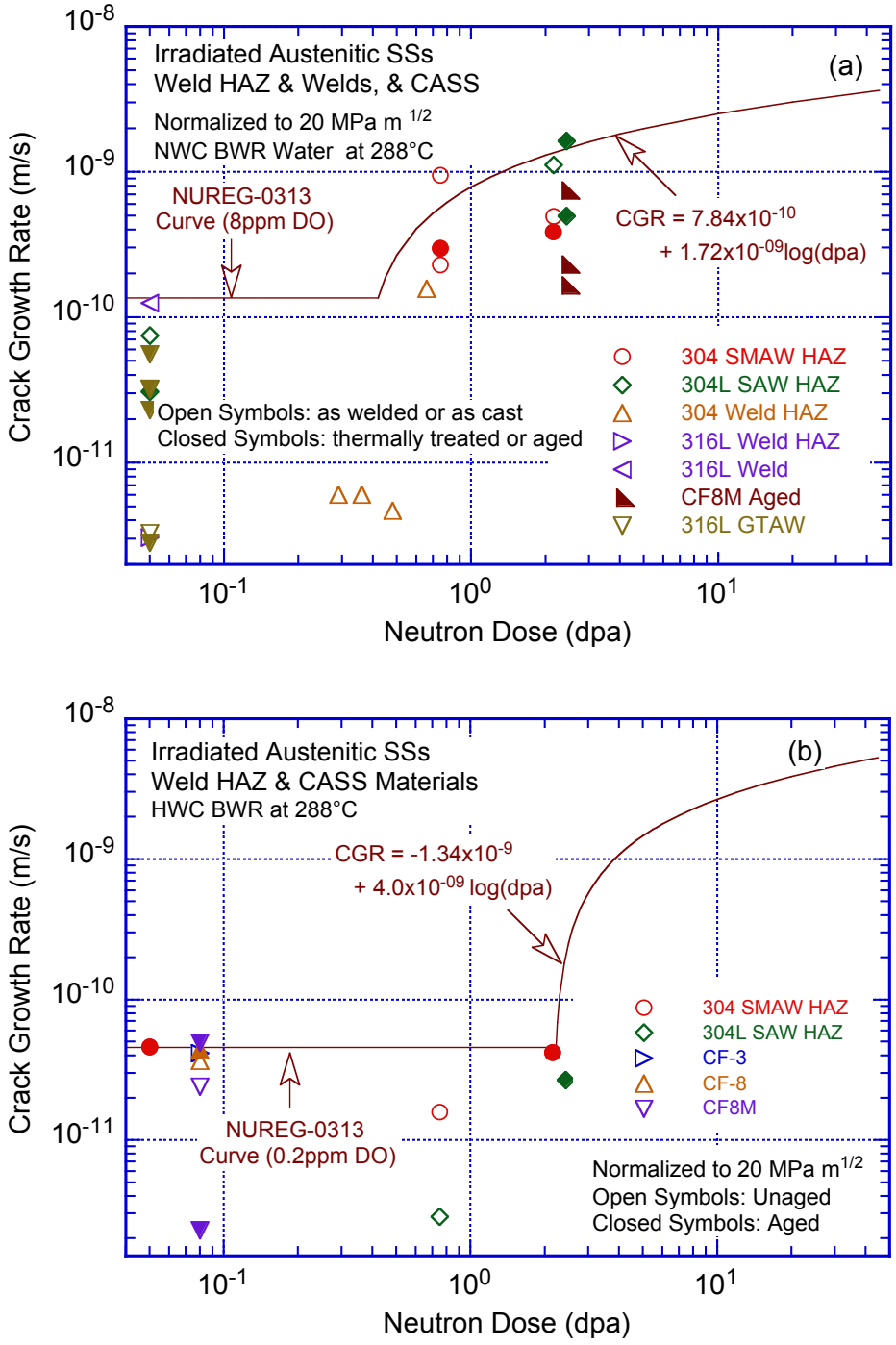

Figure 50. SCC growth rates of nonirradiated and irradiated austenitic SS weld HAZs and welds and CASS materials in (a) NWC and (b) HWC BWR environments at 288°C and K of 20 MPa $m^{1/2}$ plotted as a function of neutron dose. The data points plotted at 0.05 dpa are for nonirradiated materials.

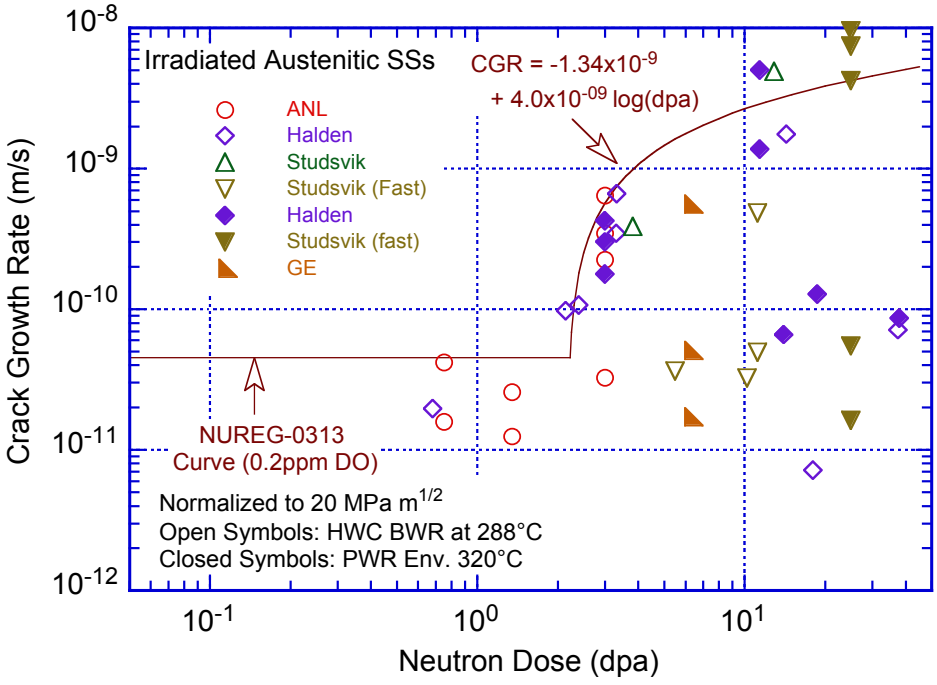

(a)

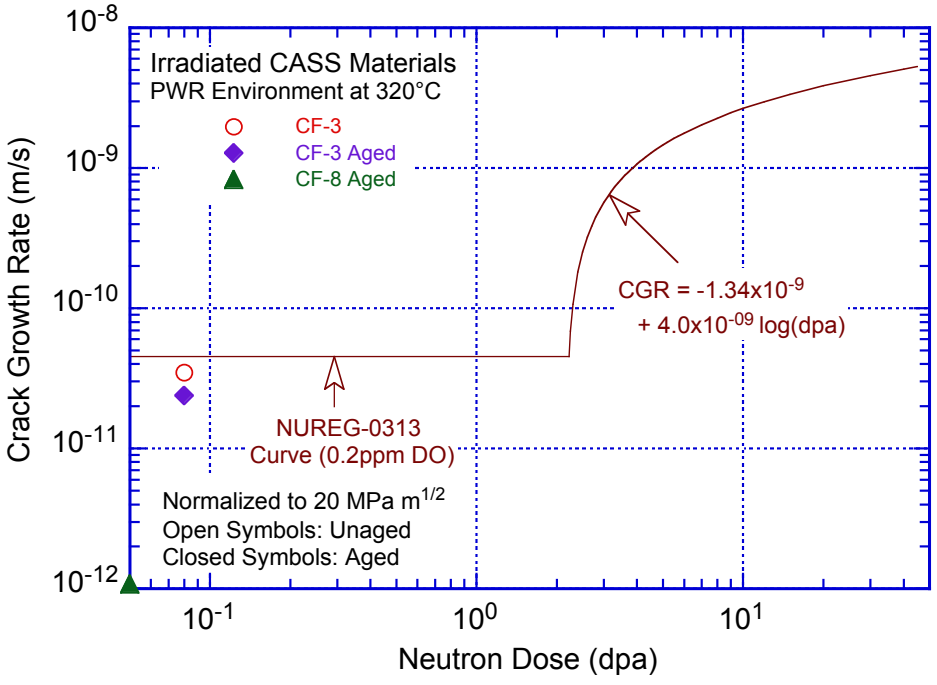

(b)

Figure 51. Crack growth rates for irradiated (a) austenitic SSs and (b) CASS materials in HWC BWR water at 288°C or PWR environment at 320°C plotted as a function of neutron dose.

4. Neutron Embrittlement

The fracture toughness of unaged and nonirradiated wrought and cast austenitic SSs and their welds fall in Category III, with J_{Ic} above 150 kJ/m^2 (857 in.-lb/in.^{2}). In these materials, fracture occurs after stable crack extension at stresses well above the yield stress. However, neutron irradiation can degrade fracture toughness of these materials to the level of Category II (J_{Ic} in the range of 30–150 kJ/m^2 [171–857 in.-lb/in.^{2}]), or Category I (J_{Ic} < 30 kJ/m^2 [< 171 in.-lb/in.^{2}]). Therefore, failure in neutron-irradiated materials may occur without general yielding. In such instances, either EPFM or LEFM is used for analysis of structural integrity and development of inspection guidelines. The EPFM analysis is used where failure is caused by plastic deformation, and involves the J-R curve approach.

As discussed earlier in Section 2, austenitic SS welds and CASS materials have a duplex microstructure consisting of austenite and ferrite phases. Embrittlement of the ferrite phase due to neutron irradiation occurs much faster than for austenitic SSs. The irradiation temperature is an important factor in establishing the extent of embrittlement of the ferrite. However, the ferrite phase is susceptible to thermal embrittlement after extended service at reactor operating temperatures. The formation of the Cr-rich α' phase in the ferrite is the primary mechanism for thermal embrittlement; thermal aging has little or no effect on the austenite phase. Although both the thermal aging embrittlement of ferrite and the neutron irradiation embrittlement of ferrite are well characterized, experimental data on the combined effect of thermal aging and neutron irradiation on the embrittlement of ferrite in SS welds and CASS materials are rather limited. The possible combined effects of thermal aging and neutron irradiation embrittlement of these materials are discussed in Section 5.

4.1 Fracture Toughness of Irradiated Austenitic Stainless Steels

Until recently, most of the published experimental data on neutron embrittlement of austenitic SSs had been obtained on materials irradiated in high-flux fast reactors. In these studies, the embrittlement of the materials has been characterized in terms of tensile properties, Charpy-impact properties, and fracture toughness. The tensile properties of Type 304, 316, and 347 SSs and their weld metals and HAZ materials, as well as CF-8 cast austenitic SSs irradiated in fast reactors or LWRs, have been discussed in Section 2.1.4 of this report.

Fracture toughness is typically characterized by the initiation toughness J_{Ic} and tearing modulus T for materials that fail after substantial plastic deformation (for EPFM analysis) and by the critical stress intensity factor K_{Ic} for materials that fail after little or no deformation (for LEFM analysis). Typically, fracture toughness data for irradiated materials have been obtained from CT or single edge bend (SE[B]) specimens and, in some cases, from Chevron notch short rod (CNSR) specimens. To reduce activity and facilitate handling, small specimens (e.g., ≈8-mm-thick ¼-T CT) have been used in several studies. For these specimens, J values above 150 kJ/m$^{1/2}$ and crack extensions beyond about 1.2 mm are above the validity limits based on ASTM Specification E 1820-06. However, comparison of fracture toughness data obtained on 1-T CT and small-size CT or SE(B) specimens shows comparable J versus Δa values even beyond the ASTM defined validity limits. The small specimens yield equivalent J-R curve data at least for materials with J_{Ic} values up to about 300 kJ/m$^{1/2}$, and maybe even higher.

Plots of J_{Ic} or K_{Ic} and K_{Jc} as a function of neutron dose are used for developing screening criteria for neutron embrittlement. In ASTM Specification E 1820-06, J_{Ic} is determined from the

intersection of the best-fit power-law J-R curve with the 0.2-offset line parallel to the blunting line, provided the specimen size criterion of Eq. 51 is satisfied. The blunting line is defined as

$$J = M\sigma_f \Delta a, \tag{51}$$

where σ_f is the flow stress, Δa is crack extension, and the constraint factor M is 2 or a value determined from the best fit of the experimental data. However, the analysis procedures, described in the ASTM specifications for J_{Ic} determination, are not applicable to austenitic SSs because of their extremely high toughness, ductility, and strain hardening ability. The main difference concerns the expression for the crack-tip blunting line. For austenitic SSs, a value of 2 for M significantly over predicts the crack extension due to crack tip blunting, and, therefore, it yields a non-conservative value of J_{Ic}.[8,137] For austenitic SSs, a value of 4 for M better defines the blunting line.

The constraint factor M, which relates J to the crack tip opening displacement (CTOD) given by the expression

$$J = M\sigma_y(\text{CTOD}). \tag{52}$$

The use of a higher value for M in Eq. 51 is consistent with the expected variation of M and σ_f with strain hardening. The factor M is 1 for materials with intermediate to high strength and low strain hardening, and 2 for materials with low strength and high strain hardening, such as austenitic SSs. For the latter, the yield strength is approximately two-thirds of the flow stress, and the crack extension associated with blunting is approximately one-third of CTOD.[8] Thus, for such materials, the crack tip blunting line is given by

$$J = M\sigma_y(\text{CTOD}) \approx 2(2\sigma_f/3)(3\Delta a) = 4\sigma_f \Delta a \tag{53}$$

(i.e., Eq. 20 with M = 4). This relationship has been used to determine J_{Ic} in most investigations on neutron embrittlement.[12,20] A value of 2 for M has also been used by some investigators.[10] The latter typically yields a higher value of J_{Ic} for Category III materials (i.e., with J_{Ic} above 150 kJ/cm^2). However, the difference in J_{Ic} values determined using values of M of 2 or 4 is insignificant for Category II materials (i.e., J_{Ic} <100 kJ/cm^2). Since it is primarily the cases in which the fracture toughness of irradiated austenitic SSs is reduced to Category II levels that are of interest, the effect of differences in the procedure to determine J_{Ic} is likely to be insignificant.

Another factor that may influence the reported values of J_{Ic} is the use of an effective yield stress instead of the measured yield stress. The K/size criteria were developed for materials that show work hardening and, therefore, may not be applicable for materials irradiated to fluence levels where, on a local level, they do not strain harden. An effective yield stress, in which the irradiation-induced increase in yield stress is discounted by a factor of 2 for moderately irradiated materials and by a factor of 3 for highly irradiated materials, has been proposed to define K/size criteria for moderate to highly irradiated materials. Some studies have used such a yield stress to determine J_{Ic}.[20] Because J_{Ic} is a measure of fracture toughness at instability without significant stable crack extension, the measured yield or flow stress of the irradiated materials seems more appropriate for J_{Ic} determinations. Nevertheless, the choice of measured or effective yield stress is likely to have an insignificant effect on the measured J_{Ic} of materials with poor fracture toughness.

4.1.1 Fracture Toughness J_{Ic}

The effect of neutron exposure (in dpa) on the fracture toughness J_{Ic} at 25–427°C (77–842°F) of austenitic SSs irradiated at 90–450°C (194–842°F) up to 90 dpa in fast reactors is shown in Fig. 52.[8,14,15,138–151] The irradiation and test temperatures were 100–155°C and 125°C for the data obtained by Sindelar et al.,[146] 90–250°C and 25–250°C for the data obtained by Alexander et al.,[145] and 325°C and 25°C for the data obtained by Kim et al.[15] The rest of the data were obtained on materials irradiated at 350–427°C and tested at 300–427°C. The fast reactor data show a rapid decrease in fracture toughness at a neutron dose of 1–2 dpa; the neutron dose at the onset of the rapid decrease varies with the chemical composition and heat treatment of the steel. The effects of irradiation may be divided into three regimes: little or no loss of toughness below an exposure of ≈1 dpa, substantial decrease in toughness at exposures of 1–10 dpa, and no further reduction in toughness above a saturation exposure of 10 dpa. The degradation in fracture properties saturates at a J_{Ic} value of ≈30 kJ/m^2 (171 in.-lb/in.^{2}) (i.e., K_{Jc} of 75 MPa m$^{1/2}$ [68.2 ksi in.$^{1/2}$]). In addition, the failure mode changes from dimple fracture to channel fracture.

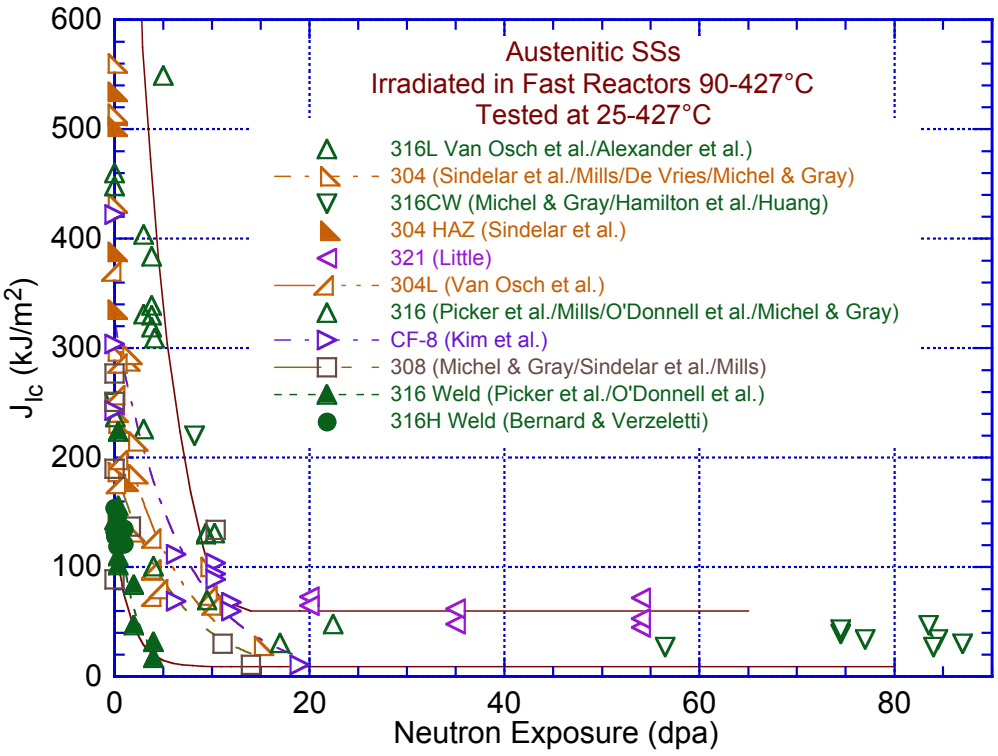

Figure 52. Change in fracture toughness J_{Ic} as a function of neutron exposure for austenitic SSs irradiated in fast reactors. Solid lines represent the scatter band for the fast reactor data on austenitic SSs (Refs. 8, 14, 15, 138–151).

The fracture toughness trend for the LWR data[6,9–12,16–20] is similar to that observed for fast reactor data (Fig. 53). Most of the fracture toughness J_{Ic} values for austenitic SSs irradiated in LWRs (288–316°C [550–601°F]) fall within the scatter band of the data obtained on materials irradiated in fast reactors, even though the LWR irradiations were at lower temperatures. There are only minor differences in the fracture toughness of the various wrought and cast austenitic SS materials. For the same irradiation conditions, the fracture toughness of thermally aged CASS material and austenitic SS weld metal is lower than that of HAZ material, which, in turn, is lower than that of solution-annealed materials. A similar behavior is also observed for the fast

reactor data in Fig. 52. The J_{Ic} values of austenitic SS welds and HAZ materials are consistently lower than those for the solution-annealed and CW materials. The data for CF-8 steel are relatively high because they were obtained at RT; the J_{Ic} values are expected to be lower at LWR operating temperatures.

Some materials irradiated above 4 dpa at LWR temperatures show very poor fracture toughness; their J_{Ic} values are below the lower-bound curve for the fast reactor data. For a Type 304 SS irradiated to 4.5–5.3 dpa (indicated by crosses in Fig. 53), nine out of 10 CT specimens showed no ductile crack extension and the K_{Ic} values were 52.5–67.5 MPa $m^{1/2}$ (47.7–61.4 ksi $in.^{1/2}$).[9] The lowest fracture toughness, with K_{Ic} or K_{Jc} values in the range of 36.8–40.3 MPa $m^{1/2}$ (33.5–36.6 ksi $in.^{1/2}$), was for a Type 347 SS irradiated to 16.5 dpa in a PWR[9] and for a Type 304 SS irradiated to 7.4–8.4 dpa in a BWR.[18]

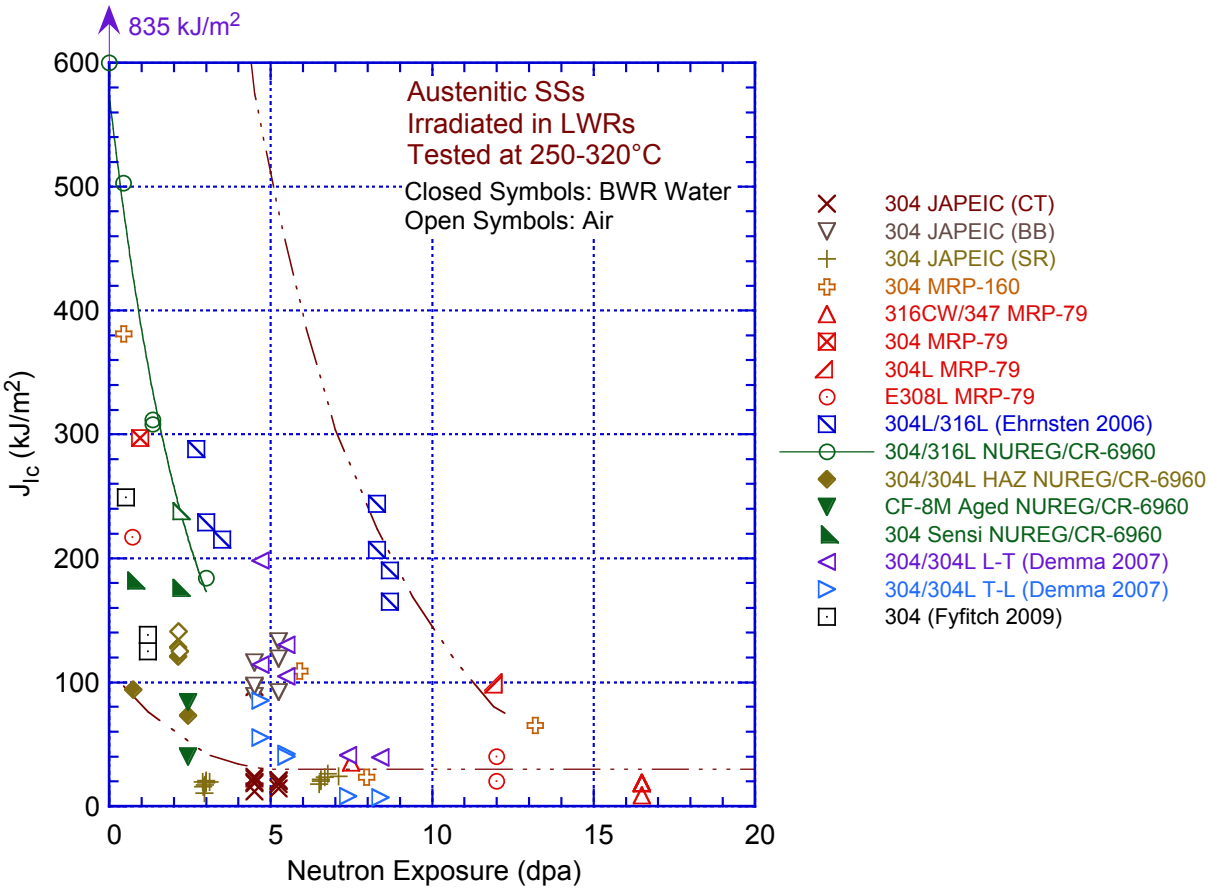

Figure 53. Change in fracture toughness J_{Ic} as a function of neutron exposure for LWR irradiated austenitic SSs. Dashed lines represent the scatter band for the fast reactor data on austenitic SSs irradiated at 350–450°C (662–843°F) (Refs. 6, 9–12, 16–20). JAPEIC = Japan Power Electric Engineering and Inspection Corp.; BB = bend bar specimen; and SR = short rod specimen.

Another significant result is a strong orientation effect on fracture toughness. Fracture toughness J-R tests and microstructural and microchemistry characterization were performed on a Type 304 control-rod and Type 304L top guide materials irradiated to 4.7–12.0 dpa in a BWR, and on Type 304 control-rod material irradiated to 7.4 and 8.4 dpa in another BWR. All

materials consistently showed lower fracture toughness in the T-L orientation than in the L-T orientation,[10] and these toughness values were lower than the limiting fracture toughness K_{Ic} of 55 MPa $m^{1/2}$ (50 ksi $in.^{1/2}$) that has been proposed by industry for flaw tolerance evaluation in austenitic SSs irradiated above 4.5 dpa (3×10^{21} n/cm^2).[10,13] The lower fracture toughness along the T-L orientation has been attributed to the presence of stringers consisting of long, narrow particles oriented in the rolling direction, which result in a long and narrow quasi-cleavage structure parallel to the crack advance, thereby accelerating the crack advance.[10]

In addition, the Type 304 control-rod material (7.4–8.4 dpa) showed very poor fracture toughness (J_{Ic} of 40 kJ/m^2 in L-T and 7.5 kJ/m^2 in T-L orientation). The authors concluded that the low J_{Ic} of this material might be considered a special case of materials containing a high density of particles aligned in the rolling direction. Nonetheless, these results show that very low fracture toughness values are possible for irradiated austenitic SSs. Microstructural characterization of the Type 304 control-rod material showed a fine distribution of γ' phase with size in the range of 2–10 nm and an average size of 4.4 nm.[10] The density was $1–3 \times 10^{22}$ m^{-3}. This phase was not observed in the Type 304 top guide material, and may influence the fracture toughness of these materials. The γ' phase has been observed at dose levels above 4 dpa in CW Type 316 SS irradiated under the PWR condition.[152] The contribution of additional precipitate phases, voids, and cavities on fracture toughness needs to be investigated.

4.1.2 Fracture Toughness J-R Curve

Fracture toughness J-R curve data have been obtained for the following materials: Type 304, 304L, and 316L SSs; SS weld materials and HAZs; and CF-3, CF-8, and CF-8M cast austenitic SSs. Data are available for materials irradiated in LWRs up to about 14 dpa,[9–13,16–20] and in fast reactors to much higher dose levels. The change in the J-R curve with neutron dose is shown in Fig. 54. The decrease in fracture toughness is quite rapid up to about 6 dpa, and the toughness continues to decrease moderately at higher dose levels. The effects of various parameters such as material type and heat treatment, test and irradiation temperature, and neutron energy spectrum, flux, and dose are discussed below.

Irradiation Conditions: Fast reactor irradiations are at fluxes and temperatures higher than those typically observed in LWRs and have a different spectrum. Until recently, most of the high neutron exposure data were from fast reactor irradiations at temperatures above 350°C (662°F) (Fig. 52). An accurate determination of the effects of neutron spectrum, flux, and temperature on the fracture properties of these materials requires data on the same heat of material irradiated in a fast reactor and an LWR to comparable neutron dose. Such information is not available. Although the general data trends appear to be similar for fast reactor and LWR irradiations, the tensile property data indicate that tensile strength is higher and ductility is lower for the BWR-irradiated materials than materials irradiated in fast reactors. However, the existing data are inadequate to determine the individual contributions of irradiation temperature, flux, and energy spectrum to the degradation of fracture properties in irradiated austenitic SSs. Therefore, additional fracture toughness data should ideally be obtained on the same heat of material that has been irradiated in both fast and thermal reactors to comparable fluence levels at the same temperature. Only such carefully controlled data can be used to accurately assess the applicability of fast reactor data to LWR irradiation conditions.

Material Type: Most of the J-R curve data on LWR-irradiated austenitic SSs have been obtained on Type 304 and 304L SS. Data on Type 316, 316L, 316CW, and 347 SSs are very limited. In addition, most of the data for SS welds are on Type 308L material irradiated to <1 dpa or 12 dpa, and a few tests on 316 weld and one test on 316LN weld. Similarly, there are only a

few J-R curve tests on weld HAZ materials and CF-8M steel irradiated to 2.1–2.5 dpa. Some differences in the fracture toughness data trends appear for the various grades of wrought austenitic SSs, but these differences may be artifacts of the limited data. For example, the heat-to-heat variation for a particular grade may be comparable to the apparent differences

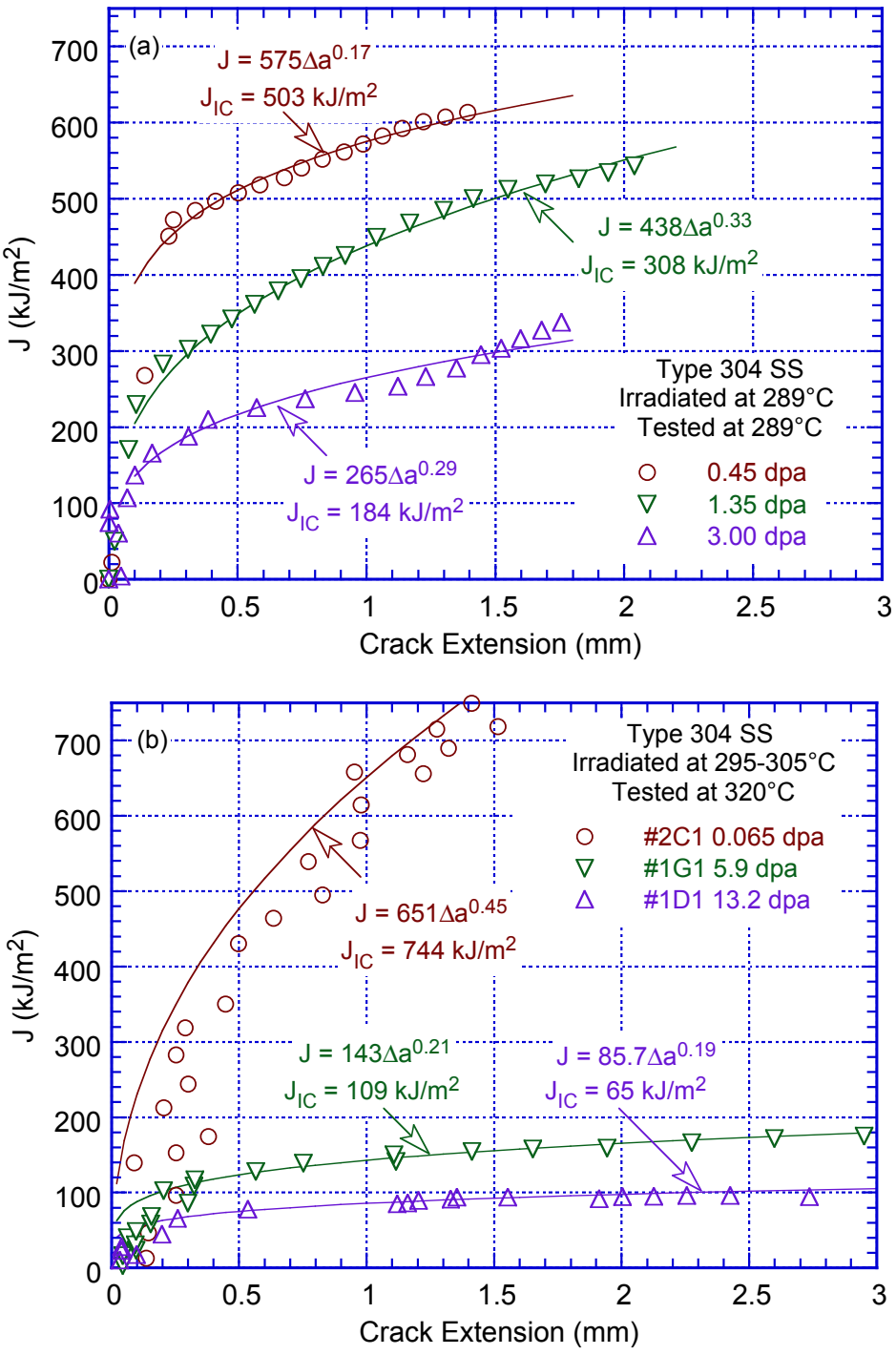

Figure 54. Change in fracture toughness J-R curve and J_{Ic} as a function of neutron exposure for Type 304 SS at (a) 289 and (b) 320°C (Refs. 18,20).

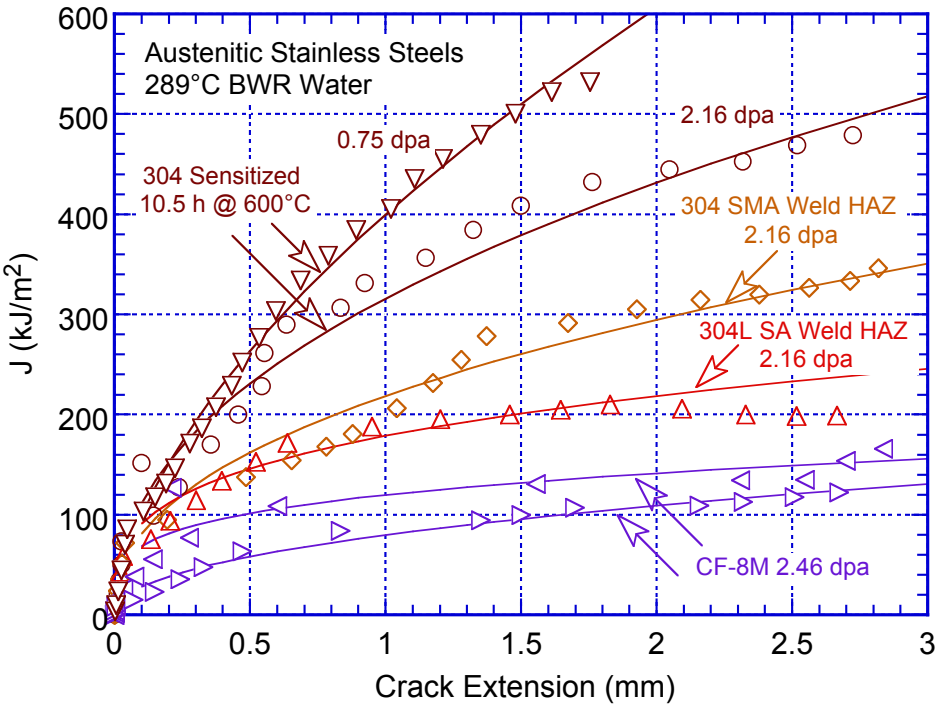

Figure 55. Fracture toughness J-R curves for sensitized Type 304 SS, weld HAZ materials of Type 304 and 304L SS, and CF-8M steel in high-purity water at 289°C (Ref. 21).

between grades in the current data. The results for different heats of Type 304 SS indicate little or no effect of sensitization treatment (green open circles and green-filled right-angle triangles in Fig. 53, respectively). In addition, for the same irradiation conditions, the fracture toughness of the weld HAZ materials is lower than that of the solution-annealed materials (olive-filled diamonds and green open circles in Fig. 53, respectively), and the toughness of austenitic SS welds and thermally aged CASS materials is lower than that of the HAZ material (Fig. 55).

Although the fracture toughness of nonirradiated CW steels is lower than that of nonirradiated solution-annealed steels, the decrease in toughness of CW steels with neutron exposure is lower and the J_{Ic} value at saturation is higher than those of irradiated solution-annealed steels (Fig. 52). However, the data for CW steels are from fast reactor irradiations at relatively high temperatures, 400–427°C (752–800°F). The saturation J_{Ic} for CW SSs is likely to be lower for irradiations at LWR operating temperatures (i.e., 290–320°C [554–608°F]), and the differences between the two are likely to be small.

Nonirradiated weld metals and thermally aged CASS materials have lower fracture toughness than wrought austenitic SSs, and their fracture toughness generally decreases more rapidly with neutron exposure than that of solution-annealed material. However, the saturation toughness for the welds is not significantly different from that of solution-annealed SSs, and the same bounding curve for J_{Ic} appears to be applicable to wrought materials as well as austenitic welds and CASS materials. Although LWR core internals are typically constructed of CF-8 or CF-3 steels, the only data for LWR irradiation of CASS materials are for CF-8M steel. The data for thermally aged CF-8 steel shown in Fig. 52 are for materials that were irradiated in the BOR-60 fast reactor, and may be non-conservative for LWR irradiation conditions. Furthermore, the data were obtained at room temperature; as discussed below in this section, fracture toughness at higher temperatures is expected to be lower. For thermal embrittlement of CASS materials,

the fracture toughness of CF-8M steel represents the worst-case scenario.[50,53] It thus might also represent a bounding case also for the combined effects of irradiation and thermal aging.

Test Environment: Nearly all of the existing fracture toughness data have been obtained from tests in air and on specimens that were fatigue precracked at relatively low load ratios (typically 0.1–0.2) in RT air. However, in reactor core components, cracks are initiated primarily by SCC and have intergranular (IG) morphology, whereas the fatigue precracks in fracture toughness tests are always transgranular (TG). In addition, the corrosion/oxidation reaction could influence fracture toughness. For example, hydrogen generated from the oxidation reaction could diffuse into the material and change the deformation behavior by changing the stacking-fault energy of the material. As discussed earlier in Section 2.5.3 for CF-8M material aged for more than 15 years at 350°C, the J-R curve data for specimens precracked in air at 54°C and then tested in PWR (SWC) at 54°C were lower relative to those tested in air. The specimens that were precracked in PWR water at 315°C and then tested in PWR water also show reduced fracture toughness but the effect was less.[88] Similarly, J-R curve data for Type 316L GTA weld indicated that the reactor coolant environment could decrease fracture toughness by up to 40% relative to that in air (Section 2.6.1).[105]

To investigate potential effects of reactor coolant environment on the fracture toughness of irradiated austenitic SSs, J-R curve tests were conducted in a BWR NWC environment.[20] The J-R data on irradiated SS weld HAZ materials (Figs. 56a and 56b) indicate that an NWC BWR environment has little or no effect on the fracture toughness. The J-R curves for irradiated Type 304L SA weld HAZ in air and water environments are essentially identical and, although the complete J-R curve could not be obtained for Type 304 SMA weld HAZ in air, ductile crack extension occurred at approximately the same value of J in air and water environments.

Figure 57 shows the J-R curves for a sensitized Type 304 SS in air and water environments. The results indicate slightly lower fracture toughness in water. In addition, the material tested in water was sensitized for a shorter time than the material tested in air. Therefore, for materials with identical sensitization treatment, the difference between the J-R curves in air and water environments might be greater than that indicated by Fig. 57. Thus, the lower J-R curve in water may be just data scatter or due to the effect of reactor coolant environment. Although these results indicate little or no effect of environment, the data presented earlier in Fig. 29, indicate a significant decrease in fracture toughness J-R curve of aged CF-8 material in PWR SWC environment at 54°C. Duplicate tests under identical material and test conditions except the environment showed significantly lower fracture toughness in the coolant environment.

The J-R curves and the load versus load-line displacement curves for the two tests on thermally aged and irradiated CF-8M steel in NWC BWR water are shown in Fig. 58. Companion tests in air have not been conducted on this material. In both tests, large load drops, accompanied by crack extensions up to 0.5 mm in Specimen 75-11TM and 1.0 mm in Specimen 75-11TT, were observed at the onset of crack extension. Such load drops are not typically observed during tests in air.[50] Fracture toughness J-R curve tests have also been conducted recently at Argonne on unaged and aged CF-3 (Heat 69) and CF-8 (Heat 68) materials in air and low corrosion potential high–purity water.[136] The tests in air were performed on 1-T CT specimens and in water on ¼-T CT specimens. The results showed lower fracture toughness of the unaged material in water environment compared to that in air. The fracture toughness J-R curves for these materials aged 10,000 h at 400°C showed little or no environmental effects; the J-R curves in in air and water environments were comparable. However, since ¼-T CT specimens were used for the tests in water, considering size effects, the J-R curves for tests in water on a 1-T CT specimen are likely to be lower than those observed for a ¼-T CT specimen.

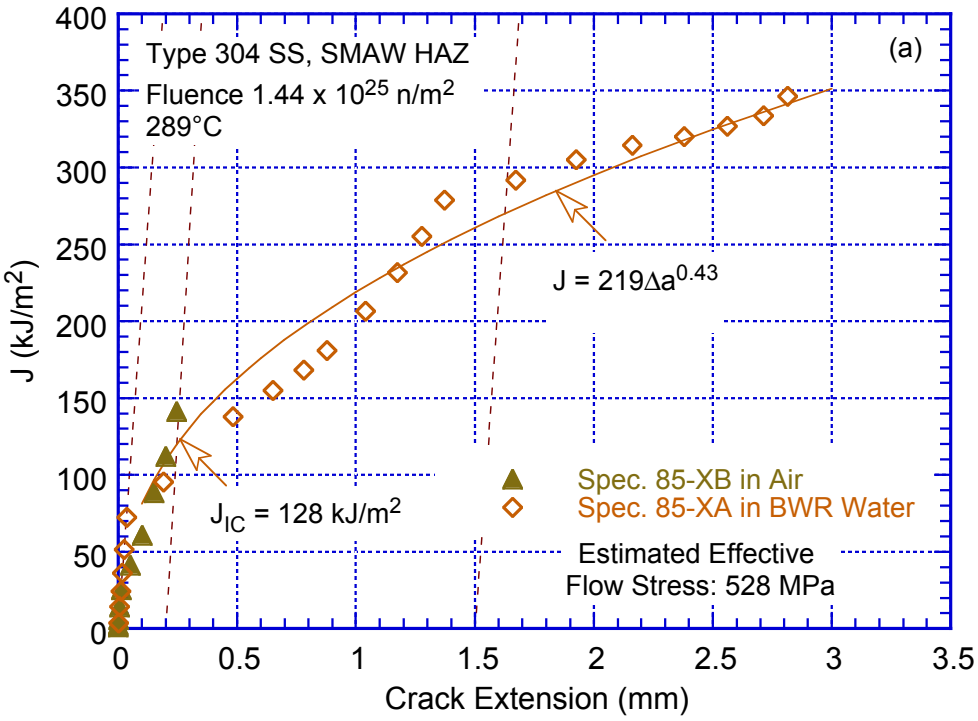

Figure 56a. Fracture toughness J-R curves for irradiated specimens of Type 304 SS SMA weld HAZ in air and NWC BWR environment (Ref. 21).

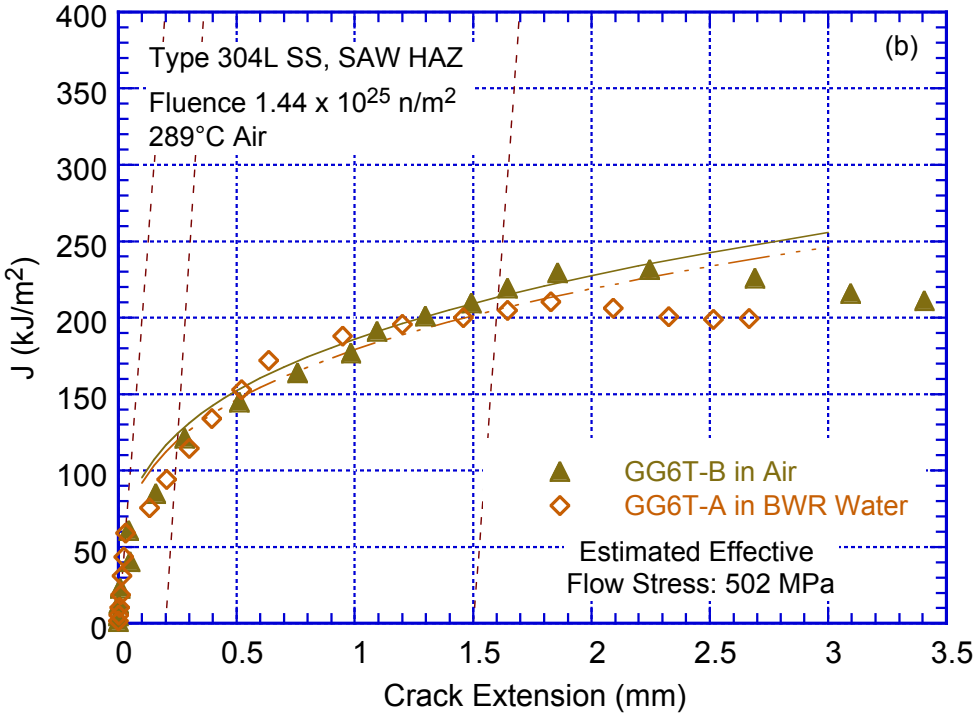

Figure 56b. Fracture toughness J-R curves for irradiated specimens of Type 304L SA weld HAZ in air and NWC BWR environment (Ref. 21).

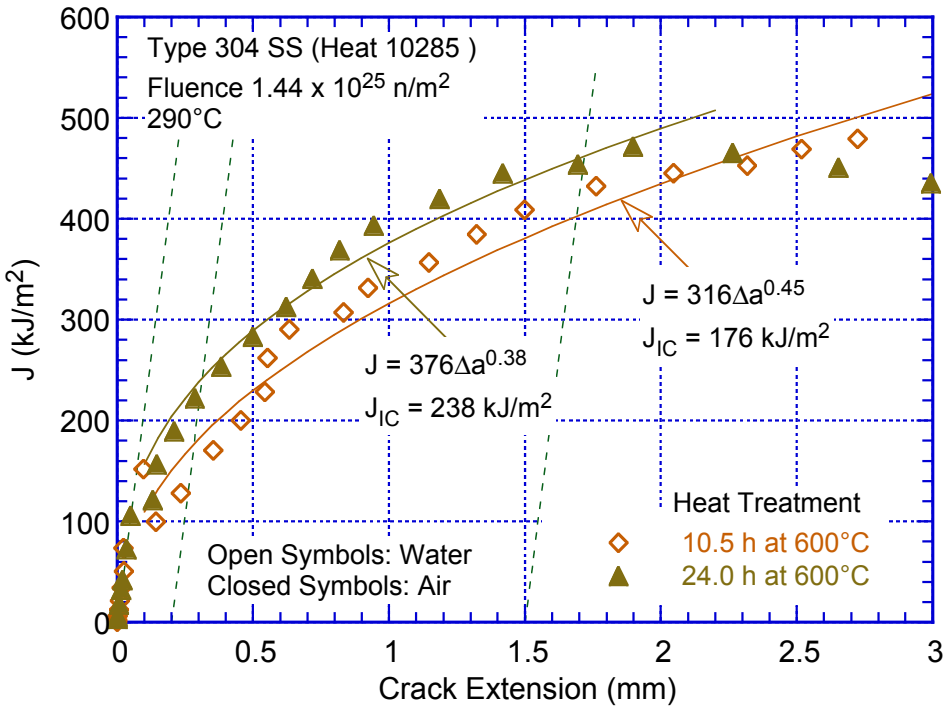

Figure 57. Fracture toughness J-R curves for sensitized Type 304 SS in air and NWC BWR water at 289°C (Ref. 21).

Thus, although available fracture toughness data in reactor coolant environments are inconclusive, the limited data suggest possible environmental effects on fracture toughness of CASS materials and austenitic SS welds, at least for materials with moderate or superior fracture toughness. Additional tests on irradiated CASS materials or SS welds in air and water environments should be conducted to determine the possible effect of LWR coolant environments on their fracture toughness.

Irradiation Temperature: The available data are inadequate to establish accurately the effects of the irradiation temperature on the fracture toughness of austenitic SSs. However, tensile data for austenitic SSs indicate that irradiation hardening is highest, and ductility loss is maximum, at an irradiation temperature of ≈300°C (≈572°F).[114] Thus, the J_{Ic} values for all materials irradiated above 350°C (662°F) (e.g., fast reactor irradiations), particularly for neutron exposures greater than 20 dpa, would be greater than for materials irradiated at temperatures of 290–320°C (554–608°F).

Test Temperature: The fracture toughness of nonirradiated austenitic SSs is known to decrease as the test temperature is increased. The change in the J_{Ic} of irradiated SSs as a function of test temperature is plotted in Fig. 59 for several grades of SSs and welds irradiated in LWRs and fast reactors. The fracture toughness of steels irradiated to relatively low doses (less than 5 dpa) decreases with increasing test temperature in most cases. However, for steels irradiated to more than 12 dpa test temperature has little effect on fracture toughness. The data on materials irradiated in LWRs or fast reactors exhibit similar trends. It should be noted that at

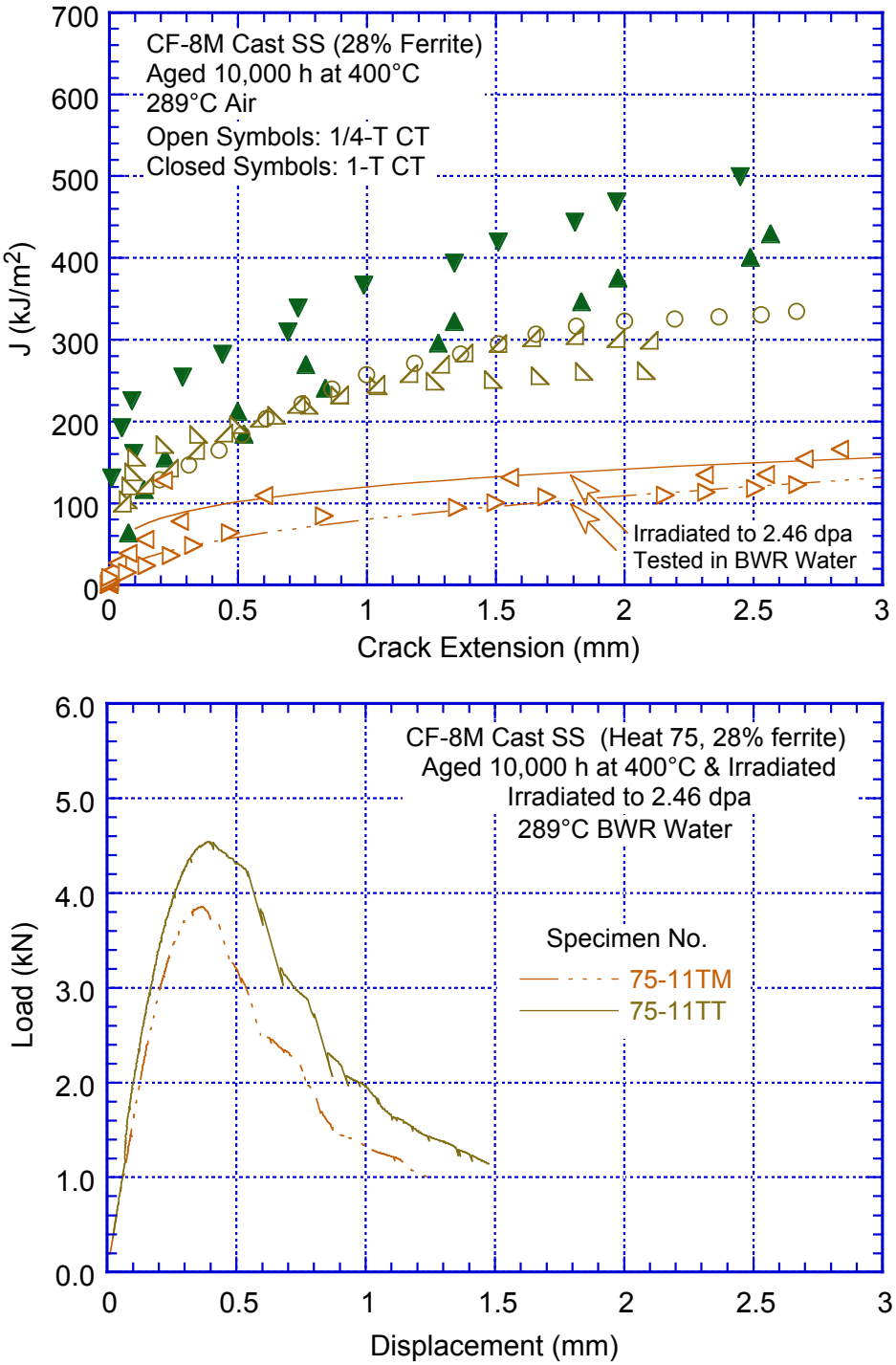

Figure 58. Fracture toughness J-R curves and load vs. loadline displacement curves for thermally aged and irradiated CF-8M steel (Ref. 21).

this fluence level the toughness value is already low, which makes it difficult to discern definitive trends. The effect of test temperature is also reflected in the fracture morphology of highly irradiated materials. At temperatures above 230°C (446°F) the failure mode is predominantly channel fracture characterized by a faceted fracture surface. It is associated with highly localized deformation along a narrow band of slip planes whereby the initial dislocation motion

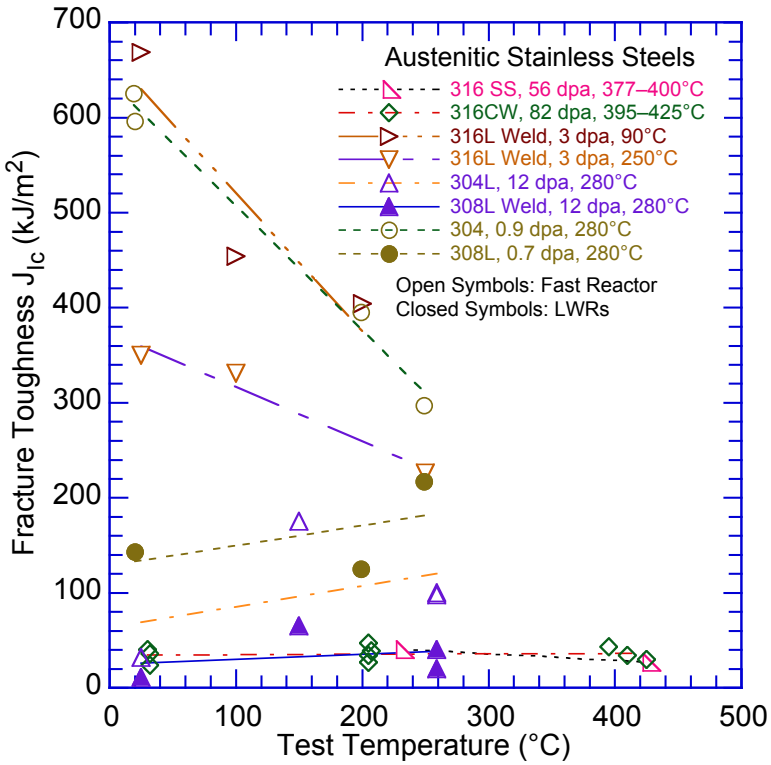

Figure 59.
Fracture toughness J_{Ic} of irradiated austenitic stainless steels and welds as a function of test temperature (Ref. 20).

along the narrow band clears away the irradiation-induced defect structure, creating a defect-free channel that offers less resistance to subsequent dislocation motion. The localization of the deformation ultimately leads to channel failure.

4.2 Fracture Toughness Trend Curve

The change in initiation toughness J_{Ic} of wrought austenitic SSs (including weld HAZ materials and sensitized SSs), CASS materials, and weld metals is shown in Fig. 60 as a function of neutron dose. [20] The fracture toughness data from both fast reactor and LWR irradiations are included. The irradiation temperatures range from 90 to 427°C (194 to 800°F) and test temperatures generally from 250 to 427°C (212 to 800°F). Only the data for CF-8 steel irradiated in a fast reactor to 10–11 dpa (inverted triangles in the Fig. 60b) were obtained at room temperature. The data in Fig. 59 indicate little or no effect of test temperature for materials irradiated to 12 dpa or higher, although the toughness values are already quite low above 12 dpa. In addition, as discussed previously in Section 3.1, the procedures for determining J_{Ic} vary among these studies. For example, in earlier studies a bilinear J-R curve was used to fit the data, whereas a power-law curve was used in the more recent studies. Different expressions have also been used for the blunting line. Overall, the results indicate little or no change in toughness below 0.5 dpa, a rapid decrease between 1 and 5 dpa, and no further change (saturation) beyond 10 dpa.

There appear to be some differences in behavior between subsets of the data in Fig. 60a. The threshold dose and the decrease in fracture toughness J_{Ic} on neutron dose seem to vary for different grades of materials. The average J_{Ic} of the Type 304 SS drops from above 150 kJ/m^2 (857 in.-lb/in.^{2}) at 1 dpa to 12–24 kJ/m^2 (69–137 in.-lb/in.^{2}) at about 2.2 dpa. The two data points at 2.25 dpa with very low J_{Ic} values are for instrumentation dry tube plunger material from an operating BWR tested using CNSR specimens.[6,9] Several data points on Type 304 SS

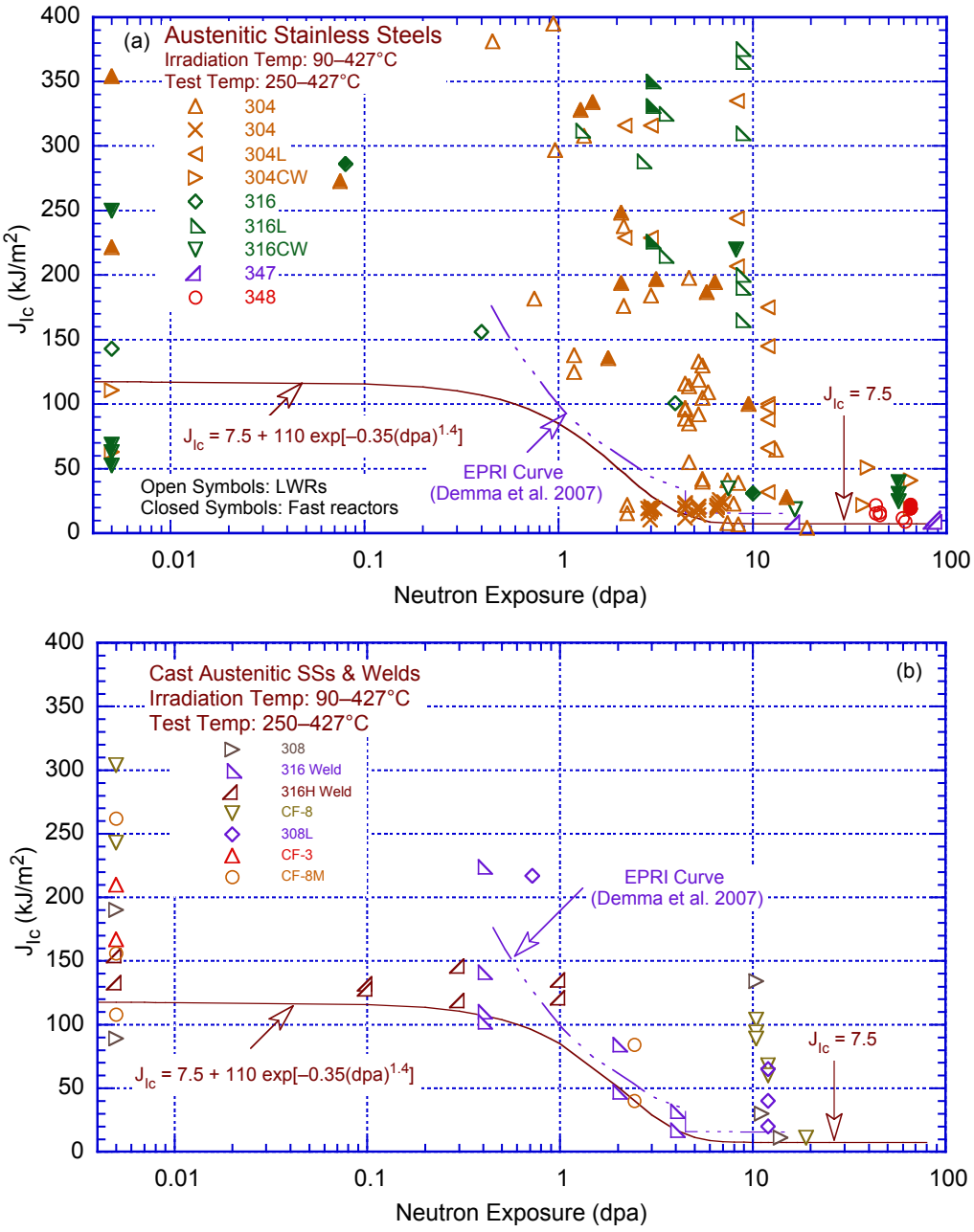

Figure 60. The change in initiation toughness J_{Ic} of (a) wrought austenitic SSs and (b) CASS materials and weld metals as a function of neutron exposure. The data points plotted at 0.005 dpa are for nonirradiated materials (Ref. 21).

irradiated to 2.25 and 3 dpa are below the lower bound curve for J_{Ic} values. In addition, for Type 316L SS the decrease in fracture toughness appears to occur at a somewhat higher fluence range (3 dpa to 10 dpa), and for Type 304L SS it occurs at a somewhat lower fluence. Therefore, the decrease in toughness with increasing fluence occurs earliest in Type 304L SS, followed by Type 304 SS and then Type 316 SS. The results indicate that for Type 304 SS, either the threshold for the decrease in fracture toughness is earlier or the decrease occurs faster.

The fracture toughness data in Fig. 60b for CASS materials and SS welds are lower than those of the wrought SSs for all dose levels less than the 10-dpa saturation level. However, the available fracture toughness data for irradiated SS welds and CASS materials are extremely limited. There are no data on any of these materials for fluences above 20 dpa. The existing data for welds suggest that ≈0.3 dpa may be considered a threshold neutron dose below which irradiation has little or no effect on fracture toughness of SS welds. The existing data for CASS materials are inadequate to define a threshold dose for irradiation effects on fracture toughness; there are no fracture toughness data for dose levels of 0.1–2.0 dpa. Furthermore, the potential combined interactions of thermal aging and neutron irradiation embrittlement of CASS materials and SS welds[50–49] have not been addressed.

The two curves shown in Fig. 60 represent a disposition curve proposed by EPRI[10] and a fracture toughness trend curve that bounds the existing data. The trend curve takes into consideration (a) a threshold neutron exposure for radiation embrittlement of austenitic SSs and a minimum fracture toughness for these materials irradiated to less than the threshold value; (b) a saturation neutron exposure and a saturation fracture toughness for materials irradiated to greater than this value; and (c) a description of the change in fracture toughness between the threshold and saturation neutron exposures. As shown in Fig. 10, the fracture toughness J_{Ic} curve that bounds the existing data for J_{Ic} as a function of neutron dose (in dpa) may be represented by

$$J_{Ic} = 7.5 + 110 \exp[-0.35(\text{dpa})^{1.4}]. \quad (54)$$

This lower bound curve represents a threshold dose of about 0.3 dpa for neutron embrittlement, a minimum fracture toughness J_{Ic} of ≈118 kJ/m^2 for neutron doses below the threshold value, a saturation threshold of 5 dpa beyond which the fracture toughness of these materials appears to saturate, a saturation fracture toughness J_{Ic} of 7.5 kJ/m^2 (or K_{Ic} or K_{Jc} of 38 MPa m$^{1/2}$), and a description of the change in toughness between 0.3 and 5 dpa. The J_{Ic} value of ≈118 kJ/m^2 for neutron doses below the threshold dose is appropriate for thermally aged and unaged CASS materials and SS flux welds. A value higher than 118 kJ/m^2 may be considered for the minimum fracture toughness J_{Ic} for wrought austenitic SSs irradiated below the threshold dose for neutron embrittlement. The description of the change in fracture toughness below 1.5 dpa will change accordingly. The lower-bound trend curve given by Eq. 54 is consistent with the Materials Reliability Program (MRP) lower-bound model proposed for PWRs.[16] The MRP model is expressed in terms of a lower-bound K_{Jc} (MPa m$^{1/2}$) curve. It bounds all the fracture toughness data from fast reactors, BWRs, and PWRs as a function of the neutron dose (in dpa) and is given by the expression,

$$K_{Jc} = 180 - 142[1-\exp(-\text{dpa})]. \quad (55)$$

Equations. 54 and 55 both predict a saturation fracture toughness K_{Ic} of 38 MPa m$^{1/2}$. For materials irradiated below the threshold dose for irradiation embrittlement, Eq. 54 predicts a minimum K_{Jc} of about 151 MPa m$^{1/2}$. However, for materials such as SS welds or weld HAZ, the fracture toughness values predicted by the MRP expression may be higher than the minimum toughness of the nonirradiated materials. Therefore, the disposition curve proposed by EPRI is not bounding for the existing data for BWR-irradiated austenitic SSs. For example, at neutron doses <0.7 dpa, the J_{Ic} values based on the EPRI curve are higher than the minimum J_{Ic} of nonirradiated SS welds (particularly flux welds), some heats of wrought SSs, and most thermally aged CASS materials with >15% ferrite.[50] The saturation K_{Ic} of 55 MPa m$^{1/2}$ at 4.5 dpa for the EPRI curve is also higher than the value of 38 MPa m$^{1/2}$ previously proposed by MRP for PWRs.[16] The saturation K_{Ic} for the EPRI curve was based on data for which the

specimen orientation was unknown. Recent data indicate that fracture toughness in the transverse orientation is nearly half of that in the longitudinal orientation.[10] Therefore, the bounding K_{Ic} values above 4.5 dpa are likely to be lower than 55 MPa $m^{1/2}$. Furthermore, as seen in Fig. 60b, some of the data for SS welds irradiated to 2–4 dpa are also below the EPRI curve.

The existing fracture toughness J_{Ic} data for irradiated austenitic SS welds, CASS materials, and austenitic SS HAZ, including some recent data published after the plot in Fig. 60 was prepared, are plotted as a function of neutron dose in Fig. 61.[9,15,16,20,53,88,105,134,138 142,148] Although most of the data were obtained in air, some of the fracture toughness J-R curve tests were performed in LWR coolant environments. As discussed before, the fracture toughness obtained from tests in LWR environments may be lower than that from tests in air; particularly for materials with high fracture toughness. The plots in Fig. 61 indicate that the lower-bound curve for J_{Ic} values may not be adequate for austenitic SS welds; some of the data for both irradiated and nonirradiated welds falls below the lower-bound curve. As discussed earlier in Section 2.6, the lower-bound fracture toughness of unaged and aged austenitic SS welds are given by Eqs. 45 and 46, respectively. The fracture toughness J_{Ic} for unaged and aged SS welds are better represented by 73.4 and 40 kJ/m^2, respectively (the lower-bound J_{Ic} for unaged welds is shown by dashed line in Fig. 61). Furthermore, some of the data obtained in LWR environments for austenitic SS HAZ, welds, and CASS materials also falls below the lower-bound curve. The data for aged CF-8 material in PWR SWC environment at 54°C are significantly lower. Therefore, based on these results the minimum acceptable fracture toughness J_{Ic} values for nonirradiated wrought and CASS materials and their welds need to be established.

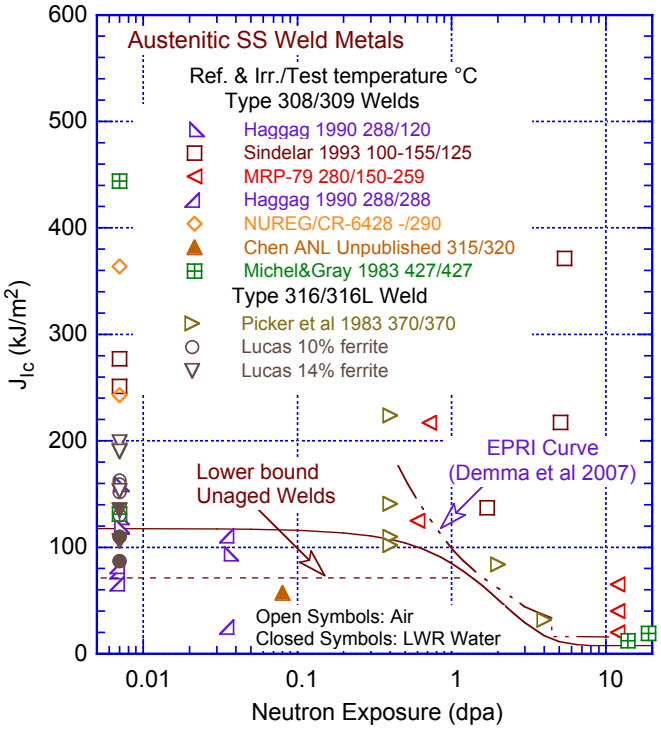

Figure 61. Plots of fracture toughness J_{Ic} values as a function of neutron dose for (a) austenitic SS welds, (b) CASS materials, and (c) austenitic SS HAZ. Solid line represents the lower-bound J_{Ic} values proposed in NUREG/CR-7027. The data points plotted at 0.007 dpa are for nonirradiated materials.

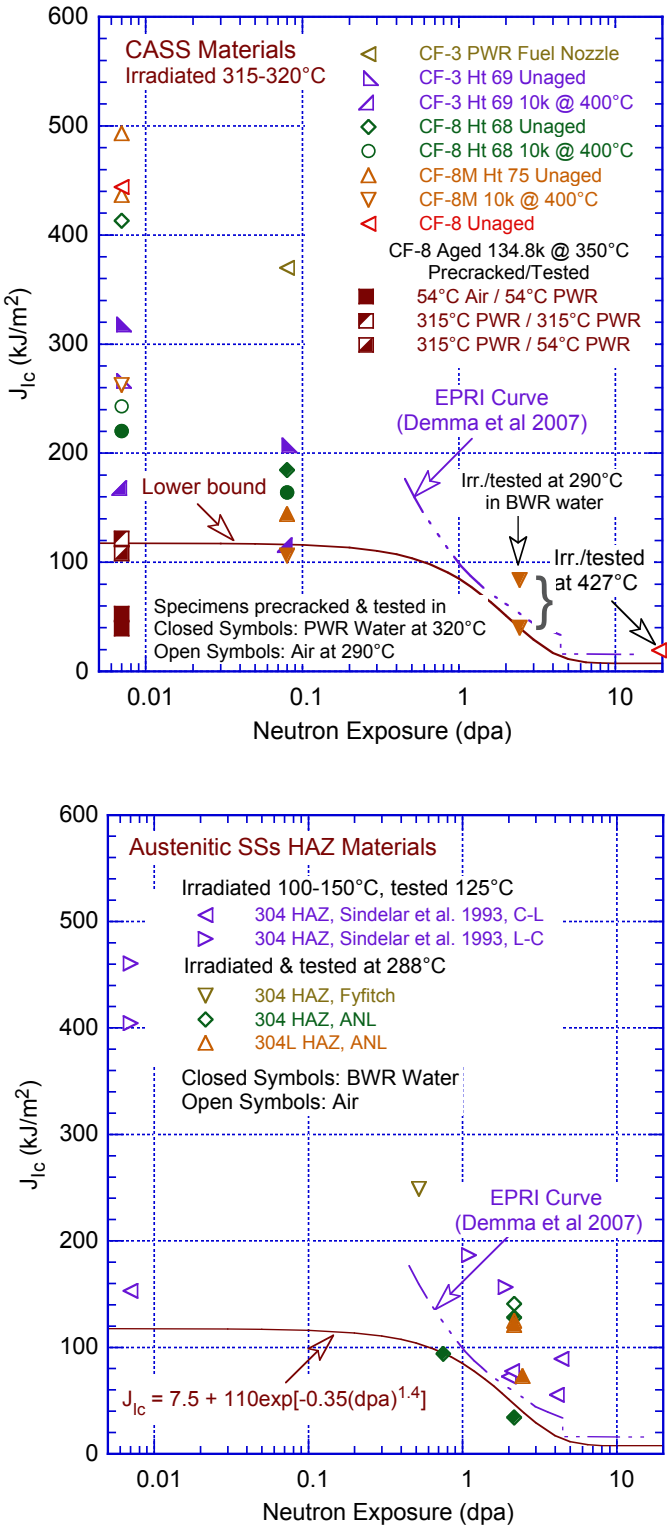

Figure 61. Continued.

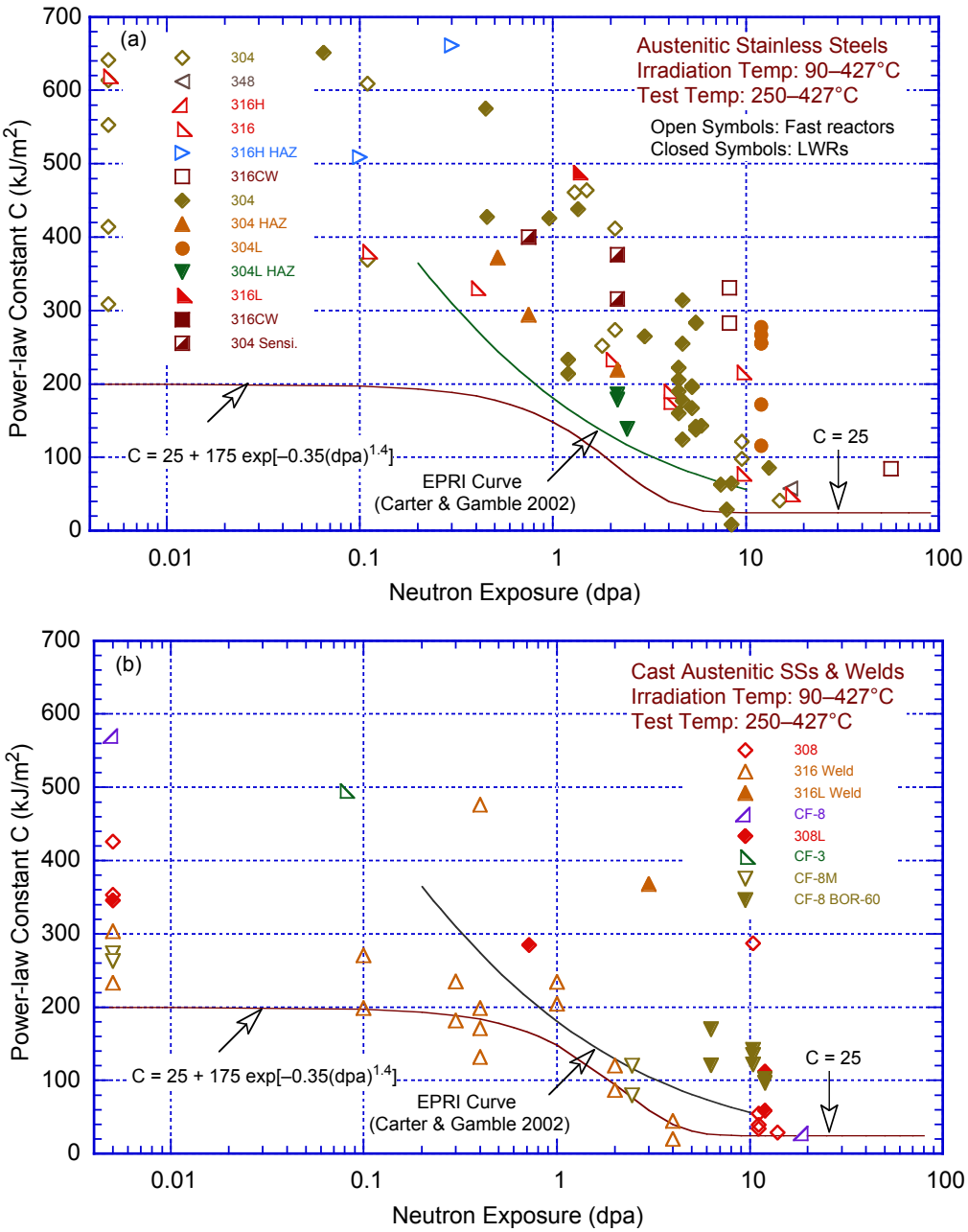

Figure 62. Change in coefficient C of the power-law J-R curve for (a) wrought austenitic SSs and (b) CASS materials and weld metals as a function of neutron exposure. The data points plotted at 0.005 dpa are for nonirradiated materials (Ref. 21).

A fracture toughness J-R curve may be used to analyze material behavior for loading beyond J_{Ic}. The J-R curve is expressed in terms of the J integral and crack extension (Δa) by the power law $J = C(\Delta a)^n$. At dose levels below the threshold dose for saturation (i.e., at dose levels less than ≈5 dpa), the effect of neutron irradiation on the fracture toughness of austenitic SSs can also be represented by a decrease in the coefficient C of the power-law correlation for the J-R curve with neutron dose. The variation of C for wrought and CASS materials and welds as a function of neutron dose is shown in Fig. 62.[21] Except for the results for CF-3 (green right-angle triangle in Fig. 62b) and CF-8 irradiated in BOR-60 reactor (filled inverted triangle in Fig. 62b),

the remaining data were obtained at temperatures above 250°C. Based on the data trends in Fig. 59, test temperature should have little or no effect on the data for CF-8 steel. However, the constant C for CF-3 steel may be more than a factor of two lower at LWR operating temperatures. The two curves in Fig. 62 represent the disposition curve proposed by EPRI for BWRs,[13] and a trend curve for coefficient C that bounds the existing data.

Even for fluence levels above 10 dpa, most heats of wrought austenitic SSs show ductile crack extension in the toughness tests. Under similar irradiation conditions, the coefficient C for CASS materials and welds is lower than that for wrought SSs. However, since most of the data are from irradiations in fast reactors and at temperatures of 370–427°C (698–800°F), the values for the power-law coefficient C are likely to be lower for irradiations at LWR operating temperatures. As mentioned previously, fracture toughness data are limited on materials irradiated in LWRs to neutron dose levels of 0.1–1.0 dpa or above 10 dpa. Therefore, it is not possible to define accurately the lower-bound trend curve for the power-law coefficient C as a function of neutron dose. For fluences less than 5 dpa, as shown in Fig. 62, the existing fracture toughness data can be bounded by the following expression for C:

$$C = 25 + 175 \exp[-0.35(\text{dpa})^{1.4}], \quad (56)$$

and an exponent n equal to 0.37 (the median value of the experimental data). The exponent n of the power-law curve typically ranges from 0.35 to 0.70 for nonirradiated materials and 0.16 to 0.65 for irradiated materials. Unlike the behavior for thermally aged cast austenitic SSs, where exponent n typically decreases with a decrease in fracture toughness,[50] no obvious trend of n with fluence is evident. For irradiated materials, the median value of n is 0.37.

Equation 56 yields a C value of ≈200 kJ/m^2 (1285 in.-lb/in.^{2}) for materials irradiated to less than 0.1 dpa and ≈31 kJ/m^2 (≈160 in.-lb/in.^{2}) for materials irradiated to ≈5 dpa. These values yield J_{Ic} values of 125 and 17 kJ/m^2, respectively, for materials irradiated to <0.1 and 5 dpa. These values are consistent with the J_{Ic} trend curve of Fig. 60. The J_{Ic} at 5 dpa is also consistent with the data for the CT specimens of Type 304 SS irradiated to ≈4.5 dpa in a BWR (closed diamonds in Fig. 60a).

As noted previously, ductile crack extension was also not observed for some specimens of a 20% CW Type 316 SS irradiated to 74–88 dpa in a fast reactor at 410–425°C (770–797°F). The specimens failed by a quasi-cleavage fracture believed to be an indirect consequence of the onset of void swelling in the material. The K_{Ic} values were 74–90 MPa m$^{1/2}$ (67–82 ksi in.$^{1/2}$).

The existing data for fracture toughness power-law constant C, including some recent data published after the plot in Fig. 62 was prepared, for irradiated austenitic SS welds, CASS materials, and austenitic SS HAZ, are plotted as a function of neutron dose in Fig. 63. The data trends for power-law constant C are similar to those observed for fracture toughness J_{Ic} values. As discussed earlier, for some materials, the fracture toughness in LWR environments may be lower than in air. The plots in Fig. 63 indicate that the lower-bound curve for constant C based on Eq. 56 may not be adequate for austenitic SS welds and CASS materials. Therefore, the minimum acceptable fracture toughness J-R curves for irradiated and even nonirradiated wrought and CASS materials and their welds need to be established.

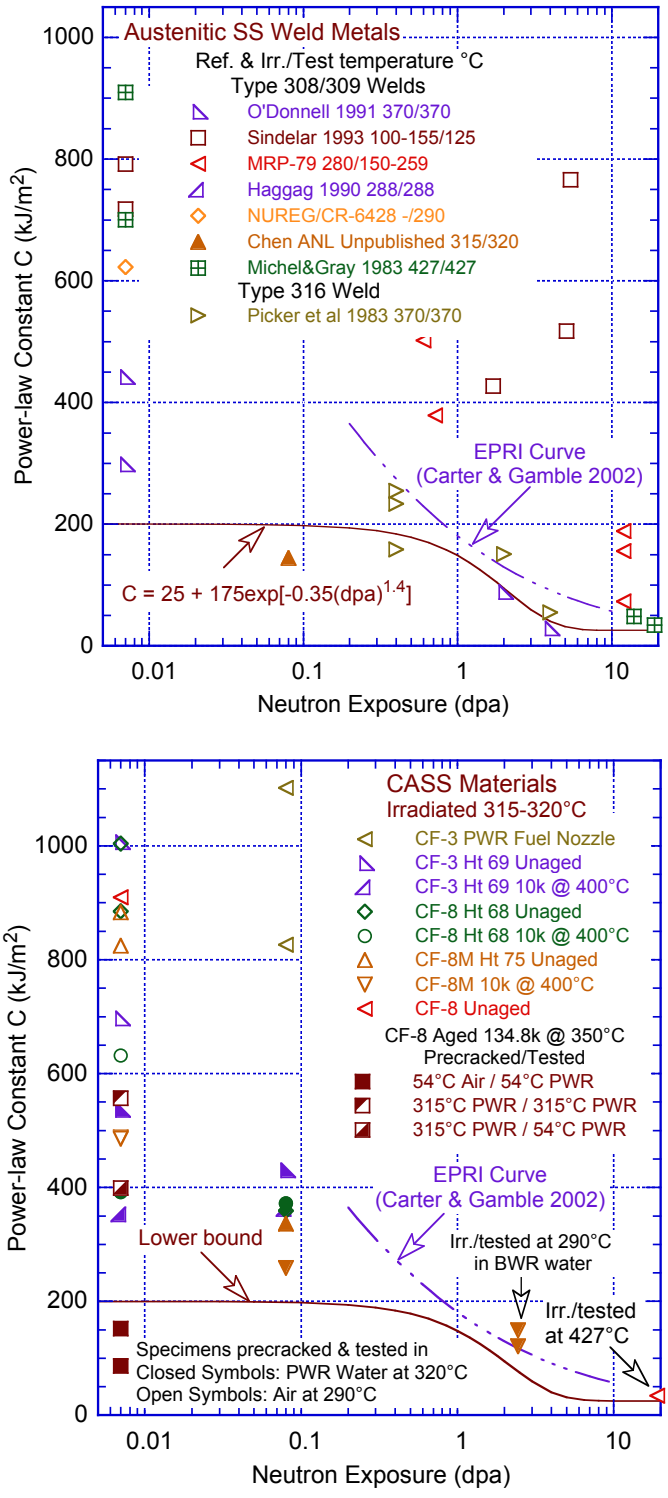

Figure 63. Plots of constant C of the power-law J-R curve as a function of neutron dose for (a) austenitic SS welds, (b) CASS materials, and (c) austenitic SS HAZ. The solid line represents the lower-bound C values proposed in NUREG/CR-7027. The data points plotted at 0.007 dpa are for nonirradiated materials.

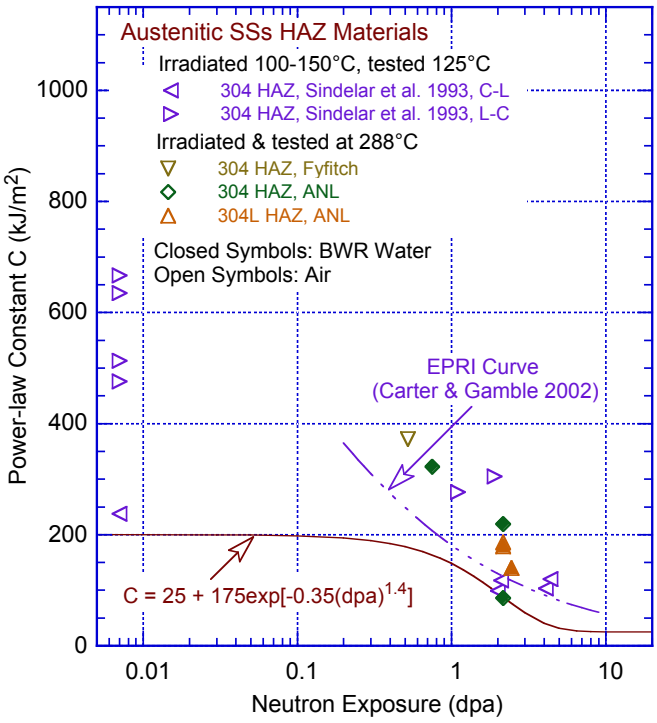

Figure 63. Continued.

5. Combined Effects of Thermal and Neutron Embrittlement

It is well known that thermal aging of CASS materials and austenitic SS welds at reactor operating temperatures leads to degradation of their fracture properties.[43,50–53] Typically wrought SSs are completely austenitic. However, austenitic SS welds and CASS materials have a duplex microstructure consisting of austenite and ferrite phases. The ferrite phase increases the tensile strength and improves resistance to SCC, but it is susceptible to thermal embrittlement after extended service at reactor operating temperatures. Thermal aging of CASS materials at 250–400°C (482–752°F) leads to precipitation of additional phases in the ferrite.[60,64,66] The formation of the Cr-rich α' phase by spinodal decomposition of ferrite is the primary mechanism for thermal embrittlement; it strengthens the ferrite phase by increasing strain hardening and the local tensile stress. Thermal aging has little or no effect on the austenite phase. Thus, thermal aging of CASS materials and SS welds leads to the development of a material with a brittle phase dispersed in a ductile matrix.

The minimum fracture toughness that can occur due to thermal aging embrittlement of CASS materials depends strongly on the chemical composition of the steel, the casting process used to construct the component, and the ferrite content and morphology.[50] A globular ferrite morphology in which the brittle ferrite phase is isolated in an austenitic matrix will have a higher fracture toughness than a lacy morphology in a material with greater than 10% ferrite, where a continuous fracture path through the embrittled ferrite is possible. The minimum toughness occurs when the ferrite is fully embrittled, and the remaining toughness depends on the toughness provided by the ductile matrix surrounding the embrittled phase. Furthermore, CASS materials with high levels of Mo (e.g., CF-8M) show greater susceptibility to thermal embrittlement than steels with low Mo content (e.g., CF-3 or CF-8). Static cast steels are more susceptible to thermal embrittlement than centrifugally-cast components. Based on this update of the previous study,[50] the predicted coefficient C and exponent n for the saturation fracture toughness J-R curves (i.e., the lowest fracture toughness that could be achieved for the steel after thermal aging) for thermally-aged CASS materials with <10%, 10–15%, 15–25%, and 25–40% ferrite were given previously in Table 3 in Section 2.5.2.

The results for austenitic SS welds indicate that the decrease in fracture toughness due to thermal aging also depends on the ferrite content and initial toughness of the weld.[53] Differences in the fracture toughness of austenitic SS welds arise from differences in the density and size of inclusions in the material. In austenitic SS welds, failure typically occurs by the formation and growth of microvoids near hard inclusions. Welds with relatively high fracture toughness (e.g., GTA or tungsten inert gas [TIG] weld) show a significant decrease due to thermal aging, whereas welds with poor fracture toughness (e.g., SA, SMA, or manual metal arc [MMA] welds) show minimal change. In the latter case, failure primarily occurs by the formation and growth of microvoids. Such processes are relatively insensitive to thermal aging. The existing data indicate that at 280–350°C, the fracture toughness J_{IC} of thermally aged welds can be as low as 40 kJ/m^2. As shown in Fig. 35, a conservative estimate of the J-R curve for aged austenitic SS welds[53] is given by $J = 40 + 83.5\ \Delta a^{0.643}$.

However, reactor core internal components are subjected to both elevated temperatures and neutron irradiation. The mechanisms of thermal embrittlement and neutron embrittlement have been discussed in detail in Sections 2 and 4, respectively. Although both the thermal aging embrittlement and the neutron irradiation embrittlement of ferrite have been well characterized, an issue that has been a concern for reactor core internal components is the possibility of a combined interaction between thermal embrittlement and irradiation embrittlement of materials with duplex microstructure such as CASS materials and austenitic SS welds. The concurrent

exposure to elevated temperatures and high neutron fluence levels could result in a combined effect wherein the service-degraded fracture toughness is reduced from the levels predicted independently for either of the two mechanisms.

The screening criteria for susceptibility of CASS materials to thermal embrittlement and the methodology for estimating thermal embrittlement of CASS materials are presented in Sections 2.5.4 and 2.5.5, respectively. An assessment of thermal embrittlement of austenitic SS welds is described in Section 2.6. The effect of neutron irradiation on the fracture toughness of wrought and CASS materials and austenitic SS welds is discussed in Section 4, and the change in fracture toughness J_{IC} and coefficient C of the power-law J-R curve with neutron dose is shown in Figs. 60 and 62, respectively.

For license renewal, to account for the effects of thermal aging and neutron irradiation embrittlement on the fracture toughness of reactor core internal components, the NRC staff has proposed an aging management program (AMP). The program is implemented for CASS components that either have (a) a fluence of greater than 1×10^{17} n/cm^2 (0.00015 dpa) or (b) are determined to be susceptible to thermal embrittlement. The AMP should consist of either a supplemental examination of the affected components as part of the applicant's 10-year ISI program during the license renewal term, or a component-specific evaluation to determine the susceptibility to loss of fracture toughness.[45] Furthermore, the program should provide for the consideration of the combined loss of fracture toughness due to neutron irradiation embrittlement and thermal aging embrittlement. The screening criteria to determine the susceptibility of CASS components to thermal aging embrittlement are outlined in Table 4.[45]

In NUREG/CR-7027, for the cast and wrought austenitic SSs and welds listed in Fig. 62, the experimental J-integral values at a crack extension of 2.5 mm are plotted as a function of neutron dose. The plots are reproduced in Fig. 64. The solid curve in Fig. 64 represents the predicted values of $J_{2.5}$ at 2.5-mm crack extension that are expected to bound the existing experimental data shown in Fig. 62. The curve was obtained using the power-law J-R curve relationship, coefficient C determined from Eq. 56 and exponent n of 0.37. The lower bound curve indicates that for CASS materials and austenitic SS welds irradiated up to 1.0 dpa, the predicted $J_{2.5}$ values are above the screening value of 255 kJ/m^2 (1456 in.-lb/in.^{2}) for all materials except some of the data for Type 316 welds are below the lower-bound curve.

In addition to possibly altering the threshold dose for neutron embrittlement, the combined effects of neutron and thermal aging embrittlement could decrease the saturation fracture toughness of irradiated austenitic SS welded and CASS materials and accelerate the change in fracture toughness between the threshold and saturation neutron exposures. Figure 64 shows the results of two tests on a CF-8M steel that was thermally aged for 10,000 h at 400°C and then irradiated to well above the threshold dose for neutron embrittlement (right-angle triangles in Fig. 64b). The resulting $J_{2.5}$ values for these two tests are bounded by the curve for other SSs irradiated to a similar level, i.e., neutron irradiation of thermal aged material does not seem to lower the toughness below that expected for irradiation alone at these neutron dose levels.

However, at the time NUREG/CR-7027 was published, fracture toughness data on irradiated SS welds and CASS materials, particularly at 0.1–2.0 dpa, were inadequate to accurately define the threshold dose beyond which the fracture toughness of austenitic SSs begins to significantly decrease. Furthermore, the evaluation in NUREG/CR-7027 did not consider the combined interaction of neutron irradiation and thermal aging embrittlement. Embrittlement of the ferrite phase from neutron irradiation occurs at lower dose levels than does embrittlement of the austenite phase. The NRC staff has proposed that CASS materials neutron dose levels greater

than 10^{17} n/cm^2 (0.00015 dpa) be considered susceptible to neutron embrittlement.[45] A shift in the nil-ductility transition temperature of up to 150°C (302°F) has been observed in pressure vessel steels irradiated to 0.07–0.15 dpa.[153] Thus, embrittlement of ferrite is expected to occur at 0.05–1.0 dpa, whereas any significant neutron embrittlement of the austenite phase occurs only above ≈0.5 dpa (Fig. 60).

The available data on fracture toughness $J_{2.5}$ for austenitic SS welds, CASS materials, and SS HAZ materials are plotted as a function of neutron dose in Figs. 65a, 65b, and 65c, respectively. The solid curve in these figures represent the J-integral values based on the lower bound trend

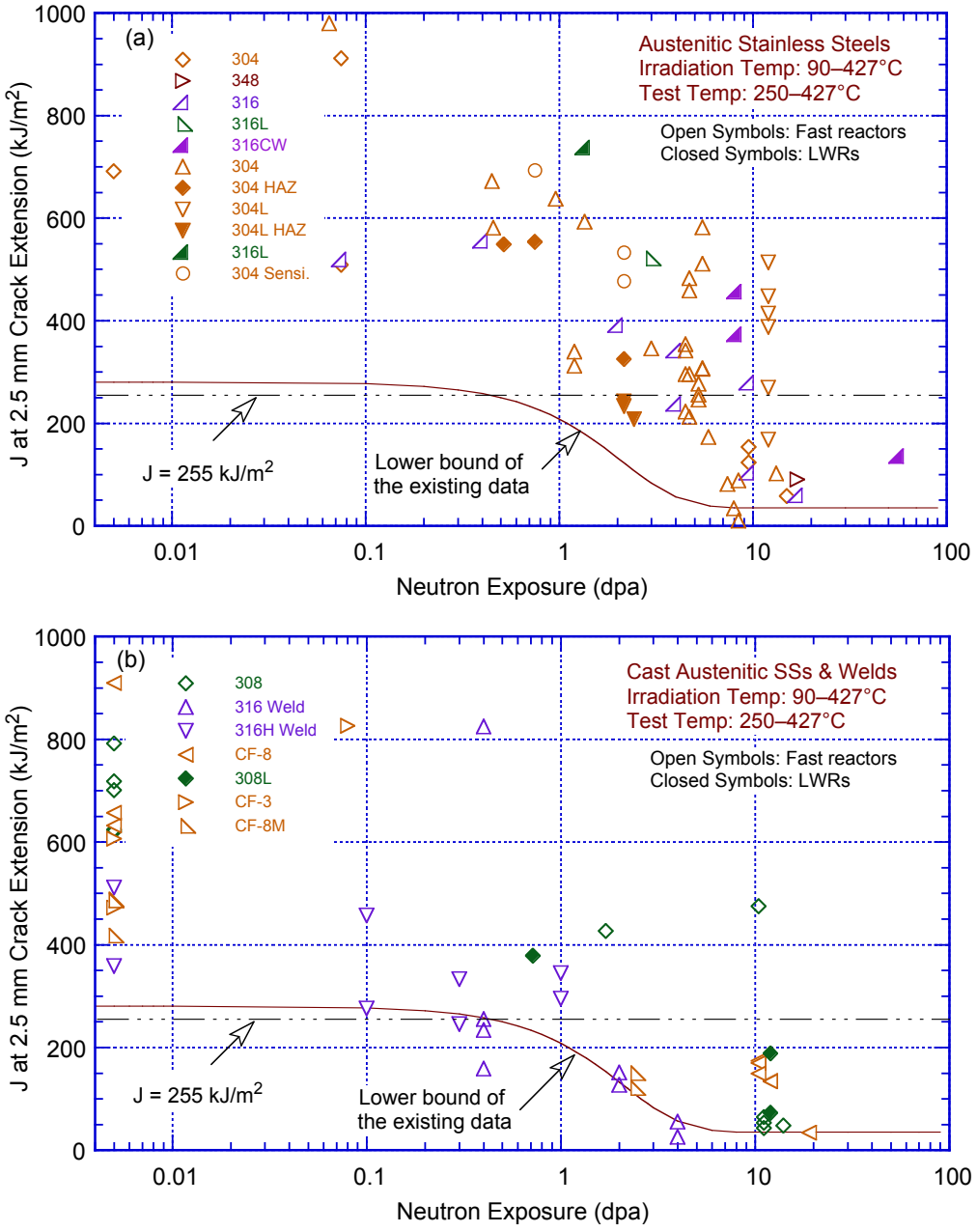

Figure 64. Experimental values of J-integral at a crack extension of 2.5 mm for (a) wrought austenitic SSs and (b) cast materials and SS weld metals plotted as a function of neutron dose. The data points plotted at 0.005 dpa are for nonirradiated materials.

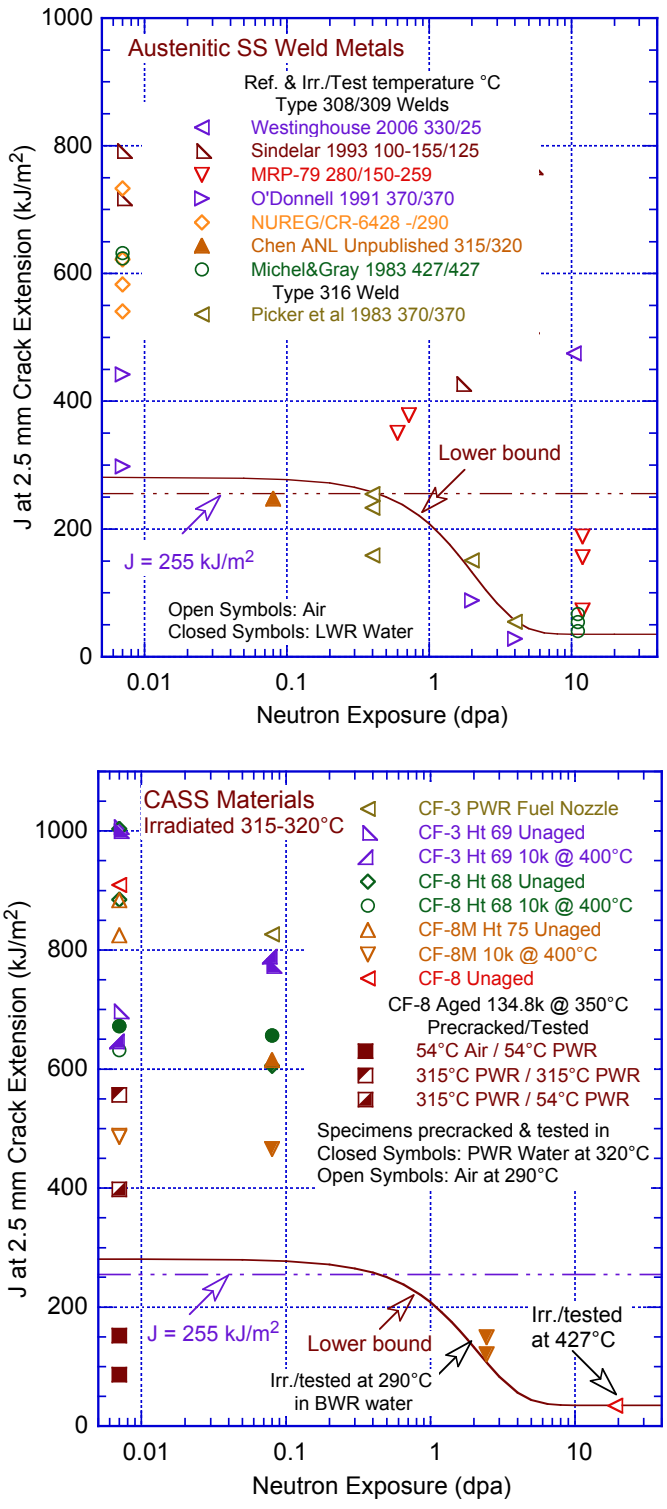

Figure 65. Plots of fracture toughness $J_{2.5}$ values as a function of neutron dose for (a) austenitic SS welds, (b) CASS materials, and (c) austenitic SS HAZ. Solid line represents the lower-bound $J_{2.5}$ values proposed in NUREG/CR-7027. The data points plotted at 0.007 dpa are for nonirradiated materials.

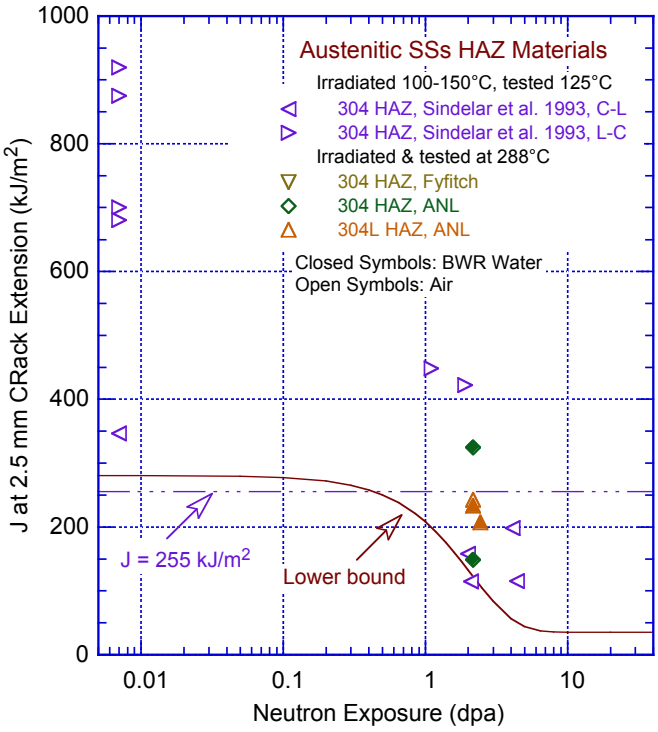

Figure 65. Continued.

curve for coefficient C given in Fig. 62 and median value of 0.37 for exponent n of the J-R curve. The open symbols in the figure represent the $J_{2.5}$ values in air and solid symbols represent the values in LWR coolant environment. The results indicate that the $J_{2.5}$ values of some of the austenitic SS welds, particularly the values for Type 316 weld, may not be bounded by the lower bound trend curve.

The limited fracture toughness data obtained from tests in LWR coolant environments indicate that the LWR coolant environment can further decrease fracture toughness of these materials relative to that obtained in air. For some heats of wrought and cast austenitic SSs and welds, some values of fracture toughness in coolant environment are likely to be below the lower-bound trend curve. The two tests on thermally aged CF-8 material tested in PWR environment at 54°C are significantly below the curve. Additional fracture toughness data in LWR coolant environments are needed to define the lower bound fracture toughness of these materials in LWR environments.

This page is intentionally left blank.

6. Summary

The significant results for thermal embrittlement; IASCC susceptibility and CGRs; and neutron embrittlement, including combined effects of thermal and neutron embrittlement, for austenitic SS welds, HAZ materials, and CASS materials are summarized below. In addition, information gaps in the data needed to address the effects of thermal and neutron embrittlement on the structural and functional integrity of CASS components and austenitic SS welds in LWR systems are identified.

6.1 Significant Results

6.1.1 Thermal Embrittlement of Duplex Stainless Steels

Cast Austenitic Stainless Steels

Stainless steels are completely austenitic in the wrought condition, but welded SSs and CASS materials have a duplex structure consisting of austenite and ferrite phases. The ferrite phase increases tensile strength and improves resistance to SCC. The ferrite content generally varies significantly in CASS components, particularly static cast components. Variations have been observed in the range of 3.0–22.5% in a CF-8M hot-leg elbow and 1.5–15.0% in a crossover-leg elbow. For centrifugally cast pipes, the ferrite content varies across the wall thickness. These observations indicate that when measured ferrite content is used for design analyses, it is important to ensure that it is representative of the entire component.

The quantitative metallographic method provides the most accurate estimate of ferrite content in CASS components. However, it may not be practical because of large variations in ferrite within a casting. Therefore, determination of ferrite from chemical composition of the material offers the most useful and common method for estimating ferrite in castings or welds. For CASS materials, the average measured ferrite is comparable with the values estimated from the material chemical composition using the Hull's equivalent factors or from the ASTM A800/A800M methodology, although the latter seems to underestimate ferrite contents above 20%. The difference between ferrite contents calculated from Hull's equivalent factor and measured values is ±6% ferrite. Both methods underestimate the ferrite contents of austenitic SS welds. The most commonly used instruments for measuring ferrite contents in CASS materials and austenitic SS welds are the Magne-Gage and Ferritescope. However, the surface roughness or curvature of the sample can introduce error because of variations in the magnetic linkage between the measuring probe and the test specimen.

It is well established that CASS materials are susceptible to thermal embrittlement when aged at temperatures between 290 and 450°C (554 and 842°F). The formation of Cr-rich α' regions in the ferrite is the primary mechanism for thermal embrittlement. The α' phase strengthens the ferrite matrix and increases strain hardening, which raises the local tensile stresses above the critical value for brittle fracture. In addition, the formation of G phase and precipitation and/or growth of carbides or nitrides at the phase boundaries lead to a brittle failure by phase boundary separation. These particles may also facilitate cleavage of the ferrite by particle cracking. The microstructural changes result in brittle transgranular fracture of the ferrite or separation of the ferrite/austenite phase boundary. The degree of embrittlement and, hence, the toughness of the material, is controlled by the amount of brittle fracture. A predominantly brittle failure occurs when either the ferrite phase is continuous (i.e., high ferrite content) or the ferrite/austenite phase boundary provides an easy path for crack propagation (i.e., high-C grades of steel). Furthermore, the microstructural changes in the ferrite phase by spinodal decomposition are

very sensitive to the initial state of the ferrite. Thus, any manufacturing process parameter that improves the homogeneity of the ferrite solid solution, such as long homogenizing heat treatments and rapid quench, delay the beginning of the ferrite decomposition, which results in a more aging-resistant CASS material.

Studies at Argonne have characterized the extent of thermal embrittlement of CF-3, CF-8, and CF-8M steels in terms of the RT Charpy-impact energy. All CASS materials attain "saturation" RT Charpy-impact energy (i.e., a minimum value that would be achieved by the material) after long-term thermal aging. The actual saturation value is independent of aging temperature but depends strongly on the chemical composition of the steel. It is lower for the CF-8M steel than for the CF-3 or CF-8 steels, and decreases with an increase in ferrite content or the concentration of C or N in the steel. The kinetics of embrittlement are controlled by three processes: spinodal decomposition, precipitation and growth of phase boundary carbides, and precipitation of G phase in ferrite. Small changes in the composition cause the kinetics to vary significantly. The activation energies range from 65 to 230 kJ/mole (15 to 55 kcal/mole). The low values are most likely due to the formation of carbides/nitrides at the phase boundaries or G-phase and/or γ_2 precipitation in ferrite. The presence of Ni-Si-Mo clusters in the ferrite matrix of an unaged material is considered a signature of steels that show low activation energy (i.e., fast embrittlement). Such materials contain G-phase particles after aging.

The laboratory data obtained for materials aged at 400°C (752°F) and the activation energy for the process of embrittlement are typically used to predict the end-of-life impact strength at reactor temperatures. This methodology, however, assumes a unique aging behavior at 400°C, which is not observed for CASS materials. For a given decrease in the RT Charpy-impact energy, the time for aging at 400°C varies by more than two orders of magnitude for the various heats of CF-3, CF-8 and CF-8M steels. In general, CASS materials that take longer for thermal embrittlement to start have low activation energy (i.e., embrittlement is fast) and materials that take short time for embrittlement to start have high activation energy (i.e., take longer to embrittle). Therefore, estimates of embrittlement at reactor temperatures (290–320°C [554–608°F]) are not likely to be significantly affected by which set of activation energy and kinetics data are used for estimations.

An earlier report, NUREG/CR-4513, Rev. 1, presented a methodology for estimating the fracture toughness J-R curves of CASS materials under LWR operating conditions. The saturation RT Charpy-impact energy was correlated to the ferrite content and chemical composition of the CASS material. The existing thermal aging data indicated that a correlation between RT Charpy-impact energy and ferrite content alone did not yield good results. The extent of embrittlement as a function of time and temperature of reactor service was estimated from the extent of embrittlement at saturation and the correlations describing the kinetics of embrittlement, which were also given in terms of chemical composition.

However, the methodology of NUREG/CR-4513, Rev. 1, is not applicable to CASS materials containing greater than 25% ferrite. A recent EPRI Report 1019128 presented a Westinghouse database of random sampling of heats of CASS material from 15 nuclear power plants. The data indicated that about 9% of the heats of CF-8M material currently in use in operating nuclear power plants contain greater than 25% ferrite. There is no acceptable methodology for estimating the reduction in fracture toughness of these materials with reactor service.

In this report, the correlations presented in NUREG/CR-4513, Rev. 1, for estimating the reduction in fracture toughness of CASS materials as a function of reactor service have been updated to cover CASS materials containing greater than 25% ferrite. The NUREG/CR-4513

expressions for estimating fracture toughness coefficient C and exponent n of the J-R curve at RT and 290–320°C (554–608°F) from RT Charpy-impact energy have been reevaluated and, if needed, updated to cover ferrite contents up to 40%. Common lower-bound J-R curves at RT and 290–320°C for thermally aged static and centrifugally cast CF-3, CF-8, and CF-8M steels with four ranges of ferrite content, <10%, 10–15%, 15–25%, and 25–40% ferrite, are also defined. Separate expressions are proposed for CF-8M steels containing <10% Ni and those containing ≥10% Ni. The latter are more susceptible to thermal embrittlement than the other grades.

A recent scoping study on low-temperature crack propagation for CASS CF-8 material in PWR environments investigated the potential synergy between hydrogen embrittlement and thermal embrittlement associated with decomposition of the ferrite at reactor temperatures. Fracture toughness J-R curve tests were conducted in air and PWR SWC at 54°C on 1-T CT specimens of CF-8 material (Argonne Heat 68) that was thermally aged for about 15.8 yr at 350°C (662°F). The results show a large effect of PWR SWC environment on fracture toughness; every material and test condition was identical for the two sets of duplicate tests except that one set of sepcimens was tested in air and the other set in water. The reason for the drastic reduction in fracture toughness is not clear.

Correlations for estimating changes in tensile stress and Ramberg/Osgood parameters for tensile strain hardening are not presented in this report; they are discussed in detail in NUREG/CR-6142, ANL-93/35 (1994). The information may be used to determine fracture toughness J_{Ic} for the aged materials. A flow diagram of the methodology for estimating mechanical properties of thermally aged CASS materials in LWR systems is discussed. Three schemes are presented for estimation of mechanical properties of CASS material of (a) unknown composition, (b) known composition and unknown service history, and (c) known composition and service history.

The correlations for estimating the degradation of mechanical properties of typical heats of CASS materials, however, do not consider the initial fracture properties of the unaged material. Some CASS materials may have low initial fracture toughness and the estimated J-R curves may be higher than the initial value. Therefore, some knowledge regarding the initial fracture toughness of the material is needed to justify the use of the estimated fracture toughness. The initial fracture toughness J-R curves may be estimated from the RT Charpy-impact energy of the unaged material, if known. Otherwise, minimum fracture toughness of the unaged material is used (i.e., Eqs. 43 and 44 of this report).

An evaluation of the NRC screening criteria established to determine the susceptibility of CASS materials to thermal aging embrittlement indicate that the existing criteria are valid, except those for CF-8M materials. The present reevaluation of the thermal embrittlement data indicates that to maintain the same level of safety margin, the existing criterion for potentially susceptible material of greater than 14% ferrite for static-cast CF-8M material and greater than 20% ferrite for centrifugally-cast CF-8M material, needs to be revised. The updated criterion for static-cast and centrifugally-cast CF-8M materials has been decreased to 13% ferrite and 17% ferrite, respectively, for materials with less than 10% Ni, and to 10% ferrite and 13% ferrite, respectively, for materials with equal to or greater than 10% Ni.

Austenitic Stainless Steel Welds

Austenitic SS welds also have a duplex structure and their chemical compositions are similar to those of CASS materials. Four distinct morphologies are observed in SS welds: vermicular,

lacy, acicular, and globular. A vermicular morphology is typically observed in austenitic SS welds with FN 5–15, and lacy or acicular morphologies are observed in welds with FN 13–15. Austenitic SS welds generally contain 5–15% ferrite, but their mechanical properties differ from those of CASS materials. For a given ferrite content, their tensile strength is higher and fracture toughness is lower than that of CASS materials. Generally, ferrite phase has little effect on the fracture toughness of austenitic SS welds because of the thin vermicular morphology and relatively low ferrite content. The welding process, however, significantly affects fracture toughness. In general, GTA welds exhibit higher fracture resistance than SMAs or SA welds. The J-R curve proposed earlier in NUREG/CR-6004 (1995) (i.e., Eq. 45 of this report) for SA and SMA welds, is defined as the lower-bound J-R curve at 288°C (550°F) for unaged austenitic SS welds.

The mechanism for thermal embrittlement of austenitic SS welds is somewhat different that of CASS materials. Thermal aging of austenitic SS welds at reactor operating temperatures results in moderate decreases in Charpy-impact strength and fracture toughness at both RT and 290°C. In SS welds, failure occurred by the formation and growth of microvoids near hard inclusions. However, since the ferrite content in austenitic SS welds is typically less than 15%, the degradation of mechanical properties occurs primarily by the presence of grain boundary or phase boundary carbides, which initiate localized intergranular cracking. Based on fracture toughness data for thermally aged SMA and SA welds, the J-R curve for fully embrittled welds at 288°C was defined in NUREG/CR-6428 (1996) (Eq. 46 of this report). The curve is about 40% lower than that for the lower-bound curve for unaged welds. However, the curve was based on very limited information. Furthermore, the possible effect of reactor coolant environment is not considered in these lower-bound curves. The lower-bound fracture toughness J-R curve can be further reduced by 40% in LWR environments relative to that in air.

6.1.2 IASCC Crack Growth Rates

Susceptibility to IASCC increases with neutron fluence, corrosion potential, and water conductivity and decreases with decrease in the corrosion potential of the coolant environment. However, low corrosion potential does not provide immunity to IASCC if the fluence is high enough. The key material parameters (such as composition, thermo-mechanical treatment, microstructure, microchemistry, yield strength, and stacking fault energy) and environmental parameters (such as water chemistry, irradiation temperature, dose, and dose rate) that influence IASCC had been identified and their effects on IASCC susceptibility of austenitic SSs were evaluated in NUREG/CR-7027. The discussions of microstructure, microchemistry, radiation hardening, yield strength, Si segregation, and stacking fault energy, are presented in this report as background.

In NUREG/CR-7027, the IASCC CGR data for irradiated wrought and CASSs and their weld metal and HAZ materials in LWR environments were compiled and compared with the K versus CGR disposition curves proposed in NRC NUREG-0313 for nonirradiated sensitized austenitic SSs and the EPRI curve for austenitic SSs. In the NWC BWR environment, the IASCC CGRs of austenitic SSs irradiated to 5 dpa could be a factor of 10 higher and those irradiated to 10–12 dpa could be a factor of 25 higher than the NUREG-0313 disposition curve for nonirradiated SSs in 8-ppm water. A significant decrease in CGRs is observed in HWC BWR environment relative to the NWC BWR environment for SSs irradiated to less than 3 dpa; little or no reduction for some SSs irradiated to 3–4 dpa; and no decrease for all SSs irradiated to 12–14.5 dpa. The CGRs for some of the materials irradiated to 3–4 dpa are above the EPRI disposition curve for the HWC BWR environment. In PWR water at 320°C, the CGR data for austenitic SSs irradiated to 3 dpa are up to a factor of 12 above the NUREG-0313 curve for nonirradiated

materials in high-purity water with 0.2 ppm DO. The CGRs for SSs irradiated to 11–25 dpa are nearly two orders of magnitude above the same curve. For the same material and irradiation condition, the CGR in PWR water increase with increasing temperature, the data were normalized using activation energy of 100 kJ/mol.

The IASCC CGRs in NWC BWR environments for SA or SMA weld HAZ materials are comparable to or higher than for wrought austenitic SSs. Materials irradiated up to about 2.5 dpa are a factor of up to 20 higher than the CGRs predicted by the NUREG-0313 curve for nonirradiated sensitized austenitic SSs in high-purity water with 8 ppm DO. Furthermore, the CGRs for these materials in HWC BWR environments are mostly below the 0.2-ppm DO NUREG-0313 curve. The available IASCC CGRs for thermally aged and unaged Type 316L weld metal at 289°C in high-purity water with 300–2000 ppb DO are bounded by the NUREG-0313 curve for nonirradiated sensitized austenitic SSs in 8-ppm DO water. Similar data for irradiated Type 316L weld metal are not available. The CGRs for CF-8M CASS material irradiated to 0.08 dpa in high-purity water with <50 ppb DO at 320°C are below the NUREG-0313 curve in 0.2-ppm DO water.

For irradiated austenitic SSs, the IASCC CGR data in NWC BWR environment at 288°C (550°F) and K = 20 MPa $m^{1/2}$ indicate that for neutron doses below about 0.42 dpa, the CGRs are below the 8 ppm DO NUREG-0313 curve, and for neutron doses above 0.42 dpa the CGRs are bounded by Eq. 49. Similar data for CASS materials and austenitic SS welds and HAZ materials also indicate that in NWC BWR environment, the IASCC CGRs for nonirradiated materials or materials irradiated below 0.42 dpa are bounded by the NUREG-0313 curve for nonirradiated sensitized austenitic SSs in high-purity water with 8 ppm DO (i.e., are also bounded by Eq. 49).

For irradiated austenitic SSs, the IASCC CGR data in HWC BWR environment at 288°C or PWR primary water at 320°C and K = 20 MPa $m^{1/2}$ indicate that for neutron doses below 2.2 dpa, the CGRs are below the 0.2 ppm DO NUREG-0313 curve; for neutron doses above 2.2 dpa, the CGRs are bounded by Eq. 50. Similar data for CASS materials, austenitic SS welds, and HAZ materials in HWC BWR environment at 288°C or PWR primary water chemistry indicate that the CGRs for nonirradiated CASS materials or materials irradiated up to 2.2 dpa are below the NUREG-0313 curve in 0.2-ppm DO water. However, CGR data are not available for CASS materials and austenitic SS welds irradiated above 2.2 dpa.

6.1.3 Neutron Embrittlement

The fracture toughness of unaged and nonirradiated wrought and cast austenitic SSs fall in Category III (J_{Ic} >150 kJ/m^2), and failure occurs after stable crack extension at stresses well above the yield stress. Neutron irradiation can degrade fracture toughness of these materials to the level of Category II (J_{Ic} of 30–150 kJ/m^2) or Category I (J_{Ic} < 30 kJ/m^2), where failure may occur without general yielding. In such instances, EPFM is generally used for analysis of structural integrity, which involves the J-R curve approach.

Plots of J_{Ic} versus neutron dose are typically used for developing screening criteria for neutron embrittlement. J_{Ic} is a measure of fracture toughness at instability without significant stable crack extension. It is determined from the intersection of the best-fit power-law J-R curve with the 0.2-offset line defined as $J = 2\sigma_f \Delta a$. However, this yields a higher value of J_{Ic} for Category III materials such as austenitic SSs because of their relatively high toughness, ductility, and strain hardening ability. For austenitic SSs, a slope of 4 better defines the blunting line, and has been used to determine J_{Ic} in most investigations.

Based on data on fast reactor irradiated austenitic SSs, the effects of neutron exposure (in dpa) on the fracture toughness J_{Ic} have been divided into three regimes: little or no loss of toughness below an exposure of ≈1 dpa, substantial decrease in toughness at exposures of 1–10 dpa, and no further reduction in toughness above a saturation exposure of 10 dpa. The degradation in fracture properties saturates at a J_{Ic} value of ≈30 kJ/m^2 (171 in.-lb/in.^{2}) (i.e., K_{Jc} of 75 MPa m$^{1/2}$ [68.2 ksi in.$^{1/2}$]). The fracture toughness trend for the LWR irradiated austenitic SSs is similar to that observed for fast reactor irradiations. Most of the fracture toughness J_{Ic} values for SSs irradiated at 288–316°C (550–601°F) fall within the scatter band observed for fast reactor data, although the LWR irradiations were at lower temperatures. However, some SSs irradiated above 4 dpa at LWR temperatures show very poor fracture toughness. For a Type 304 SS irradiated to 4.5–5.3 dpa, nine out of 10 specimens showed no ductile crack extension and the K_{Ic} values were 52.5–67.5 MPa m$^{1/2}$ (47.7–61.4 ksi in.$^{1/2}$). The lowest fracture toughness K_{Ic} or K_{Jc} values were in the range of 36.8–40.3 MPa m$^{1/2}$ (33.5–36.6 ksi in.$^{1/2}$).

Specimen orientation has a strong effect on the fracture toughness of irradiated austenitic SSs. Types 304 and 304L materials irradiated to 4.7–12.0 dpa in BWRs showed lower fracture toughness in the T-L orientation than in the L-T orientation. The toughness values for T-L orientation were lower than the limiting fracture toughness K_{Ic} of 55 MPa m$^{1/2}$ (50 ksi in.$^{1/2}$) proposed by industry for flaw tolerance evaluation for austenitic SSs irradiated above 4.5 dpa. The effects of various parameters such as material type, heat treatment, test and irradiation temperature, and neutron energy spectrum, flux, and dose are discussed.

There are only minor differences in the fracture toughness of the various wrought and cast austenitic SS materials. For the same irradiation conditions, the fracture toughness of thermally aged CASS material and austenitic SS weld metal is lower than that of HAZ material, which, in turn, is lower than that of solution-annealed materials. The fracture toughness J_{Ic} of austenitic SSs irradiated to less than 5 dpa decreases with increasing test temperature. For steels irradiated to more than 12 dpa, test temperature has little effect on fracture toughness.

The threshold dose and the rate of the decrease in fracture toughness J_{Ic} with neutron dose seem to vary for different grades of materials. The decrease in toughness with increasing fluence occurs earliest in Type 304L SS, followed by Type 304 SS and then Type 316 SS. However, it is not clear whether the threshold for irradiation effects on fracture toughness is earlier or the decrease in fracture toughness occurs faster. The average J_{Ic} of Type 304 SS decreases from more than 150 kJ/m^2 (857 in.-lb/in.^{2}) at 1 dpa to 12–24 kJ/m^2 (69–137 in.-lb/in.^{2}) at about 2.2 dpa.

A fracture toughness trend curve, represented by either the J_{Ic} value or coefficient C of the power-law J-R curve, has been developed that bounds the existing neutron embrittlement data. The trend curve describes (a) a threshold neutron exposure for radiation embrittlement of austenitic SSs and a minimum fracture toughness for these materials irradiated to less than the threshold value, (b) a saturation neutron exposure and a saturation fracture toughness for materials irradiated to greater than this value, and (c) a description of the change in fracture toughness between the threshold and saturation neutron exposures. The lower bound curve represents a threshold dose of about 0.3 dpa for neutron embrittlement, a minimum fracture toughness J_{Ic} of ≈118 kJ/m^2 for neutron doses below the threshold value, a saturation threshold of 5 dpa beyond which the fracture toughness of these materials appears to saturate, a saturation fracture toughness J_{Ic} of 7.5 kJ/m^2 (or K_{Ic} or K_{Jc} of 38 MPa m$^{1/2}$), and a description of the change in toughness between 0.3 and 5 dpa. The disposition curve proposed by EPRI for BWRs is not bounding for the existing data for BWR-irradiated austenitic SSs.

The lower bound trend curve is consistent with the MRP lower bound model proposed for PWRs. The MRP curve also predicts a saturation fracture toughness K_{Ic} of 38 MPa $m^{1/2}$. However, the MRP curve predicts fracture toughness values that, for some austenitic SS welds or weld HAZ, may be higher than the minimum toughness of the materials in the nonirradiated condition.

The existing fracture toughness data have been used to develop the lower-bound curve for the decrease in the coefficient C of the power-law J-R curve with neutron dose. The lower-bound trend curve for the change in coefficient C of the power-law J-R curve versus neutron dose may be used to analyze material behavior for loading beyond J_{Ic}. A median value of 0.37 is assumed for exponent n of the J-R curve. The existing data indicate that the lower-bound curve for coefficient C based developed in this study may not be adequate for austenitic SS welds. Furthermore, the effects of LWR coolant environments may also decrease fracture toughness of wrought and CASSs and their welds.

6.1.4 Combined Effects of Thermal and Neutron Embrittlement

The NRC accepted the industry proposal of using fracture toughness $J_{2.5}$ = 255 kJ/m^2 to determine susceptibility of CASS materials to loss of fracture toughness due to thermal embrittlement. However, at the time when these screening criteria were proposed, the combined effects of thermal and neutron embrittlement of CASS materials and austenitic SS welds were not well established. Although both the thermal aging embrittlement and the neutron irradiation embrittlement of ferrite have been well characterized, the combined effect of thermal and irradiation embrittlement is not well established. The concurrent exposure to elevated temperatures and high neutron fluence levels could result in a combined effect wherein the service-degraded fracture toughness is reduced from the levels predicted independently for either of the two mechanisms alone.

As discussed above, the available fracture toughness data on austenitic SS welds and associated HAZ materials as well as CASS materials indicate that some of the data for austenitic SS welds, particularly Type 316 weld, may not be bounded by the lower-bound fracture toughness versus neutron dose curve proposed in NUREG/CR-7027. Furthermore, limited J-R curve data in LWR coolant environments indicate that the reactor coolant environment may further decrease fracture toughness of these materials relative to that in air. Therefore, the combined effects of thermal and neutron embrittlement and the potential effect of coolant environment on fracture toughness of CASS materials and austenitic SS welds need to be established for performing flaw tolerance evaluations for these materials. However, the existing fracture toughness data are inadequate to evaluate the combined effects of thermal and neutron embrittlement on the threshold dose for embrittlement.

6.2 Information Gaps

6.2.1 Thermal Embrittlement of Duplex Stainless Steels

The updated expressions presented in this report for estimating mechanical properties of CASS materials are based on data that contained little or no fracture toughness J-R curve results for thermally aged CF-3 and CF-8 materials with more than 25% ferrite. The use of the methodology proposed in this report for CF-3 and CF-8 materials with more than 25% ferrite needs to be validated. The fracture toughness lower-bound J-R curve for fully embrittled SMA and SA welds was defined in NUREG/CR-6428. However, the curve was based on very limited information, particularly for Type 316 welds. Additional data on austenitic SSs welds aged at

reactor operating temperature are needed to better establish the lower-bound J-R curve for thermally aged welds, including the effect of reactor coolant environment.

6.2.2 IASCC Crack Growth Rates

As discussed in NUREG/CR-7027, additional data on PWR materials irradiated between 15 and 40 dpa at temperatures of 300–350°C are needed to better understand the IASCC susceptibility of austenitic SSs in PWR environments, and to understand the reason for high CGRs and large data scatter for SSs irradiated to 7–18 dpa and relatively low CGRs in SSs irradiated to 37.5 dpa.

A review of the existing IASCC susceptibility data for CASS materials and austenitic SS welds indicates that the data are too limited to accurately establish the IASCC CGRs of these materials in LWR environments. Additional data on irradiated CASS materials and austenitic SS weld welds, including weld HAZ, are needed, particularly in low-DO environments.

6.2.3 Neutron Embrittlement

Most of the data for CASS materials and austenitic SS welds shown in Fig. 62b for the fracture toughness coefficient C versus neutron dose trend curve, are from irradiations in fast reactors and at temperatures of 370–427°C (698–800°F). The values for coefficient C for LWR irradiated materials are likely to be lower. Furthermore, there are few or no fracture toughness data on LWR irradiated austenitic SS and CASS materials for dose levels of 1.0–10.0 dpa. Additional data on LWR irradiated materials should be obtained to accurately define the lower bound trend curve for coefficient C.

Some of the data obtained in LWR environments falls below the lower-bound fracture toughness curve. Therefore, the potential effects of the LWR coolant environment also need to be investigated. Furthermore, the contribution of additional precipitate phases, voids, and cavities on fracture toughness needs to be investigated.

6.2.4 Combined Effects of Thermal and Neutron Embrittlement

Additional fracture toughness J-R curve data on the combined effects of thermal and neutron embrittlement of austenitic SS welds and CASS materials, including the potential effects of LWR coolant environments, are needed to accurately define the lower-bound fracture properties of these materials in LWR environments.

References

1. Bruemmer, S. M., et al., "Critical Issue Reviews for the Understanding and Evaluation of Irradiation-Assisted Stress Corrosion Cracking," EPRI TR-107159, Electric Power Research Institute, Palo Alto, CA, 1996.

2. Scott, P., "A Review of Irradiation Assisted Stress Corrosion Cracking," *J. Nucl. Mater.* **211**, 101–122, 1994.

3. Was, G. S., and P. L. Andresen, "Stress Corrosion Cracking Behavior of Alloys in Aggressive Nuclear Reactor Core Environments," *Corrosion* **63**, 19–45, 2007.

4. Andresen, P. L., F. P. Ford, S. M. Murphy, and J. M. Perks, "State of Knowledge of Radiation Effects on Environmental Cracking in Light Water Reactor Core Materials," *Proc. 4th Intl. Symp. on Environmental Degradation of Materials in Nuclear Power Systems—Water Reactors*, NACE, Houston, TX, pp. 1.83–1.121, 1990.

5. Bruemmer, S. M., E. P. Simonen, P. M. Scott, P. L. Andresen, G. S. Was, and J. L. Nelson, "Radiation-Induced Material Changes and Susceptibility to Intergranular Failure of Light-Water-Reactor Core Internals," *J. Nucl. Mater.* **274**, 299–314, 1999.

6. Herrera, M. L., et al., "Evaluation of the Effects of Irradiation on the Fracture Toughness of BWR Internal Components," *Proc. ASME/JSME 4th Intl. Conf. on Nucl. Eng.* (ICONE-4), Vol. 5, A. S. Rao, R. M. Duffey, and D. Elias, eds., American Society of Mechanical Engineers, New York, pp. 245–251, 1996.

7. Mills, W. J., "Fracture Toughness of Irradiated Stainless Steels Alloys," *Nucl. Technol.*, **82**, 290–303, 1988.

8. Mills, W. J., "Fracture Toughness of Type 304 and 316 Stainless Steels and Their Welds," *Intl. Mater. Rev.* **42**, 45–82, 1997.

9. Xu, H., and S. Fyfitch, "Materials Reliability Program: A Review of Radiation Embrittlement for Stainless Steels (MRP-79)," Rev. 1, EPRI Report 1008204, Electric Power Research Institute, Palo Alto, CA, Sept. 2004.

10. Demma, A., R. Carter, A. Jenssen, T. Torimaru, and R. Gamble, "Fracture Toughness of Highly Irradiated Stainless Steels in Boiling Water Reactors," *Proc. 13th Intl. Conf. on Environmental Degradation of Materials in Nuclear Power Systems—Water Reactors*, T. R. Allen, P. J. King, and L. Nelson, eds., Canadian Nuclear Society, Toronto, Canada, Paper No. 114, 2007.

12. Ehrnsten, U., K. Wallin, P. Karjalainen-Roikonen, S. van Dyck, and P. Ould, "Fracture Toughness of Stainless Steels Irradiated to ≈9 dpa in Commercial BWRs," *Proc. 6th Intl. Symp. on Contribution of Materials Investigations to Improve the Safety and Performance of LWRs*, Vol. 1, Fontevraud 6, French Nuclear Energy Society, SFEN, Fontevraud Royal Abbey, France, pp. 661–670, Sept. 18–22, 2006.

13. Carter, R. G., and R. M. Gamble, "Assessment of the Fracture Toughness of Irradiated Stainless Steel for BWR Core Shrouds," *Fontevraud 5 Intl. Symp., Contribution of Materials Investigation to the Resolution of Problems Encountered in Pressurized Water Reactors*, Avignon, France, Sept. 25, 2002.

14. O'Donnell, I. J., H. Huthmann, and A. A. Tavassoli, "The Fracture Toughness Behaviour of Austenitic Steels and Weld Metal Including the Effects of Thermal Aging and Irradiation," *Intl. J. Pressure Vessels and Piping* **65** (3), 209–220, 1996.

15. Kim C., R. Lott, S. Byrne, M. Burke, and G. Gerzen, "Embrittlement of Cast Austenitic Stainless Steel Reactor Internals Components," *Proc. 6th Intl. Symp. on Contribution of Materials Investigations to Improve the Safety and Performance of LWRs*, Vol. 1, Fontevraud 6, French Nuclear Energy Society, SFEN, Fontevraud Royal Abbey, France, Sept. 18–22, 2006.

16. Fyfitch, S., H. Xu, A. Demma, R. Carter, R. Gamble, and P. Scott, "Fracture Toughness of Irradiated Stainless Steel in Nuclear Power Systems," *Proc. 14th Intl. Conf. on Environmental Degradation of Materials in Nuclear Power Systems—Water Reactors, American Nuclear Society*, Lagrange Park, IL, 2009.

17. Fyfitch, S., H. Xu, K. Moore, and R. Gurdal, "Materials Reliability Program: PWR Internals Material Aging Degradation Mechanism Screening and Threshold Values (MRP-175)," EPRI Report 1012081, Dec. 2005.

18. Electric Power Research Institute, Materials Reliability Program, "Fracture Toughness Testing of Decommissioned PWR Core Internals Material Samples (MRP-160)," EPRI Report 1012079, Sept. 2005.

19. Chopra, O. K., and A. S. Rao, "A Review of Irradiation Effects on LWR Core Internal Materials - Neutron Embrittlement," *J. Nucl. Mater.* **412**, 195–208, 2011.

20. Chopra, O. K., and W. J. Shack, "Crack Growth Rates and Fracture Toughness of Irradiated Austenitic Stainless Steels in BWR Environments," NUREG/CR-6960, ANL-06/58, March 2008.

21. Chopra, O. K., "Degradation of LWR Core Internal Materials Due to Neutron Irradiation," NUREG/CR-7027, December 2010.

22. Andresen, P. L. "Emerging Issues and Fundamental Processes in Environmental Cracking in Hot Water," *Proc. Research Topical Symposium on Environmental Cracking, Corrosion/07*, NACE, 2007.

23. Bruemmer, S. M., "New Issues Concerning Radiation-Induced Material Changes and Irradiation-Assisted Stress Corrosion Cracking in Light-Water Reactors," *Proc. Tenth Intl. Symp. on Environmental Degradation of Materials in Nuclear Power Systems—Water Reactor*, Paper No. 0008V, NACE, Houston, TX, 2001.

24. Edwards, D., E. Simonen, and S. Bruemmer, "Radiation-Induced Segregation Behavior in Austenitic Stainless Steels: Fast Reactor versus Light Water Reactor Irradiations," *Proc. 13th Intl. Conf. on Environmental Degradation of Materials in Nuclear Power Systems—Water Reactors*, T. R. Allen, P. J. King, and L. Nelson, eds., Canadian Nuclear Society, Toronto, Canada, Paper No. P0139, 2007.

25. Fyfitch, S., H. Xu, P. Scott, L. Fournier, and A. Demma, "Criteria for Initiation of Irradiation-Assisted Stress Corrosion Cracking in Stainless Steels in PWR Systems," *Proc. 14th Intl. Conf. on Environmental Degradation of Materials in Nuclear Power Systems—Water Reactors*, American Nuclear Society, Lagrange Park, IL, 2009.

26. Jenssen, A., J. Stjarnsater, and R. Pathania, "Crack Growth Rates of Irradiated Commercial Stainless Steels in BWR and PWR Environments," *Proc. 15th Intl. Conf. on Environmental Degradation of Materials in Nuclear Power Systems—Water Reactors*, J. T. Busby, G. Ilevbare, and P. L. Andresen, eds., The Minerals, Metals & Materials Society, Warrendale, PA, pp. 1229–1240, 2011.

27. Jenssen, A., and L. G. Ljungberg, "Irradiation Assisted Stress Corrosion Cracking: Post Irradiation CERT Tests of Stainless Steels in a BWR Test Loop," *Proc. Seventh Intl. Symp. on Environmental Degradation of Materials in Nuclear Power Systems—Water Reactor*, G. Airey et al., eds., NACE, Houston, TX, pp. 1043–1052, 1995.

28. Jenssen, A., and L. G. Ljungberg, "Irradiation Assisted Stress Corrosion Cracking of Stainless Alloys in BWR Normal Water Chemistry and Hydrogen Water Chemistry," *Proc. Sixth Intl. Symp. on Environmental Degradation of Materials in Nuclear Power Systems—Water Reactor*, R. E. Gold and E. P. Simonen, eds., Minerals, Metals & Materials Society, Warrendale, PA, pp. 547–553, 1993.

29. Chopra, O. K., and A. S. Rao, "A Review of Irradiation Effects on LWR Core Internal Materials - IASCC Susceptibility and Crack Growth Rates of Austenitic Stainless Steels," *J. Nucl. Mater.* **409**, 235–256, 2011.

30. Trautwein, A., and W. Gysel, "Influence of Long Time Aging of CF-8 and CF-8M Cast Steel at Temperatures Between 300 and 500°C on the Impact Toughness and the Structure Properties," in *Spectrum, Technische Mitteilungen aus dem+GF+Konzern, No. 5* (May 1981); also in *Stainless Steel Castings*, V. G. Behal and A. S. Melilli, eds., STP 756, ASTM, Philadelphia, PA, pp. 165–189, 1982.

31. Landerman, E. I., and W. H. Bamford, "Fracture Toughness and Fatigue Characteristics of Centrifugally Cast Type 316 Stainless Steel Pipe after Simulated Thermal Service Conditions," in *Ductility and Toughness Considerations in Elevated-Temperature Service*, MPC 8, ASME, New York, pp. 99–127, 1978.

32. Solomon, H. D., and T. M. Devine, "Influence of Microstructure on the Mechanical Properties and Localized Corrosion of a Duplex Stainless Steel," in *Micon 78: Optimization of Processing, Properties, and Service Performance through Microstructural Control*, H. Abrams, G. N. Maniar, D. A. Nail, and H. D. Solomon, eds., ASTM STP 672, p. 430, 1979.

33. Solomon, H. D., and T. M. Devine, Jr., "Duplex Stainless Steels - A Tale of Two Phases," in *Duplex Stainless Steels*, R. A. Lula, ed., ASM, Metals Park, 1983, pp. 693–756.

34. Slama, G., P. Petrequin, and T. Mager, "Effect of Aging on Mechanical Properties of Austenitic Stainless Steel Castings and Welds," presented at SMIRT Post-Conference Seminar 6, Assuring Structural Integrity of Steel Reactor Pressure Boundary Components, Aug. 29–30, 1983, Monterey, CA.

35. McConnell, P., and J. W. Sheckherd, "Fracture Toughness Characterization of Thermally Embrittled Cast Duplex Stainless Steel, Report NP-5439, Electric Power Research Institute, Palo Alto, CA, Sept. 1987.

36. Meyzaud, Y., P. Ould, P. Balladon, M. Bethmont, and P. Soulat, "Tearing Resistance of Aged Cast Austenitic Stainless Steel," *Int. Conf. on Thermal Reactor Safety* (NUCSAFE 88), Avignon, France, Oct. 1988.

37. Bethmont, M., Y. Mezaud, and P. Soulat, "Properties of Cast Austenitic Materials for Light Water Reactors," *Int. J. Pres. Ves. & Piping* **66**, 221–229, 1996.

38. Jayet-Gendrot, S., P. Ould, and T. Meylogan, "Fracture Toughness Assessment of In-Service Aged Primary Circuit Elbows Using Mini-CT Specimens Taken from Outer Skin," *Nucl. Eng. and Design* **184**, 3–11, 1998.

39. Mills, W. J., "Heat-to-Heat Variations in the Fracture Toughness of Austenitic Stainless Steels," *Eng. Fract. Mech.*, **30**(4**)**, 469–492, 1988.

40. Mills, W. J., "Fracture Toughness of Stainless Steel Welds," in *Fracture Mechanics: Nineteenth Symposium*, STP 969, ASTM, Philadelphia, PA, 330–355, 1988.

41. Mills, W. J., "Fracture Toughness of Aged Stainless Steel Primary Piping and Reactor Vessel Materials," *J. Pressure Vessel Technol.* (Trans ASME) **109**, 440–448, 1987.

42. Chung, H. M., and O. K. Chopra, "Kinetics and Mechanism of Thermal Aging Embrittlement of Duplex Stainless Steels," *Environmental Degradation of Materials in Nuclear Power Systems—Water Reactors*, G. J. Theus and J. R. Weeks, eds., Metallurgical Society, Warrendale, PA, pp. 359–370, 1988.

43. Bonnet, S., J. Bourgoin, J. Champredonde, D. Guttmann, and M. Guttmann, "Relationship between Evolution of Mechanical Properties of Various Cast Duplex Stainless Steels and Metallurgical and Aging Parameters: An Outline of Current EDF Programmes," *Mater. Sci. Technol.*, 6, 221–229, 1990.

44. Pumphrey, P. H., and K. N. Akhurst, "Aging Kinetics of CF3 Cast Stainless Steel in Temperature Range 300–400°C," *Mater. Sci. Technol.*, 6, 211–219, 1990.

45. Grimes, C. I., U.S. Nuclear Regulatory Commission, License Renewal and Standardization Branch, letter to Douglas J. Walters (Nuclear Energy Institute), License Renewal Issue No. 98-0030, "Thermal Aging Embrittlement of Cast Stainless Steel Components," May 19, 2000.

46. Nickell, R. E., and M. A. Rinckel, "Evaluation of Thermal Aging Embrittlement for Cast Austenitic Stainless Steels Components in LWR Reactor Coolant Systems," EPRI TR-106092, Electric Power Research Institute, Palo Alto, CA, 1997.

47. Rinckel, M. A., "Evaluation of Thermal Aging Embrittlement for Cast Austenitic Stainless Steels Components," EPRI 1000976, Electric Power Research Institute, Palo Alto, CA, Jan. 2001.

48. Chopra, O. K., and A. Sather, "Initial Assessment of the Mechanisms and Significance of Low-Temperature Embrittlement of Cast Stainless Steels in LWR Systems," NUREG/CR-5385, ANL-89/17, Aug. 1990.

49. Chopra, O. K., and H. M. Chung, "Effect of Low-Temperature Aging on the Mechanical Properties of Cast Stainless Steels," in *Properties of Stainless Steels in Elevated Temperature Service*, M. Prager, ed., MPC-Vol. 26 / PVP-Vol. 132, ASME, New York, pp. 79–105,1988.

50. Chopra, O. K., "Estimation of Fracture Toughness of Cast Stainless Steels during Thermal Aging in LWR Systems," NUREG/CR-4513, Rev. 1, ANL-93/22, Aug. 1994.

51. Chopra, O. K. and W. J. Shack, “Mechanical Properties of Thermally Aged Cast Stainless Steels from Shippingport Reactor Components,” NUREG/CR-6275, ANL-94/37, April 1995.

52. Michaud, W. F., P. T. Toben, W. K. Soppet, and O. K. Chopra, “Tensile-Property Characterization of Thermally Aged Cast Stainless Steels,” NUREG/CR-6142, ANL-93/35, Feb. 1994.

53. Gavenda, D. J., W. F. Michaud, T. M. Galvin, W. F. Burke, and O. K. Chopra, “Effects of Thermal Aging on Fracture Toughness and Charpy-Impact Strength of Stainless Steel Pipe Welds,” NUREG/CR-6428, ANL-95/47, 1996.

54. Heger, J. J., “885°F Embrittlement of the Ferritic Chromium-Iron Alloys,” *Met. Progress*, p. 55, 1951.

55. Lagneborg, R., “Metallography of the 475°C Embrittlement in an Iron-30% Chromium Alloy,” *Trans. ASM* **60**, 67, 1967.

56. Grobner,, P. J. “The 885°F (475°C) Embrittlement of Ferritic Stainless Steels,” *Metall. Trans*. **4**, 251, 1973.

57. Nichol, T. J., A. Datta, and G. Aggen, “Embrittlement of Ferritic Stainless Steels,” *Metall. Trans*. **11A**, 573, 1980.

58. Chung, H. M., and O. K. Chopra, “Long-Term Aging Embrittlement of Cast Austenitic Stainless Steels - Mechanism and Kinetics,” in *Properties of Stainless Steels in Elevated-Temperature Service*, M. Prager, ed., MPC Vol. 26, PVP Vol. 132, ASME, New York, pp. 17–34, 1988.

59. Chung, H. M., and T. R. Leax, “Embrittlement of Laboratory- and Reactor-Aged CF3, CF8, and CF8M Duplex Stainless Steels,” *Mater. Sci. Technol.*, **6**, 249–262, 1990.

60. Auger, P., F. Danoix, A. Menand, S. Bonnet, J. Bourgoin, and M. Guttmann, “Atom Probe and Transmission Electron Microscopy Study of Aging of Cast Duplex Stainless Steels, *Mater. Sci. Technol.*, **6**, 301–313, 1990.

61. Vrinat, M., P. Cozar, and Y. Meyzaud, “Precipitated Phases in the Ferrite of Aged Cast Duplex Stainless Steels,” *Scripta Metall.*, **20**, 1101–1106, 1986.

62. Joly, P., R. Cozar, and A. Pineau, “Effect of Crystallographic Orientation of Austenite on the Formation of Cleavage Cracks in Ferrite in an Aged Duplex Stainless Steel,” *Scripta Metall.*, **24**, 2235–2240, 1990.

63. Sassen, J. M., M. G. Hetherington, T. J. Godfrey, and G. D. W. Smith, “Kinetics of Spinodal Reaction in the Ferrite Phase of a Duplex Stainless Steel,” in *Properties of Stainless Steels in Elevated Temperature Service*, M. Prager, ed., MPC Vol. 26, PVP Vol. 132, ASME, New York, pp. 65–78, 1988.

64. Brown, J. E., A. Cerezo, T. J. Godfrey, M. G. Hetherington, and G. D. W. Smith, “Quantitative Atom Probe Analysis of Spinodal Reaction in Ferrite Phase of Duplex Stainless Steel,” *Mater. Sci. Technol.*, **6**, 293–300, 1990.

65. Bentley, J., M. K. Miller, S. S. Brenner, and J. A. Spitznagei, “Identification of G-phase in Aged Cast CF-8 Type Stainless Steel,” in *Proc. 43rd Electron Microscopy Society of America*, G. W. Bailey, ed., San Francisco Press, pp. 328–329, 1985.

66. Miller, M. K., and J. Bentley, “Characterization of Fine-Scale Microstructures in Aged Primary Coolant Pipe Steels,” in *Environmental Degradation of Materials in Nuclear Power Systems—Water Reactors*, G. J. Theus and J. R. Weeks, eds., The Metallurgical Society, Warrendale, PA, pp. 341–349, 1988.

67. Kawaguchi, S., N. Sakamoto, G. Takano, F. Matsuda, Y. Kikuchi, and L. Mraz, "Microstructural Changes and Fracture Behavior of CF8M Duplex Stainless Steel after Long-Term Aging," Nucl. Eng. and Design **174**, 273–285, 1997.

68. Massoud, Jean-Paul, Claude Boveyron, Pascal Ould, Georges Bezdikian, and Henriette Churier-Bossenec, “Effect of the Manufacturing Process on the Thermal Aging of PWR Duplex Stainless Steel Components,” *ASME 6th Intl. Conf. on Nucl. Eng.* (ICONE-6), American Society of Mechanical Engineers, New York, paper ICINE-6085, 1998.

69. Jansson, C., “Degradation of Cast Stainless Steel Elbows after 15 Years in Service,” presented at Fontevraud II Intl. Symp., Royal Abbey of Fontevraud, France, Sept. 10–14, 1990.

70. David, S. A., “Ferrite Morphology and Variations in Ferrite Content in Austenitic Stainless Steel Welds,” Welding Research Supplement, American Welding Society and Welding Research Council, pp73-s–71-s, April 1981.

71. AWS A4.2-74, Standard Procedures for Calibrating Magnetic Instruments to Measure Delta Ferrite Content of Austenitic Stainless Steel Weld Metal,” American Welding Society, Miami, FL, 1974.

72. Hull, F. C., “Delta Ferrite and Martensite Formation in Stainless Steels,“ *Welding Journal*, Vol. **52** (5), Research Supplement, pp. 193s–203s, May 1973.

73. ASTM A 800/A 800M, “Standard Practice for Steel Casting, Austenitic Alloy, Estimating Ferrite Content thereof,” American Society of Testing and Materials, West Conshohocken, PA, 2001.

74. Schoefer, E. A., “A Diagram for Estimation of Ferrite Content in Stainless Steel Castings,” in Appendix to Mossbauer-Effect Examination of Ferrite in Stainless Steel Welds and Castings, by L. J. Schwartzgruber et al., *Welding Journal*, Research Supplement, **53**, 10s–12s, 1974.

75. Schaeffler, A. L., “Selection of Austenitic Electrodes for Welding Dissimilar Metals,” *Welding Journal*, Vol. **26** (10), 601–620, 1947.

76. DeLong, W. T., “Ferrite in Austenitic Stainless Steel Weld Metal,” *Welding Journal*, Research Supplement, **53** (7), 273s–286s, 1974.

77. Chopra, O. K., A. Sather, and L. Y. Bush, "Long Term Embrittlement of Cast Stainless Steels in LWR Systems: Semiannual Report, April-September 1989," NUREG/CR-4744, Vol. 4, No. 2, ANL-90/49, June 1991.

78. Chopra, O. K., "Long Term Embrittlement of Cast Stainless Steels in LWR Systems: Semiannual Report, October 1990-March 1991," NUREG/CR-4744, Vol. 6, No. 1, ANL-91/22, August 1992.

79. Chopra, O. K., and L. Y. Bush, "Long Term Embrittlement of Cast Stainless Steels in LWR Systems: Semiannual Report, October 1989-March 1990," NUREG/CR-4744, Vol. 4, No. 1, ANL-91/7, July 1991.

80. Hale, G. E., and S. J. Garwood, "The Effect of Aging on the Fracture Behaviour of Cast Stainless Steel and Weldments," *Mater. Sci. Technol.*, **6**, 230–235, 1990.

81. Hiser, A. L., "Fracture Toughness Characterization of Nuclear Piping Steels," NUREG/CR-5118, MEA-2325, Materials Engineering Associates, Inc., Nov. 1989.

82. Lee, S., P. T. Kuo, K. Wichman, and O. Chopra, "Flaw Evaluation of Thermally Aged Cast Stainless Steel in Light-Water Reactor Applications," *Int. J. Pres. Ves. and Piping*, pp. 37–44, 1997.

83. Griesbach, T. J., V. Marthandam, and H. Qian, "Nondestructive Evaluation: Flaw Tolerance Evaluation of Thermally Aged Cast Austenitic Stainless Steel Piping," EPRI 1019128, Electric Power Research Institute, Palo Alto, CA, December 2009.

84. Chopra, O. K., "Estimation of Fracture Toughness of Cast Stainless Steels during Thermal Aging in LWR Systems," NUREG/CR-4513, Rev. 0, ANL-90/42, June 1991.

85. Leone, G. L., and H. W. Kerr, "Ferrite to Austenite Transformation in Stainless Steels," Welding Research Supplement, American Welding Society and Welding Research Council, pp13-s to 21-s, January 1982.

86. Section XI Task Group for Piping Flaw Evaluation, Nuclear Power Division, "Evaluation of Flaws in Austenitic Piping," EPRI NP-4690-SR, Electric Power Research Institute, Palo Alto, CA, July 1986.

87. Section XI Task Group for Piping Flaw Evaluation, ASME Code, "Evaluation of Flaws in Austenitic Steel Piping." *J. Press. Vessel Technol.* **108** (3), 352–366, 1986.

88. M. Morra, "Program on Technology Innovation: Scoping Study of Low Temperature Crack Propagation for 182 Weld Metal in BWR Environments and for Cast Austenitic Stainless Steel in PWR Environments (Revision 1)," EPRI 1020957, Electric Power Research Institute, Palo Alto, CA, May 2010.

89. Vitek, J. M., S. A. David, D. J. Alexander, J. R, Keiser, and R. K. Nanstad, "Low Temperature Aging Behavior of Type 308 Stainless Steel Weld Metal," *Acta Metall.*, **39**, 503–516 (1991).

90. Hale, G. E., and S. J. Garwood, "Effect of Aging on Fracture Behaviour of Cast Stainless Steel and Weldments," *Mater. Sci. Technol.* **6**, 230–236, 1990.

91. Garwood, S. J., "Fracture Toughness of Stainless Steel Weldments at Elevated Temperatures," in *Fracture Mechanics: 15th Symposium*, R. J. Sanford, ed., ASTM STP 833, American Society for Testing and Materials, Philadelphia, PA, pp. 333–359, 1984.

92. Vassilaros, M. G., R. A. Hays, and J. P. Gudas, “Investigation of the Ductile Fracture Properties of Type 304 Stainless Steel Plate, Welds, and 4-inch Pipe,” in *Proc. 12th Water Reactor Safety Research Information Meeting*, NUREG/CP-0058, Vol. 4, U.S. Nuclear Regulatory Commission, pp. 176–189, 1985.

93. Faure, F., B. Houssin, and P. Balladon, “Mechanical Properties of Automatic TIG/GTA Welds of Stainless Steel Piping in Nuclear Reactors,” in *Trends in Welding Research*, ASM Conf., Gatlinburg, May 14–18, 1989.

94. Horn, R. M., H. S. Mehta, W. R. Andrews, and S. Ranganath, "Evaluation of the Toughness of Austenitic Stainless Steel Pipe Weldments," EPRI NP-4668, Electric Power Research Institute, Palo Alto, CA, June 1986.

95. Landes, J. D., and D. E. McCabe, "Toughness of Austenitic Stainless Steel Pipe Welds," EPRI NP-4768, Electric Power Research Institute, Palo Alto, CA, Oct. 1986.

96. Gudas, J. P., and D. R. Anderson, “J-R Curve Characteristics of Piping Material and Welds,” in *Proc. 9th Water Reactor Safety Research Information Meeting*, Oct. 1981, U.S. Nuclear Regulatory Commission.

97. Wilkowski, G., et al., "Analysis of Experiments on Stainless Steel Flux Welds," NUREG/CR-4878, BMI-2151, April 1987.

98. Nakagaki, M., C. Marshall, and F. Brust, "Analysis of Cracks in Stainless Steel TIG Welds," NUREG/CR-4806, BMI-2144, Dec. 1986.

99. Hiser, A. L., and G. M. Callahan, "A User's Guide to the NRC's Piping Fracture Mechanics Database (PIFRAC)," NUREG/CR-4894, May 1987.

100. Wilkowski, G. M., et al., "Short Cracks in Piping and Piping Welds," NUREG/CR-4599, Vols. 1–3, Nos. 1 and 2, May 1991–March 1994.

101. Wilkowski, G. M., et al., "Probabilistic Pipe Fracture Evaluations for Leak-Rate-Detection Applications," NUREG/CR-6004, April 1995.

102. Purtscher, Patrick, private communications, Division of Engineering, Office of Nuclear Reactor Regulation, U.S. Nuclear Regulatory Commission, May 2014.

103. Ould, P., P. Balladon, and Y. Meyzaud, Bull. Cercle Etud. Metaux **15**, 31.1–31.12, 1988.

104. Chipperfield, C. G., “A Toughness and Defect Size Assessment of Welded Stainless Steel Components,” *Tolerance of Flaws in Pressurized Components*, Inst. Mech. Eng. pp. 125–137, 1978.

105. Lucas, T., R. G. Ballinger, H. Hanninen, and T. Saukkonen, "Effect of Thermal Aging on SCC, Material Properties and Fracture Toughness of Stainless Steel Weld Metals," *15th Intl. Conf. on Environmental Degradation of Materials in Nuclear Power Systems—Water Reactors*, J. T. Busby, G. Ilevbare, and P. L. Andresen, eds., The Minerals, Metals & Materials Society, Warrendale, PA, pp. 883–900, 2011.

106. Lucas, Timothy R., "The Effect of Thermal Aging and Boiling Water reactor Environment on Type 316L Stainless Steel Welds," Doctoral Thesis, Massachusetts Institute of Technology, Cambridge, MA, May 2011.

107. Brown, K. S., and G. M. Gordon, “Effects of BWR Coolant Chemistry on the Propensity for IGSCC Initiation and Growth in Creviced Reactor Internals Components,” *Proc. Third Intl. Symp. on Environmental Degradation of Materials in Nuclear Power Systems—Water Reactor*, Metallurgical Society, Warrendale, PA, pp. 243–248, 1987.

108. Gordon, G. M., and K. S. Brown, “Dependence of Creviced BWR Component IGSCC Behavior on Coolant Chemistry,” *Proc. 4th Intl. Symp. on Environmental Degradation of Materials in Nuclear Power Systems—Water Reactor*, Daniel Cubicciotti, ed., NACE, Houston, TX, pp. 14.46–14.61, 1990.

109. Garzarolli, F., D. Alter, and P. Dewes, “Deformability of Austenitic Stainless Steels and Nickel-Base Alloys in the Core of a Boiling and a Pressurized Water Reactor,” *Proc. Intl. Symp. on Environmental Degradation of Materials in Nuclear Power Systems—Water Reactor*, American Nuclear Society, Lagrange, IL, pp. 131–138, 1986.

110. Kodama, M., et al., “IASCC Susceptibility of Austenitic Stainless Steels Irradiated to High Neutron Fluence,” *Proc. Sixth Intl. Symp. on Environmental Degradation of Materials in Nuclear Power Systems—Water Reactor*, R. E. Gold and E. P. Simonen, eds., The Minerals, Metals & Materials Society, Warrendale, PA, pp. 583–588, 1993.

111. Kodama, M., et al., “Effects of Fluence and Dissolved Oxygen on IASCC in Austenitic Stainless Steels,” *Proc. Fifth Intl. Symp. on Environmental Degradation of Materials in Nuclear Power Systems—Water Reactor*, American Nuclear Society, Lagrange, IL, pp. 948–954, 1991.

112. Clark, W. L., and A. J. Jacobs, “Effect of Radiation Environment on SCC of Austenitic Materials,” *Proc. First Intl. Symp. on Environmental Degradation of Materials in Nuclear Power Systems - Water Reactor*, NACE, Houston, TX, p. 451, 1983.

113. Jacobs, A. J., G. P. Wozadlo, K. Nakata, T. Yoshida, and I. Masaoka, “Radiation Effects on the Stress Corrosion and Other Selected Properties of Type-304 and Type-316 Stainless Steels,” *Proc. Third Intl. Symp. on Environmental Degradation of Materials in Nuclear Power Systems—Water Reactor*, Metallurgical Society, Warrendale, PA, pp. 673–681, 1987.

114. Lucas, G. E., “The Evolution of Mechanical Property Change in Irradiated Austenitic Stainless Steels,” *J. Nucl. Mater.* **206**, 287–305, 1993.

115. Chen, Y., O. K. Chopra, W. K. Soppet, N. L. Dietz Rago, and W. J. Shack, “ ,” *Proc. 13th Intl. Conf. on Environmental Degradation of Materials in Nuclear Power Systems—Water Reactors*, T. R. Allen, P. J. King, and L. Nelson, eds., Canadian Nuclear Society, Toronto, Canada, Paper No. P0026, 2007.

116. Chung, H. M., and W. J. Shack, “Irradiation-Assisted Stress Corrosion Cracking Behavior of Austenitic Stainless Steels Applicable to LWR Core Internals,” NUREG/CR-6892, ANL-04/10, 2006.

117. Andresen, P. L., “Similarity of Cold Work and Radiation Hardening in Enhancing Yield Strength and SCC Growth of Stainless Steel in Hot Water,” *Corrosion/02*, NACE, Houston, TX, Paper No. 02509, 2002.

118. Andresen, P. L., and F. P. Ford, “Irradiation Assisted Stress Corrosion Cracking: From Modeling and Prediction of Laboratory & In-Core Response to Component Life Prediction,” *Corrosion/95*, NACE, Houston TX, Paper No. 419, 1995.

119. R. Stoenescu, M. L. Castano, S. van Dyck, A. Roth, B. van der Schaaf, C. Ohms, and D. Gavillet, “Irradiation-Assisted Stress Corrosion Cracking of Heat-Affected Zones of Austenitic Stainless Steel Welds,” *Proc. 12th Intl. Conf. on Environmental Degradation of Materials in Nuclear Power System—Water Reactors*, T. R. Allen, P. J. King, and L. Nelson, eds., Minerals, Metals, & Materials Society, pp. 267–275, 2005.

120. Maziasz, P. J., “Overview of Microstructural Evolution in Neutron-Irradiated Austenitic Stainless Steels,” *J. Nucl. Mater.* **205**, 118–145, 1993.

121. Zinkle, S. J., P. J. Maziasz, and R. E. Stoller, “Dose Dependence of the Microstructural Evolution in Neutron-Irradiated Austenitic Stainless Steels,” *J. Nucl. Mater.* **206**, 266–286, 1993.

122. Edwards, D. J., E. P. Simonen, and S. M. Bruemmer, “Evolution of Fine-Scale Defects in Stainless Steels Neutron-Irradiated at 275°C,” *J. Nucl. Mater.* **317**, 13–31, 2003.

123. Bruemmer, S. M., D. J. Edwards, B. W. Arey, and L. A. Charlot, “Microstructural, Microchemical and Hardening Evolution in LWR-Irradiated Austenitic Stainless Steels,” *Proc. Ninth Intl. Symp. on Environmental Degradation of Materials in Nuclear Power Systems—Water Reactor*, Metallurgical Society, Warrendale, PA, pp. 1079–1087, 1999.

124. Ooki, S., Y. Tanaka, K. Takamori, S. Suzuki, S. Tanaka, Y. Saito, T. Nakamura, T. Kato, K. Chatani, and M. Kodama, “Study on SCC Growth Behavior of BWR Core Shroud,” *Proc. 12th Intl. Conf. on Environmental Degradation of Materials in Nuclear Power Systems—Water Reactors*, T. R. Allen, P. J. King, and L. Nelson, eds., Minerals, Metals & Materials Society, Warrendale, PA, pp. 365–376, 2005.

125. Andresen, P. L. and M. M. Morra, “Effects of Si on SCC of Irradiated and Unirradiated Stainless Steels and Nickel Alloys,” *Proc. 12th Intl. Conf. on Environmental Degradation of Materials in Nuclear Power System—Water Reactors*, T. R. Allen, P. J. King, and L. Nelson, eds., Minerals, Metals, & Materials Society, pp. 87–106, 2005.

126. Hazelton, W. S., and W. H. Koo, “Technical Report on Material Selection and Processing Guidelines for BWR Coolant Pressure Boundary Piping, Final Report,” NUREG-0313, Rev. 2, 1988.

127. Pathania, R., R. Carter, R. Horn, and P. Andresen, “Crack Growth Rates in Irradiated Stainless Steels in BWR Internals,” *Proc. 14th Intl. Conf. on Environmental Degradation of Materials in Nuclear Power Systems—Water Reactors*, American Nuclear Society, Lagrange Park, IL, Paper No. 203178, 2009.

128. Karlsen, T. M., and A. Horvath, “Final Report on the In-pile Crack Growth Behavior of Irradiated Compact Tension Specimens in IFA-639,” HWR-770, OECD Halden Reactor Project, Dec. 2004.

129. Karlsen, T. M., M. Espeland, and A. Horvath, “Summary Report on the PWR Crack Growth Rate Investigation, IFA-657,” HWR-773, OECD Halden Reactor Project, May 2005,

130. Nakano, J., T. M. Karlsen, and M. Espeland, “Summary Report on the BWR Crack Growth Rate Experiment, IFA-658,” HWR-862, OECD Halden Reactor Project, Feb. 2007.

131. Nakano, J., T. M. Karlsen, and M. Espeland, “Summary of Results from the PWR Crack Growth Rate Investigation, IFA-670,” HWR-843, OECD Halden Reactor Project, Aug. 2008.

132. Karlsen, T. M., P. Bennett, and N. W. Hogberg, “In-core Crack Growth Rate Studies on Irradiated Austenitic Stainless Steels in BWR and PWR Conditions in the Halden Reactor,” *Proc. 12th Intl. Conf. on Environmental Degradation of Materials in Nuclear Power Systems—Water Reactors*, T. R. Allen, P. J. King, and L. Nelson, eds., Minerals, Metals & Materials Society, Warrendale, PA, pp. 337–348, 2005.

133. Jenssen, A., K. Gott, P. Efsing, and P. O. Andersson, “Crack Growth Behavior of Irradiated Type 304L Stainless Steel in Simulated BWR Environment,” *Proc. 11th Intl. Symp. On Environmental Degradation of Materials in Nuclear Power Systems—Water Reactor*, pp. 1015–1024, 2003.

134. Chen, Y., O. K. Chopra, E. E. Gruber, and W. J. Shack, "Irradiated Assisted Stress Corrosion Cracking of Austenitic Stainless Steels in BWR Environments," NUREG/CR-7018, ANL-09/17, June 2010.

135. Lu, Z., T. Shoji, Y. Takeda, Y. Ito, A. Kai, and N. Tsuchiya, "Effects of Loading Mode and Water Chemistry on Stress Corrosion Crack Growth Behavior of 316L HAZ and Weld Metal Materials in High Temperature Pure Water," *Corrosion Sc.*, **50**, 625–638, 2008.

136. Chen, Y., personal communication from Yiren Chen (Argonne) to Omesh Chopra (Argonne), Jan. 2014.

137. Balladon, P., J. Heritier, and P. Rabbe, “Influence of Microstructure on the Ductile Rupture Mechanisms of a 316L Steel at Room and Elevated Temperatures,” *Fracture Mechanics: 14th Symp.*, Vol. II: Testing and Applications, ASTM STP 791, American Society for Testing and Materials, Philadelphia, PA, pp. 496–516, 1983.

138. Picker, C., A. L. Stott, and H. Cocks, “Effects of Low-Dose Fast Neutron Irradiation on the Fracture Toughness of Type 316 Stainless Steel and Weld Metal,” *Proc. Specialists Meeting on Mechanical Properties of Fast Reactor Structural Material*s, Chester, UK, Paper IWGFR 49/440-4, 1983.

139. Huang, F. H., “The Fracture Characterization of Highly Irradiated Type 316 Stainless Steel,” *Int. J. Fracture* **25**, 181–193, 1984.

140. Bernard, J., and G. Verzeletti, “Elasto-Plastic Fracture Mechanics Characterization of Type 316H Irradiated Stainless Steel up to 1 dpa,” *Effects of Radiation on Materials: 12th Intl. Symp.*, ASTM STP 870, F. A. Garner and J. S. Perrin, eds., American Society for Testing and Materials, Philadelphia, PA, pp. 619–641, 1985.

141. Mills, W. J., L. A. James, and L. D. Blackburn, “Results of Fracture Mechanics Tests on PNC SU 304 Plate,” Westinghouse Hanford Report HEDL-7544, Hanford Engineering Development Laboratory, Richland, WA, 1985.

142. Michel, D. J., and R. A. Gray, “Effects of Irradiation on the Fracture Toughness of FBR Structural Materials,” *J. Nucl. Mater.* **148**, 194–203, 1987.

143. Van Osch, E. V., M. G. Horsten, and M. I. De Vries, “Fracture Toughness of PWR Internals,” ECN Contribution to CEC Contract on PWR Internals-Part 2 (ETNU/CT/94/0136-F), ECN-I-97-010 (71747/NUC/EvO/mh/006274), Netherlands Energy Research Foundation ECN, Petten, the Netherlands, 1997.

144. De Vries, M. I., “Fatigue Crack Growth and Fracture Toughness Properties of Low Fluence Neutron-Irradiated Type 316 and Type 304 Stainless Steels,” *Influence of Radiation on Mechanical Properties: 13th Symposium (Part II)*, ASTM STP 956, F. A. Garner et al., eds., American Society of Testing and Materials, Philadelphia, PA, pp. 174–190, 1987.

145. Alexander, D. J., J. E. Pawel, L. M. Grossbeck, A. F. Rowcliffe, and K. Shiba, “Fracture Toughness of Irradiated Candidate Materials for ITER First Wall/Blanket Structures,” *Effect of Radiation on Materials: 17th Intl. Symp.*, ASTM STP 1270, American Society of Testing and Materials, Philadelphia, PA, pp. 945–970, 1996.

146. Sindelar, R. L., G. R. Caskey, Jr., J. K. Thomas, J. R. Hawthorne, A. L. Hiser, R. A. Lott, J. A. Begley, and R. P. Shogan, “Mechanical Properties of 1950s Vintage Type 304 Stainless Steel Weldment Components after Low Temperature Neutron Irradiation,” *16th Intl. Symp. on Effects of Radiation on Materials*, ASTM STP 1175, American Society of Testing and Materials, Philadelphia, PA, pp. 714–746, 1993.

147. Sindelar, R. L., P. Lam, A. J. Duncan, B. J. Wiersma, K. H. Subramanian, and J. B. Edler, “ Development and Application of Materials Properties for Flaw Stability Analysis in Extreme Environment Service,” *Proc. of PVP2007 ASME Pressure Vessel and Piping Conf.*, July 22–26, 2007, San Antonio, TX, PVP2007-26660, 2007.

148. Haggag, F. M., W. R. Corwin, and R. K. Nanstad, “Effects of Irradiation on the Fracture Properties of Stainless Steel Weld Overlay Cladding,” *Nucl. Eng. and Design* **124**, 129–141, 1990.

149. Hamilton, M. L., F. H. Huang, W. J. S. Yang, and F. A. Garner, “Mechanical Properties and Fracture Behavior of 20% Cold-Worked 316 Stainless Steel Irradiated to Very High Neutron Exposures,” *Influence of Radiation in Material, Properties: 13th Intl. Symp. (Part II)*, ASTM STP 956, American Society of Testing and Materials, Philadelphia, PA, pp. 245–270, 1987.

150. Little, E. A., “Dynamic J-Integral Toughness and Fractographic Studies of Fast Reactor Irradiated Type 321 Stainless Steel,” *Effects of Radiation on Material, Properties: 12th Intl. Symp.*, ASTM STP 870, American Society of Testing and Materials, Philadelphia, PA, pp. 563–579, 1985.

151. Haggag, F. J., W. L. Server, W. G. Reuter, and J. M. Beeston, “Effects of Irradiation Fluence and Creep on Fracture Toughness of Type 347/348 Stainless Steels,” ASTM STP 870, American Society of Testing and Materials, Philadelphia, PA, pp. 548–562, 1985.

152. Fukuya, K., K. Fuji, H. Nishioka, and Y. Kitsunai, “Evolution of Microstructure and Microchemistry in Cold-Worked 316 Stainless Steels under PWR Irradiation,” *J. Nucl. Sci. and Technol.* **43** (2) 159–173. 2006.

153. Eason, E. D., J. E. Wright, and G. R. Odette, "Improved Embrittlement Correlations for Reactor Pressure Vessels," NUREG/CR-6551 (MSC 970501), Nov. 1998.